



# University of HUDDERSFIELD

## University of Huddersfield Repository

Cox, Nicola Michelle

Synthesis of Functional Metallosupramolecular Complexes

### Original Citation

Cox, Nicola Michelle (2012) Synthesis of Functional Metallosupramolecular Complexes. Doctoral thesis, University of Huddersfield.

This version is available at <http://eprints.hud.ac.uk/id/eprint/17502/>

The University Repository is a digital collection of the research output of the University, available on Open Access. Copyright and Moral Rights for the items on this site are retained by the individual author and/or other copyright owners. Users may access full items free of charge; copies of full text items generally can be reproduced, displayed or performed and given to third parties in any format or medium for personal research or study, educational or not-for-profit purposes without prior permission or charge, provided:

- The authors, title and full bibliographic details is credited in any copy;
- A hyperlink and/or URL is included for the original metadata page; and
- The content is not changed in any way.

For more information, including our policy and submission procedure, please contact the Repository Team at: [E.mailbox@hud.ac.uk](mailto:E.mailbox@hud.ac.uk).

<http://eprints.hud.ac.uk/>

# Synthesis of Functional Metallosupramolecular Complexes

Nicola Michelle Cox



*University of*  
**HUDDERSFIELD**

This thesis is submitted in partial fulfilment of the requirements for the award of Doctor of Philosophy awarded by the University of Huddersfield.

November 2012

## Acknowledgements

Firstly I would like to thank my supervisor Dr Lindsay Harding for giving me the opportunity to undertake this work and for her guidance and support throughout my PhD. I would also like to thank Prof. Craig Rice for all his help and patience in the lab and all his expertise, especially with the X-ray crystallographic analysis.

I would like to thank the University of Huddersfield for providing me with the funding that has also made this PhD possible.

To all the technical staff members who have helped me throughout this process I would like to thank, especially Dr Neil McLay. His support both professional and personal was and still is gratefully appreciated.

A big thank you has to be said to my fellow researchers and friends, especially Dr Ilyas Qamar for all his words of wisdom, keeping me focused and making me believe in myself when times got tough. This also extends to Adam Zahid and Sean Piela, again, their support throughout was deeply appreciated and I cannot thank them enough.

Lastly but most importantly thank you to my sisters who have never doubted me and encouraged me to carry on till the end, also I would like to say a special thank you with all my heart to the two most important people in my life, my sons Sian and Wayde. None of my achievements would have been possible without their unconditional love and constant support and belief in me.

# Table of Contents

Acknowledgements.....	ii
Abstract .....	v
Chapter 1 Introduction .....	1
1.1 Supramolecular Chemistry .....	1
1.2 Supramolecular Interactions.....	1
1.3 Hydrogen Bonding .....	2
1.4 $\pi$ - $\pi$ Stacking .....	2
1.5 Electrostatic Interactions .....	3
1.6 Hydrophobic Effects .....	4
1.7 Host-guest Chemistry.....	5
1.8 Coordination Chemistry.....	7
1.9 Metallosupramolecular Chemistry .....	8
1.10 Helicates .....	10
1.10.1 Homoleptic Helicates.....	12
1.10.2 Heteroleptic Helicates .....	13
1.11 Pyridyl-thiazole Donor Units .....	14
1.12 References.....	17
Chapter 2 Using Pyrene Fluorescence to Elucidate Supramolecular Structures in Solution.....	21
2.1 Introduction .....	21
2.2 Aims .....	30
2.3 Experimental .....	31
2.3.1 Ligand Synthesis .....	31
2.3.2 Characterisation .....	32
2.4 Results and Discussion .....	33
2.4.1 Ligand synthesis.....	33
2.4.2 Coordination Chemistry of $L^1$ .....	37
2.4.3 Coordination Chemistry of $L^2$ .....	43
2.4.4 Photophysical Measurements .....	50
2.5 Conclusion .....	53
2.6 References.....	54
2.7 Appendix: Crystallographic Data Tables .....	59

Chapter 3	Novel pyridyl-thiazole-containing complexes capable of binding anions .....	63
3.1	Introduction .....	63
3.2	Aims .....	72
3.3	Experimental .....	73
3.3.1	Ligand synthesis ( $L^3$ ).....	73
3.3.2	Ligand synthesis ( $L^4$ ).....	78
3.4	Results and Discussion .....	84
3.4.1	Results and Discussion – $L^3$ .....	84
3.4.2	Coordination Chemistry - $L^3$ .....	90
3.4.3	Results and Discussion – $L^4$ .....	102
3.4.4	Coordination Chemistry - $L^4$ .....	108
3.5	Conclusion .....	113
3.6	References .....	114
3.7	Appendix: Crystallographic Data Tables .....	118
Chapter 4	Allosteric control of metal specificity in formation of coordination complexes.....	122
4.1	Introduction .....	122
4.2	Aims .....	131
4.3	Experimental .....	132
4.3.1	Ligand synthesis ( $L^5$ ).....	132
4.4	Results and Discussion .....	137
4.4.1	Coordination Chemistry of $L^5$ .....	138
4.4.2	Metal specificity of $L^5$ .....	150
4.5	Conclusion .....	171
4.6	References .....	172
4.7	Appendix: Crystallographic Data Tables .....	175
Appendix: Publication .....		180

## Abstract

This thesis describes three areas of research which involve preparation of novel pyridyl-thiazole-containing ligands and the formation of their complexes with transition metal ions.

Chapter 2 describes the preparation, complexation chemistry and photophysical behaviour of ligands  $L^1$  and  $L^2$  which contain pyrene moieties. The emission properties of pyrene are highly dependent on its environment, and so it was proposed that it could be used as a probe to elucidate solution conformations of complexes. It was shown that incorporation of a pyrene moiety into the ligand strand and subsequent measurement of the emission spectra of its complexes with  $Cu^+$  and  $Cd^{2+}$  gave information about their solution state conformations which correlated well with the solid state structures.

In Chapter 3, synthesis and coordination complexes of ligands  $L^3$  and  $L^4$ , which contain substituents capable of binding anions, are described.  $L^3$  forms a mononuclear complex with  $Zn(II)$  which binds two perchlorate anions *via* the amide groups on the two substituents. However, with  $Cu(I)$ ,  $L^3$  and  $L^4$  form dinuclear double helicates which have a binding "pocket" at each end of the complex. Both  $[Cu_2(L^3)_2](ClO_4)_2$  and  $[Cu_2(L^4)_2](PF_6)_2$  form one-dimensional polymers; the complexes are held together by bridging perchlorate and hexafluorophosphate anions, respectively.

Finally, in Chapter 4, allosteric control of the complexation behaviour of ligand  $L^5$  is described.  $L^5$  contains amine groups on the 3,3'-positions of the bipyridine core which can react with ketones, forming a cyclic aminal product. Reaction with cyclohexanone was used to control the metal specificity of the ligand by restraining the torsion angle between the two pyridine groups and forcing the ligand into planarity. In general,  $L^5$  formed dinuclear double helicates with tetrahedral metals and mononuclear complexes with octahedral metals, as expected. Upon reaction with cyclohexanone, mononuclear species were observed with  $Hg^{2+}$ ,  $Zn^{2+}$ ,  $Cd^{2+}$  and  $Ag^+$ . Experiments were then carried out with mixtures of metal ions and two trends were observed: firstly, when  $L^5$  is mixed with octahedral and tetrahedral metals, species containing the octahedral metal are favoured. Where two octahedral metals are used species containing the metal with the larger ionic radius are formed preferentially. After reaction with cyclohexanone, only mononuclear species of the octahedral metals are observed in every case.

# Chapter 1 Introduction

## 1.1 Supramolecular Chemistry

Supramolecular chemistry is a fast growing area within chemical research which spans inorganic, organic and physical chemistry as well as biochemistry.<sup>1</sup> Supramolecular chemistry is often described as *chemistry beyond the molecule*, mainly focusing on the non-covalent bonding interactions between molecules and the spontaneous self-assembly of the resulting complexes.<sup>1</sup> Supramolecular chemistry is a relatively new field of chemistry which can be dated back to the late 1960s when Lehn and Pedersen synthesised various macrocyclic ligands which can form supramolecular complexes. Jean-Marie Lehn was one of the first, most influential scientists to help define supramolecular chemistry and he won the Nobel Prize in 1987 along with C. J. Pedersen and D. J. Cram for their pioneering work in this field of chemistry.<sup>2-4</sup>

All three research groups developed innovative macrocyclic ligands and investigated their coordination of different metal cations.<sup>5</sup> Studies within supramolecular chemistry in the past have partly focused on the synthesis and design of macrocyclic ligands for coordination with different guest species. Synthesis and design is constantly changing and becoming more complex within these supramolecular systems. The vast majority of these systems include host units where the binding of one or more guest species will occur at well-defined binding sites with the host. More recently however, the design and synthesis of supramolecules has changed immensely, with the development of self-assembly, allosteric interactions and ligand recognition.

## 1.2 Supramolecular Interactions

There are numerous interactions or forces used to assemble supramolecules; such interactions are often weak and reversible and can generally be regarded as non-covalent processes. This covers an extensive range of repulsive and attractive forces between a host, a guest and the surrounding environment.

These interactions include hydrogen bonding,  $\pi$ - $\pi$  stacking interactions, electrostatic effects, hydrophobic and solvophobic effects, among others.<sup>6</sup>

### 1.3 Hydrogen Bonding

Within supramolecular chemistry the hydrogen bond can be said to be the most important non-covalent interaction used in the design of supramolecular architectures.<sup>1</sup> This is mainly due to the high level of directionality and strength of hydrogen bonds. These bonds can be regarded as strong dipole-dipole interactions (4-120 kJ mol<sup>-1</sup>) between a proton donor and a proton acceptor. These interactions occur when a hydrogen atom is bound to a highly electronegative atom such as nitrogen or oxygen which therefore will form a dipole with the hydrogen atom that then gains a partial positive charge (Figure 1.1).<sup>1</sup>

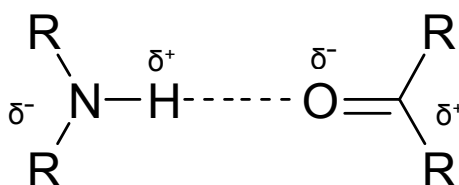


**Figure 1.1:** A carbonyl oxygen accepting a hydrogen bond from a secondary amine donor

### 1.4 $\pi$ - $\pi$ Stacking

$\pi$ - $\pi$  Stacking interactions are weak electrostatic interactions (0-50 kJ mol<sup>-1</sup>) that occur between systems containing aromatic rings. There are two types of  $\pi$ - $\pi$  stacking interactions that can occur: *face-to-face* where the interaction is between the corner of one ring and the centre of another and *edge-to-face* where a hydrogen atom from one of the aromatic rings interacts in a perpendicular orientation with respect to the centre of another ring (Figure 1.2).<sup>1</sup>

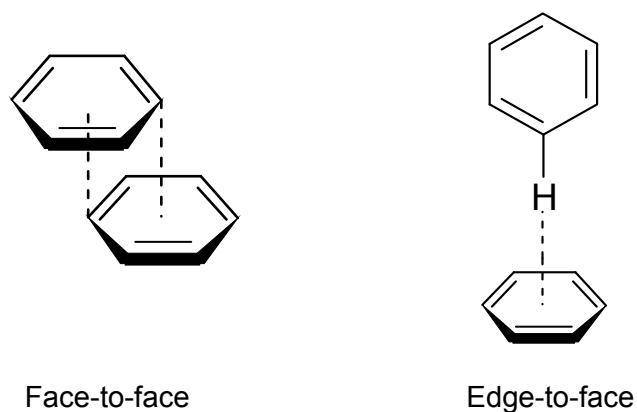


**Figure 1.2:**  $\pi$ - $\pi$  stacking interactions

## 1.5 Electrostatic Interactions

Electrostatic interactions such as ion-dipole and dipole-dipole interactions are all based on the Coulombic attraction between opposite charges.<sup>6</sup> Ion-ion interactions are the strongest of the three interactions ( $100\text{-}350\text{ kJ mol}^{-1}$ ) and are non-directional, allowing the reaction to occur in any orientation.

Ion-dipole interactions are directional and therefore have orientation-dependent aspects requiring the dipole to be suitably aligned for the best possible binding efficiency ( $50\text{-}200\text{ kJ mol}^{-1}$ ) (Figure 1.3).<sup>1</sup>

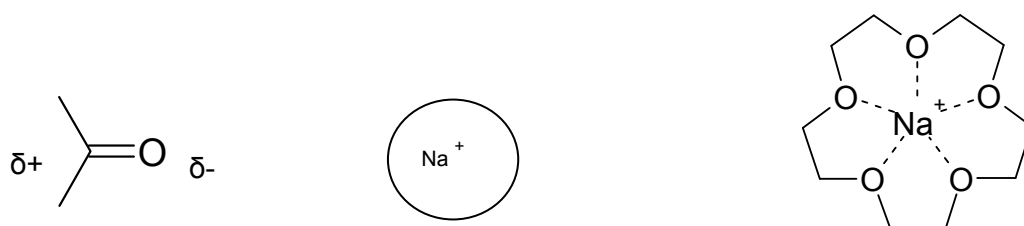


**Figure 1.3:** Ion-dipole interaction, in the sodium complex of [15]crown-5

Dipole-dipole interactions also have orientation-dependent aspects like ion-dipole interactions but as directional interactions are moderately inflexible, only spatially complementary dipoles will be able to form aggregates (Figure 1.4).

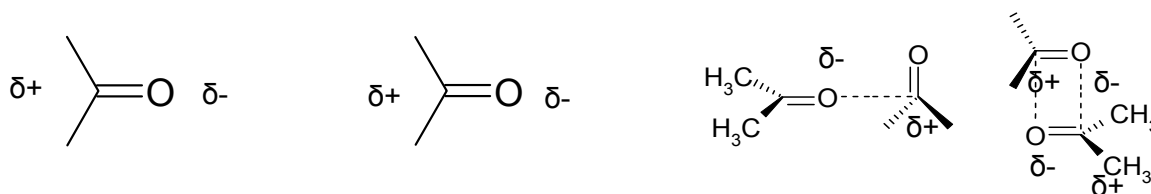


**Figure 1.4:** Dipole-dipole interactions in acetone

Whereas ion-ion interactions can stabilise a vast range of molecular pairing, dipole-dipole interactions are the weakest of the three forces ( $5\text{-}50\text{ kJ mol}^{-1}$ ) due to the fact that ions have a higher charge density than dipoles and the strength of these directional interactions depends on the species involved.<sup>1</sup>

## 1.6 Hydrophobic Effects

The hydrophobic effect involves the exclusion of non-polar molecules from aqueous solutions. The hydrophobic effect is energetically favourable as the water molecules will only interact with other polar molecules or themselves preferentially, with the formation of micelles being an excellent example.<sup>1</sup>

Micelles are formed when molecules such as fatty acids, salts of fatty acids and other similar molecules containing both hydrophobic and hydrophilic regions are added to water.<sup>5</sup> Such molecules contain polar head groups and a long hydrophobic chain (hydrocarbon tail); due to the heads being polar, in water they tend to form the outer surface of the micelle. The tails tend to be repelled from the aqueous environment due to their hydrophobicity and thus form the inner core of the micelle (Figure 1.5a). If a hydrophobic liquid such as an organic solvent or oil is added to water, then the structure of micelles can change and they can invert (Figure 1.5b); the long hydrophobic chain will be forced to face outwards turning the polar head groups inwards.

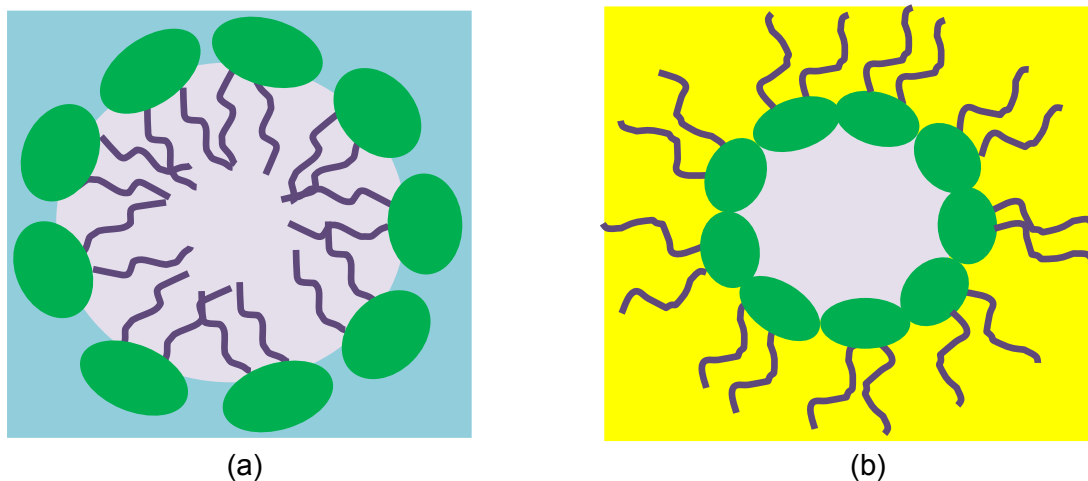


**Figure 1.5:** Diagrams showing formations of micelles in water (a) and in an organic solvent (b)

## 1.7 Host-guest Chemistry

Supramolecular chemistry can also be described as *host-guest* chemistry where, in its simplest form, assemblies are held together by non-covalent interactions between two or more different species. The host is a molecule which contains convergent binding sites and is capable of binding a guest species which has divergent binding sites.<sup>1</sup> This can be achieved by hydrogen bonding, ion pairing, metal to ligand bonding or electrostatic effects.<sup>5</sup> With non-covalent bonds being weaker than covalent bonds, assembly of host-guest complexes normally involves multiple binding interactions. Thus, the arrangement of the binding sites in the host and the guest must be complementary for efficient binding to take place.<sup>5</sup> It can be said, therefore, that the host will *recognise* suitable guests.

The archetypal example of this recognition behaviour is the binding between biological receptors and their substrates, providing a deep source of inspiration and a high standard of challenges for supramolecular chemists to attempt to match.<sup>6</sup> Emil Fischer described the *lock and key* principle which illustrated the specificity required in enzyme-substrate recognition.<sup>6</sup> The binding sites' size, shape and position have to correspond with the specific substrate in order for there to be ideal substrate recognition (Figure 1.6).<sup>6</sup>

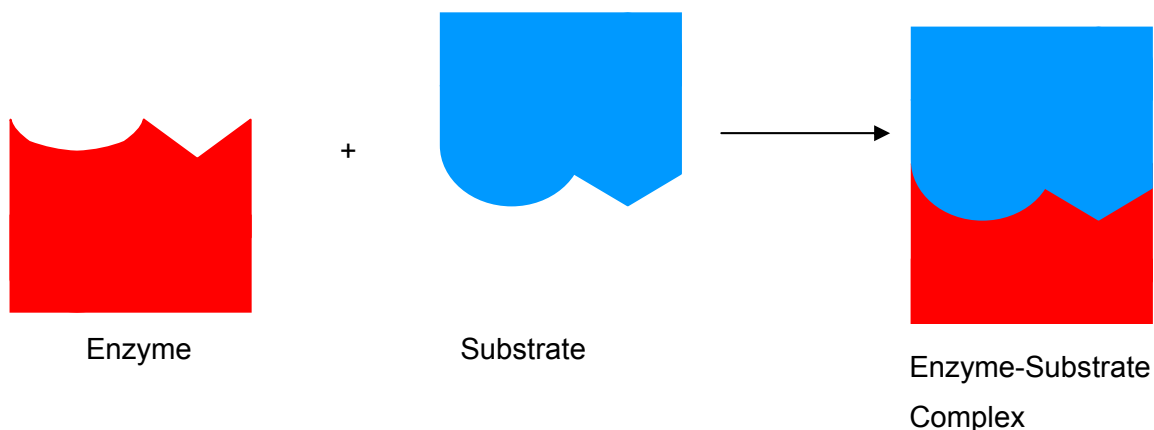


**Figure 1.6:** *Lock and key model* – the substrate and the enzyme binding site have complementary shapes

One of the most important and well known examples of molecular recognition in supramolecular chemistry is the double helicate structure of DNA, where hydrogen bonding interactions link the two separate strands together.<sup>6</sup> A single DNA strand is made up of pyrimidine and purine bases linked to a backbone of phosphorylated sugars. The double helix of DNA merges two anti-parallel strands which are held together by  $\pi$ - $\pi$  stacking interactions and complementary hydrogen bonds between the base pairs (Figure 1.7).

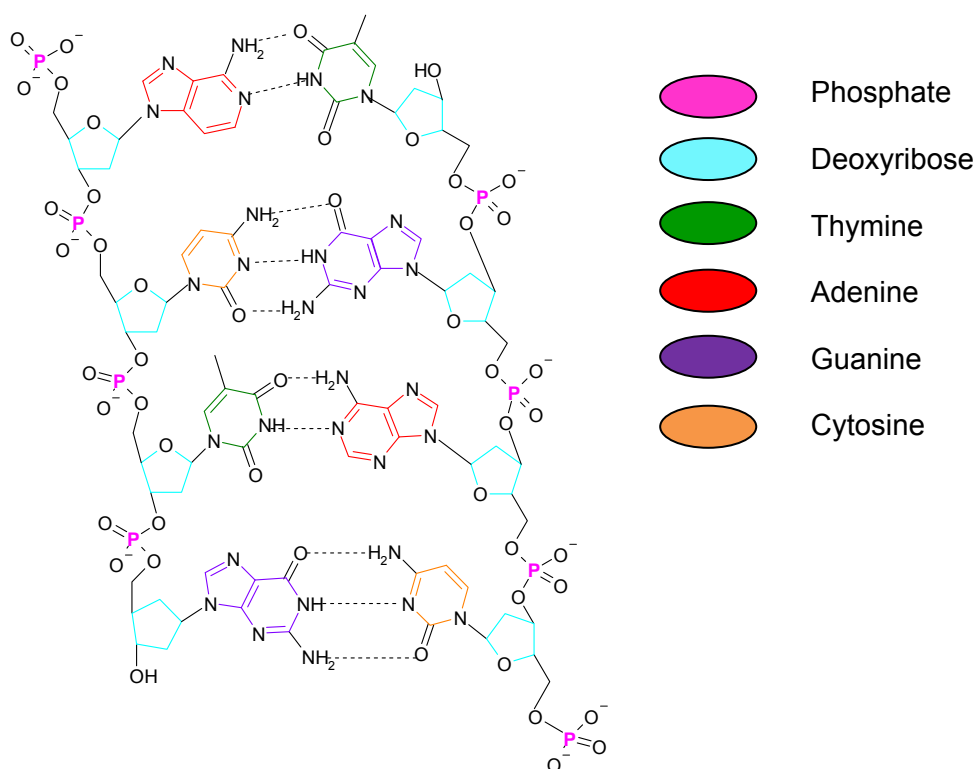


**Figure 1.7:** The chemical structure of DNA (hydrogen bonds are shown as dotted lines)

The hydrogen bonds occur between adenine and thymine or guanine and cytosine bases. Each species will recognise its specific partner and will not link or join in any other formation.<sup>1</sup> This has definitely made researchers in the field of supramolecular chemistry determined to try to achieve the same level of precision among non-biological systems.

## 1.8 Coordination Chemistry

Researchers have studied for years how metal complexes play vital roles within everyday life and industry.<sup>8</sup> Scientists have already proven that haemoglobin, an iron complex, transports oxygen through the red blood cells of vertebrates, and how chlorophyll, which is a magnesium complex, is critical to the photosynthesis process in plants.<sup>8</sup> Coordination compounds are used considerably in qualitative analysis as a means for positively identifying certain unknown ions and for separating specific metal ions.

Our understanding of the nature of metal complexes is mainly due to the pioneering work from Nobel Prize winner Alfred Werner. He was awarded the prize in 1913 due to his development of the basic concepts of coordination chemistry.<sup>9</sup> Metal amines and ammonium salts made up the core focus of Werner's work, and were the compounds of choice largely investigated within his research.<sup>10-12</sup> He documented the discovery of several different forms of cobalt-ammonia chlorides, where each compound had a different colour and other characteristics.<sup>11</sup> To date, his discovery is more commonly known as 'Werner's Coordination Theory' which when broken down follows three important main rules:

- 1)** Elements exhibit two types of valences: primary (oxidation number) and secondary (coordination number).
- 2)** Every atom tends to satisfy both primary and secondary valences.
- 3)** The secondary valence is directed towards fixed orientations in space.<sup>9</sup>

Werner was one of the first scientists to recognise that stereochemistry was not limited to organic chemistry. His understanding and discoveries in coordination chemistry opened new avenues in research, especially inorganic chemistry. Subsequently, researchers have pushed Werner's work past the boundaries of inorganic chemistry and it has been of incredible value in the areas of analytical, physical and biological

chemistry.<sup>10</sup> Areas such as crystallography and mineralogy have even benefited from Werner's pioneering knowledge in coordination chemistry.

## 1.9 Metallosupramolecular Chemistry

Metallosupramolecular chemistry is a subdivision of supramolecular chemistry involving spontaneous self-assembly of metal ions with ligands through coordinate bonds. Metal-ligand interactions are of keen interest due to their high levels of directionality and the ability of ligands to easily replace other ligands in an equilibrium reaction due to the predictable nature of metal ion coordination environments.<sup>13</sup> Metal ions have ideal coordination numbers and coordination geometries that can be matched with the intrinsic bonding properties of polydentate ligands.<sup>14</sup> These ligands can contain more than one metal binding site which makes it possible for researchers to create a vast range of innovative and functional assemblies.<sup>14</sup> Metallosupramolecular building blocks involve metal ions and organic ligands with the most common ligands used incorporating heterocyclic rings containing nitrogen.<sup>15</sup> Lehn contributed hugely towards work in this field, especially in his work involving pyridyl complexes, discussed further below.<sup>16-18</sup>

Assembly of supramolecular hosts brings concern to researchers. We can construct a stable host-guest complex using non-covalent interactions which are often weak, ensuring there are as many as possible of these interactions stabilising the complex.<sup>5</sup> Stabilisation energy is gained from each interaction; when these small energies are all added together a substantial binding energy is created giving the complex stability.<sup>5</sup>

Host binding sites are usually donor atoms in ligands whereas the metal is usually the guest.<sup>6</sup> Stabilisation of the chelate will rely on the size of both the chelate and the guest. Generally, a chelate has donor atoms positioned at certain intervals along its length; the host chain will wrap itself around the guest making a stable host-guest complex; this type of chain is known as a podand.<sup>5</sup>

Metal complexes of bidentate ligands (such as 1,2-diaminoethane) are much more stable than those containing monodentate ligands (such as ammonia) and this extra stabilisation is due to the *chelate effect*.<sup>6</sup> Complexes containing bidentate ligands are more stable than those containing monodentate ligands due to entropic effects. Figure 1.8 shows how six monodentate ligands are replaced by three bidentate ligands in an equilibrium reaction between  $\text{Ni}^{2+}$ , ammonia and 1,2-diaminoethane (en). During this

process a number of molecules will become free in solution giving a higher degree of freedom in the system, thereby favourably increasing entropy.

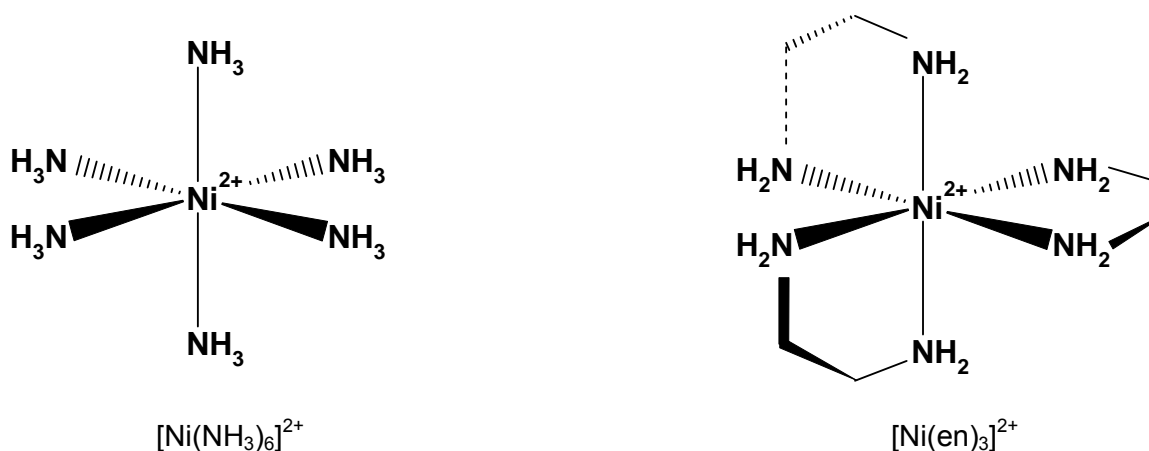
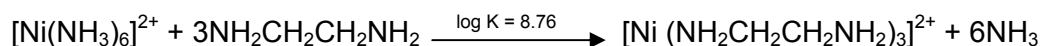


**Figure 1.8:** The equilibrium between  $[\text{Ni}(\text{NH}_3)_6]^{2+}$  and  $[\text{Ni}(\text{en})_3]^{2+}$ . The value of  $\log K$  indicates that the 1, 2-diaminoethane chelate complex is more than  $10^8$  times more stable<sup>5</sup>

Stabilisation offered by the chelate effect is extremely dependent on the size of the chelate ring. Five-membered rings are the most stable having the least amount of ring strain.<sup>5</sup> As chelate ring size increases the probability of two donor atoms pointing towards the same metal ion directly decreases leading to decreased coordination and unfavourable entropy.<sup>5</sup> The chelate effect can enhance the thermodynamic stability of a host-guest complex.

However, numerous supramolecular host-guest complexes are more stable than would be expected from the chelate effect alone; these compounds are stabilised additionally by the *macrocyclic effect*. The macrocyclic effect relates both chelation of the guest by multiple binding sites and the organisation of the binding sites spatially.<sup>5</sup> With cyclic hosts such as crown ethers, the stability can increase by a factor of  $10^4$  times more than podands with the same type of binding sites due to the spatial pre-organisation of the binding sites in the chelate.<sup>5</sup>

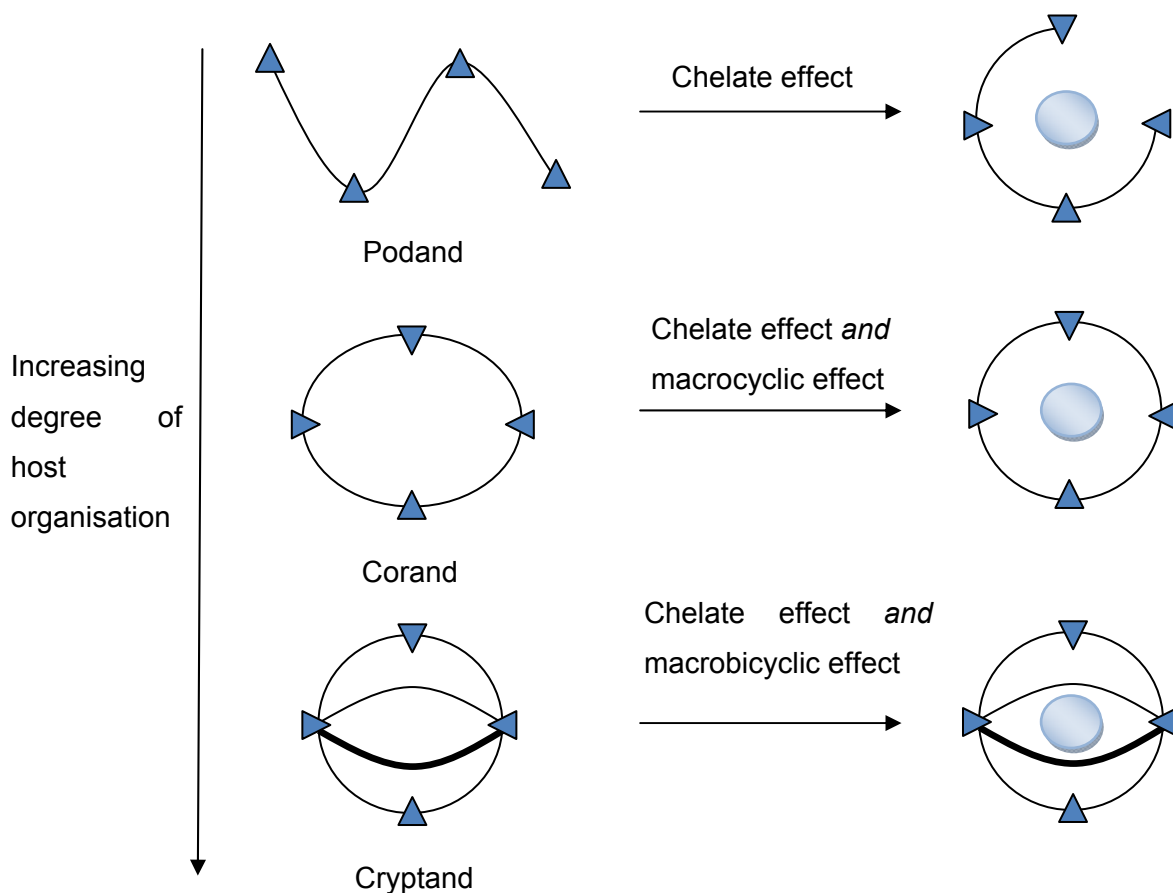


**Figure 1.9:** The chelate, macrocyclic and macrobicyclic effects

Thus, careful consideration of these effects can lead to control of assembly formation.

## 1.10 Helicates

One of the major areas of activity within supramolecular coordination chemistry is the assembly of double and triple helicate complexes. Such helicate assemblies have demonstrated how the specific formation of architecturally complex assemblies is directed by the interaction between simple parameters such as the stereoelectronic preference of the metal ion and the disposition of binding sites in the ligand.<sup>19,20</sup> The term “helicate” was first introduced in 1987 by Lehn and co-workers to describe a complex containing two or more ligand strands coordinated by two or more metal centres in a helical arrangement (Figure 1.10).<sup>6,21</sup>

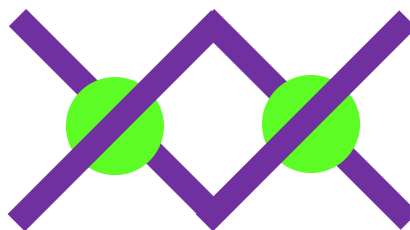


**Figure 1.10:** Illustration showing the basic formation of a helicate, in this case a dinuclear double helicate

Helicate complexes usually contain multidentate bridging ligands that contain more than one set of donor atoms which are capable of chelating different metal centres. The formation of a helicate complex will depend on both the design of the ligand and the choice of metal ion used, for example, the ligand may vary in number and disposition of the binding sites; this would make the ligand capable of coordinating a metal ion with a particular coordination geometry. The ligand may also be flexible enough to form various supramolecular architectures and be capable of self-recognition and self-assembly processes.<sup>19</sup> The metal ion may vary in size, binding strength and stability and may also have a preferred coordination geometry. An important aspect in the assembly of helicates is how a flexible polydentate ligand becomes partitioned into different metal binding sites. In the past, ligands have been constructed which contain several bidentate or terdentate domains which are so arranged that each site must essentially bind a separate metal ion rather than chelating a single metal ion.<sup>19,22</sup>

There are numerous types of helicate species, which in turn can cause the classification to become quite complicated. Many different aspects need to be taken into consideration, such as the number of ligands, the number of metal centres and the number of binding sites. Simple helicates are named in terms of the number of metal centres and the number of ligand strands involved; mononuclear, dinuclear, trinuclear and so on, refer to one, two and three metal centres respectively. The helicate can be made up from two ligand strands which results in a double helicate or three ligand strands which results in a triple helicate. One of the important factors in the assembly of helicates is the ligand strands themselves; helicates comprising identical strands are termed homoleptic helicates while helicates that consist of different ligand strands are termed heteroleptic. Heteroleptic systems and asymmetric ligands can form helicates that can exist in two different isomeric forms according to the orientations of the coordinated ligand strands. The terms for these isomeric forms are head-to-head (HH) and head-to-tail (HT) (Figure 1.11).

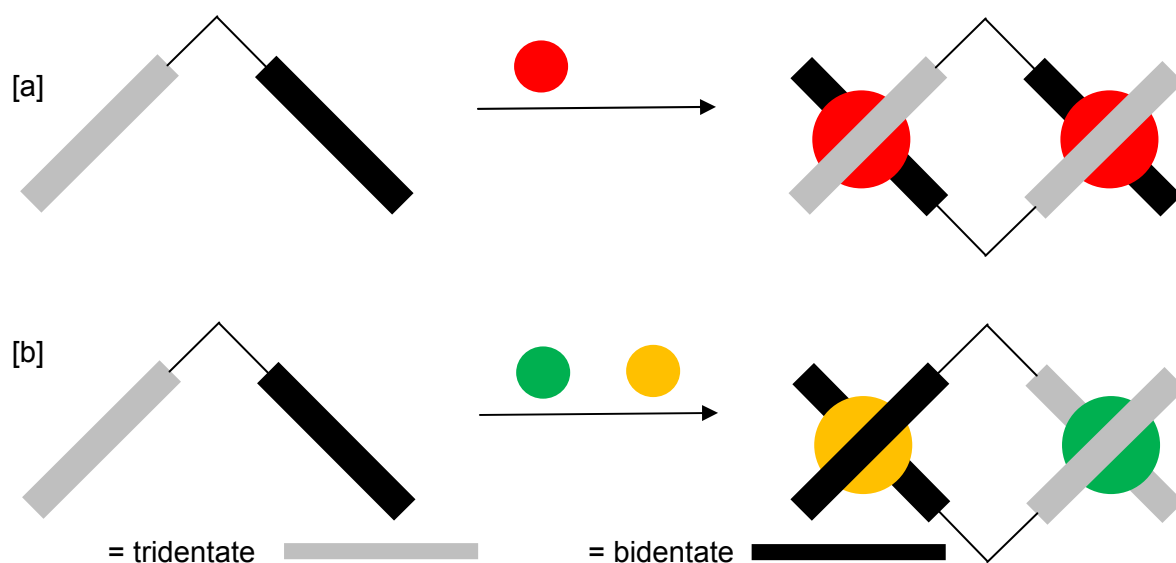


**Figure 1.11:** Schematic representation of (a) the formation of a double-stranded (HT) helicate, (b) a double-stranded (HH) helicate (red, yellow and green circles represent five-, four- and six-coordinate metal ions, respectively)

### 1.10.1 Homoleptic Helicates

Homoleptic helicates are assembled from identical ligand strands and have attracted a considerable amount of attention from researchers throughout the years.<sup>23-25</sup> An excellent example of this was demonstrated by Constable *et al.*<sup>26</sup> This research showed that reaction of the potentially tetradentate *ortho*-linked quarterpyridine ligand  $L^a$  with equimolar amounts of copper(I) resulted in the formation of a homoleptic dinuclear double helicate  $[Cu_2(L^a)_2]^{2+}$  (Figure 1.12). The copper(I) centres have occupied a distorted tetrahedral coordination geometry which is formed by two bidentate binding domains, one from each of the ligands, in a double helical arrangement. However, reacting ligand  $L^a$  with a metal ion that favours octahedral coordination geometry such as Cu(II), would result in a mononuclear complex due to the four N-donor atoms coordinating in the equatorial plane of the  $Cu^{II}$  ion (Figure 1.13).

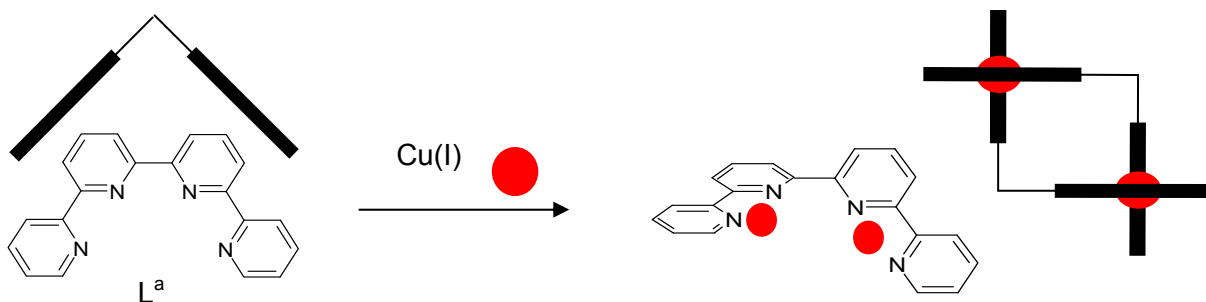


**Figure 1.12:** Schematic representation of the homoleptic dinuclear double helicate  $[\text{Cu}_2(\text{L}^a)_2]^{2+}$  formed upon reaction of  $\text{L}^a$  with  $\text{Cu(I)}$  ions<sup>26</sup>

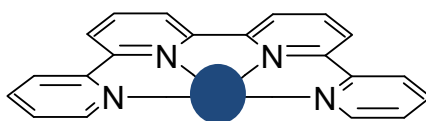


**Figure 1.13:** Representation of the  $[\text{Cu(II)}\text{L}^a]^{2+}$  mononuclear complex<sup>26</sup>

### 1.10.2 Heteroleptic Helicates

Heteroleptic helicates are assembled from different ligand strands. Even though homoleptic helicates have been researched for longer, heteroleptic helicates have been reported in great detail and the interest in these systems has grown immensely.<sup>18,19,24</sup> One example was demonstrated by Cohen *et al.*; two structurally similar ligands  $\text{L}^b$  and  $\text{L}^c$  were prepared which consisted of alternating 1,10-phenanthroline units and 2,2'-bipyridine units linked together by methylene spacers.<sup>27</sup> Due to the disposition of the N-donor units, the ligands partition into a sequence of bidentate binding domains. It was shown that reacting  $\text{L}^b$  and  $\text{L}^c$  with copper(I) resulted in the formation of both the homoleptic and heteroleptic helicates (Figure 1.14). For all three formations, the copper(I) centres occupied a distorted tetrahedral coordination geometry which is formed by two bidentate binding domains, one from each of the ligand strands in a trinuclear double helical arrangement.

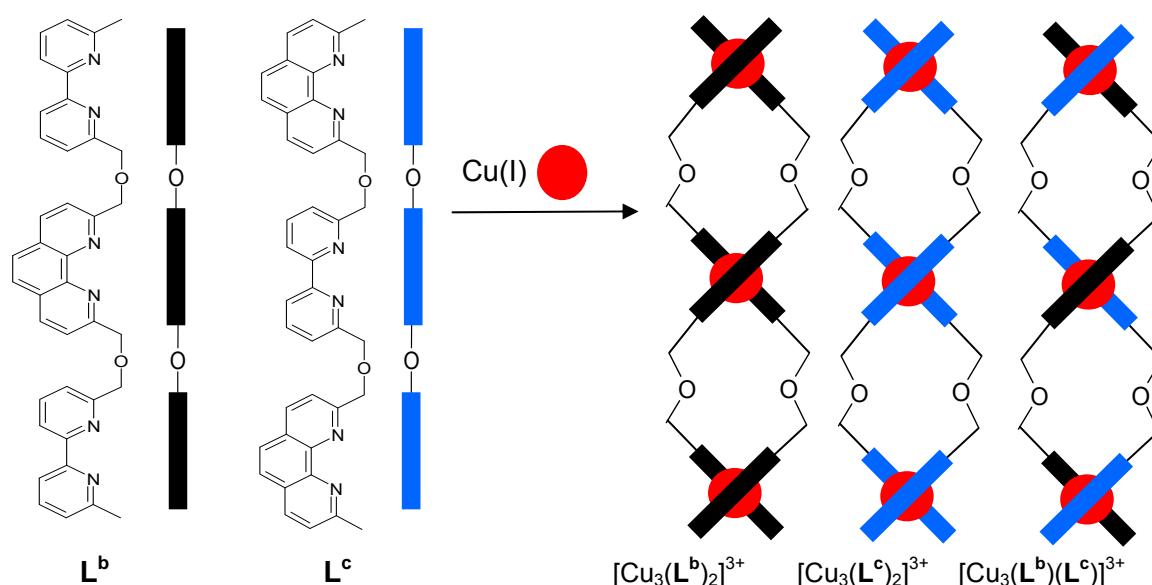


**Figure 1.14:** Schematic representation of the formation of homoleptic and heteroleptic helicates upon reaction of  $L^b$  and  $L^c$  with copper(I) ions<sup>27</sup>

## 1.11 Pyridyl-thiazole Donor Units

Pyridyl-thiazole N-donor ligands have been of great interest within metallosupramolecular chemistry since incorporation of a five-membered thiazole ring within the ligand forces it to partition into separate binding domains. Pyridyl-thiazole ligands are very similar to the well-known oligopyridines, although they have different coordination properties due to the presence of five-membered thiazolyl rings.

Two major features which make such ligands particularly interesting are that they are readily available in much higher quantities than the analogous polypyridines and are very simple to prepare. The thiazole unit can be easily introduced into polydentate ligands which leads them to partition themselves naturally into specific binding domains; this is due to the fact that two adjacent thiazolyl units cannot chelate the same metal ion (Fig. 1.15).<sup>15,28</sup> With octahedral metals such as  $\text{Cd}^{2+}$  and  $\text{Cu}^{2+}$ , an oligopyridine ligand such as 2,2',6',2'',6'',2'''-quaterpyridine can coordinate all four equatorial coordination sites of the metal ion since the bite angles between adjacent pyridine rings are sufficiently convergent (Figure 1.15(a)).

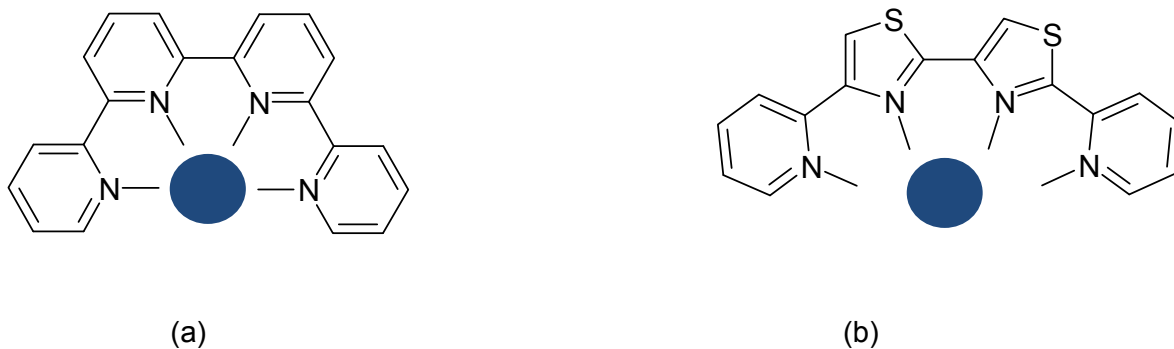


**Figure 1.15:** Showing how ligand (b) is more divergent than ligand (a) due to the addition of the five-membered thiazole rings

However, upon reaction with a metal such as Cu(I) which prefers tetrahedral coordination geometry, the ligand cannot bend to accommodate all of the coordination sites of the metal and the backbone twists causing the ligand to partition into two separate binding domains, resulting in a double helicate (Figure 1.16).

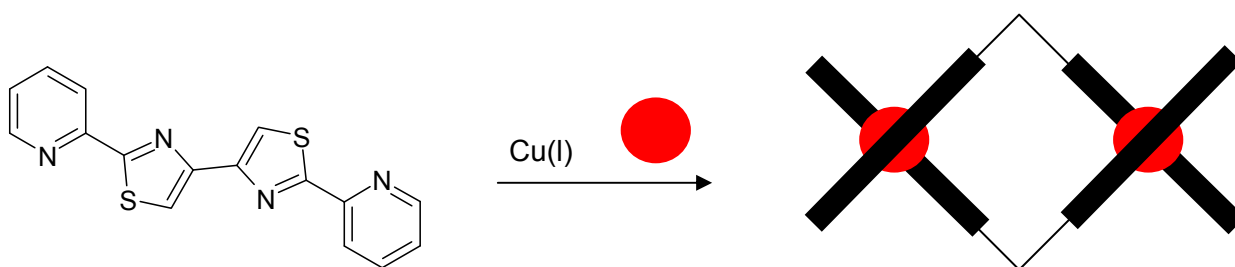


**Figure 1.16:** Reaction of a pyridyl-thiazole ligand with Cu(I), a metal ion which prefers tetrahedral coordination geometry. The backbone of the ligand twists partitioning it into two separate binding domains, which in turn results in a dinuclear double helicate<sup>29</sup>

Using these principles, researchers within this field of chemistry have designed ligands containing various combinations of pyridyl-thiazole donor units and prepared their complexes with metal ions of different coordination geometries.<sup>15,30-33</sup> An excellent example of this was demonstrated by Rice *et al.*<sup>33</sup> Ligands **L<sup>d</sup>** and **L<sup>e</sup>** (Figure 1.17) which contained chelating pyridyl-thiazolyl fragments were successfully prepared for the assembly of double and triple helicates with Cu(II) ions.<sup>29</sup>

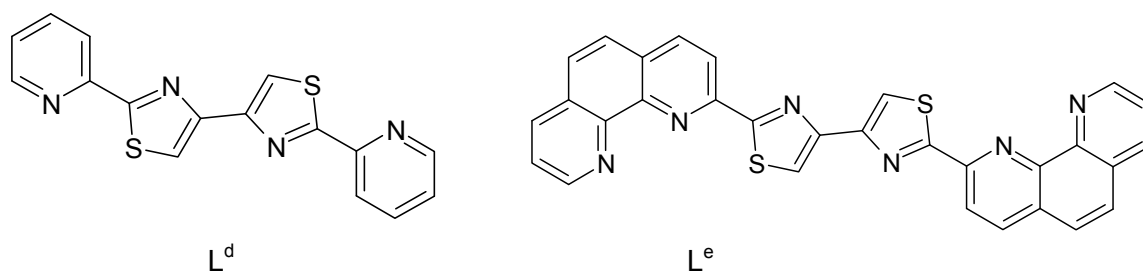


**Figure 1.17:** Ligands L<sup>d</sup> and L<sup>e(29)</sup>

Upon reaction of L<sup>d</sup> with Cu(II) the dinuclear triple helicate complex [Cu<sub>2</sub>(L<sup>d</sup>)<sub>3</sub>](PF<sub>6</sub>)<sub>4</sub> was formed. X-ray crystallography confirmed the structure of the complex and showed a triple helical arrangement with two Cu(II) ions coordinated by three bridging ligands. Each copper centre adopts an octahedral coordination geometry and is coordinated by three thiazole-pyridyl bidentate units; the backbone of L<sup>d</sup> has twisted about the inter-thiazole bond.

Upon reaction of L<sup>e</sup> with Cu(II), a dinuclear double helicate [Cu<sub>2</sub>(L<sup>e</sup>)<sub>2</sub>](ClO<sub>4</sub>)<sub>4</sub> was formed. Again, each copper centre adopts an octahedral coordination geometry and is coordinated by two thiazolyl-phenanthroline tridentate units. Each ligand again has twisted at the inter-thiazole bond.

It is clear that these types of ligand are very versatile due to their ability to adopt wide varieties of different coordination modes. Results from Rice *et al.* show clearly how, due to the incorporation of the two five-membered thiazole rings within both L<sup>d</sup> and L<sup>e</sup>, the nitrogen atoms within these rings cannot chelate the same metal ion therefore the ligand naturally partitions into separate binding domains. Such principles can be used to “design” ligands which will form particular assemblies with certain metal ions.

This thesis presents three chapters which use novel pyridyl-thiazole ligands to create a variety of functional metallosupramolecular complexes. In Chapter 2, two ligands (L<sup>1</sup> and L<sup>2</sup>) are appended with pyrene moieties whose luminescence properties are used to probe solution state conformations of the complexes formed on reaction of the ligands with transition metals.<sup>34</sup> Chapter 3 describes synthesis of ligands L<sup>3</sup> and L<sup>4</sup>, which are capable of binding anions, and their resultant complexes with a series of transition metal salts. In Chapter 4, the coordination behaviour of ligand L<sup>5</sup>, which contains a 3,3'-diamino-2,2'-bipyridyl moiety, is examined and is subsequently modified allosterically by reaction of the amino groups with cyclohexanone.

## 1.12 References

1. Steed, J. W., Turner, D. R., Wallace, K. J., (2007). *Core Concepts in Supramolecular Chemistry and Nanochemistry*. Chichester: John Wiley & Sons.
2. Pedersen, C. J., Cyclic Polyethers and Their Complexes with Metal Salts, *J. Am. Chem. Soc.*, 1967, **89**, 7017-7036.
3. Lehn, J. M., Cryptates: The Chemistry of Macropolycyclic Inclusion Complexes, *Am. Chem. Rev.*, 1978, **11**, 49-57.
4. Cram, D. J., The Design of Molecular Hosts, Guests, and Their Complexes (Nobel Lectures), *Angew. Chem.*, 1988, **27**, 1009-1112.
5. Steed, J. W. & Atwood, J. L., (2000). *Supramolecular Chemistry*. Chichester: John Wiley & Sons.
6. Beer, P. D., Gale, P. A., Smith, D. K., (1999). *Supramolecular Chemistry*. New York: Oxford University Press Inc.
7. Lehn, J. M., From Matter to Life: Chemistry?!, *Resonance*, 1996, **1**, 39-53.
8. Basolo, F., Johnson, R.C., (1986). *Coordination Chemistry*. Northwood: Science Reviews.
9. Graddon, D. P. (1968). *An Introduction to Co-ordination Chemistry*. 2<sup>nd</sup> ed. Oxford: D. R. Hillman & Sons Ltd.
10. Kauffman, G. B., "Quinquevalent" Nitrogen and the Structure of Ammonium Salts: Contributions of Alfred Werner and Others, *Isis*, 1973, **64**, 78-95.
11. Ramberg, P. J. (2003). Chemical Structure, Spatial Arrangement: The Early History of Stereochemistry, 1874-1914. Google [online]. Available at: <<http://books.google.co.uk/bkshp?hl=en&tab=wp>> [Accessed 1<sup>st</sup> February 2011].

12. Bowman-James, K. Alfred Werner Revisited: The Coordination Chemistry of Anions, *Acc. Chem. Res.*, 2005, **38**, 671-678.
13. Dobraza, R., Würthner, F., Metallosupramolecular Approach Toward Functional Coordination Polymers, *J. Poly. Chem.*, 2005, **43**, 4981-4995.
14. Constable, E. C., Novel Oligopyridines for Metallosupramolecular Chemistry, *Pure & Appl. Chem.*, 1996, **68**, 253-260.
15. Steel, P. J., Ligand Design in Multimetallic Architectures: Six Lessons Learned, *Acc. Chem. Res.*, 2005, **38**, 243-250.
16. Ziener, U., Breuning, E., Lehn, J. M., Wegelius, E., Rissanen, K., Baum, G., Fenske, D., Vaughan, G., Recognition-Directed Supramolecular Assemblies of Metal Complexes of Terpyridine Derived Ligands with Self-Complementary Hydrogen Bonding Sites, *Chem. Eur. J.*, 2000, **6**, 4132-4139.
17. Lehn, J. M., Ziessel, R., Polybipyridine Ligands Derived from Acyclic and Macrocyclic Polyamines; Synthesis and Metal Binding Studies, *J. Chem. Soc., Chem. Commun.*, 1987, 1292-1294.
18. Lehn, J. M., (1995). *Supramolecular Chemistry. Concepts and Perspectives.* Weinheim: VCH.
19. Rice, C. R., Wörl, S., Jeffery, J. C., Paul, R. L., Ward, M. D., New Multidentate Ligands for Supramolecular Coordination Chemistry: Double and Triple Helical Complexes of Ligands Containing Pyridyl and Thiazoyl Donor Units, *J. Chem. Soc., Dalton Trans.*, 2001, 550-559.
20. Piguet, C., Bernardinelli, G., Hopfgartner, G., *Chem. Rev.*, 1997, **97**, 2005; Constable, E. C., *Polynuclear Transition Metal Helicates*, vol. 9, *Comprehensive Supramolecular Chemistry*, editor: Sauvage, J. P., Elsevier, Oxford, 1996, 213-252.

21. Lehn, J. M., Rigault, A., Siegel, J., Harrowfield, J., Chevrier, B., Moras, D., Spontaneous Assembly of Double-Stranded Helicates from Oligobipyridine Ligands and Copper(I) Cations: Structure of an Inorganic Double Helix, *Proc. Natl. Acad. Sci.*, 1987, **84**, 2565-2569.
22. Machado, V. G., Baxter, P. N., Lehn, J. M., Self-Assembly in Self-Organized Inorganic Systems: A View of Programmed Metallosupramolecular Architectures, *J. Braz. Chem. Soc.*, 2001, **12**, 431-462.
23. Baylies, C. J., Harding, L. P., Jeffery, J. C., Moon, R., Rice, C. R., Riis-Johannessen, T., Electrostatic Control of the Formation of Heteroleptic Transition Metal Helicates, *New. J. Chem.*, 2007, **31**, 1525-1529.
24. Greenwald, M., Wessely, D., Katz, E., Willner, I., Cohen, Y., From Homoleptic Double to Heteroleptic Stranded Copper(I) Helicates: The Role of Self-Recognition in Self-Assembly Processes, *J. Org. Chem.*, 2000, **65**, 1050-1058.
25. Piguet, C., Bernardinelli, G., Bocquet, B., Quattropiani, A., Williams, A. F., Self-Assembly of Double and Triple Helices Controlled by Metal Ion Stereochemical Preference, *J. Am. Chem. Soc.*, 1992, **114**, 7440-7451.
26. Baum, G., Constable, E. C., Fenske, D., Housecroft, C. E., Kulke, T., Stereoselective Double Helicate Assembly from Chiral 2,2':6',2'':6'',2'''-Quaterpyridines and Tetrahedral Metal Centres, *Chem. Eur. J.*, 1999, **5**, 1862-1873.
27. Shaul, M., Cohen, Y., Novel Phenanthroline-Containing Trinuclear Double-Stranded Helicates: Self-Recognition between Helicates with Phenanthroline and Bipyridine Binding Sites, *J. Org. Chem.*, 1999, **64**, 9358-9364.
28. Rice, C. R., Baylies, C. J., Harding, L. P., Jeffery, J. C., Paul, R. L., Ward, M. D., Pyridyl-thiazole Multidentate Ligands: Metal-specific Recognition of a Combination of Ligands from a Mixture, *J. Chem. Soc., Dalton Trans.*, 2001, 3039-3044.

29. Rice, C. R., Wörl, S., Jeffery, J. C., Paul, R. L., Ward, M. D., Pyridyl-Thiazoles as a New Class of Ligand for Metallosupramolecular Chemistry: Formation of Double and Triple Helicates with Cu(II), *Chem. Commun.*, 2000, 1529-1530.
30. Gavrilova, A. L., Bosnich, B., Principles of Mononucleating and Binucleating Ligand Design, *Chem. Rev.*, 2004, **104**, 349-383.
31. Teng, P. F., Tsang, C. S., Yeung, H. L., Wong, W. L., Kwong, H. L., Williams, I. D., New Chiral Bidentate Ligands Containing Thiazolyl and Pyridyl Donors for Copper-Catalyzed Asymmetric Allylic Oxidation of Cyclohexene, *Journal of Organometallic Chemistry*, 2006, **691**, 2237-2244.
32. Bullock, S., Gillie, L. J., Harding, L. P., Rice, C. R., Riis-Johannessen, T., Whitehead, M., Isomeric Pyridyl-Thiazole Donor Units for Metal Ion Recognition in Bi- and Tri-Metallic Helicates, *Chem. Commun.*, 2009, 4856-4858.
33. Rice, C. R., Baylies, C. J., Harding, L. P., Jeffery, J. C., Paul, R. L., Ward, M. D., Cadmium-containing Pyridyl-Thiazole Complexes: Crystal Structures and Solution Behaviour of Mononuclear, Dinuclear Double Helicate and Dinuclear Triple Helicate Complexes, *Polyhedron*, 2003, **22**, 755-762.
34. Cox, N. M., Harding, L. P., Jones, J. E., Pope, S. J. A., Rice, C. R., Adams, H., Probing Solution Behaviour of Metallosupramolecular Complexes using Pyrene Fluorescence, *J. Chem. Soc., Dalton Trans.*, 2012, **41**, 1568-1573.

## Chapter 2 Using Pyrene Fluorescence to Elucidate Supramolecular Structures in Solution

### 2.1 Introduction

The main focus of this chapter involves the use of pyrene fluorescence to elucidate supramolecular structures in solution. As stated earlier, metallosupramolecular chemistry is a sub-division of supramolecular chemistry involving spontaneous self-assembly of metal ions with ligands through coordinate bonds. Usually, N-donor heterocyclic ligands are reacted with transition metal ions which prefer either octahedral or tetrahedral coordination geometry which in turn gives rise to many interesting self-assembled architectures.

With luminescence being a sensitive and easy way of retrieving chemical information, fluorescent sensing is a popular technique due to the fact that it has excellent sensitivity, gives a rapid response and is a non-destructive technique. Previous work in the fields of both chemical and biological science has shown how pyrene has been used with numerous complexes towards the development of fluorescent probes and chemosensors.<sup>1-6</sup>

Luminescence can be defined as the generation of light without heat. For something to be described as luminescent it will undergo a process where it absorbs electromagnetic radiation then re-emits electromagnetic radiation at a different wavelength.<sup>7</sup> There are two types of luminescence: fluorescence and phosphorescence. The difference between these two is the spin state of the electron upon promotion to the excited state.<sup>7</sup> With fluorescence, the spin state of the electron does not change but with phosphorescence the spin state of the electron does change as it undergoes an intersystem crossing so the electron will go from a singlet state to the triplet state, as shown in Figure 2.1.

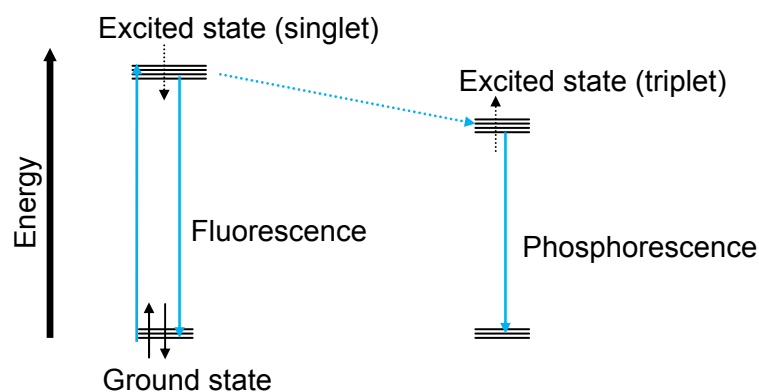


**Figure 2.1:** A simplified Jablonski diagram illustrating the electronic states of a molecule and the transitions between them, indicating fluorescence and phosphorescence

The absorption of UV radiation by a molecule will excite the molecule from a vibrational level which is in the electronic ground state to one of numerous vibrational levels in the electronic excited state. This excited state is usually the first excited singlet state and once a molecule arrives at the lowest vibrational level of an excited singlet state a number of things can happen. Fluorescence will occur when the excited singlet state of a molecule returns to the ground state by photon emission. The spin state of an excited electron can also be reversed. This leaves the molecule in an excited triplet state which is known as intersystem crossing (ISC). The triplet state is of a lower electronic energy than that of the excited singlet state and therefore with phosphorescence, the lifetime of the excited 'triplet' state will last longer in comparison to that of the lifetime of the excited singlet state in fluorescence. Phosphorescence transitions are easily distinguished from fluorescence as they occur much more slowly. Fluorescence occurs over time scales of  $10^{-6} - 10^{-9}$  seconds while phosphorescence occurs over time scales of seconds to hours.

Luminescence has various applications in sensing ranging from environmental to chemical and biological applications. Molecular sensors are an area of particular interest for chemists especially towards the identification of molecular substances and how they actually occur in tissues and cells.<sup>7</sup> Optical sensors are the most suitable type of sensors for use in biological systems as the physical output is relatively easy to interpret. The most common type of optical sensor is a fluorescent sensor, which contains a fluorophore (fluorescent unit) and a binding site.<sup>8</sup> For the sensor to work, there has to be efficient coupling between both the binding site and the fluorophore for the sensor to detect the presence of the bound guest, and therefore the fluorescent sensors will give a physical output in the form of light.

Pyrene is a polycyclic aromatic hydrocarbon that consists of four benzene rings which are fused together giving a planar aromatic system (Figure 2.2).

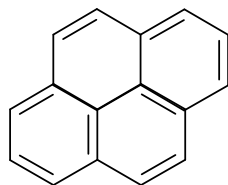


**Figure 2.2:** Pyrene

Pyrene was first isolated from coal tar in 1837 from the revolutionary work of French chemist Auguste Laurent.<sup>9</sup> Since then, pyrene has been the subject of immense investigations and is still the chromophore of choice in a variety of scientific areas.<sup>9</sup> Some characteristics of pyrene and its many derivatives include easy derivatisation and versatile redox properties. However, the most interesting property of pyrene is its photophysical behaviour as it is a highly emissive species with a long-lived excited state in deoxygenated solvents and this emission is very sensitive to its chemical environment. As a single species, excitation of pyrene at 350 nm results in emission at 390 nm which possesses a short luminescence lifetime. However, if two pyrenes come into close proximity to one another due to  $\pi$ - $\pi$  stacking then energy can be transmitted from one pyrene to another and the emission changes from 390 nm for the monomer to 480 nm for the dimer (Figure 2.3).<sup>10</sup> When such a short lived dimeric molecule is formed from two species with at least one of the molecules in an electronic excited state, the resultant species is termed an excimer.<sup>11</sup> As a result, the luminescent emission of pyrene can be used to study the proximity of one pyrene to another and correspondingly it is proposed that adding pyrene moieties to ligands can be used to probe self-assemblies in solution (Figure 2.4).<sup>12</sup>

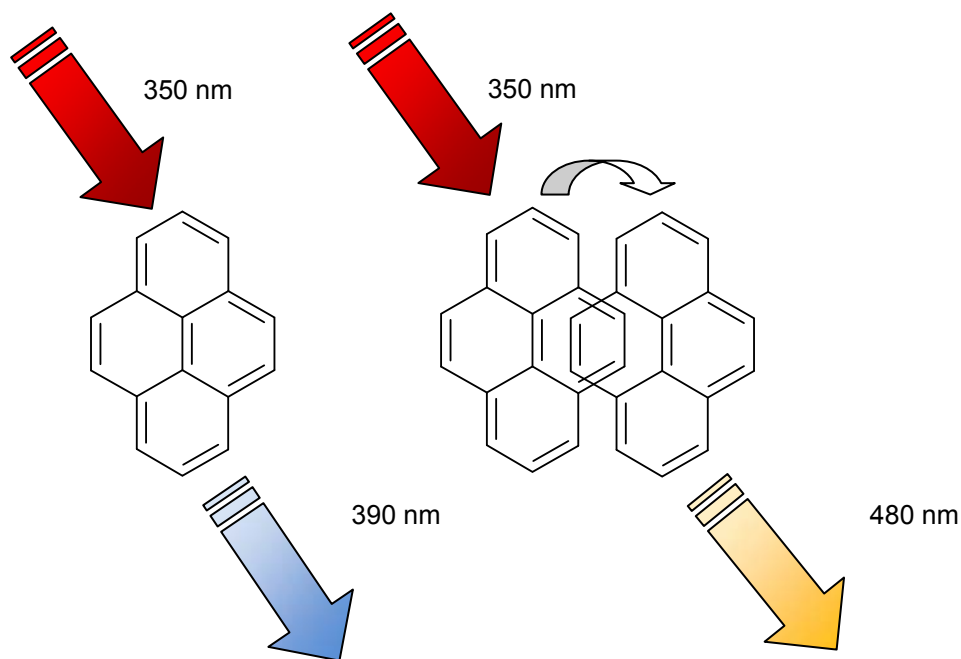


**Figure 2.3:** Illustration of pyrene showing short lifetime monomer emission at 390 nm and long lifetime excimer emission at 480 nm

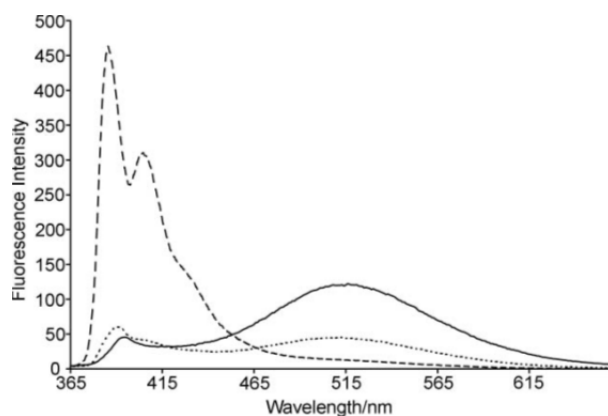


**Figure 2.4:** Typical fluorescence spectra of pyrene-containing species showing monomer emission (at 390 nm) and excimer emission (at 515 nm) profiles<sup>12</sup>

The formation of self-assembled supramolecular structures has received much attention in recent years and the generation of large assemblies in the solid state is well understood.<sup>11</sup> However, studying the formation of these self-assemblies in solution is much more difficult. Mass spectrometry and NMR techniques such as NOESY and DOSY can be helpful in solution state determination but these techniques can be time consuming, difficult to interpret and often can only be applied retrospectively.<sup>13</sup> As a result they can confirm that the solution behaviour of an

assembly is the same as the structurally characterised species, but often cannot be used to ascertain structures without single crystal data.

Pyrene has been used extensively for sensing applications, ranging from work involving polysaccharides<sup>14</sup> and sugars<sup>12,15,16</sup>, to metal detection<sup>1,17,18</sup> both in and out of the body. Successful fluorescent sensors usually include the following important factors: the fluorophore, a binding recognition unit and a signal conducting system (Figure 2.5).

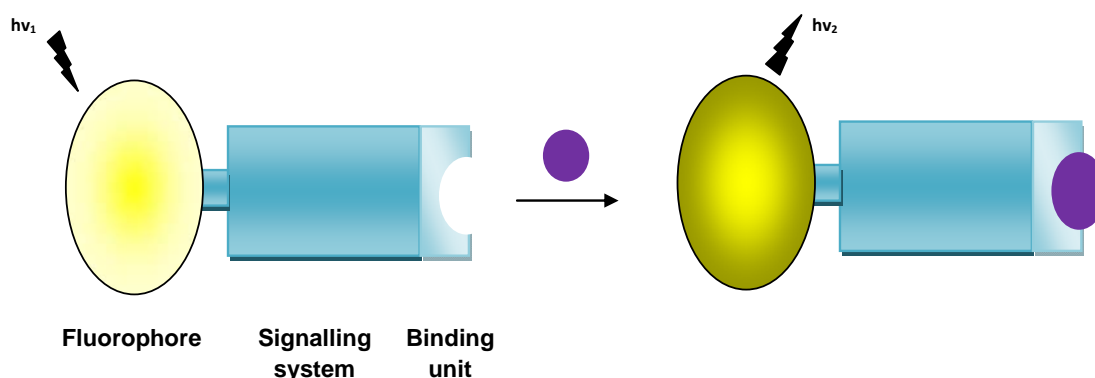


**Figure 2.5:** Diagram showing the fluorophore unit emission when the binding recognition unit is unoccupied and a change in luminescence when a guest is coordinated in the binding recognition unit

Pyrene is one of the most useful fluorogenic units, this is mainly due to the fact that it emits not only from the monomer but from the excimer also; additionally, the ratio between the monomer and excimer emission is a sensitive probe for conformational change.<sup>1,17</sup>

Carlsson *et al.* researched the unfolding of the protein human carbonic anhydrase II when under denaturing conditions using a pyrene-appended version of the protein.<sup>19</sup> The overall shape of this protein is ellipsoidal; the upper half of the structure contains the active site and the N-terminal region, and the lower half contains a large hydrophobic core. This hydrophobic core is the main reason behind this research group's investigations, due to the fact that it has been shown that this protein is very resistant to unfolding even under strongly denaturing conditions.<sup>20,21</sup> The protein has been examined by conventional optical methods and has been reported to be completely unfolded, however, residual structures have been detected by employing different techniques such as NMR spectrometry. Therefore, pyrenyl fluorophores were attached to specific sections of the protein in order to study the conformational changes in the unfolded state. Once the pyrene moieties had been attached to the

protein, various concentrations of guanidinium hydrochloride (GuHCl) were added and the monomer and excimer emission intensities were recorded (Figure 2.6).

Initially, mainly excimer fluorescence was detected but as the concentration of GuHCl was increased the protein began to unfold, making the pyrene groups more distant from each other, and monomer emission became predominant. Thus, it was shown that this method of using pyrene to probe protein unfolding provided structural information which complemented the information gained by chemical reactivity measurements and the use of single spectroscopic probes.

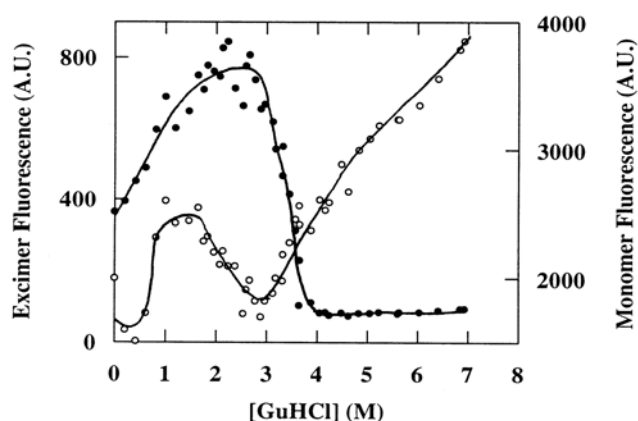


**Figure 2.6:** Unfolding transition curves for pyrene-attached human carbonic anhydrase II as monitored by pyrene fluorescence. Monomer fluorescence intensity (o) recorded at 379 nm and excimer fluorescence intensity (●) recorded at 465 nm<sup>19</sup>

A recent paper published by Freeman *et al.* showed how pyrene was used as a fluorescent probe in conformational studies of the complex of *myo*-inositol 1,2,3-triphosphate with Fe<sup>3+</sup>.<sup>12</sup> In solution, the preferred conformation of the sugar is the penta-equatorial structure shown in Figure 2.7[a]; this conformation is more favourable in energy than that of the penta-axial conformer (Figure 2.7[b]) due to the steric bulk of the phosphate groups.

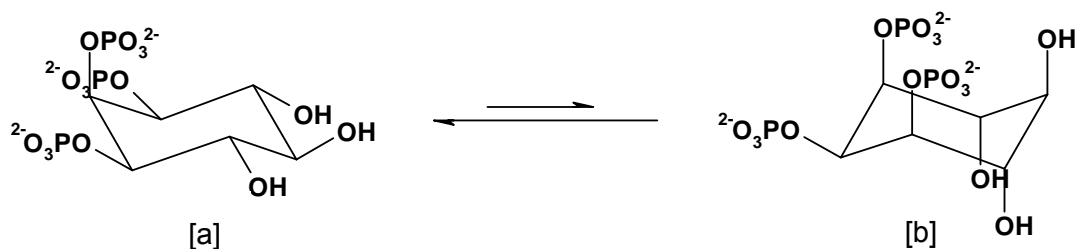


**Figure 2.7:** Penta-equatorial [a] and penta-axial [b] conformations of *myo*-inositol 1,2,3-triphosphate

These authors proposed the use of pyrene as a fluorescent probe to elucidate which conformation (penta-axial or penta-equatorial) was adopted on binding  $\text{Fe}^{3+}$  ions to the sugar. Pyrene was therefore appended onto the sugar and, as Freeman proposed, with the addition of  $\text{Fe}^{3+}$  it was shown that the complex adopts the less stable penta-axial conformation (Figure 2.8). This causes the two pyrene units to come into close proximity and an excimer is formed.

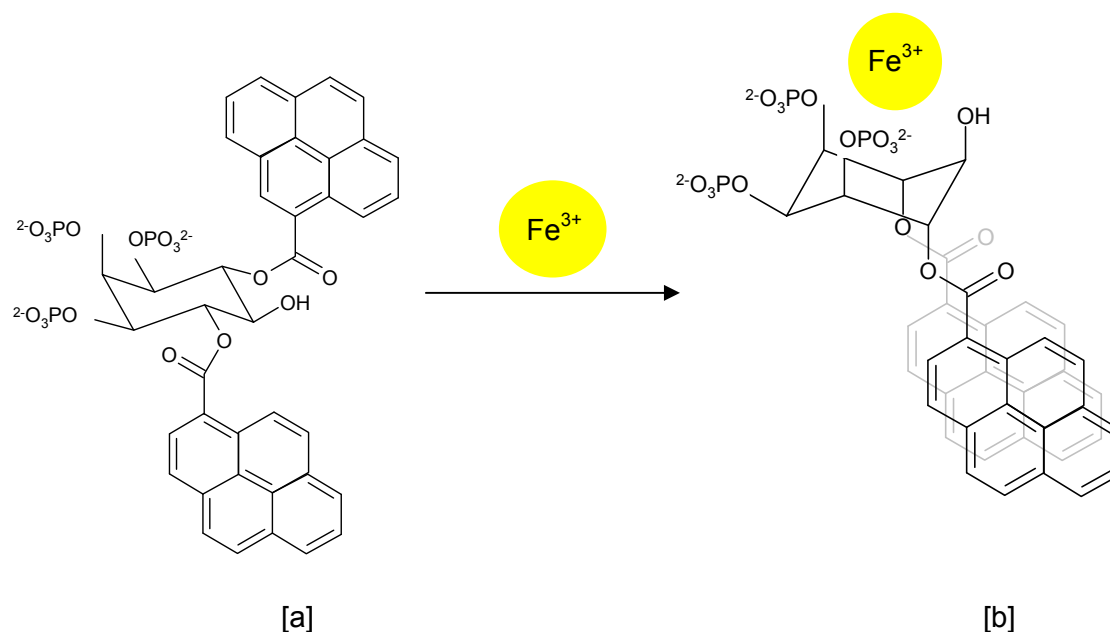


**Figure 2.8:** The proposed conformational change upon the addition of  $\text{Fe}^{3+}$  causes the pyrene units to come into close proximity to one another<sup>12</sup>

Freeman's results showed that on analysis of the free sugar-pyrene complex (Figure 2.8[a]), blue fluorescence is observed at 386 nm. This is credited to the locally excited state of the pyrene monomer. However, when the sugar is complexed with  $\text{Fe}^{3+}$  the emission changes substantially and an emission is now noted at 510 nm (green fluorescence). This is due to excimer emission as a result of the two pyrene groups being in close proximity to one another.

Within chemistry, there are far fewer examples of the use of synthetic pyrene appended systems. The majority of these systems are used as sensors with conformational changes induced on binding the target analyte causing either increased or decreased excimer emission from the pyrene groups.

Cao *et al.* report a pyrene-based fluorescent sensor for the detection of  $\text{Hg}^{2+}$  ions.<sup>17</sup> Within the body, mercury is of great interest among researchers and the need to develop rapid detection methods for mercury with a high sensitivity has received tremendous attention throughout the years.<sup>22</sup> Fluorescent sensors have proven to be a

very powerful tool towards monitoring  $\text{Hg}^{2+}$ .<sup>23-25</sup> One of the major problems within these sensors is that they have poor solubility; Cao's paper has shown that the incorporation of indolium to a pyrene based mercury(II) sensor (PMS) (Figure 2.9) has enhanced the solubility of the sensor in aqueous solutions.

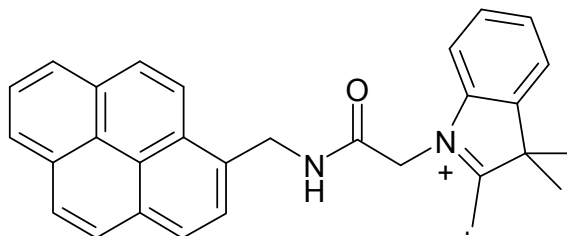


**Figure 2.9:** Pyrene-based mercury(II) sensor (PMS)<sup>17</sup>

Reaction of PMS with various metal ions showed no change in the absorption spectrum compared to the free ligand, however, upon the continuous addition of  $\text{Hg}^{2+}$ , the emission spectrum was gradually quenched with no wavelength shift and the emission spectrum showed peaks which were typical for pyrene monomeric emission. The formation of the complex of PMS with  $\text{Hg}^{2+}$  could lead to two pyrene units closely approaching each other to give an intermolecular ground-state dimer however this was not observed indicating that the orientation of the two pyrene moieties meant that they did not undergo sufficient  $\pi$ - $\pi$  interaction for excimer formation (Figure 2.10).

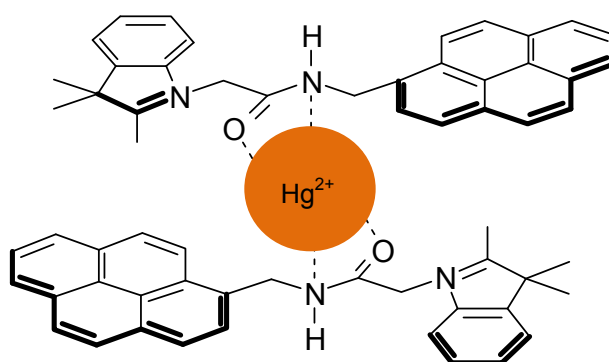


**Figure 2.10:** Complex formed by PMS and  $\text{Hg}^{2+}$  in a 2:1 ratio<sup>17</sup>

Another excellent example demonstrated by Chung *et al.* showed the dual-mode recognition of transition metal ions with bis-triazole-tethered pyrenes (Figure 2.11[a-e]).<sup>1</sup> This study was prompted by previous research showing how two pyrenyl moieties

connected by a series of polyoxyethylenes<sup>26</sup> or dioxaoctanediamides<sup>28</sup> had moderate to excellent selectivities towards  $\text{Ca}^{2+}$  and  $\text{Hg}^{2+}$  ions.

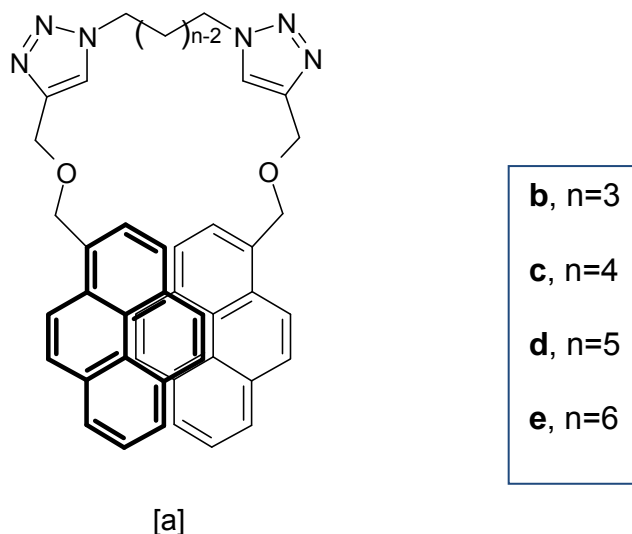


**Figure 2.11:** 1,*n*-Bispyrenyl-methoxymethyltriazole-alkanes [a-e]<sup>1</sup>

The main focus of Chung's work was to synthesise 1,*n*-bispyrenyl-methoxymethyltriazole-alkanes and to study their reversible conformational transformation in the presence of metal ions using the pyrene monomer and excimer emission as a probe. All ligands showed strong excimer emission around 482 nm and also weak signals due to monomer emission in the 370-400 nm region. Compound **e** showed differences in its emission profiles on complexation with different metal ions. Two metal-binding modes are proposed in which **e** coordinates  $\text{Pb}^{2+}$  and  $\text{Ni}^{2+}$  via the triazole nitrogens and the ether oxygens but coordinates  $\text{Cd}^{2+}$  and  $\text{Zn}^{2+}$  via the thiazole moieties alone. This leads to conformational differences in the complexes such that with  $\text{Pb}^{2+}$  and  $\text{Ni}^{2+}$  both the monomer and excimer emission are quenched, but with  $\text{Cd}^{2+}$  and  $\text{Zn}^{2+}$  separation of the pyrene moieties leads to quenching of the excimer emission but monomer emission is enhanced (Fig. 2.12).

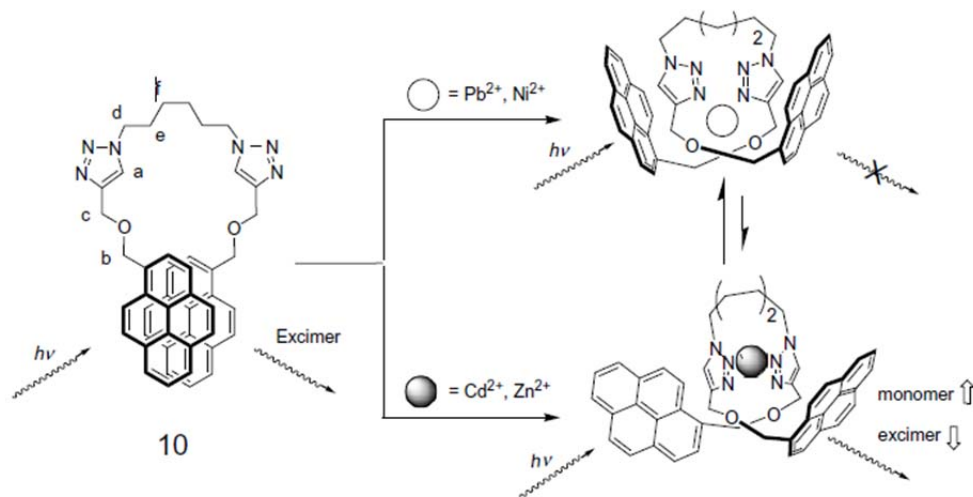


**Figure 2.12:** Alternative binding modes of compound e with different metal ions<sup>1</sup>

## 2.2 Aims

This chapter describes the synthesis of two potentially tetradentate N-donor ligands **L**<sup>1</sup> and **L**<sup>2</sup> and their coordination chemistry with transition metal ions. These ligands comprise a pyridyl-pyridyl-pyridyl-thiazole backbone (**L**<sup>1</sup>) and thiazole-pyridyl-pyridyl-thiazole backbone (**L**<sup>2</sup>). Each ligand has four nitrogen donor atoms which allow the backbone to act as a simple tetradentate donor or to partition into bis-bidentate binding domains. In order to probe solution state assemblies, each thiazole unit was appended with a pyrene group for use as a luminescent tag resulting in the mono-substituted ligand **L**<sup>1</sup> and the di-substituted ligand **L**<sup>2</sup> (Figure 2.13).

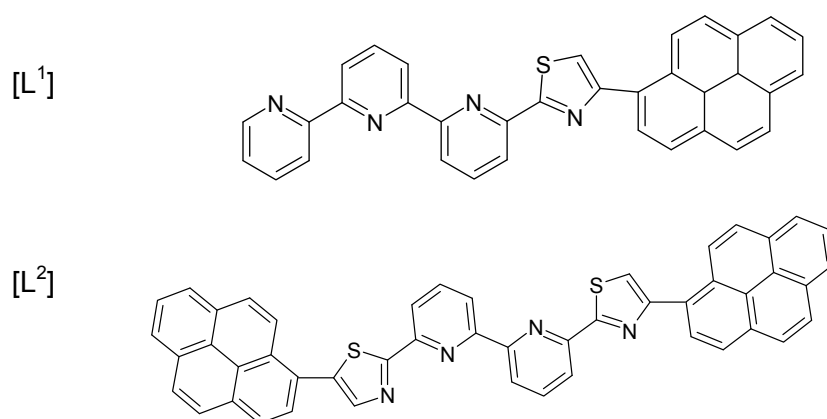


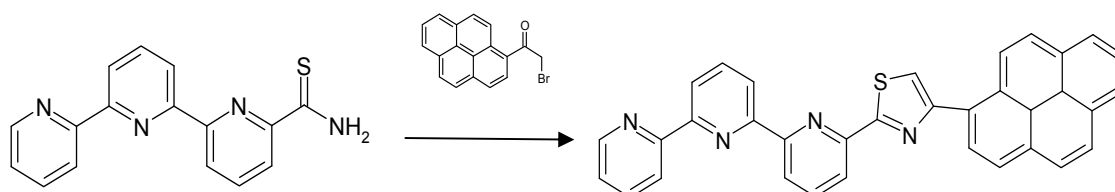
**Figure 2.13:** Ligands **L**<sup>1</sup> and **L**<sup>2</sup>

## 2.3 Experimental

### 2.3.1 Ligand Synthesis

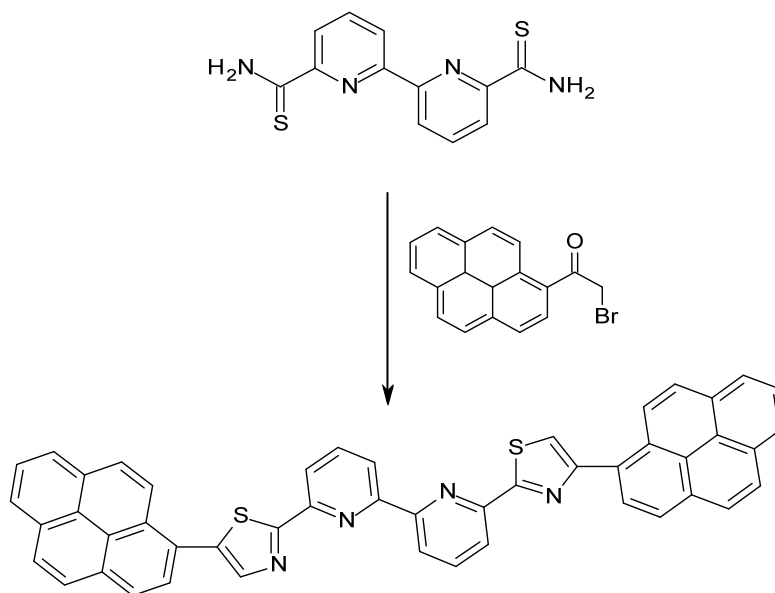
2,2'-Bipyridine-6,6'-dithioamide and 2,2':6',2''-terpyridine-6-thioamide were prepared according to literature methods.<sup>28-30</sup>

#### 2.3.1.1 Synthesis of L<sup>1</sup>



To a round bottom flask charged with 2,2':6',2''-terpyridine-6-thioamide (0.05 g, 0.17 mmol) and 1-(bromoacetyl)pyrene (0.06 g, 0.19 mmol) was added EtOH (20 mL) and the reaction was left to reflux for 12 hrs, after which time a yellow precipitate was formed. The precipitate was filtered and washed with EtOH (2 x 10 mL) and Et<sub>2</sub>O (2 x 10 mL). The yellow solid was suspended in NH<sub>3</sub> (aq) (10 mL, conc, 0.88 g) for 10 hrs. Filtration followed by washing with H<sub>2</sub>O (2 x 10 mL) and Et<sub>2</sub>O (2 x 10 mL) gave the ligand L<sup>1</sup> as a yellow solid (0.052 g, 65%).

### 2.3.1.2 Synthesis of L<sup>2</sup>



To a round bottom flask charged with 2,2'-bipyridine-6,6'-dithioamide (0.05 g, 0.2 mmol) and 1-(bromoacetyl)pyrene (0.129 g, 0.4 mmol) was added EtOH (50 mL) and the reaction was refluxed for 12 hrs, after which time a yellow precipitate formed. The precipitate was filtered and washed with EtOH (2 x 10 mL) and Et<sub>2</sub>O (2 x 10 mL) then suspended in NH<sub>3</sub> (aq) (10mL, conc, 0.88 sg) for 10 hrs. Filtration followed by washing with H<sub>2</sub>O (2 x 10 mL), EtOH (2 x 10 mL) and Et<sub>2</sub>O (2 x 10 mL) gave the ligand L<sup>2</sup> as a yellow solid (0.075 g, 58%).

### 2.3.2 Characterisation

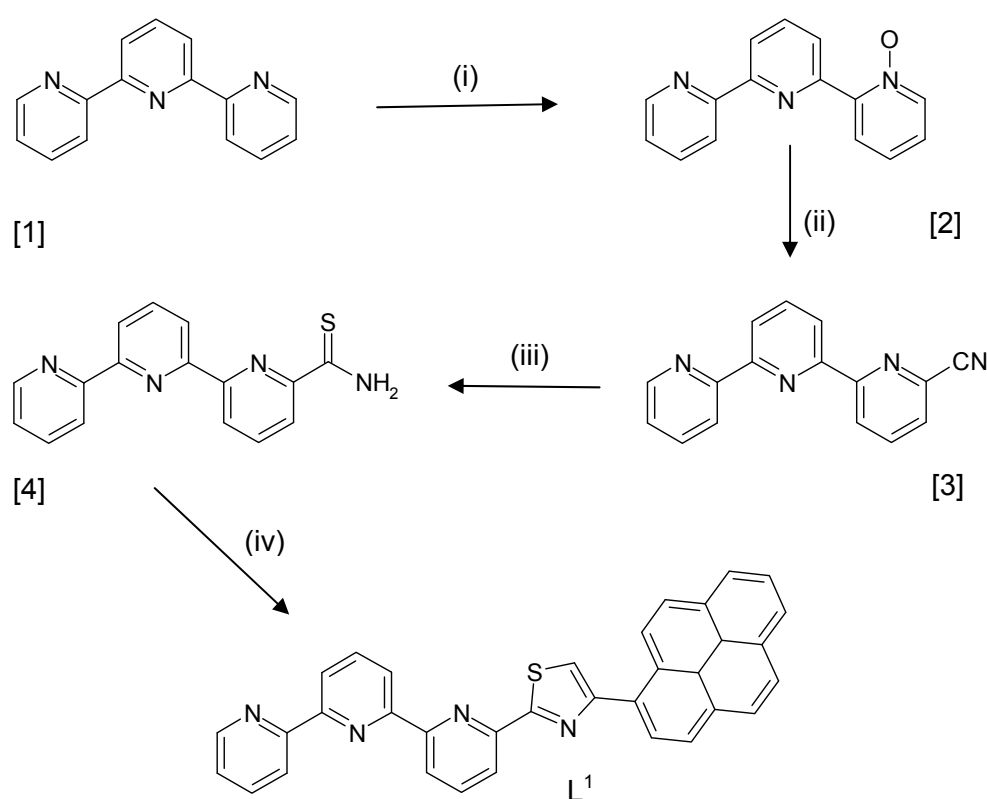
All photophysical data were obtained at the University of Cardiff on a JobinYvon-Horiba Fluorolog spectrometer fitted with a JY TBX picosecond photodetection module. Lifetimes were obtained using the provided deconvolution software DAS6. Electrospray ionisation mass spectra were recorded from 10<sup>-3</sup> M solutions on a Bruker MicrOTOF-q instrument. Assignments of ions from the mass spectra of the complexes were confirmed by comparison of the measured and calculated isotope patterns for each species. NMR spectra were recorded on a Bruker DPX400 MHz spectrometer. The ligands and complexes were, in some cases, poorly soluble leading to broad, unresolved peaks which were frequently coincident with other signals.

## 2.4 Results and Discussion

### 2.4.1 Ligand synthesis

The two potentially tetradentate ligands  $L^1$  and  $L^2$  were prepared by reaction of their corresponding thioamides (2,2':6'2''-terpyridine-6-thioamide for  $L^1$  and 2,2'-bipyridine-6,6'-dithioamide for  $L^2$ ) with 1-(bromoacetyl)pyrene according to literature methods.<sup>28-30</sup>

#### 2.4.1.1 Synthesis of $L^1$



**Scheme 2.1:** Synthesis of  $L^1$ . Reagents and conditions: (i) mCPBA, DCM, room temp (ii) Benzoyl chloride, TMS cyanide, reflux (iii) Triethylamine, ethanol,  $H_2S$  (iv) 1-(bromoacetyl)pyrene, reflux

The synthesis of  $L^1$  is outlined in Scheme 1.1. To a solution of 2,2':6'2''-terpyridine in DCM was added mCPBA and the reaction stirred at room temperature. The reaction was monitored using TLC and on completion the 2,2':6'2''-terpyridine-1-N-oxide product **[2]** was isolated as a white solid *via* column chromatography and gave an NMR spectrum (Figure 2.14), which is consistent with previously reported data.<sup>26</sup>

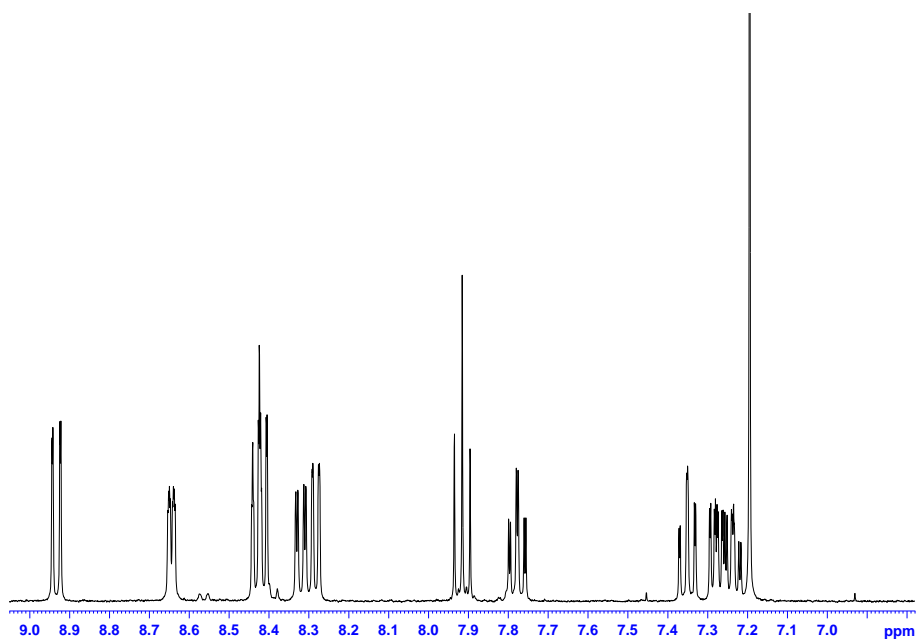


**Figure 2.14:** Aromatic region of the  $^1\text{H}$  NMR ( $\text{d}_6\text{-DMSO}$ ) spectrum of [2]

If 2,2':6',2''-terpyridine had not oxidised at all, then the amount of signals present in the NMR spectrum would be considerably less than that shown in Figure 2.13 due to the compound being symmetrical. If 2,2':6',2''-terpyridine had fully oxidised to form the bis-N-oxide, again the amount of signals expected would be the same as when the oxidation did not take place. The mono-N-oxide species, however, is unsymmetrical and accounts for the more complex NMR spectrum shown in Fig. 2.14.

Addition of a nitrile group to the 6-position of the terminal pyridine group was achieved by reaction of [2] with benzoyl chloride and trimethylsilylcyanide in DCM under reflux. Confirmation of the 6-nitrile derivative [3] was given by  $^1\text{H}$  NMR (Figure 2.15), which showed 10 aromatic signals, again due to the complex being unsymmetrical.

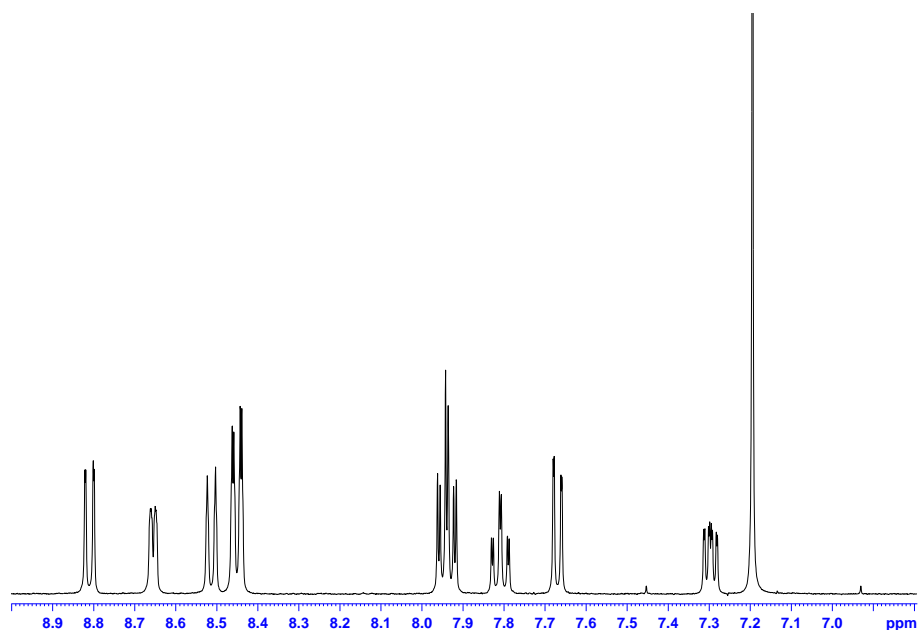


**Figure 2.15:** Aromatic region of the  $^1\text{H}$  NMR ( $\text{d}_6$ -DMSO) spectrum of [3]

Reaction with  $\text{H}_2\text{S}$  in EtOH gave the 6-thioamide [4] with two broad signals at low field in the  $^1\text{H}$  NMR spectrum which are characteristic of this functional group (Figure 2.16).

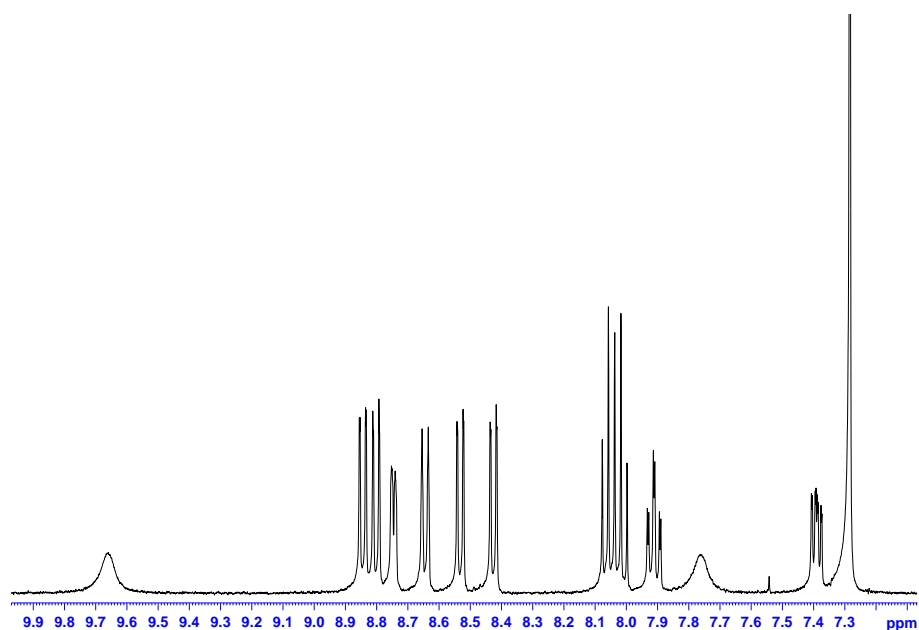


**Figure 2.16:** Aromatic region of the  $^1\text{H}$  NMR ( $\text{d}_6$ -DMSO) spectrum of [4]

Reaction of 2,2':6',2''-terpyridine-6-thioamide in EtOH with a slight excess of 1-(bromoacetyl)pyrene gave a yellow precipitate which was isolated by filtration and neutralized with concentrated ammonia. This ligand gave a total of 19 aromatic signals

in the  $^1\text{H}$  NMR consistent with the successful formation of  $\text{L}^1$  (Figure 2.17), despite numerous solubility problems encountered with this ligand, even in DMSO.

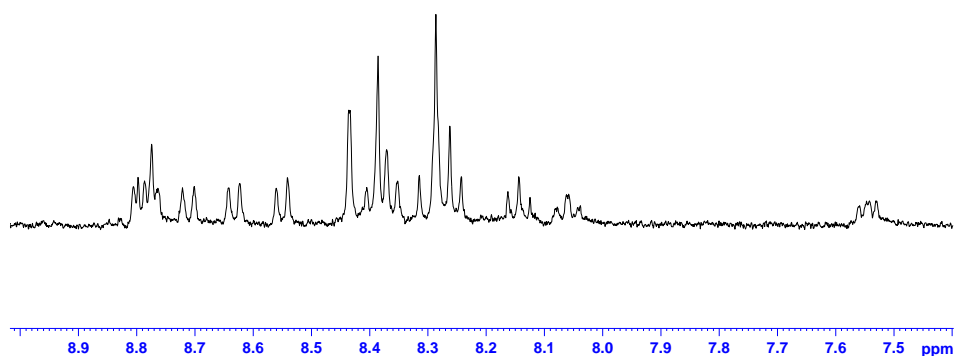
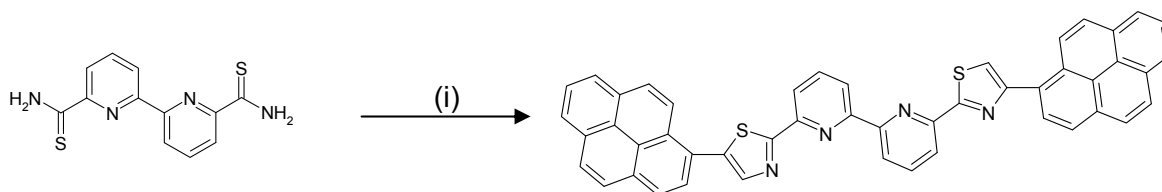


**Figure 2.17:** Aromatic region of the  $^1\text{H}$  NMR ( $d_6$ -DMSO) spectrum of  $\text{L}^1$

#### 2.4.1.2 Synthesis of $\text{L}^2$



**Scheme 2.2:** Reagents and conditions: (i) 1-(bromoacetyl)pyrene, EtOH, reflux

$\text{L}^2$  was prepared by reaction of 2,2'-bipyridine-6,6'-dithioamide with 1-(bromoacetyl)pyrene in ethanol under reflux for 12 hours, as shown in Scheme 1.2. The resulting yellow precipitate was filtered, washed with ethanol and diethyl ether and neutralised using aqueous ammonia. The yellow solid product was recovered by filtration and washed with ethanol and diethyl ether.

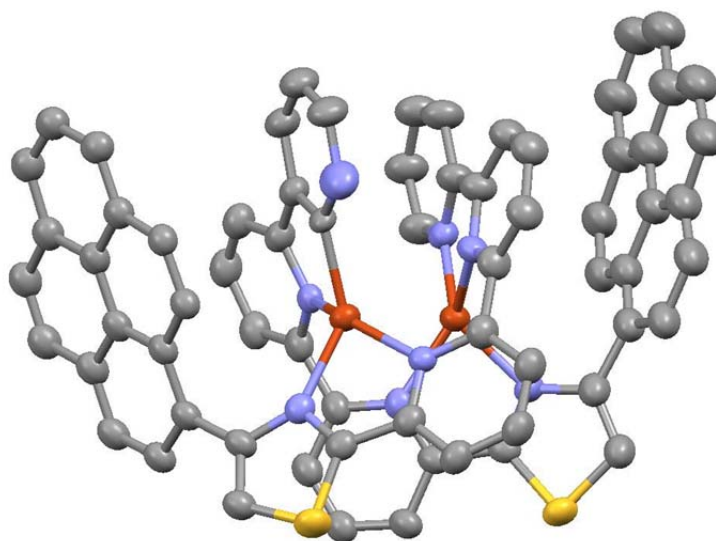
The poor solubility of  $\text{L}^2$  prevented characterisation by  $^1\text{H}$  NMR and even at  $70^\circ\text{C}$  in  $d_6$ -DMSO no peaks could be observed in the spectrum. However, mass spectrometry characterisation was carried out using a product ion scan of its cadmium complex. An ion was observed in the product ion spectrum at  $m/z$  723.1 corresponding to  $[\text{L}^2+\text{H}]^+$ ; accurate mass measurement of this ion confirmed the product had the correct molecular formula.

## 2.4.2 Coordination Chemistry of $L^1$

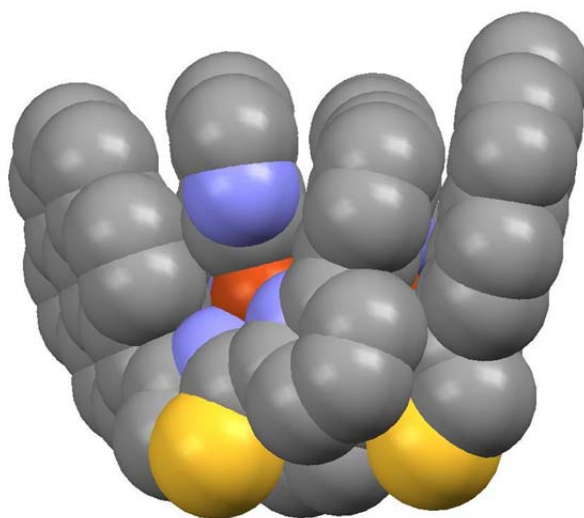
### 2.4.2.1 Reaction of $L^1$ with copper(I)

The reaction of  $L^1$  with one equivalent of  $[Cu(MeCN)_4]PF_6$  in the presence of excess tetraethylammonium perchlorate produced a red solution, from which slow diffusion of ethyl acetate afforded red crystals from the resulting red solution. Single crystal X-ray analysis showed the formation of a dinuclear double helicate species  $[Cu_2(L^1)_2](PF_6)_2$ , in the solid state (Figure 2.18).

(a)



(b)



(c)

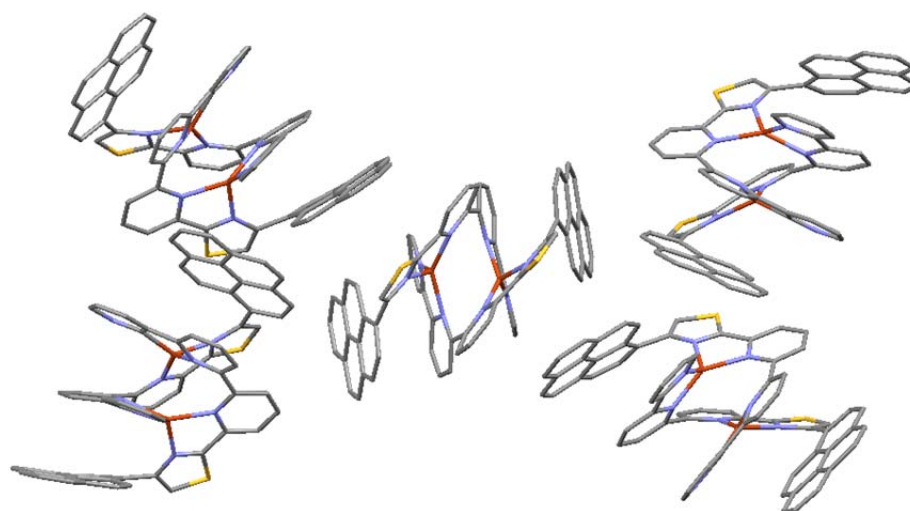


**Figure 2.18:** Single crystal X-ray structure of [Cu<sub>2</sub>(L<sup>1</sup>)<sub>2</sub>](PF<sub>6</sub>)<sub>2</sub>: (a) as a displacement ellipsoid plot drawn at the 50% probability level; (b) as a space-filling model; (c) showing the molecular packing in the unit cell (counter ions omitted for clarity)

The crystal structure of the complex cation of  $[\text{Cu}_2(\text{L}^1)_2](\text{PF}_6)_2$  shows how the ligand partitions into two bidentate nitrogen donor domains. Each copper ion is coordinated by two of the bidentate domains, one from each ligand (Figure 2.18a). The copper(I) centre has assumed a distorted tetrahedral geometry (Cu-N distances 1.98-2.104 Å), as shown in Table 2.1. As the ligand is unsymmetrical it can be considered as having a head (i.e. the terminal pyridyl-pyridyl unit) and a tail (i.e. pyridyl-thiazole unit, with the appended pyrene group). In the solid state there is only one species present i.e. the head-to-tail isomer, with each of the copper ions coordinated by both a pyridyl-pyridyl and a pyridyl-thiazole donor unit. The driving force for this is probably the pyrene units which adopt an arrangement such that they are far apart minimising unfavourable steric interactions; the interstrand centroid...centroid distance is 11.138 Å. However, other interactions, such as  $\pi$ -stacking between the pyrene and the pyridyl-pyridyl donor unit, or the electronic preference of the metal centres (i.e. each copper ion is coordinated in an identical manner) cannot be completely discounted.

Examination of the extended molecular packing (Fig. 2.18(c)) shows that each of the pyrene units in adjacent molecules aligns in an edge-to-face manner. The intermolecular distances are relatively long, with the average of the four shortest centroid...centroid separations being 6.591 Å.

Selected bond angles are shown in Table 2.2.

Bond	Bond length (Å)
Cu(1)-Cu(2)	2.9153(13)
Cu(1)-N(1)	2.056(7)
Cu(1)-N(3)	2.106(7)
Cu(1)-N(4)	2.073(7)
Cu(1)-N(5)	2.010(4)
Cu(2)-N(2)	2.069(6)
Cu(2)-N(6)	1.987(7)
Cu(2)-N(7)	2.070(6)
Cu(2)-N(10)	2.058(7)
Cu(3)-Cu(3)	2.909(2)
Cu(3)-N(8)	2.054(8)
Cu(3)-N(9)	2.082(8)
Cu(3)-N(11)	2.078(5)
Cu(3)-N(12)	1.983(9)

**Table 2.1:** Selected bond lengths (Å) for the complex cation  $[\text{Cu}_2(\text{L}^1)_2]^{2+}$

Bond	Bond angle (°)	Bond	Bond angle (°)
N(1)-Cu(1)-N(3)	80.7(3)	N(6)-Cu(2)-N(10)	135.8(3)
N(1)-Cu(1)-N(4)	143.3(2)	N(10)-Cu(2)-N(2)	81.3(2)
N(4)-Cu(1)-N(3)	105.4(3)	N(10)-Cu(2)-N(7)	104.5(3)
N(5)-Cu(1)-N(1)	121.1(2)	N(8)-Cu(3)-N(9)	79.7(3)
N(5)-Cu(1)-N(3)	135.5(2)	N(8)-Cu(3)-N(11)	107.2(3)
N(5)-Cu(1)-N(4)	80.1(2)	N(9)-Cu(3)-N(11)	141.9(3)
N(2)-Cu(2)-N(7)	139.9(2)	N(12)-Cu(3)-N(8)	136.5(3)
N(6)-Cu(2)-N(2)	121.9(3)	N(12)-Cu(3)-N(9)	121.3(3)
N(6)-Cu(2)-N(7)	81.7(3)	N(12)-Cu(3)-N(11)	80.0(3)

**Table 2.2:** Selected bond angles (°) for the complex cation  $[\text{Cu}_2(\text{L}^1)_2]^{2+}$

The formation of the dinuclear double helicate species  $[\text{Cu}_2(\text{L}^1)_2]^{2+}$  was also observed in the solution state with an ion observed in the ESI-MS at  $m/z$  1305.1 corresponding to  $\{[\text{Cu}_2(\text{L}^1)_2](\text{PF}_6)\}^+$ . The  $^1\text{H}$  NMR spectrum (Figure 2.19), was consistent with the formation of the complex  $[\text{Cu}_2(\text{L}^1)_2]^{2+}$ , as up to 40 proton aromatic signals could be expected for this complex. The spectrum showed that major and minor components were present which is consistent with formation of the head-to-tail and head-to-head isomers in solution. However, in light of the results in the solid state it seems likely that the major component is the head-to-tail double helicate.

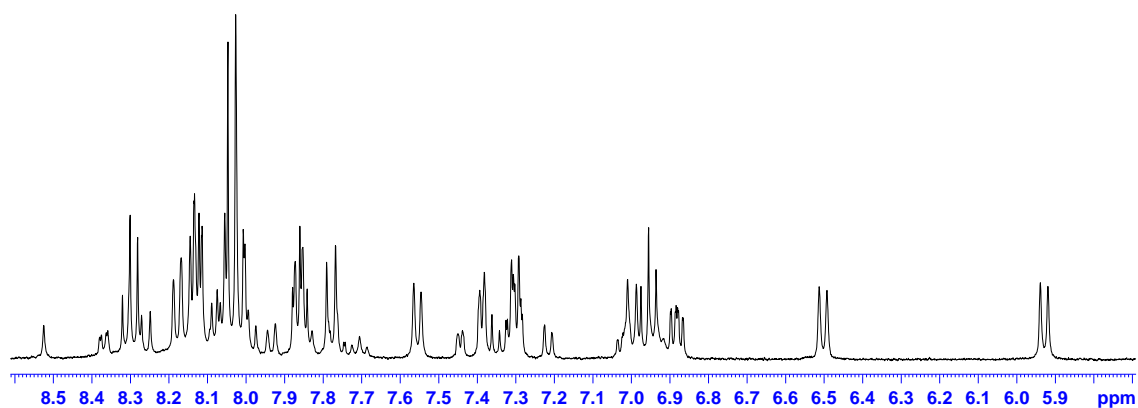


**Figure 2.19:** Aromatic region of the  $^1\text{H}$  NMR ( $d_6$ -DMSO) of the complex  $[\text{Cu}_2(\text{L}^1)_2]^{2+}$

#### 2.4.2.2. Reaction of $L^1$ with cadmium(II)

$L^1$  is expected to act as a simple tetradentate nitrogen donor. Three pyridyl nitrogens and one thiazole nitrogen atom could coordinate all four equatorial positions of the metal centre in an analogous fashion to that observed in similar compounds reported previously.<sup>28-31</sup>

The reaction of  $L^1$  with one equivalent of  $Cd(ClO_4)_2 \cdot 6H_2O$  in nitromethane produced a yellow solution. Slow diffusion of diethyl-ether into the resulting solution produced orange crystals however, these crystals were not of sufficient quality for single crystal X-ray analysis.

An ion at  $m/z$  729.0 was present in the ESI-mass spectrum, corresponding to  $\{[Cd(L^1)](ClO_4)\}^+$ . The  $^1H$  NMR spectrum of the complex showed 20 aromatic proton signals present (Figure 2.20); this is consistent with the formation of the mononuclear species  $[Cd(L^1)]^{2+}$ .

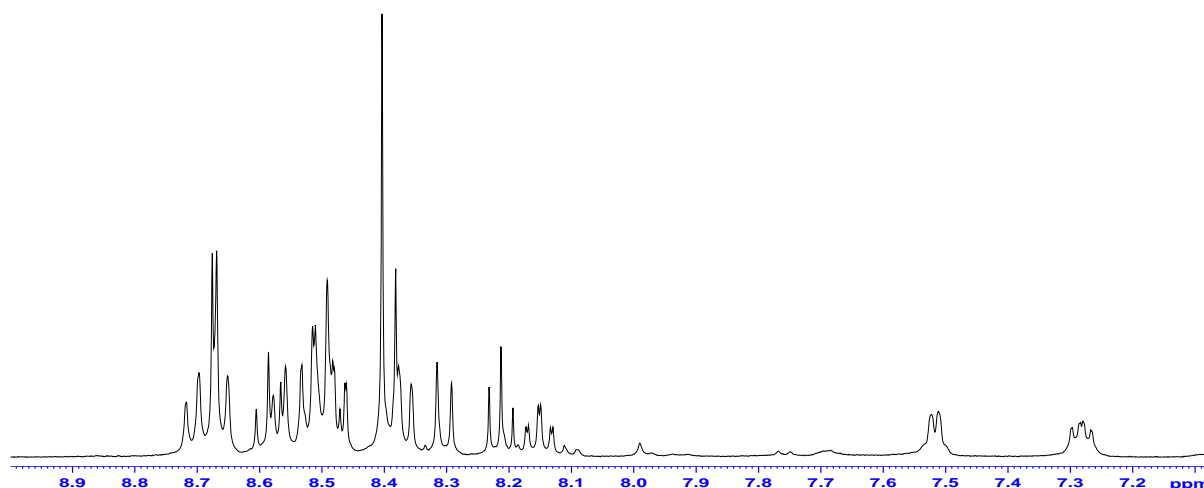


**Figure 2.20:** Selected region of the  $^1H$  NMR spectrum of  $[Cd(L^1)]^{2+}$

## 2.4.3 Coordination Chemistry of $L^2$

### 2.4.3.1 Reaction of $L^2$ with copper(I)

The reaction of  $L^2$  with one equivalent of  $Cu(MeCN)_4 \cdot PF_6$  in nitromethane in the presence of excess tetraethylammonium perchlorate produced a red solution. Slow diffusion of ethyl acetate into the resulting solution produced red crystals, single crystal X-ray analysis of which showed the formation of a dinuclear double helicate species. The crystal structure of  $[Cu_2(L^2)_2](PF_6)_2$  shows how the ligand has partitioned into two bidentate nitrogen donor domains. Each copper ion is coordinated by two of the bidentate domains, one from each ligand (Figure 2.21). Since each of the pyrene units lies at the end of a ligand strand, the intramolecular pyrene-pyrene distances are quite large, with intrastrand centroid $\cdots$ centroid distances of 8.080 and 8.315 Å; the interstrand centroid $\cdots$ centroid distances are 8.669 and 9.241 Å.

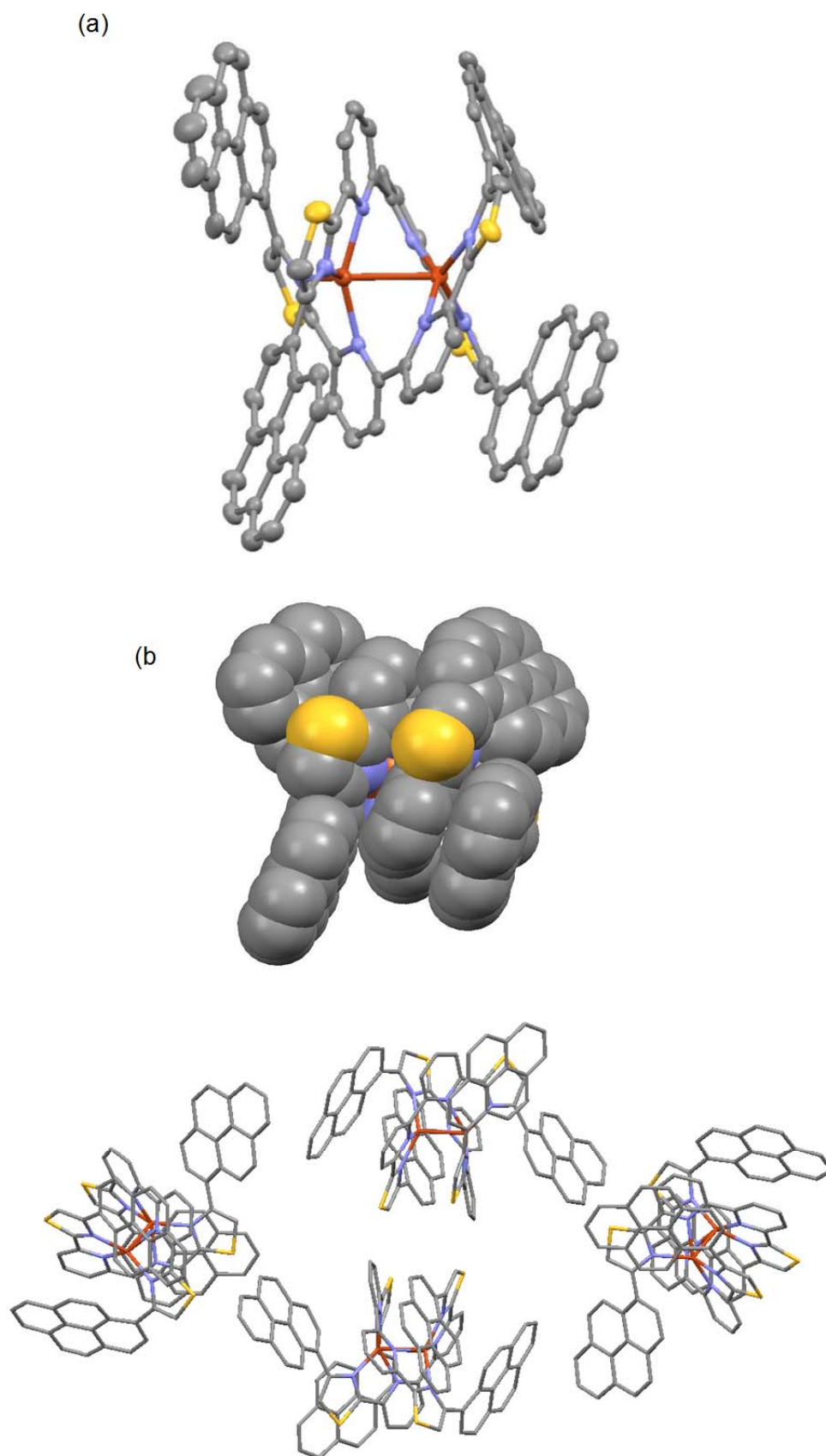


**Figure 2.21:** Single crystal X-ray structure of the complex cation  $[\text{Cu}_2(\text{L}^2)_2](\text{PF}_6)_2$ : (a) as displacement ellipsoid plot drawn at the 50% probability level; (b) as a space-filling model; (c) showing the molecular packing in the unit cell (counter ions and solvent molecules omitted for clarity)

The copper(I) centres have assumed a distorted tetrahedral geometry, with Cu-N distances ranging from 2.050(4) – 2.132(4) Å as shown in Table 2.3.

Bond	Bond length (Å)
Cu(1)-Cu(2)	2.7483(9)
Cu(1)-N(1)	2.056(3)
Cu(1)-N(2)	2.132(4)
Cu(1)-N(5)	2.102(4)
Cu(1)-N(6)	2.078(4)
Cu(2)-N(3)	2.057(4)
Cu(2)-N(4)	2.108(4)
Cu(2)-N(7)	2.081(4)
Cu(2)-N(8)	2.050(4)

**Table 2.3:** Selected bond lengths (Å) for the complex cation  $[\text{Cu}_2(\text{L}^2)_2]^{2+}$

Bond	Bond angle (°)	Bond	Bond angle (°)
N(1)-Cu(1)-N(2)	80.61(14)	N(3)-Cu(2)-N(4)	81.03(15)
N(1)-Cu(1)-N(5)	134.74(14)	N(3)-Cu(2)-N(7)	149.47(15)
N(1)-Cu(1)-N(6)	119.64(14)	N(7)-Cu(2)-N(4)	104.55(15)
N(5)-Cu(1)-N(2)	102.55(15)	N(8)-Cu(2)-N(3)	117.90(16)
N(6)-Cu(1)-N(2)	146.88(14)	N(8)-Cu(2)-N(4)	131.57(15)
N(6)-Cu(1)-N(5)	81.90(15)	N(8)-Cu(2)-N(7)	81.23(15)

**Table 2.4:** Selected bond angles (°) for the complex cation  $[\text{Cu}_2(\text{L}^2)_2]^{2+}$

Examination of the intermolecular packing (Fig. 2.21(c)) shows that the pyrene units align in an edge-to-face manner in an analogous manner to  $[\text{Cu}_2(\text{L}^1)_2]^{2+}$ , with the shortest centroid···centroid distance being 6.077 Å.

The formation of the dinuclear double helicate species  $[\text{Cu}_2(\text{L}^2)_2]^{2+}$  was supported by the solution state analysis; an ion was observed in the ESI-mass spectrum at  $m/z$  1717.2, which corresponds to  $\{[\text{Cu}_2(\text{L}^2)_2](\text{PF}_6)\}^+$ .

The  $^1\text{H}$  NMR spectrum of the complex (Figure 2.22) showed 13 proton aromatic signals, consistent with the formation of  $[\text{Cu}_2(\text{L}^2)_2]^{2+}$ . However, these signals show significant line broadening; recording the spectrum at 343K did not improve the peak shapes. It is probable that, due to the steric bulk of the pyrene units, free rotation of these groups is prevented resulting in a significantly broadened  $^1\text{H}$  NMR spectrum.

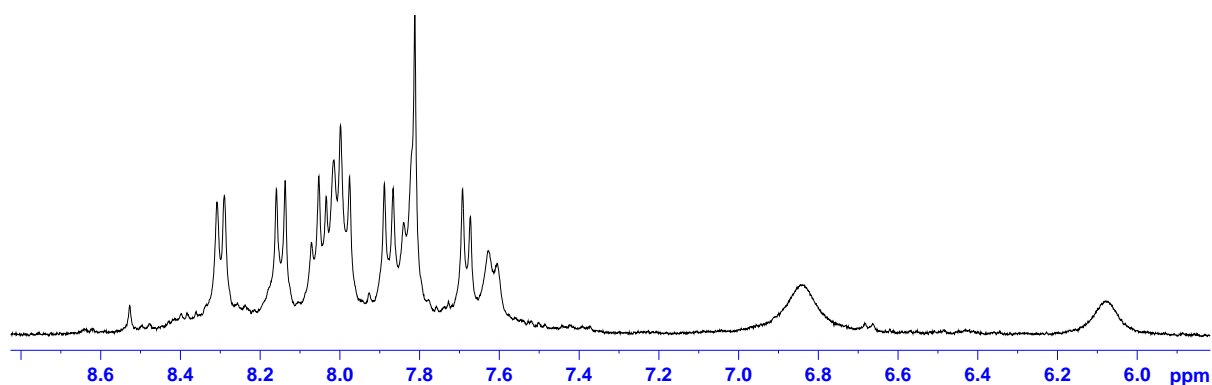


**Figure 2.22:** Selected region of the  $^1\text{H}$  NMR spectrum of  $[\text{Cu}_2(\text{L}^2)_2]^{2+}$

#### 2.4.3.2 Reaction of $\text{L}^2$ with cadmium(II)

The reaction of  $\text{L}^2$  with one equivalent of  $\text{Cd}(\text{ClO}_4)_2 \cdot 6\text{H}_2\text{O}$  in nitromethane produced a yellow solution. Slow diffusion of ethyl acetate into this resulting solution afforded orange crystals; single crystal X-ray analysis of these crystals showed the formation of a monomeric species,  $\{[\text{Cd}(\text{L}^2)](\text{ClO}_4)_2\}$ , in the solid state (Figure 2.23).

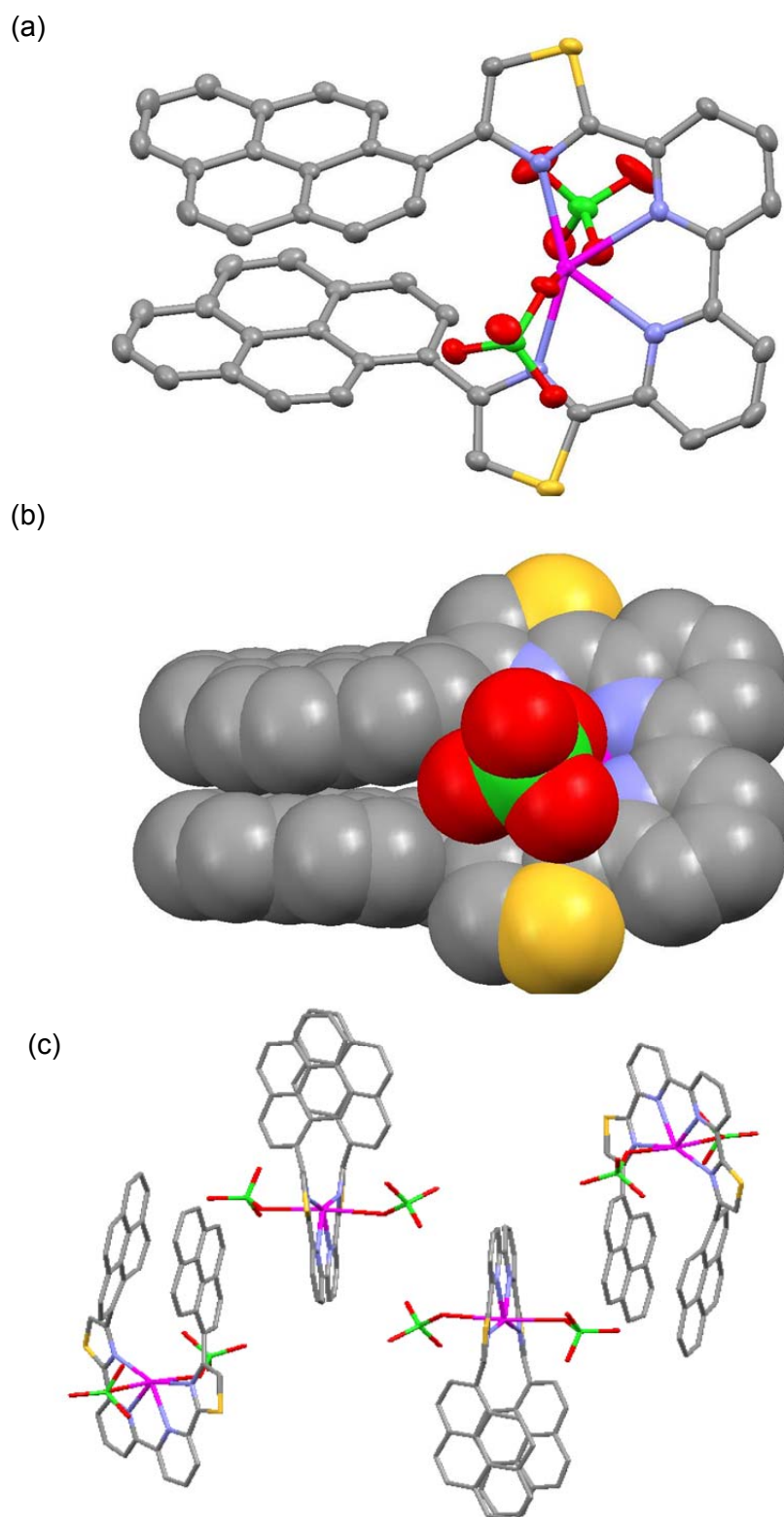


**Figure 2.23:** Single crystal X-ray structure of  $\{[\text{Cd}(\text{L}^2)](\text{ClO}_4)_2\}$ : (a) as displacement ellipsoid plot drawn at the 50% probability level; (b) as a space-filling model; (c) showing the molecular packing in the unit cell (solvent molecules omitted for clarity)

The crystal structure of  $\{[\text{Cd}(\text{L}^2)](\text{ClO}_4)_2\}$  shows that the ligand acts as a tetradentate donor and the metal ion is coordinated in the equatorial position by all four nitrogen

donor atoms (Cd-N distances 2.276(2) – 2.340(2) Å as shown in Table 3.5). Two perchlorate ions are also coordinated to the cadmium ion (Cd-O distances 2.4022(2) – 2.4180(2) Å), which results in a six-coordinate metal centre. The two pyrene moieties overlap significantly and are in close proximity (centroid···centroid distance 3.783 Å). The intermolecular pyrene-pyrene separations are, however, quite long with the shortest centroid···centroid distance being 9.915 Å. The pyrene units  $\pi$ -stack with the planar pyridyl-thiazole domains (Fig. 2.23(c)); the shortest centroid···centroid distance is 4.824 Å, which is significantly longer than the intramolecular pyrene-pyrene separation (3.783 Å).

Bond	Bond length (Å)
Cd(1)-N(6)	2.2825(19)
Cd(1)-N(7)	2.3402(19)
Cd(1)-N(8)	2.3380(2)
Cd(1)-N(9)	2.2763(19)
Cd(1)-O(1)	2.4180(2)
Cd(1)-O(5)	2.4022(19)

**Table 3.5:** Selected bond lengths (Å) for the complex cation  $[\text{Cd}(\text{L}^2)]^{2+}$

Selected bond angles are shown in Table 3.6.

Bond	Bond angle (°)
N(6)-Cd(1)-N(7)	71.59(7)
N(6)-Cd(1)-N(8)	138.51(7)
N(6)-Cd(1)-O(1)	90.72(7)
N(6)-Cd(1)-O(5)	89.30(6)
N(7)-Cd(1)-O(1)	88.04(7)
N(7)-Cd(1)-O(5)	86.59(7)
N(8)-Cd(1)-N(7)	67.37(7)
N(8)-Cd(1)-O(1)	82.15(7)
N(8)-Cd(1)-O(5)	94.10(7)
N(9)-Cd(1)-N(6)	149.32(7)
N(9)-Cd(1)-N(7)	139.09(7)
N(9)-Cd(1)-N(8)	71.92(7)
N(9)-Cd(1)-O(1)	90.48(7)
N(9)-Cd(1)-O(5)	92.39(7)
O(5)-Cd(1)-O(1)	174.33(7)

**Table 3.6:** Selected bond angles (°) for the complex cation  $[\text{Cd}(\text{L}^2)]^{2+}$

Analysis by ESI-MS confirmed the formation of a mononuclear species with an ion at  $m/z$  935.0 corresponding to the complex  $\{[\text{Cd}(\text{L}^2)](\text{ClO}_4)\}^+$ . The  $^1\text{H}$  NMR spectrum of the complex in  $\text{d}_3$ -nitromethane (Figure 2.24), showed 13 reasonably well resolved proton signals were present in the aromatic region, along with some broad peaks corresponding to a small amount of an impurity. However, this spectrum is consistent with the formation of  $[\text{Cd}(\text{L}^2)]^{2+}$  as the major species in solution.

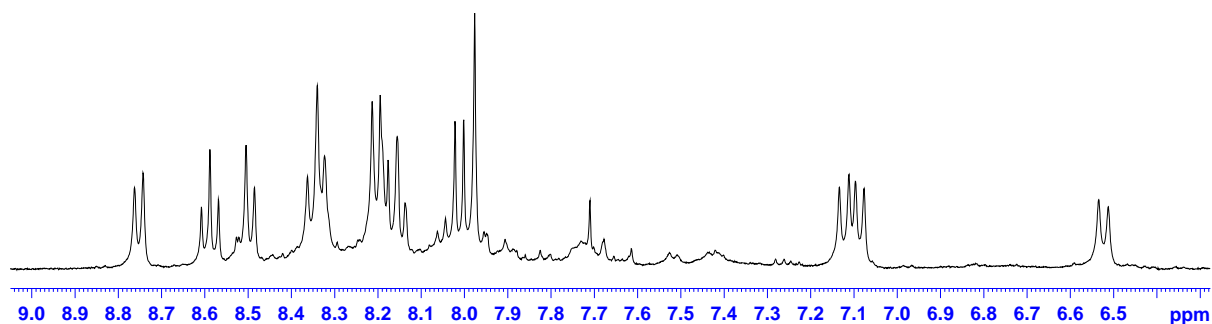


**Figure 2.24:** Selected region of the  $^1\text{H}$  NMR spectrum of  $[\text{CdL}^2]^{2+}$ .

## 2.4.4 Photophysical Measurements

### 2.4.4.1 $\underline{\text{L}}^1$

The steady state luminescence spectrum of the free ligand  $\text{L}^1$  in dilute solution ( $10^{-6}$  M) displayed a strong, broad emission band at 462 nm, which is characteristic of excimer-based fluorescence emission; this is likely to be due to  $\pi$ -stacking of the relatively planar ligand strands in solution. The lifetime of this emission was found to be 1.1 ns. The ligand solution was then diluted sequentially and vibronically structured features began to appear between 370 and 440 nm in the emission spectrum due to emission from monomeric pyrene units (Fig. 2.25).

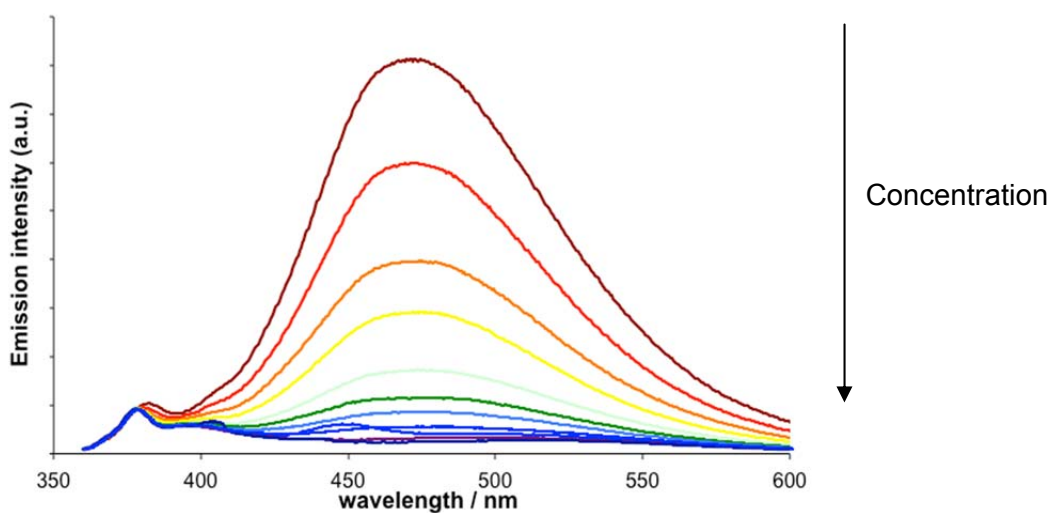


**Figure 2.25:** Emission spectra (MeCN;  $\lambda_{\text{ex}} = 340$  nm) for  $\text{L}^1$  with decreasing concentration ( $2.1 \times 10^{-6}$  M to  $2.1 \times 10^{-9}$  M)

The photophysical behaviour of the  $\text{Cd}^{2+}$  and  $\text{Cu}^+$  complexes of  $\text{L}^1$  was similar; addition of either metal ion to a dilute solution of  $\text{L}^1$  resulted in a decrease in intensity of the excimer emission band and the appearance of new features at higher energy (between 360 and 460 nm). These signals can be attributed to monomeric pyrene fluorescence, which was associated with lifetimes of 4.1-6.9 ns and therefore easily distinguished from the shorter-lived excimer emission of the free ligand (Fig. 2.26).

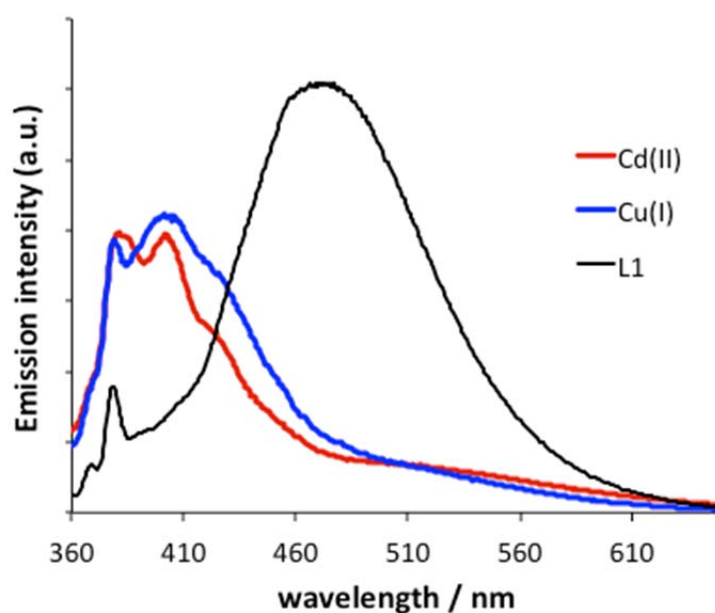


**Figure 2.26:** Comparison of the emission spectra ( $2.1 \times 10^{-6}$  M MeCN;  $\lambda_{\text{ex}} = 340$  nm) of  $\text{L}^1$ ,  $[\text{Cd}(\text{L}^1)](\text{ClO}_4)_2$  and  $[\text{Cu}_2(\text{L}^1)_2](\text{PF}_6)_2$

The spectra for  $[\text{Cd}(\text{L}^1)]^{2+}$  and  $[\text{Cu}_2(\text{L}^1)_2]^{2+}$  both display monomeric pyrene emission, with no emission attributable to excimer formation; this corroborates the solid state structures since there are no proximate pyrene units in these species seen in the single-crystal X-ray analyses (Section 2.4.2). The emission spectra of both  $[\text{Cd}(\text{L}^1)]^{2+}$  and  $[\text{Cu}_2(\text{L}^1)_2]^{2+}$  are remarkably similar indicating that the metal ions (which are of different oxidation states) have little effect on the emission profile and the emission is independent of the metals present.

#### 2.4.4.2 $\text{L}^2$

In contrast to  $\text{L}^1$ , the steady state spectrum of bis-pyrenyl ligand  $\text{L}^2$  ( $1.7 \times 10^{-6}$  M) was dominated by typical monomeric pyrene emission, with classical vibronic features

prominently displayed between 360-450 nm, and a corresponding lifetime of 5.5 ns. This indicates that the disubstituted ligands cannot stack in solution to form excimers, probably due to their steric bulk. Mixing of  $L^2$  at  $1.7 \times 10^{-6}$  M with  $Cu^+$  gave an emission spectrum almost superimposable with that of the free ligand, but with a slight increase in emission intensity and a notable reduction in the resolution of the vibronic structure. Again, as with the copper(I) complex of  $L^1$ , this is in agreement with the X-ray structure which shows a dinuclear double helicate is formed in the solid state; in this complex the pyrene units are too distant from one another to form excimers within a molecule.

Upon reaction of  $L^2$  with  $Cd^{2+}$ , however, significantly different results were obtained. A significant quenching of the overall emission intensity was observed along with the appearance of an additional weakly intense band at ca. 540 nm, which is attributed to excimeric emission (Fig. 2.27).

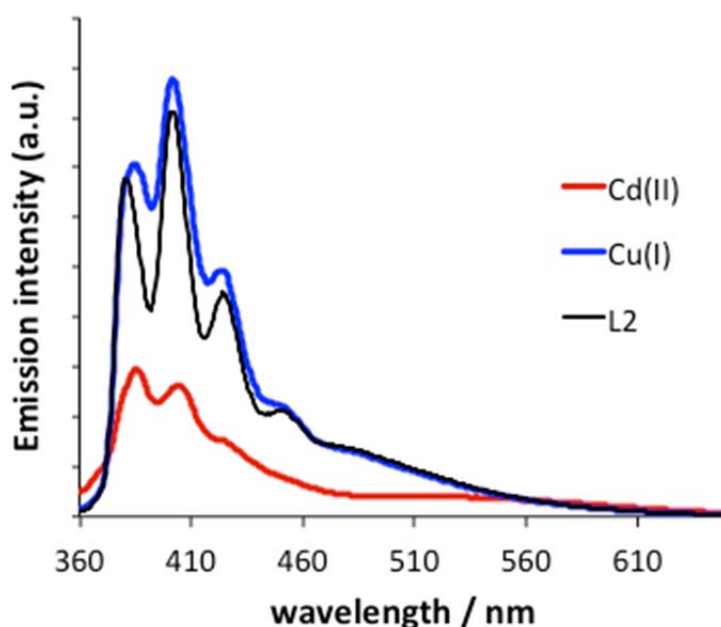


**Figure 2.27:** Comparison of the emission spectra ( $1.7 \times 10^{-6}$  M MeCN;  $\lambda_{ex} = 340$  nm) of  $L^2$ ,  $[Cd(L^2)]^{2+}$  and  $[Cu_2(L^2)_2]^{2+}$

This solution-state behaviour shows good correlation with the solid state structure as the two pyrene units in  $[Cd(L^2)]^{2+}$  are coplanar and in close proximity; hence, a general quenching is observed (which is consistent with excimer formation) together with appearance of a new, weak emission at 540 nm (Fig. 2.28). However, there is still emission at  $\sim 410$  nm indicating that although in  $[Cd(L^2)]^{2+}$  the two pyrene units are in close proximity not all the energy is transferred to give excimer emission. It is also possible that in solution the two pyrene units adopt a different conformation. Rotation

about the thiazole-pyrene carbon-carbon single bonds, of both units, will result in a conformer where overlap of the aromatic units would be less than that observed in the solid-state. Adopting this conformation would result in less energy transfer giving rise to some monomer emission.

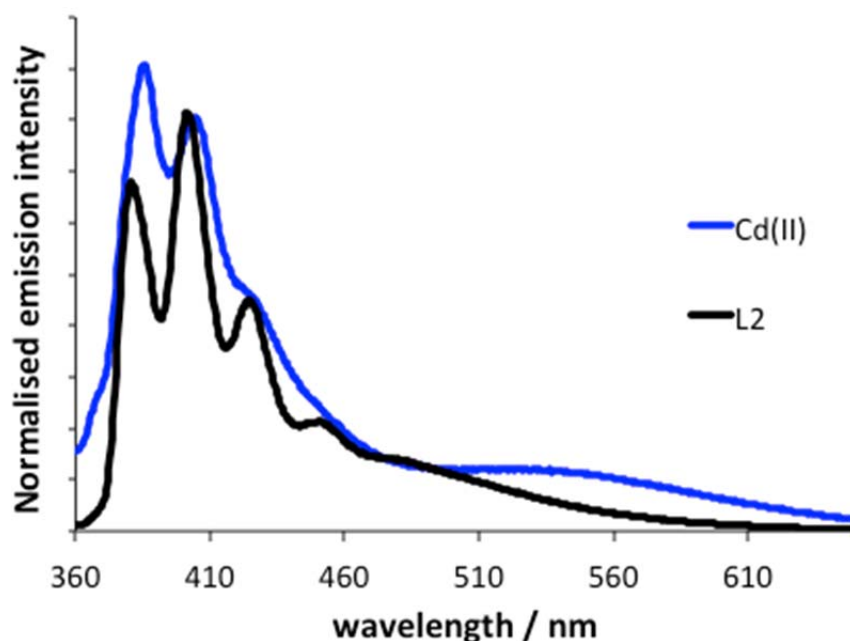


**Figure 2.28:** Comparison of the normalized (400 nm) emission spectra ( $1.7 \times 10^{-6}$  M MeCN;  $\lambda_{\text{ex}} = 340$  nm) of  $\text{L}^2$  and  $[\text{Cd}(\text{L}^2)]^{2+}$

As the spectra of  $[\text{Cd}(\text{L}^1)]^{2+}$  and  $[\text{Cu}_2(\text{L}^1)_2]^{2+}$  are very similar the difference between the emission profiles of  $[\text{Cd}(\text{L}^2)]^{2+}$  and  $[\text{Cu}_2(\text{L}^2)_2]^{2+}$  can be attributed to the different species formed (i.e. mononuclear versus dinuclear double helicate). The solution state spectroscopic results indicates that inclusion of pyrene units within a ligand strand can help ascertain the self-assembled species in solution through monitoring of monomer *versus* excimer type emission from the fluorescent pyrene units.

## 2.5 Conclusion

Fluorescent pyrene units can be successfully incorporated into multidentate ligands capable of forming supramolecular assemblies. The inclusion of a pyrene unit within a ligand strand can be a useful probe into the resultant self-assembled species due to the environment-sensitive fluorescent properties of the pyrene fluorophore. Although the difference in emission spectra for  $[\text{Cd}(\text{L}^2)]^{2+}$  and  $[\text{Cu}_2(\text{L}^2)_2]^{2+}$  is not as dramatic as

would be expected from the solid state structures the profiles are noticeably different correlating well with the structures observed in the solid state.

## 2.6 References

1. Hung, H. C., Cheng, C. W., Ho, I. T., Chung, W. S., Dual-mode Recognition of Transition Metal Ions by Bis-triazoles Chained Pyrenes., *Tetrahedron Letters*, 2009, **50**, 302-305.
2. Winnik, F. M., Photophysics of Preassociated Pyrenes in Aqueous Polymer Solutions and in Other Organized Media., *J. Am. Chem. Soc.*, 1993, **93**, 587-614.
3. Gao, C., Qian, H., Wang, S., Yan, D., Chen, W., Yu, G., Self-association of Hyperbranched Poly(sulfone-amine) in Water: Studies with Pyrene-fluorescence Probe and Fluorescence Label., *Polymer*, 2003, **44**, 1547-1552.
4. Jones, G., Vullev, V., Ground- and Excited-State Aggregation Properties of a Pyrene Derivative in Aqueous Media., *J. Phys. Chem. A.*, 2001, **105**, 6402-6406.
5. Xu, Z., Singh, N. J., Lim, J., Kim, H. N., Park, S., Kim, K. S., Yoon, J., Unique Sandwich Stacking of Pyrene-Adenine-Pyrene for Selective and Ratiometric Fluorescent Sensing of ATP at Physiological pH., *J. Am. Chem. Soc.*, 2009, **131**, 15528-15533.
6. Shiraishi, Y., Tokitoh, Y., Hirai, T., pH- and H<sub>2</sub>O-Driven Triple-Mode Pyrene Fluorescence., *Organic Letters*, 2006, **8**, 3841-3844.
7. Bowen, E. J., (1968). *Luminescence in Chemistry*. Canada: D. Van Nostrand Company.

8. Beer, P. D., Gale, P. A., Smith, D. K., (1999). *Supramolecular Chemistry*. New York: Oxford University Press Inc.
9. Leroy, S., Soujanaya, T., Sohna Sohna, J. E., Fages, F., Ion-Induced Luminescence Control in Pyrene-tethered Bipyridine Ligand Systems., *International Journal of Photoenergy*., 2001, **3**, 49-53.
10. Focsaneanu, K. S., Scaiano, J. C., Potential Analytical Applications of Differential Fluorescence Quenching: Pyrene Monomer and Excimer as Sensors of Electron Deficient Molecules., *Photochem. Photobiol. Sci.*, 2005, **4**, 817-821.
11. Steed, J. W., Turner, D. R., Wallace, K. J., (2007). *Core Concepts in Supramolecular Chemistry and Nanochemistry*. Chichester: John Wiley & Sons.
12. Mansell, D., Rattray, N., Etchells, L. L., Schwalbe, C. H., Blake, A. J., Bichenkova, E. V., Bryce, R. A., Barker, C. J., Diaz, A., Kremer, C., Freeman, S., Fluorescent Probe: Complexation of Fe<sup>3+</sup> with the Myo-inositol 1,2,3-trisphosphate Motif., *Chem. Commun.*, 2008, 5161-5163.
13. Friebolin, H., (2005). *Basic One and Two Dimensional NMR Spectroscopy*. Germany: Wiley-VHC.
14. Zeng, L., Wang, P., Zhang, H., Zhuang, X., Dai, Q., Liu, W., Highly Selective and Sensitive Heparin Probing from Supramolecular Assembly of Pyrene Derivatives., *Organic Letters*, 2009, **11**, 4294-4297.
15. Ueno, A., Host-Guest Sensory Systems for Detecting Organic Compounds by Pyrene Excimer Fluorescence., *Anal. Chem.*, 1990, **62**, 2461-2466.

16. Yuasa, H., Miyagawa, N., Nakatani, M., Izumi, M., Hashimoto, H., A Tong-like Fluorescence Sensor for Metal Ions: Perfect Conformational Switch of Hinge Sugar by Pyrene Stacking., *Org. Biomol. Chem.*, 2004, **2**, 3548-3556.
17. Yang, Y., Gou, X., Blecha, J., Cao, H., A Highly Selective Pyrene Based Fluorescent Sensor Towards Hg<sup>2+</sup> Detection., *Tetrahedron Letters*, 2010, **51**, 3422-3425.
18. Yang, J. S., Lin, C. S., Hwang, C. Y., Cu<sup>2+</sup>-Induced Blue Shift of the Pyrene Excimer Emission: A New Signal Transduction Mode of Pyrene Probes., *Organic Letters*, 2001, **3**, 889-892.
19. Hammarström, P., Kalman, B., Jonsson, B. H., Carlsson. U., Pyrene Excimer Fluorescence as a Proximity Probe for Investigation of Residual Structure in the Unfolded State of Human Carbonic Anhydrase II., *FEBS Letters*, 1997, **420**, 63-68.
20. Svensson, M., Jonasson, P., Freskgård, P. O., Jonsson, B. H., Lindgren, M., Mårtensson, L. G., Gentile, M., Borén, K., Carlsson, U., Mapping the Folding Intermediate of Human Carbonic Anhydrase II. Probing Substructure by Chemical Reactivity and Spin and Fluorescence Labeling of Engineered Cysteine Residues., *Biochemistry*, 1995, **34**, 8606-8620.
21. Mårtensson, L. G., Jonsson, B. H., Freskgård, P. O., Kihlgren, A., Svensson, M., Carlsson, U., Characterization of Folding Intermediates of Human Carbonic Anhydrase II: Probing Substructures by Chemical Labeling of SH Groups Introduced by Site-Directed Mutagenesis., *Biochemistry*, 1993, **32**, 224-231.
22. Tseng, C. M., Hammerschmidt, C. R., Fitzgerald, W. F., Determination of Methylmercury in Environmental Matrixes by On-line Flow Injection and Atomic Fluorescence Spectrometry., *Anal. Chem.*, 2004, **76**, 7131-7136.

23. Chen, X., Nam, S. W., Jou, M. J., Kim, Y., Kim, S. J., Park, S., Yoon, J., Hg<sup>2+</sup> Selective Fluorescent and Colorimetric Sensor: Its Crystal Structure and Application to Bioimaging, *Organic Letters*, 2008, **10**, 5235-5238.
24. Zhu, M., Yuan, M., Liu, X., Xu, J., Lv, J., Huang, C., Liu, H., Li, Y., Wang, S., Zhu, D., Visible Near-Infrared Chemosensor for Mercury Ion., *Organic Letters*, 2008, **10**, 1481-1484.
25. Liu, B., Tian, H., A Selective Fluorescent Ratiometric Chemodosimeter for Mercury Ion., *Chem. Commun.*, 2005, 3156-3158.
26. Suzuki, Y., Morozumi, T., Nakamura, H., Shimomura, M., Hayashita, T., Bartsh, R. A., New Fluorimetric Alkali and Alkaline Earth Metal Cation Sensors Based on Noncyclic Crown Ethers by Means of Intramolecular Excimer Formation of Pyrene., *J. Phys. Chem. B.*, 1998, **102**, 7910-7917.
27. Kim, J. S., Choi, M. G., Song, K. C., No, K. T., Ahn, S., Chang, S. K., Ratiometric Determination of Hg<sup>2+</sup> Ions Based on Simple Molecular Motifs of Pyrene and Dioxaoctanediamide., *Organic Letters*, 2007, **9**, 1129-1132.
28. Rice, C. R., Wörl, S., Jeffery, J. C., Paul, R. L., Ward, M. D., New Multidentate Ligands for Supramolecular Coordination Chemistry: Double and Triple Helical Complexes of Ligands Containing Pyridyl and Thiazolyl Donor Units., *J. Chem. Soc., Dalton Trans.*, 2001, 550-559.
29. Thummel, R. P., Jahng, Y., N-Oxides of 2,2'6',2"-Terpyridine., *J. Org. Chem.*, 1985, **50**, 3635-3636.
30. Rice, C. R., Baylies, C. J., Clayton, H. J., Jeffery, J. C., Paul, R. L., Ward, M. D., Novel Multidentate Pyridyl/Thiazolyl Ligands Containing Terpyridine Units: Formation of Dinuclear and Trinuclear Double Helicate Complexes., *Inorganica Chimica Acta.*, 2003, **351**, 207-216.

31. Clayton, H. J., Harding, L. P., Irvine, J. P., Jeffery, J. C., Riis-Johannessen, T., Laws, A. P., Rice, C. R., Whitehead, M., Metal-specific Allosteric Activation and Diactivation of a Diamine., *Chem. Commun.*, 2008, 108-110.

## 2.7 Appendix: Crystallographic Data Tables

Compound	<b>{[Cu<sub>2</sub>(L<sup>1</sup>)<sub>2</sub>](PF<sub>6</sub>)<sub>2</sub>}</b>
Formula	C <sub>204</sub> H <sub>118</sub> Cu <sub>6</sub> F <sub>36</sub> N <sub>24</sub> P <sub>6</sub> S <sub>6</sub>
M	4348.64
System, space group	Orthorhombic, <i>Iba</i> 2
a/Å	45.237(2)
b/Å	18.6332(10)
c/Å	23.8739(13)
V/ Å <sup>3</sup>	20122.5(2)
Z	4
$\rho_{\text{calc}}/\text{Mg m}^{-3}$	1.435
<i>F</i> (000)	8776
Dimensions/mm	0.35 x 0.12 x 0.10
$\mu/\text{mm}^{-1}$	0.71073
T/K	150(2)
Reflections collected (range)	31846 (2.08 ≤ $\theta$ ≤ 23.31°)
<i>hkl</i> range indices	-48 ≤ <i>h</i> ≤ 50, -20 ≤ <i>k</i> ≤ 20, -21 ≤ <i>l</i> ≤ 26
Unique reflections	12922
Total, independent <i>R</i> <sub>int</sub>	0.0377
<i>R</i> <sub>w</sub>	0.1802
<i>R</i>	0.0659
Reflections with <i>I</i> > 2 $\sigma$ ( <i>I</i> )	10183
GOF	1.011
Refined parameters	1227
Restraints	955
Largest peak and hole/eÅ <sup>-3</sup>	1.058, -0.682

Compound	<b>{[Cd(L<sup>2</sup>)](ClO<sub>4</sub>)<sub>2</sub>(MeNO<sub>2</sub>)}</b>
Formula	C <sub>49</sub> H <sub>29</sub> CdCl <sub>2</sub> N <sub>5</sub> O <sub>10</sub> S <sub>2</sub>
M	1095.19
System, space group	Monoclinic, <i>P2<sub>1</sub>/c</i>
a/Å	20.2402(8)
b/Å	10.3881(4)
c/Å	20.5791(7)
β/°	101.4650(10)
V/ Å <sup>3</sup>	4240.6(3)
Z	4
ρ <sub>calc</sub> /Mg m <sup>-3</sup>	1.715
F(000)	2208
Dimensions/mm	0.40 x 0.35 x 0.07
μ/mm <sup>-1</sup>	0.71073
T/K	101(2)
Reflections collected (range)	38944 (2.02 ≤ θ ≤ 27.88°)
hkl range indices	-26 ≤ h ≤ 26, -13 ≤ k ≤ 13, -27 ≤ l ≤ 26
Unique reflections	10120
Total, independent R <sub>int</sub>	0.0483
R <sub>w</sub>	0.0800
R	0.0330
Reflections with I > 2σ(I)	8049
GOF	0.950
Refined parameters	623
Restraints	0
Largest peak and hole/eÅ <sup>-3</sup>	0.637, -0.653

Compound	<b>{[Cu<sub>2</sub>(L<sup>2</sup>)<sub>2</sub>](ClO<sub>4</sub>)<sub>2</sub>(MeNO<sub>2</sub>)(EtOAc)}</b>
Formula	C <sub>101</sub> H <sub>63</sub> Cl <sub>2</sub> Cu <sub>2</sub> N <sub>9</sub> O <sub>12</sub> S <sub>4</sub>
M	1920.82
System, space group	Monoclinic, <i>P2<sub>1</sub>/n</i>
a/Å	15.462(2)
b/Å	33.213(5)
c/Å	16.066(2)
β/°	98.734(2)
V/ Å <sup>3</sup>	8155.0(2)
Z	4
ρ <sub>calc</sub> /Mg m <sup>-3</sup>	1.564
F(000)	3936
Dimensions/mm	0.20 x 0.10 x 0.10
μ/mm <sup>-1</sup>	0.71073
T/K	150(2)
Reflections collected (range)	63702 (1.77 ≤ θ ≤ 26.43°)
hkl range indices	-19 ≤ h ≤ 18, -41 ≤ k ≤ 41, -19 ≤ l ≤ 20
Unique reflections	16577
Total, independent R <sub>int</sub>	0.0692
R <sub>w</sub>	0.1498
R	0.0629
Reflections with I > 2σ(I)	9947
GOF	1.006
Refined parameters	1175
Restraints	41
Largest peak and hole/eÅ <sup>-3</sup>	1.059, -0.827

## Chapter 3 Novel pyridyl-thiazole-containing complexes capable of binding anions

### 3.1 Introduction

Ion binding is one of the many avenues of interest within supramolecular chemistry since cations have many roles in biological processes with a few being essential to life.<sup>1</sup> Cations such as sodium and potassium are involved with the transmission of nerve impulses, whereas calcium ions are vital towards cellular signalling control.<sup>1</sup> Medically, complexes containing platinum have been proven to show disturbance towards the growth of tumour cells when coordinating DNA, with the subsequent effect of hindering replication of the cells.<sup>2</sup> Toxic metals such as lead and mercury are also of interest both medically (where an individual has been poisoned) and where there is a toxic heavy metal build up in the environment.<sup>1</sup>

There are numerous cation binding hosts suitable for metal ions which have good reactivity and selectivity properties.<sup>3</sup> One of the most common structural features used for this purpose is the crown ether. Research into crown ethers initially started due to the discovery made by Pedersen<sup>1,4</sup>; the 18-membered ring, dibenzo-[18]crown-6 (Figure 3.1) was the first of the aromatic crown ether compounds to be prepared.<sup>4</sup>

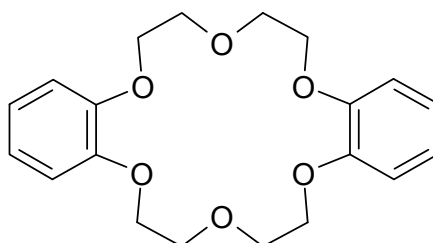


**Figure 3.1:** The aromatic crown ether compound, dibenzo-[18]crown-6

The discovery of this compound was a crucial step within development of the discipline of supramolecular chemistry and the initial results led to the rapid synthesis of related macrocyclic species (Figure 3.2).

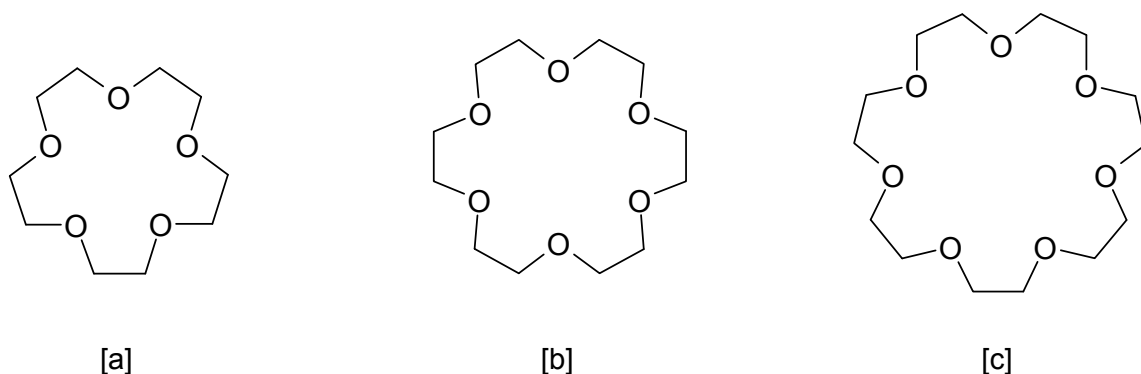


**Figure 3.2:** The structures of [15]crown-5 [a], [18]crown-6 [b] and [21]crown-7 [c]

Upon discovery of dibenzo-[18]crown-6 Pedersen showed that a sodium ion was being held in the centre of the ring by the electrostatic attraction between the positive charge from the sodium ion and the negative charge of the six oxygen atoms which are arranged symmetrically around the sodium ion in the polyether ring. Pedersen used other alkali metal ions and ammonium ions which behaved in the same way as the sodium ion, forming stable complexes with crown ethers.

Following the discovery of crown ethers a vast range of macrocyclic ligands now exists with thousands of examples available, many of which contain different types of ring system. The different types of ring system include coronands, podands, cryptands and spherands. All of these systems can be regarded as well developed ring systems where the structures vary but still contain oxygen atoms which are linked by dimethylene groups.<sup>1</sup>

Crown ethers are members of the coronand family which, in their simplest form, comprise a cyclic array of ethylene glycol units (-O-CH<sub>2</sub>-CH<sub>2</sub>-O-), with the most well known crown ether being [18]crown-6 as shown in Figure 3.2. Podands however are acyclic analogues of the crown ethers such as pentaethyleneglycol dimethylether (Figure 3.3[a]), which is analogous to [18]crown-6. Another simple podand is its diol analogue (Figure 3.3[b]).

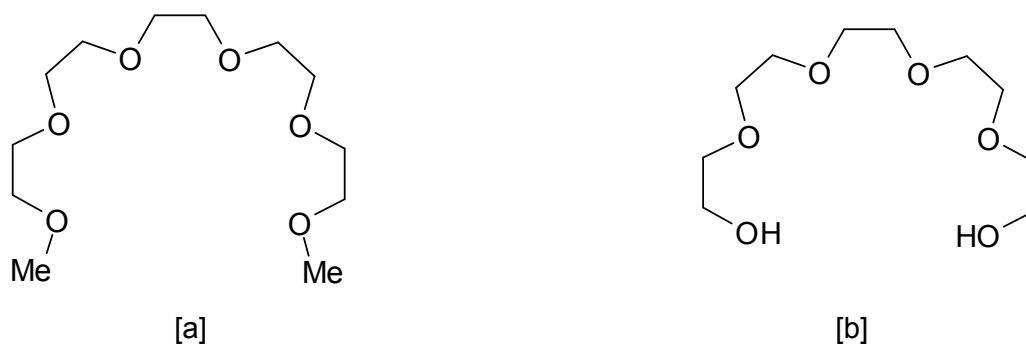


**Figure 3.3:** Crown ethers pentaethyleneglycol dimethylether [a] and the diol analogue [b]

Cryptands, three dimensional analogues of the original crown ethers, have also been prepared. Lehn contributed towards this work immensely with the first and most important member in this group being [2.2.2]cryptand (Figure 3.4).<sup>3</sup>

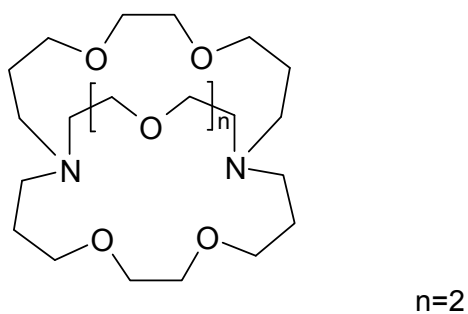


**Figure 3.4:** The structure of [2.2.2]cryptand

Spherands are complex cryptands which have an almost spherical structure and are able to form complexes by enveloping metal cations. The donor atoms (O, N, S) are arranged in such a way that they can provide a coordination sphere to the encapsulated cation. An all-aromatic spherand was amongst one of the earliest examples produced by D. J. Cram (Figure 3.5).<sup>5</sup>

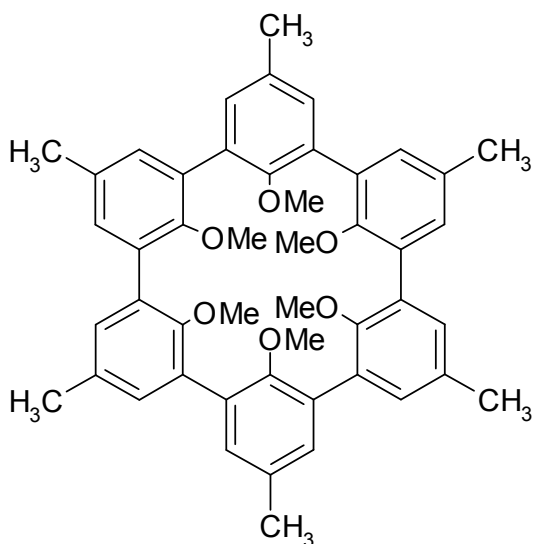


**Figure 3.5:** The structure of an aromatic spherand discovered by Cram<sup>5</sup>

Each of these types of system can exist with varying ring sizes. Variations of crown ethers have a series of O-donor atoms which generate a cavity that is suitable for coordinating guest species, usually s-block metal cations. The basis of molecular recognition is the selective binding of a particular guest and can be easily explained by the size match between the host cavity and the cation.

A specific crown ether will bind strongly a cation that is complementary to its host cavity. By varying the number of alkyl spacers or O-donors then the size of the cavity can easily be changed within the macrocycle. By changing the size of the cavity the suitability of the cation for coordination with the host will also change.

For example, the internal cavity diameter for [18]crown-6 is between 2.60-3.20 Å and is an ideal match for coordination with K<sup>+</sup> ions whose diameter is 2.66 Å, whereas Li<sup>+</sup> ions with a diameter of 1.36 Å are not suitable for coordination to [18]crown-6. Li<sup>+</sup> ions are however complementary to [12]crown-4 which has an internal cavity diameter between 1.20-1.50 Å. Further cation diameters and crown ether cavity diameters are shown in Table 3.1.

Crown Ether	Cavity Diameter	Cation	Cation Diameter/Å
[12]crown-4	1.20-1.50	Li <sup>+</sup>	1.36
		Mg <sup>2+</sup>	1.44
[15]crown-5	1.70-2.20	Na <sup>+</sup>	1.90
		Ca <sup>2+</sup>	2.20
		Sr <sup>2+</sup>	2.26
[18]crown-6	2.60-3.20	K <sup>+</sup>	2.66
		Ba <sup>2+</sup>	2.68
[21]crown-7	3.40-4.30	Cs <sup>+</sup>	3.38

**Table 3.1:** Selected crown ether cavity diameters and compatible cation diameters

Anions also have roles in both biological and chemical processes. The development of receptors for anion recognition is an innovative and active development in supramolecular chemistry.<sup>2,6</sup> In chemical processes anions mainly take on the role of catalysts and bases; using receptors that will bind to anions can vary the anions' reactivity. In biological processes, the majority of enzyme substrates are negatively charged and anion recognition is highly important within this field as receptors and cells must recognise and discriminate very similar anions such as  $\text{SeO}_4^{2-}$  and  $\text{SO}_4^{2-}$ .<sup>2</sup> Anions are also very important in diseases, such as cystic fibrosis which involves problems with regulation of chloride channels, therefore the investigation of anion coordination and selective anion recognition is a growing area in anion research.<sup>2</sup>

Anion receptors have many characteristics contributing towards the strength of their binding to the desired donor and each of these should be taken into consideration. These characteristics include charge, size, solvation, geometry and pH dependence. The main characteristic of anions is their negative charge. Electrostatic interactions can be introduced to help with coordination and receptors normally exploit this fact.<sup>2</sup> Cations are smaller than their corresponding isoelectronic anions so with host-guest chemistry, cavities have to be large enough to incorporate anionic guests.

As stated earlier, when comparing cation coordination chemistry to anion chemistry, anion recognition is a fairly new discipline. The existing difficulties with anionic guests,

which may be the main reason for the slow development in this area, include the characterisation of the size of the anionic guests (which are generally larger than cations) and the wider range of shapes available along with the pH dependence as certain anions, especially amphiprotic anions, only exist over a small pH range.<sup>7</sup>

Electrostatic interactions are probably the most obvious and simple way to bind anions by designing a host containing a positive charge which will provide a strong electrostatic ion-ion interaction. With the knowledge of that strong interaction, it would make sense that incorporating more positively charged groups within the receptor would make it even more effective. This would however cause a major problem with the design as all these charges will have a tendency to repel each other. This can be counteracted to some extent by use of a cyclic or rigid system which has the added advantage of creating a preorganised binding cavity.

When utilizing neutral receptors, a typical approach with anion recognition is to incorporate hydrogen bond arrays. Amides and their many derivatives have been found to be eminently suitable when pursuing this avenue; this is due to the relatively acidic protons which are maintained in rigid conformations.<sup>7-9</sup>

There are multiple variations of anion receptors which can range from organometallic, organic-metallocene or just solely organic frameworks.<sup>10</sup> At present, inorganic-based hosts are the main class and focus of anion receptors used and the complexity of these receptors is ever increasing with the only limitation being the researchers' imagination and capabilities.

The most common approach used by chemists is to avoid any interference between the anion recognition process and the metal coordination chemistry. Therefore, the main priority when designing these metal-based systems are that they are both kinetically and thermodynamically stable over a range of conditions. Two organometallic compounds which are both thermodynamically and kinetically stable, that have most commonly been used previously are ferrocene and cobaltocenium. Beer has reported the binding behaviour of multiple mono-cobaltocenium derivatives based on both the negative charge (on an amide arm) and the positive charge of the organometallic centre. This provides the receptor with an assortment of both acceptor and donor hydrogen bonding groups.<sup>7,18-20</sup>

The synthesis of similar derivatives which take advantage of the neutral ferrocene building blocks, combined with hydrogen bonding units, have also been widely published.<sup>6,21-23</sup> These systems were shown to also demonstrate binding behaviours

that obeyed the general rules already established and also, an innovative selectivity principle was established known as *chemical selectivity*.

Receptors used in this research are shown in Figure 3.6. Beer *et al.* showed by incorporating a basic amine moiety into the binding cavity, the corresponding new receptor [L4] displayed a preferential response to  $\text{HSO}_4^-$  over  $\text{H}_2\text{PO}_4^-$ .<sup>21</sup> Normally the selectivity pattern would be reversed due to the stronger hydrogen bonding capability of the acidic anionic guest  $\text{H}_2\text{PO}_4^-$ . However, the presence of the receptor's basic centre causes the  $\text{HSO}_4^-$  moiety to transfer a proton to the amine group. This induces a charge separation in the host-guest complex, which contributes to the overall binding strength.

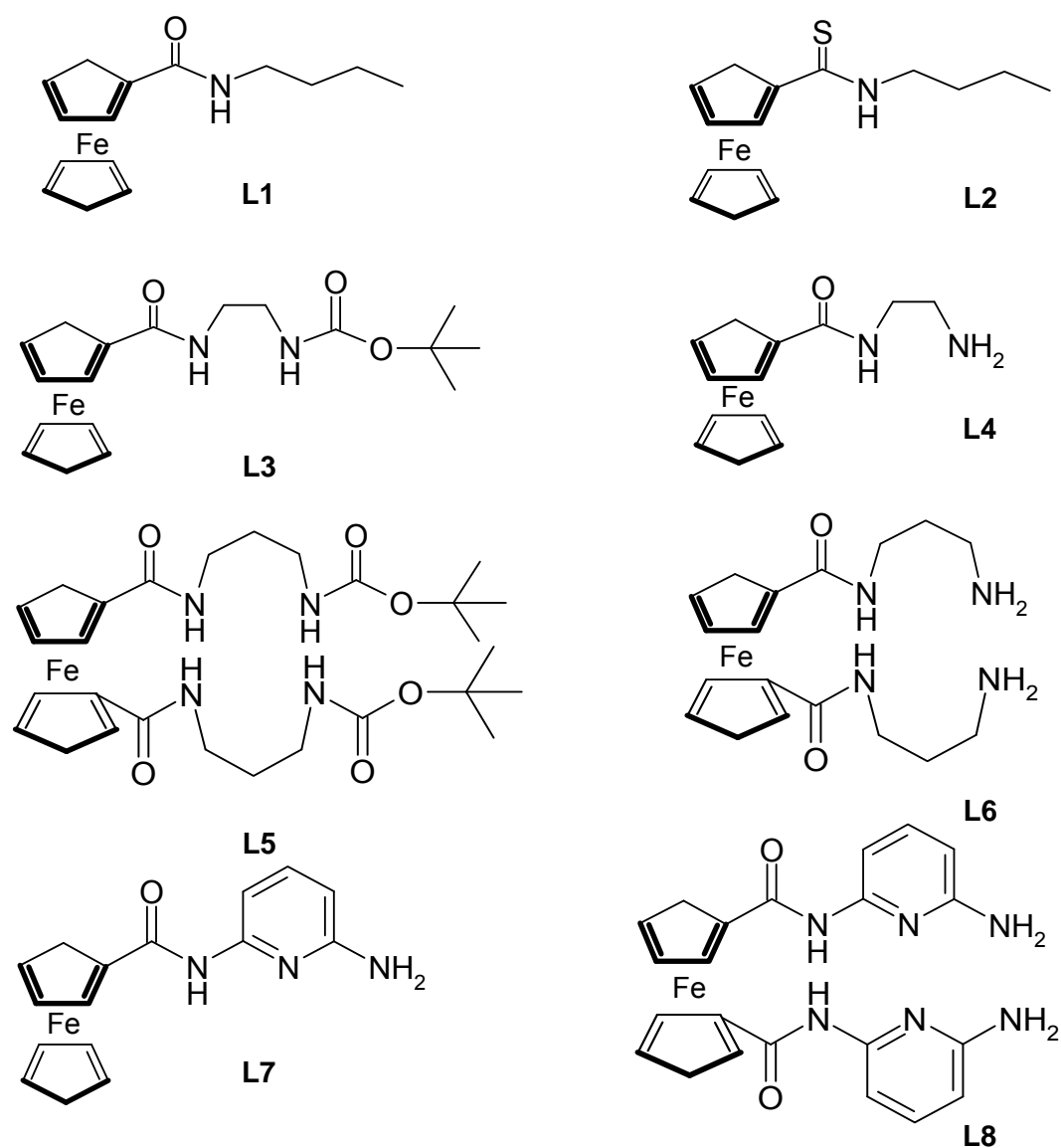
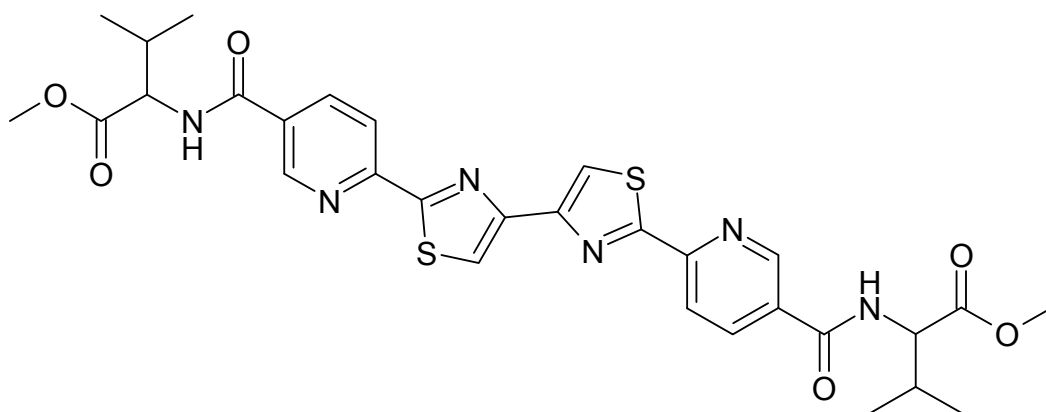


Figure 3.6: Structures of receptors L1-L8 used by Beer *et al.*<sup>21</sup>

Anion receptors which are assembled using transition metal ions can be synthesised by numerous different routes. Self-assembly/coordination about a metal centre can result in the formation of a cavity capable of anion binding, as long as suitable ligands are available.<sup>10</sup> Therefore, the use of transition metal cations to assemble anion receptors is very appealing to researchers.

Research published by Rice *et al.* showed the self-assembly of a novel potentially tetradentate N-donor ligand (Figure 3.7) with  $\text{Co}^{2+}$  into a triple helicate complex.<sup>26</sup> The self-assembly of such metallo-supramolecular complexes and their derivatives has been discussed in a previous chapter.<sup>27-30</sup>

This research showed that, upon reacting the potentially tetradentate ligand with a cation such as cobalt(II) perchlorate hexahydrate  $[\text{Co}(\text{ClO}_4)_2] \cdot 6\text{H}_2\text{O}$ , the complex formed a dinuclear triple helicate. On formation of this self-assembled complex two cavities were formed, one at either end of the helicate (Figure 3.8).



**Figure 3.7:** Structure of the potentially tetradentate N-donor pyridyl-thiazole ligand  $\text{L}^{1(26)}$

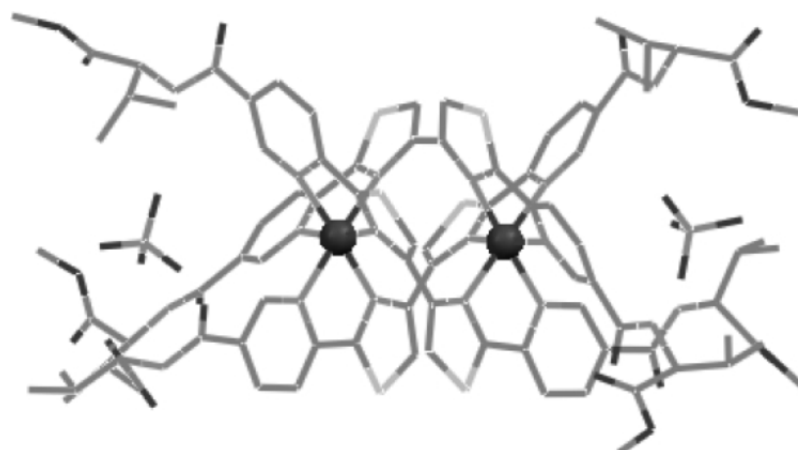


**Figure 3.8:** Crystal structure of the complex cation  $[\text{Co}_2(\text{L}^1)_3](\text{ClO}_4)_2^{2+(26)}$

The amide-containing “arms” of this complex formed an anion binding pocket which encapsulated perchlorate anions. As shown in the crystal structure, a perchlorate anion has been encapsulated within each of the two self-assembled cavities at either end of the complex.

Another example of self-assembled anion receptors includes Beer’s work.<sup>10, 31</sup> With the use of 2,2'-bipyridine-substituted ligands and the incorporation of the metal cation ruthenium (II), Beer showed that with the formation of the multiple complexes achieved, in turn resulted in good anion receptors. As shown in Figure 3.9, when the ligand 5,5'-diamido-2,2'-bipyridine is reacted with RuCl<sub>3</sub>, the ligand coordinates the metal ion which results in a distorted octahedral geometry around the metal centre.

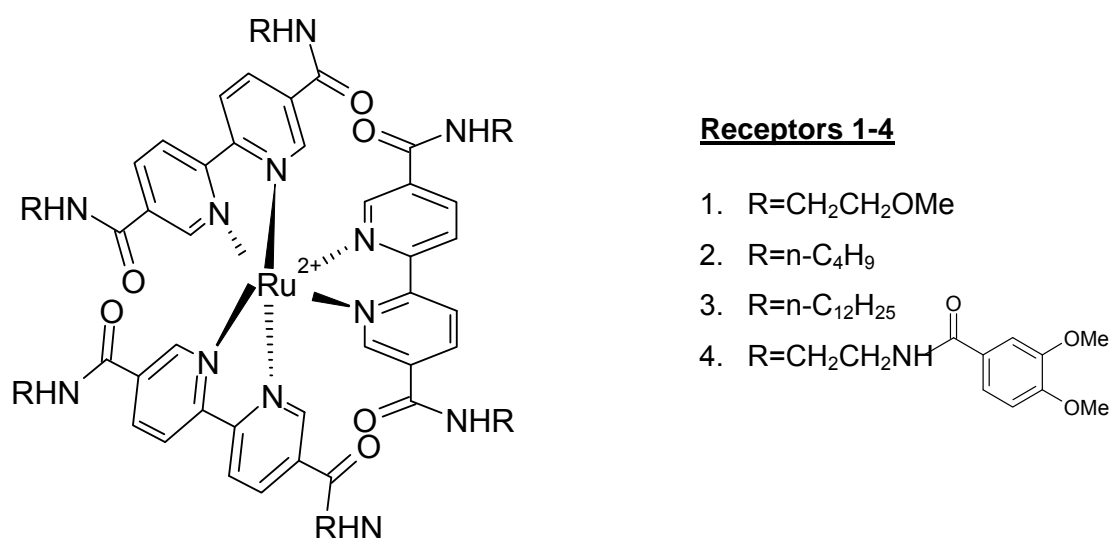


**Figure 3.9:** The structure of 2,2'-bipyridine substituted ligand and Ru(II) showing the coordination and distorted octahedral geometry<sup>33</sup>

By achieving this geometry, the complex has produced a C<sub>3</sub>-symmetric cavity containing three amide functional groups at each end of the molecule. Each of these cavities is capable of forming hydrogen bonds to anions.

UV-vis spectroscopic anion titrations were performed by adding various chloride and nitrate salts to the anion receptors 1-4. The selectivity of these assembled anion receptors were shown to be extremely dependant on both the nature of the substituent present on the amide groups and the solvent medium.

## 3.2 Aims

The aim of this chapter was to synthesise ligands which are capable of binding anions and to explore their coordination chemistry and anion binding potential. The desired ligands contain a mixture of N-donor domains, capable of coordination of transition metal ions, and amide functional groups which will interact with anions.

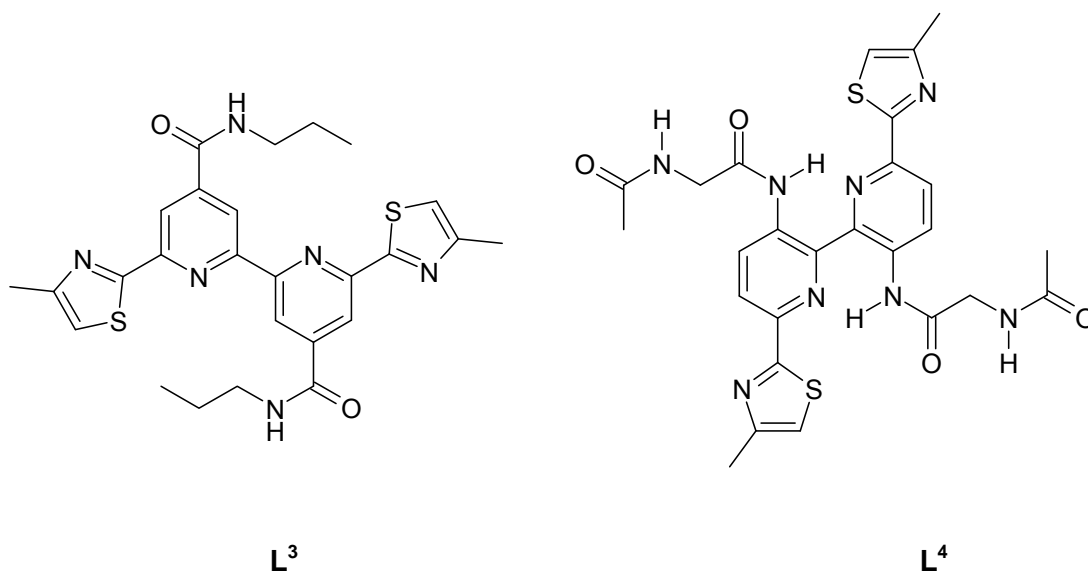


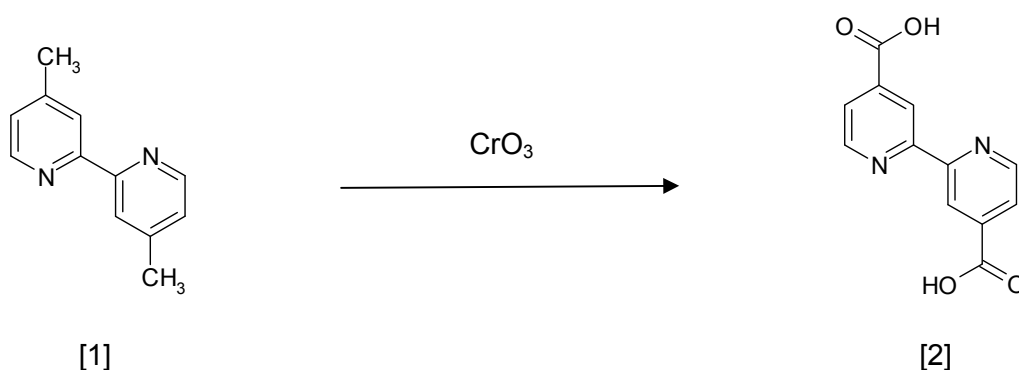
Figure 3.10: Structures of target ligands L<sup>3</sup> and L<sup>4</sup>

### 3.3 Experimental

#### 3.3.1 Ligand synthesis ( $L^3$ )

Compound **[1]** was purchased and used as received; compound **[2]** was prepared according to literature methods.<sup>32,33</sup>

##### 3.3.1.1 Synthesis of 2,2'-bipyridine-4,4'-dicarboxylic acid, [2]

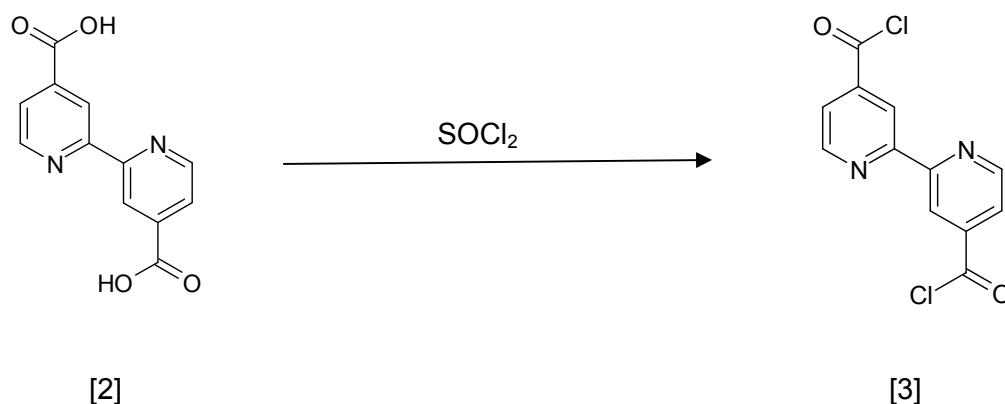


To a round bottom flask charged with **[1]** (1 g, 0.54 mmol) was added sulfuric acid (conc., 20 mL) and the reaction was cooled to 0° C. Chromium (VI) oxide (3.25 g, 0.03 mmol) was added with stirring over a 1 hr period. The reaction was stirred at 75° C for 4 hrs, then at room temperature overnight. After this time the reaction was poured over ice (40 mL) and after stirring for half an hour a light green precipitate formed. The precipitate was filtered and washed with  $H_2O$  (2 x 10 mL) giving a green solid.

The solid was suspended in  $H_2O$  (40 mL) with potassium hydroxide (0.05 g, 0.89 mmol) added with stirring, to achieve a pH above 7. The solution was filtered and an aliquot of conc. HCl added to achieve a pH below 7. Filtration followed by washing with  $H_2O$  (2 x 10 mL), MeOH (2 x 10 mL) and  $Et_2O$  (2 x 10 mL) gave **[2]** as a grey solid (1.21g, 92%).

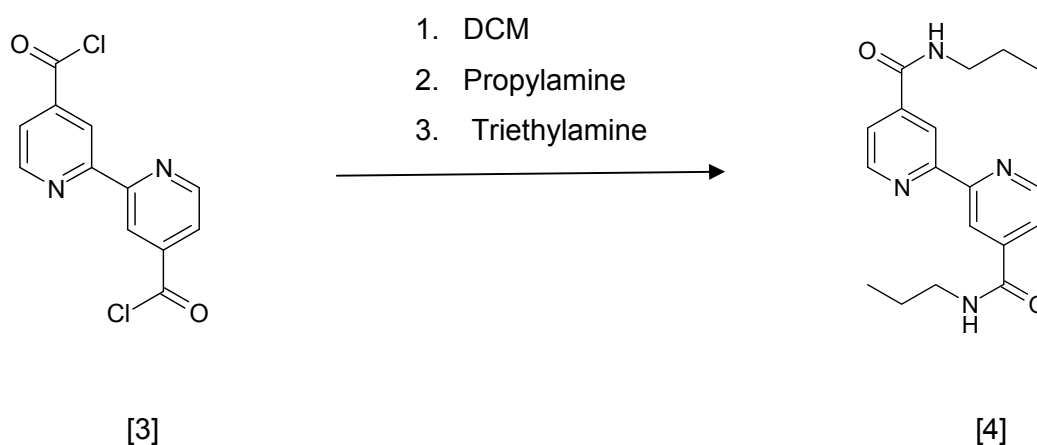
$^1H$  NMR (400 MHz,  $d_6$ -DMSO)  $\delta$  13.85 (s, br, 2H, COOH), 8.92 (d, 2H, py,  $J = 4.92$ ), 8.85 (s, 2H, py), 7.92 (dd, 2H, py,  $J = 4.94, 1.54$  Hz). The signal at 8.85 ppm should be a doublet but, in common with the NMR spectra for some subsequent steps, the *meta*-coupling is not observed and the signal appears as a singlet. High res. ESI-MS found  $m/z$  267.0380  $C_{12}H_8N_2O_4Na_1$  ( $[M+Na]^+$ ) requires  $m/z$  267.0376.<sup>32, 33</sup>

### 3.3.1.2 Synthesis of 2,2'-bipyridine-4,4'-dicarbonyl dichloride, [3]



To a round bottom flask charged with **[2]** (0.5 g, 0.21 mmol) was added thionylchloride (1 mL). The reaction was stirred at 85°C for 16 hrs after which time removal of the thionyl chloride *in vacuo* gave a beige solid (0.4 g, 69%). Further reaction of **[3]** was carried out immediately without purification or characterisation due to its hydrolytic susceptibility.

### 3.3.1.3 Synthesis of bis-N-propyl- 2,2'-bipyridine-4,4'-dicarboamide, [4]

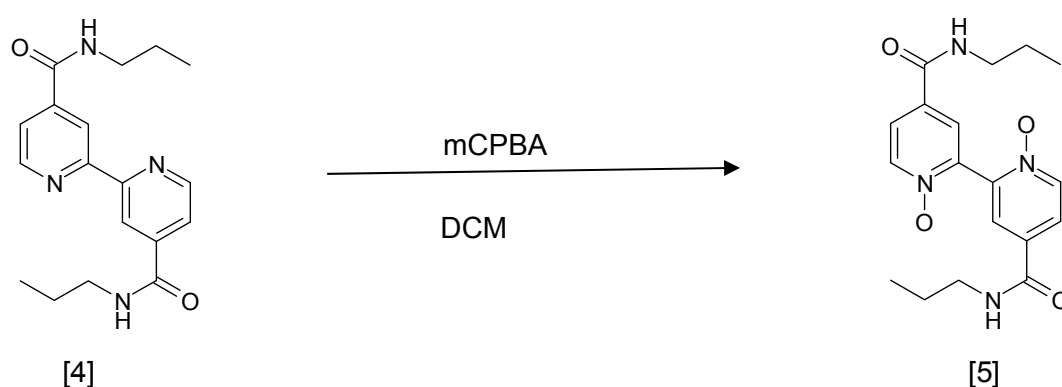


A solution of **[3]** (1.5 g, 0.53 mmol) and anhydrous DCM (15 mL) was cooled to 0° C, after which time propylamine (0.5 mL, 6.08 mmol) and triethylamine (0.6 mL, 4.32

mmol) were added slowly with stirring over half an hour. Filtration followed by washing with (DCM 2 x 10 mL) gave a light pink solid (1.20 g, 69%).

$^1\text{H}$  NMR (400 MHz,  $d_6$ -DMSO)  $\delta$  8.97 (t, 2H, NH,  $J = 5.54$ ), 8.87 (d, 2H, py,  $J = 5.00$ ), 8.79 (s, 2H, py), 7.86 (dd, 2H, py,  $J = 5.02, 1.70$ ), 3.27 (dt, overlap, 4H,  $J = 5.44$ ), 1.57 (tq, overlap, 4H,  $J = 7.20$ ), 0.92 (t, 6H,  $J = 7.40$  Hz). High res. ESI-MS found  $m/z$  327.1854  $\text{C}_{18}\text{H}_{23}\text{N}_4\text{O}_2$  ( $[\text{M}+\text{H}]^+$ ) requires  $m/z$  327.1856.

#### 3.3.1.4 Synthesis of bis-N-propyl-2,2'-bipyridine-N,N-dioxide-4,4'-dicarboamide, [5]

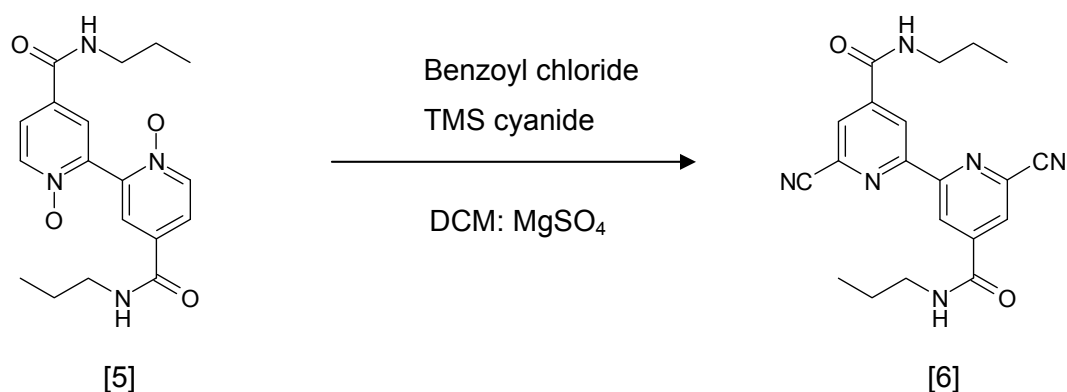


To a round bottom flask charged with [4] (0.10 g, 0.31 mmol) was added 10% MeOH in DCM (50 mL) and the reaction was stirred at room temperature. To this was added mCPBA (77%, 0.21 g, 1.22 mmol) and the reaction was stirred at room temperature for 4-6 weeks. The reaction was monitored by TLC and upon completion purification *via* column chromatography (10% MeOH in DCM,  $\text{Al}_2\text{O}_3$ ) gave [5] as a white solid (0.058 g, 53%).

$^1\text{H}$  NMR (400 MHz,  $d_6$ -DMSO)  $\delta$  8.76 (t, 2H, NH,  $J = 5.52$ ), 8.50 (d, 2H, py,  $J = 6.84$ ), 8.15 (d, 2H, py,  $J = 2.52$ ), 7.98 (dd, 2H, py,  $J = 6.84, 2.68$ ), 3.23 (dt, 4H,  $J = 6.20$ ), 1.53 (tq, 4H,  $J = 7.08$ ), 0.90 (t, 6H,  $J = 7.40$  Hz). High res. ESI-MS found  $m/z$  359.1701  $\text{C}_{18}\text{H}_{23}\text{N}_4\text{O}_4$  ( $[\text{M}+\text{H}]^+$ ) requires  $m/z$  359.1714.

### 3.3.1.5 Synthesis of bis-N-propyl-2,2'-bipyridine-4,4'-dicarboamide-6,6'-carbonitrile

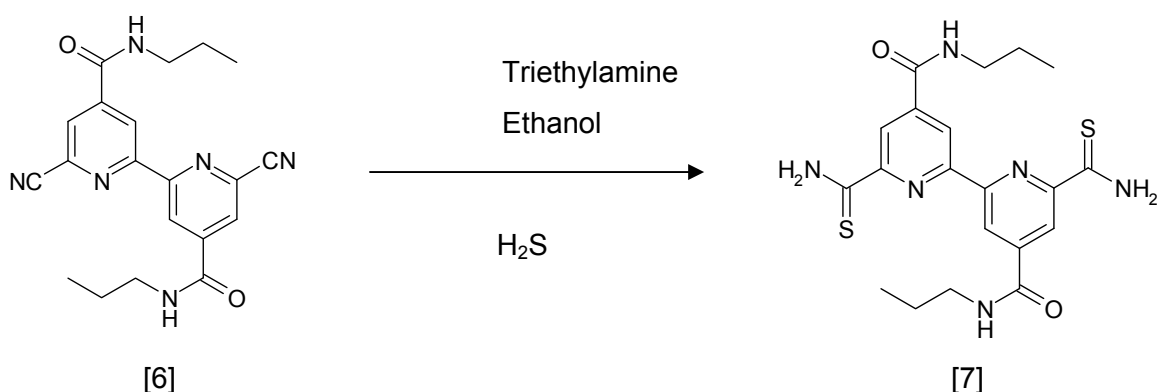
**[6]**



A solution of **[5]** (0.058 g, 0.16 mmol), benzoyl chloride (0.2 mL, 1.72 mmol) and trimethylsilylcyanide (0.2 mL, 1.50 mmol) in anhydrous DCM (20 mL) was refluxed for 16 hrs, during which time a solid precipitated. Filtration followed by washing with anhydrous DCM (2 x 10 mL) gave a yellow solid (0.031 g, 52%).

<sup>1</sup>H NMR (400 MHz, d<sub>6</sub>-DMSO) δ 9.10 (t, 2H, NH, *J* = 5.52), 8.91 (d, 2H, py, *J* = 1.48), 8.47 (d, 2H, py, *J* = 1.52), 3.25 (dt, coincident with HOD peak), 1.57 (tq, overlap, 4H, *J* = 7.16), 0.87 (t, 6H, *J* = 7.40 Hz). High res. ESI-MS found *m/z* 377.1731 C<sub>20</sub>H<sub>21</sub>N<sub>6</sub>O<sub>2</sub> ([M+H]<sup>+</sup>) requires *m/z* 377.1721.

### 3.3.1.6 Synthesis of bis-N-propyl-2,2'-bipyridine bis-thioamide-4,4'-dicarboamide, [7]

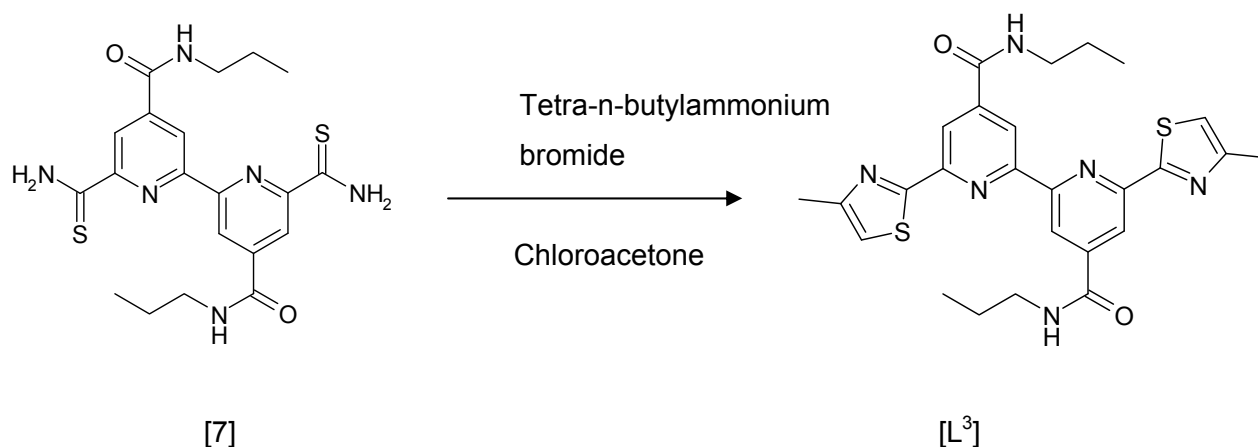


A solution of **[6]** (0.05 g, 0.13 mmol) and triethylamine (10 mL) in EtOH (10 mL) was placed in a flask and H<sub>2</sub>S was slowly bubbled through the solution for 15 minutes,

during which time the solution turned yellow. The yellow solution was allowed to stand for 48 hrs during which time a yellow solid slowly precipitated. Collection via filtration gave bis-N-propyl-2,2'-bipyridine bis-thioamide-4,4'-dicarboamide **[7]** as a yellow solid (0.03 g, 51%).

$^1\text{H}$  NMR (400 MHz,  $d_6$ -DMSO)  $\delta$  10.51 (s, 2H,  $\text{NH}_2$ ), 10.30 (s, 2H,  $\text{NH}_2$ ), 9.19 (d, 2H, py,  $J = 1.44$ ), 9.03 (t, 2H, NH,  $J = 5.64$ ), 8.94 (d, 2H, py,  $J = 1.48$ ), 3.31 (dt, coincident with HOD peak), 1.61 (tq, 4H,  $J = 7.16$ ), 0.94 (t, 6H,  $J = 7.36$  Hz). High res. ESI-MS found  $m/z$  445.1479  $\text{C}_{20}\text{H}_{25}\text{N}_6\text{O}_2\text{S}_2$  ( $[\text{M}+\text{H}]^+$ ) requires  $m/z$  445.1475.

### 3.3.1.7 Synthesis of $\text{L}^3$

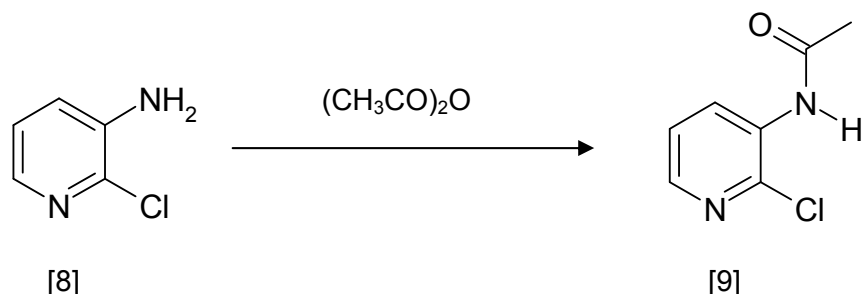


To a round bottom flask charged with **[7]** (0.02 g, 0.038 mmol) and tetra-*n*-butylammonium bromide (0.5 g, 1.35 mmol) was added EtOH (25 mL) and chloroacetone (1 mL) and the reaction was heated at 90°C and left to stir for 4 hrs. A yellow solid slowly precipitated out and the precipitate was filtered and washed with EtOH (2 x 10 mL) and Et<sub>2</sub>O (2 x 10 mL). The yellow solid was suspended in aqueous ammonia (10 mL) for 10 hrs. Filtration followed by washing with H<sub>2</sub>O (2 x 10 mL), EtOH (2 x 10 mL) and Et<sub>2</sub>O (2 x 10 mL) gave ligand  $\text{L}^3$  as a yellow solid (0.017 g, 81%).

$^1\text{H}$  NMR (400 MHz,  $d_6$ -DMSO)  $\delta$  9.19 (t, 2H, NH,  $J = 4.60$ ), 8.84 (d, 2H, py,  $J = 1.19$ ), 8.57 (d, 2H,  $J = 1.11$ ), 7.58 (s, 2H, th), 3.30 (dt, coincident with HOD peak), 1.60 (tq, overlap, 4H,  $J = 5.78$ ), 1.09 (dt, 6H,  $J = 14.08, 5.58$ ,  $\text{CH}_3$ ), 0.96 (t, 6H,  $J = 5.92$  Hz,  $\text{tz-CH}_3$ ). High res. ESI-MS found  $m/z$  521.1767  $\text{C}_{26}\text{H}_{29}\text{N}_6\text{O}_2\text{S}_2$  ( $[\text{M}+\text{H}]^+$ ) requires  $m/z$  521.1788.

### 3.3.2 Ligand synthesis ( $L^4$ )

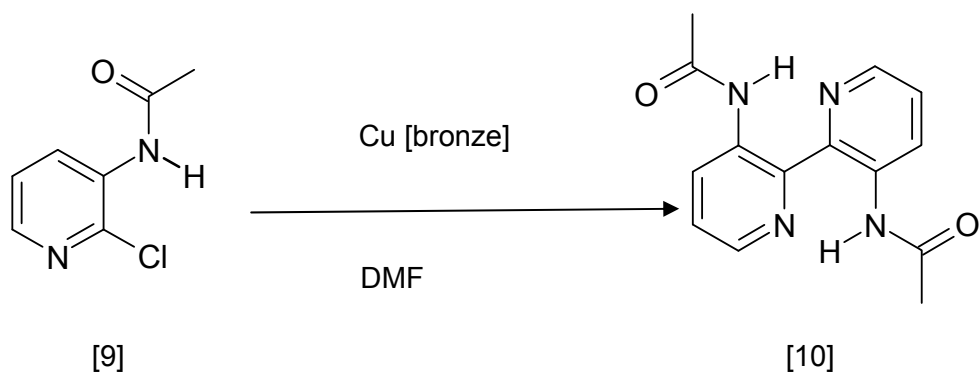
#### 3.3.2.1 Synthesis of 2-chloro-3-acetylamidopyridine, [9]



To a round bottom flask charged with 3-amino-2-chloropyridine **[8]** (0.70 g, 5.49 mmol) was added acetic anhydride (10 mL) and the reaction was allowed to stir for 24 hrs. Removal of the solvent by rotary evaporation gave the product as a clear oil, resulting in **[9]** as a beige crystalline solid upon cooling (0.90 g, 97%).

$^1H$  NMR (500 MHz,  $CDCl_3$ )  $\delta$  9.10 (dd, 1H,  $J = 8.4, 1.57$ , py), 8.13 (dd, 1H,  $J = 4.5, 1.55$ ), 7.30 (d, 1H,  $J = 8.4, 4.5$  Hz, py), 7.1 (s, 1H, -CONH). High res. ESI-MS found  $m/z$  171.0316  $C_7H_8N_2O_1Cl_1$  ( $[M+H]^+$ ) requires  $m/z$  171.0320.<sup>32, 33</sup>

#### 3.3.2.2 Synthesis of 2,2'-bipyridine-3,3'-diacetamide, [10]



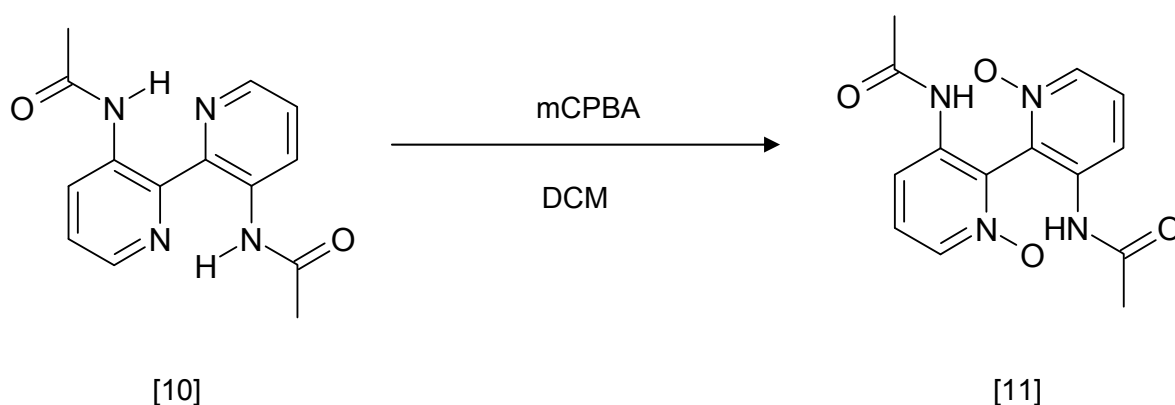
Under an atmosphere of nitrogen, a 250 mL two neck round bottom flask was charged with **[9]** (3.5 g, 0.02 mmol) and copper bronze (3.5 g, 0.06 mmol) and dimethylformamide (20 mL) was added. The reaction was stirred at 80 °C for 16 hrs then cooled to 0 °C and poured over ice (100 mL). The cold solution was filtered through a sintered glass funnel charged with celite then washed with  $NH_3$  (aq.) (200

mL) giving a turquoise solid. The solid was dried and the product was extracted with DCM (5 x 50 mL) giving **[10]** as a yellow solid (1.4 g, 25%).

$^1\text{H}$  NMR (500 MHz,  $\text{CDCl}_3$ )  $\delta$  13.17 (s, 2H, NH), 9.12 (dd, 2H, py,  $J = 8.54, 1.60$ ), 8.36 (dd, 2H, py,  $J = 4.58, 1.60$ ), 7.40 (dd, 2H, py,  $J = 8.20, 4.60$  Hz), 2.26 (s, 6H,  $\text{CH}_3$ ). High res. ESI-MS found  $m/z$  271.1193  $\text{C}_{14}\text{H}_{15}\text{N}_4\text{O}_2$  ( $[\text{M}+\text{H}]^+$ ) requires  $m/z$  271.1190.<sup>32</sup>

33

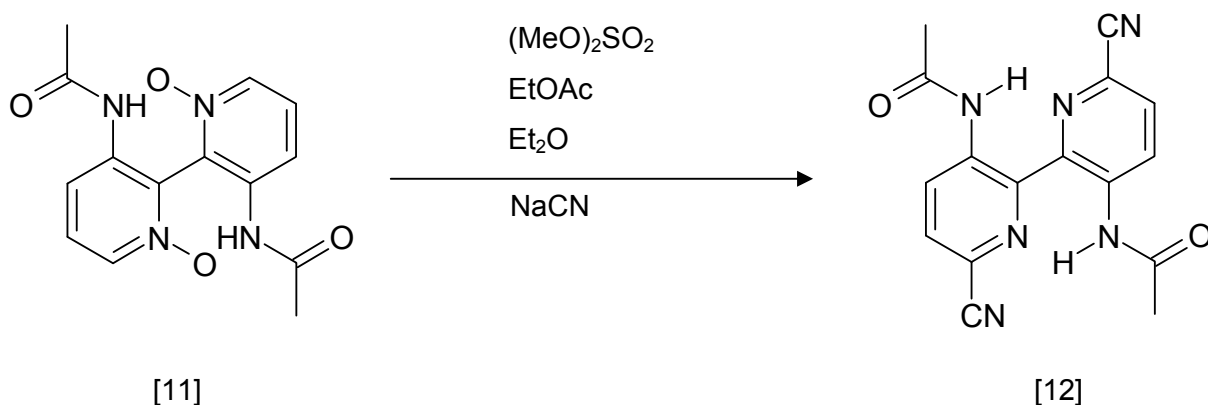
### 3.3.2.3 Synthesis of 3,3'-diacetylamino-2,2'-bipyridine-*N,N*-dioxide, **[11]**



To a solution of **[10]** (0.25 g, 0.92 mmol) in DCM (50 mL) was added *m*CPBA (77%, 0.61 g, 2.76 mmol) and the reaction monitored by TLC (5% MeOH/ $\text{CH}_2\text{Cl}_2$ ,  $\text{Al}_2\text{O}_3$ ) over a period of 1 week. During this time the starting material disappeared and an intermediate spot appeared (presumably the mono-*N*-oxide). After this intermediate spot was consumed, which was facilitated by the addition of more *m*CPBA if necessary, the reaction was reduced in volume and the resulting solution purified by column chromatography (5% MeOH/ $\text{CH}_2\text{Cl}_2$ ,  $\text{Al}_2\text{O}_3$ ) giving the bis-*N,N*-dioxide **[11]** (0.18 g, 65%) as a white solid.

$^1\text{H}$  NMR (500 MHz,  $\text{CDCl}_3$ )  $\delta$  9.41 (s, 2H, NH), 8.15 (d, 2H,  $J = 6.4$  Hz, py), 7.66 (d, 2H,  $J = 8.4$  Hz), 7.46 (dd, 2H,  $J = 6.5, 8.4$  Hz, py), 1.84 (s, 3H,  $-\text{CH}_3$ ). High res. ESI-MS found  $m/z$  303.1093  $\text{C}_{14}\text{H}_{15}\text{N}_4\text{O}_4$  ( $[\text{M}+\text{H}]^+$ ) requires  $m/z$  303.1088.

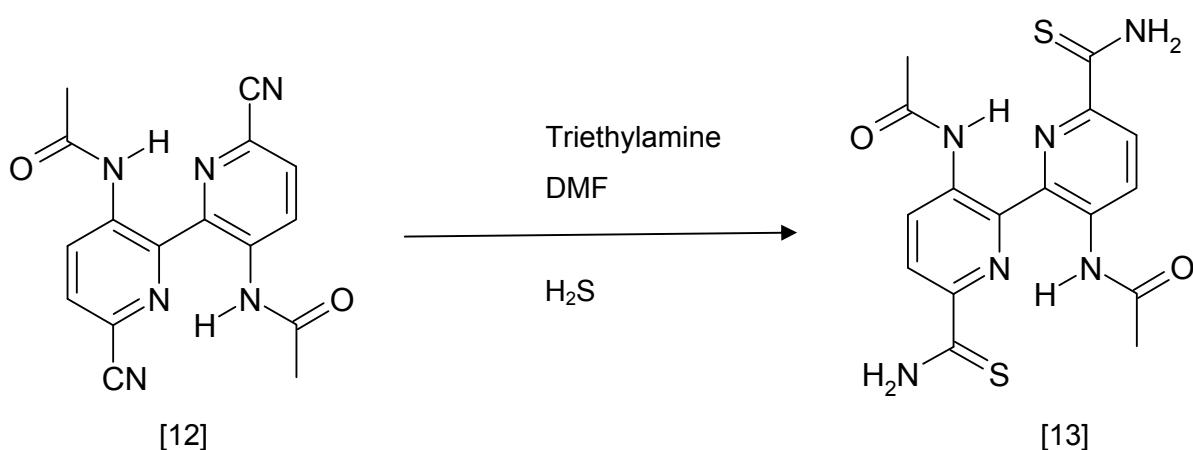
### 3.3.2.4 Synthesis of 3,3'-diacetylamino-6,6'-dicyano-2,2'-bipyridine, [12]



To a 50ml round bottomed flask charged with the bis-*N,N*-dioxide [11] (0.25 g, 0.83 mmol) was added enough (MeO)<sub>2</sub>SO<sub>2</sub> to completely cover the solid and the reaction heated at 80°C under nitrogen overnight. The reaction was then cooled and ethyl acetate (10 mL) and diether ether (30 mL) added sequentially. After leaving to stand for 24 hrs the organic solvents were removed by decanting and the resulting brown oil washed with Et<sub>2</sub>O (2 x 30 mL). The oil was then dissolved in water (25 mL) and neutralised with NaHCO<sub>3</sub>. To this was added a solution of NaCN (0.12 g, 2.49 mmol) in water (10mL) and the reaction stirred for 30 mins. The resulting precipitate was isolated by filtration and washed with water (2 x 15 mL) giving 3,3'-diacetylamino-6,6'-dicyano-2,2'-bipyridine [12] (0.19 g, 71%) as a cream solid.

<sup>1</sup>H NMR (500 MHz, DMSO-*d*<sub>6</sub>) δ 9.93 (s, 2H, NH), 8.57 (d, 2H, J = 8.6 Hz, py), 8.01 (brs, 2H, py), 1.98 (s, 6H, -CH<sub>3</sub>). High res. ESI-MS found *m/z* 343.0912 C<sub>16</sub>H<sub>12</sub>N<sub>6</sub>NaO<sub>2</sub> ([M+Na]<sup>+</sup>) requires *m/z* 343.0914.

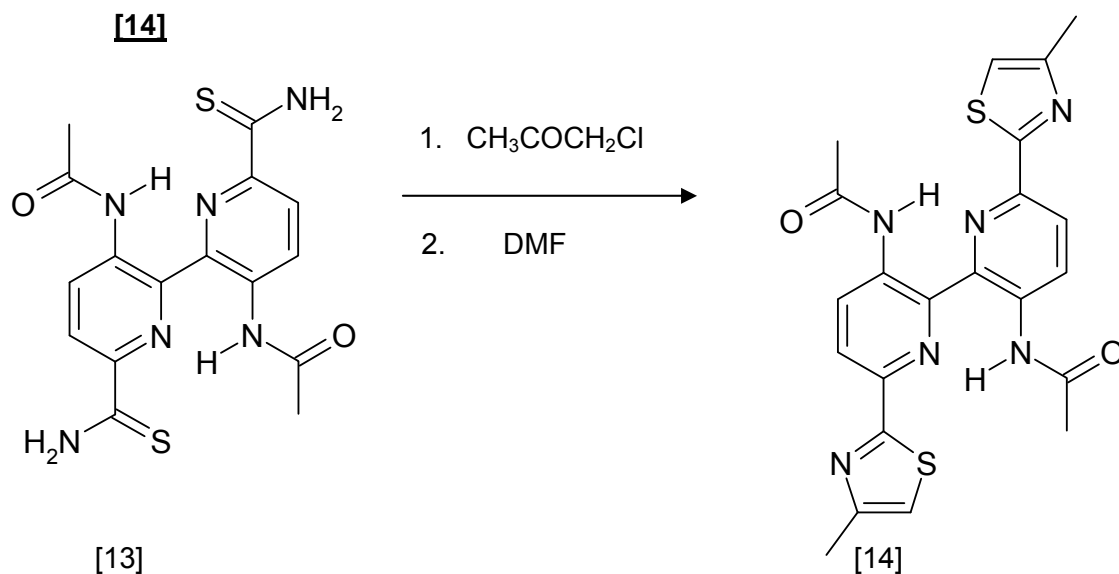
### 3.3.2.5 Synthesis of 3,3'-diacetylamino-6,6'-dithioamide-2,2'-bipyridine, [13]



A solution of the 6,6'-dicyano derivative **[12]** (0.10g, 0.31 mmol) was added to Et<sub>3</sub>N (0.5 mL) in DMF (25 mL), then H<sub>2</sub>S gas was bubbled through the reaction for 20 mins. The reaction was then sealed and allowed to stand for 2 days. After this time the reaction was concentrated (ca. 10 mL) and the resulting solid isolated by filtration, giving the 6,6'-dithioamide derivative **[13]** (0.08 g, 66%) as a yellow solid.

<sup>1</sup>H NMR (500 MHz, DMSO-*d*<sub>6</sub>) δ 10.48 (s, 2H, CONH), 10.15 (s, 2H, CSNH<sub>2</sub>), 9.75 (s, 2H, CSNH<sub>2</sub>), 8.65 (d, 2H, J = 8.7 Hz, py), 8.46 (d, 2H, J = 8.7 Hz, py), 2.03 (s, 6H, -COCH<sub>3</sub>). High res. ESI-MS found *m/z* 389.0846 C<sub>16</sub>H<sub>17</sub>N<sub>6</sub>O<sub>2</sub>S<sub>2</sub> ([M+H]<sup>+</sup>) requires *m/z* 389.0849.

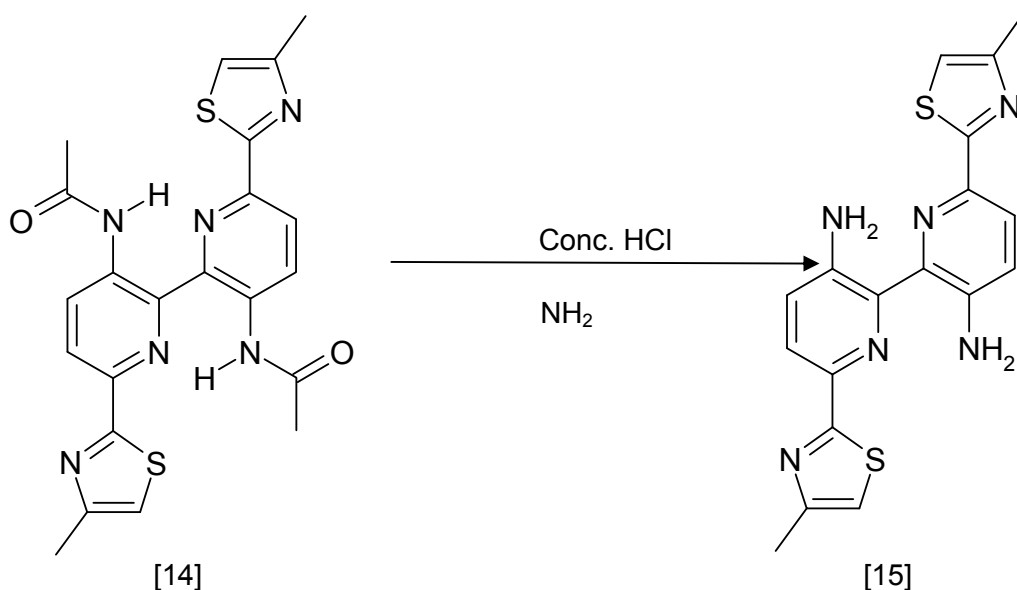
### 3.3.2.6 Synthesis of 3,3'-diacetylamino-6,6'-bis(4-methylthiazol-2-yl)-2,2'-bipyridine, [14]



To a solution of 3,3'-diacetylamino-6,6'-dithioamide-2,2'-bipyridine **[13]** (0.1 g, 0.25 mmol) in DMF (10 mL) was added chloroacetone (0.1 mL) and the reaction heated at 80°C. After 4 hrs the resulting precipitate was isolated by filtration, washed with EtOH (2 x 10 mL) and Et<sub>2</sub>O (2 x 10 mL), giving **[14]** (0.09 g, 77%) as a pale yellow solid.

<sup>1</sup>H NMR (500 MHz, DMSO-*d*<sub>6</sub>) δ 10.44 (s, 2H, NH), 8.76 (d, 2H, J = 8.7 Hz, py), 8.18 (d, 2H, J = 8.7 Hz, py), 7.41 (s, 2H, tz), 2.47 (s, 3H, tz-CH<sub>3</sub>), 2.08 (s, 3H, -COCH<sub>3</sub>). High res. ESI-MS found *m/z* 465.1171 C<sub>22</sub>H<sub>21</sub>N<sub>6</sub>O<sub>2</sub>S<sub>2</sub> ([M+H]<sup>+</sup>) requires *m/z* 465.1162.

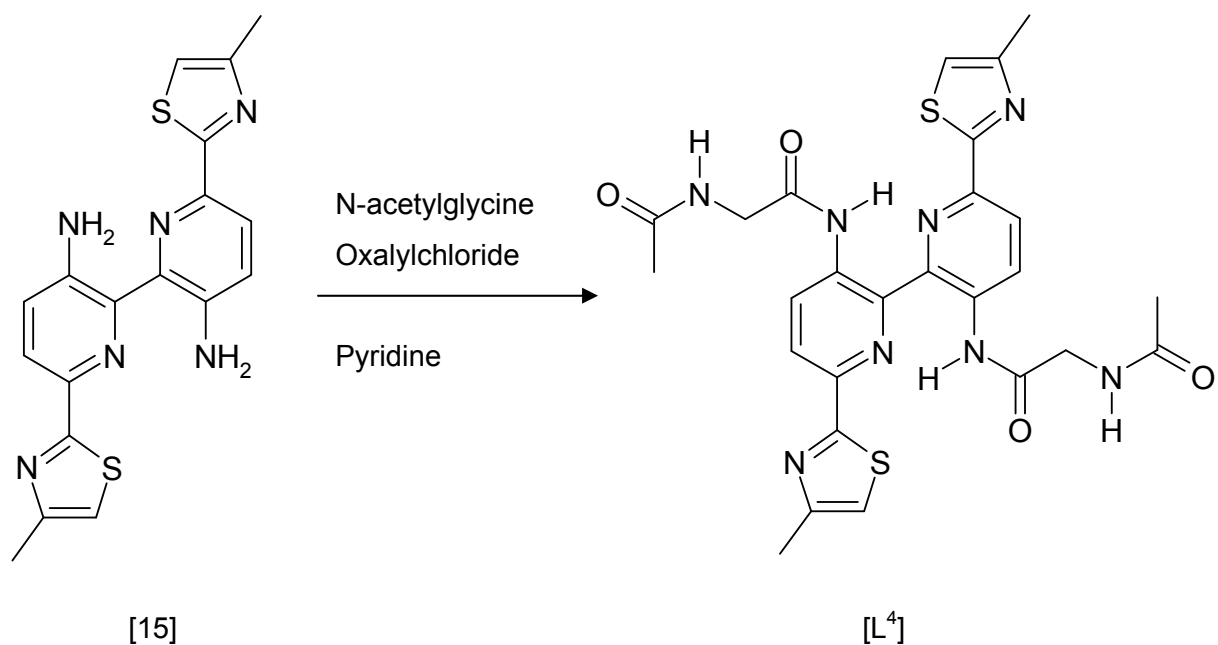
### 3.3.2.7 Synthesis of 3,3'-diamino-6,6'-bis(4-methylthiazol-2-yl)-2,2'-bipyridine, [15]



To a 50 mL round bottom flask charged with the 3,3'-diacetylamino derivative **[14]** (0.1 g, 0.21 mmol) was added HCl (conc, 25 mL) and the reaction refluxed for 3 hrs. After this time the solution was poured into water (50 mL) and the resulting orange precipitate isolated by filtration. This solid was then suspended in NH<sub>3</sub>(conc.) overnight during which time the colour changed from orange to yellow. Filtration and washing with H<sub>2</sub>O (2 x 10 mL), EtOH (2 x 10 mL) and Et<sub>2</sub>O (2 x 10 mL) gave **[15]** (0.05 g, 63%) as a bright yellow solid.

<sup>1</sup>H NMR (500 MHz, DMSO-*d*<sub>6</sub>) δ 7.90 (d, 2H, J = 8.55 Hz, py), 7.77 (brs, 4H, -NH<sub>2</sub>), 7.35 (d, 2H, J = 8.55 Hz, py), 7.26 (s, 2H, tz), 2.43 (s, 6H, tz-CH<sub>3</sub>). High res. ESI-MS found *m/z* 381.0962 C<sub>18</sub>H<sub>17</sub>N<sub>6</sub>S<sub>2</sub> ([M+H]<sup>+</sup>) requires *m/z* 381.0951.

### 3.3.2.8 Synthesis of L<sup>4</sup>



To a round bottom flask charged with N-acetylglycine (0.068 g, 0.57 mmol) was added anhydrous pyridine (50 mL) and the reaction was cooled to 0°C. Oxalylchloride solution (0.3 mL, 2.0M in methylene chloride) was added drop wise to the reaction and stirred at room temperature for 1 hr. Compound **[15]** (0.028 g, 0.074 mmol) was added to the reaction and left to stir at room temperature for 72 hrs, after which time a yellow precipitate formed. The precipitate was filtered and washed with EtOH (2 x 10 mL) and Et<sub>2</sub>O (2 x 10 mL) giving ligand **L<sup>4</sup>** as a yellow solid. The ligand was

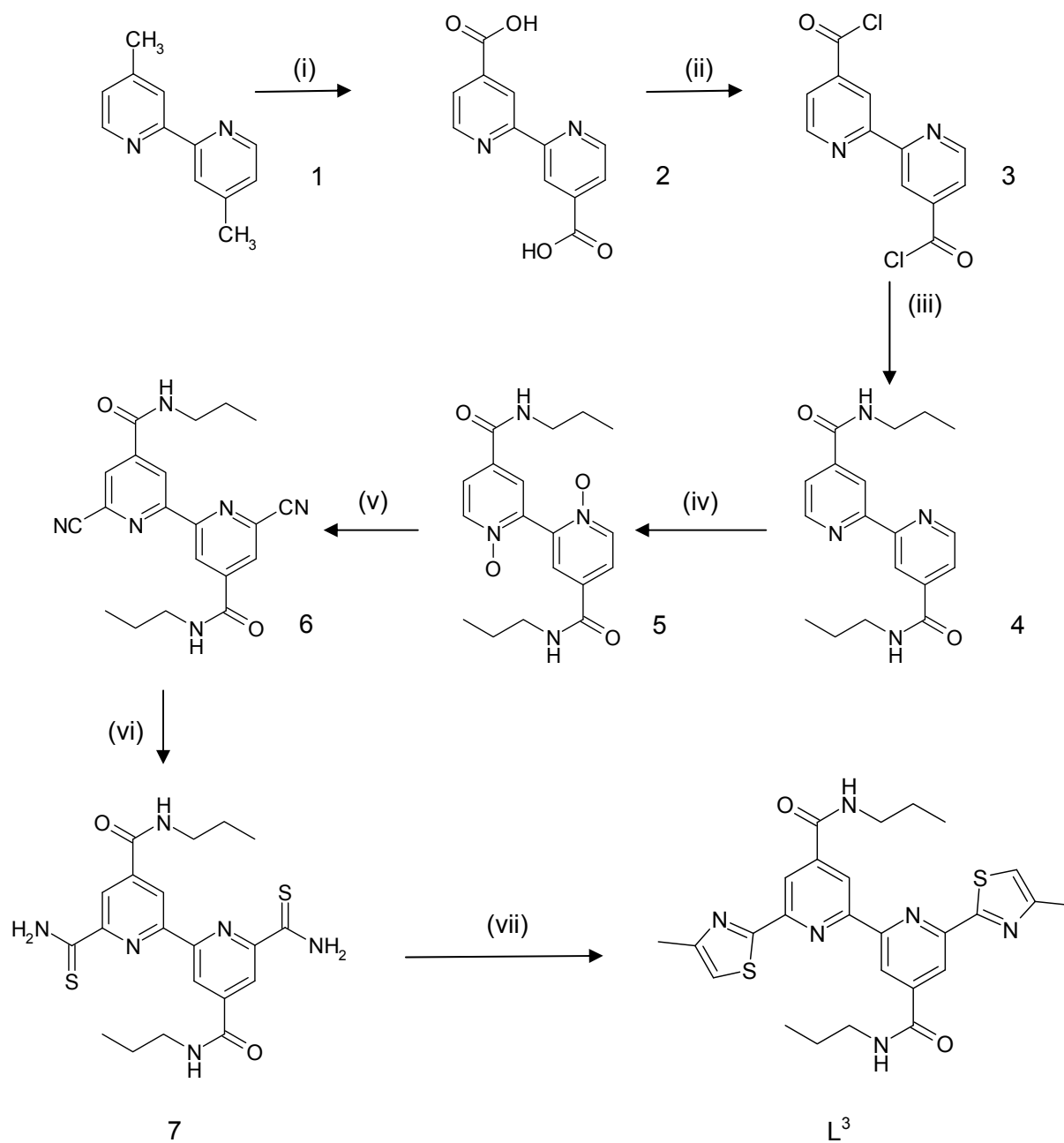
suspended in H<sub>2</sub>O (20 mL), sonicated, refiltered and washed with EtOH (2 x 10 mL) and Et<sub>2</sub>O (2 x 10 mL) giving ligand **L**<sup>4</sup> as an orange solid (0.009g, 21%).

<sup>1</sup>H NMR (500 MHz, d<sub>6</sub>-DMSO) δ 10.28 (s, 2H, ar-NH), 8.78 (d, 2H, *J* = 8.75, py), 8.21 (d, 2H, *J* = 8.75, py), 8.20 (t, 2H, *J* = 5.5, NH), 7.43 (s, 2H, tz<sup>3</sup>), 3.84 (d, 4H, *J* = 5.5 Hz), 2.47 (s, 6H, -COCH<sub>3</sub>), 1.67 (s, 6H, tz-CH<sub>3</sub>). High res. ESI-MS found *m/z* 579.1619 C<sub>26</sub>H<sub>27</sub>N<sub>8</sub>O<sub>4</sub>S<sub>2</sub> ([M+H]<sup>+</sup>) requires *m/z* 579.1591.

### 3.4 Results and Discussion

#### 3.4.1 Results and Discussion – **L**<sup>3</sup>

The synthesis of the ligand **L**<sup>3</sup> was performed using a seven-step linear synthesis (Scheme 3.1). Structural elucidation was performed at each step of the synthesis using <sup>1</sup>H NMR and mass spectrometry.



**Scheme 3.1:** Synthesis of L<sup>3</sup> from 4,4'-dimethyl-2,2'-bipyridine [1]. Reagents and conditions: (i) sulfuric acid, CrO<sub>3</sub>, 75°C, 4 hrs (ii) thionylchloride, 85°C, 16 hrs (iii) DCM, 0°C, propylamine, triethylamine, RT, 30 mins (iv) DCM, mCPBA, RT, 4-6 weeks (v) benzoyl chloride, TMS cyanide, anhydrous DCM, reflux, 16 hrs (vi) triethylamine, ethanol, H<sub>2</sub>S (vii) tetra-n-butylammonium bromide, chloroacetone, 90°C, 4 hrs

As stated earlier, the first two steps within this synthesis were performed using previous literature methods, therefore **[3]** was reacted with triethylamine and propylamine in DCM at 0°C for half an hour. Filtration followed to produce a pale pink solid **[4]**.

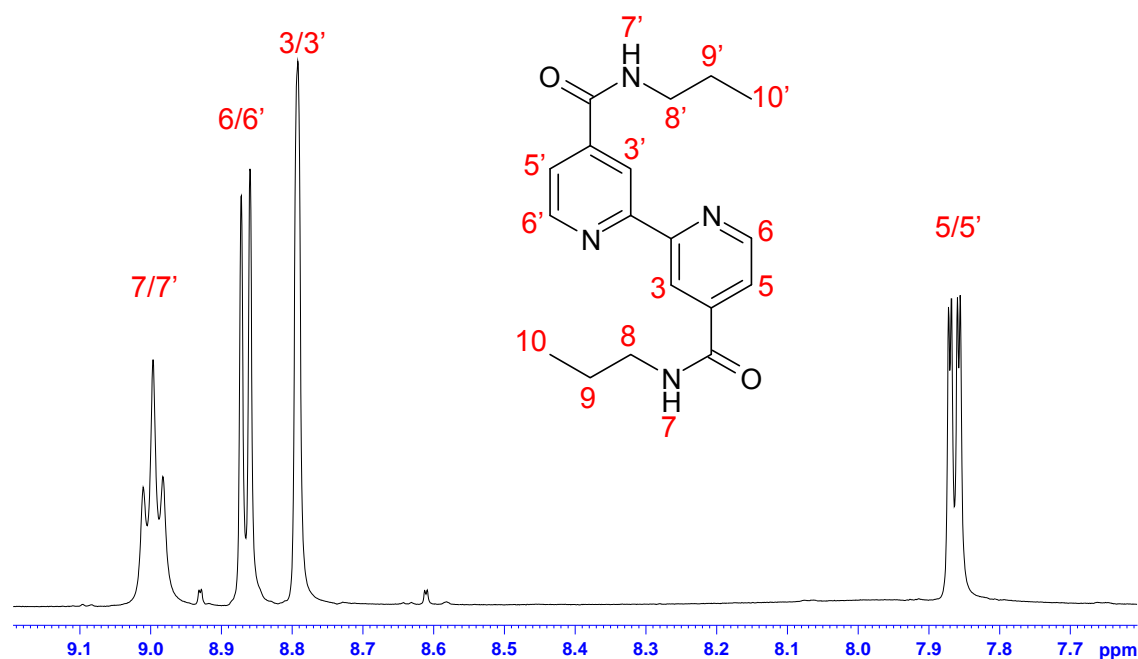


**Figure 3.11:** Aromatic region of the <sup>1</sup>H NMR (d<sub>6</sub>-DMSO) spectrum of **[4]**

Three peaks are expected in the aromatic region excluding the peak relating to the NH groups. The <sup>1</sup>H NMR spectrum shown in Figure 3.11 shows two doublet aromatic signals and a doublet of doublets aromatic signal. These represent the hydrogens labelled 3/3', 5/5' and 6/6' on the bipyridine ring.

To achieve the bis-N-oxidation of **[4]**, the complex was allowed to stand in DCM with an excess of mCPBA for a period of 4-6 weeks. The reaction was monitored during this time using TLC. Once the bis-N-oxidation had gone to completion the product **[5]** was purified by column chromatography to give a white solid.

Structural elucidation of **[5]** was performed using <sup>1</sup>H NMR. The structure of the ligand is symmetrical and therefore there are only 7 different hydrogen environments. The spectrum, as shown in Figure 3.12 reveals two doublet aromatic signals at δ 8.47 and 8.12 and a doublet of doublet aromatic signal at δ 7.94. These peaks represent the hydrogens labelled 3/3', 5/5' and 6/6' on the bipyridine ring, as also shown in Figure 3.12.

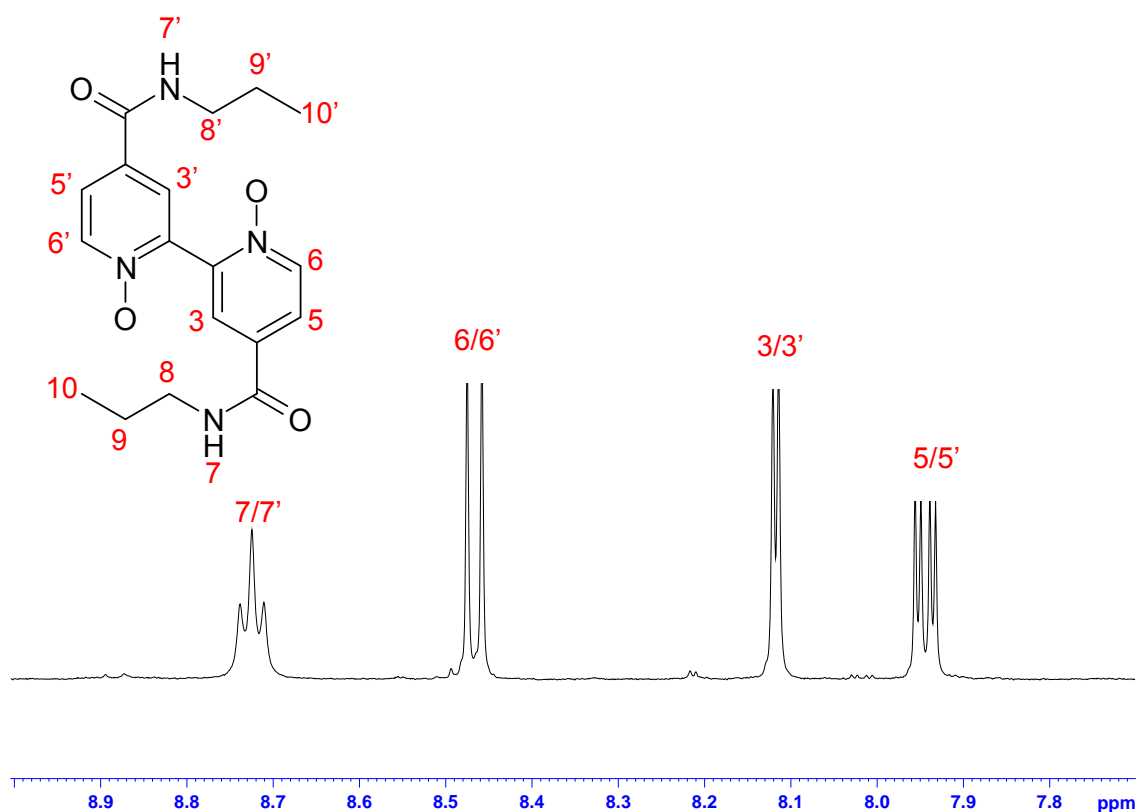


**Figure 3.12:** Aromatic region of the  $^1\text{H}$  NMR ( $d_6$ -DMSO) spectrum of **[5]**

The same number of signals is expected for the oxidation step as with step (iii). Comparisons between the spectrum of complex **[4]** shown in Figure 3.11 and the spectrum of the bis-N-oxidation product (Figure 3.12) showed that the three aromatic signals had shifted considerably which is due to the presence of the N-oxidised nitrogens, confirming completion of this step.

The spectrum also displayed three signals in the aliphatic region which are attributed to the aliphatic hydrogen atoms labelled 8/8', 9/9, and 10/10'.

The bis-N,N'-dioxide **[5]** was reacted with trimethylsilyl cyanide and benzoyl chloride under reflux in anhydrous DCM for 16 hours. This resulted in a yellow precipitate which, when isolated by filtration, gave a yellow solid **[6]**. The  $^1\text{H}$  NMR spectrum shown in Figure 3.13 shows two doublet aromatic signals which represent the hydrogens labelled 3/3' and 5/5' on the bipyridine ring.

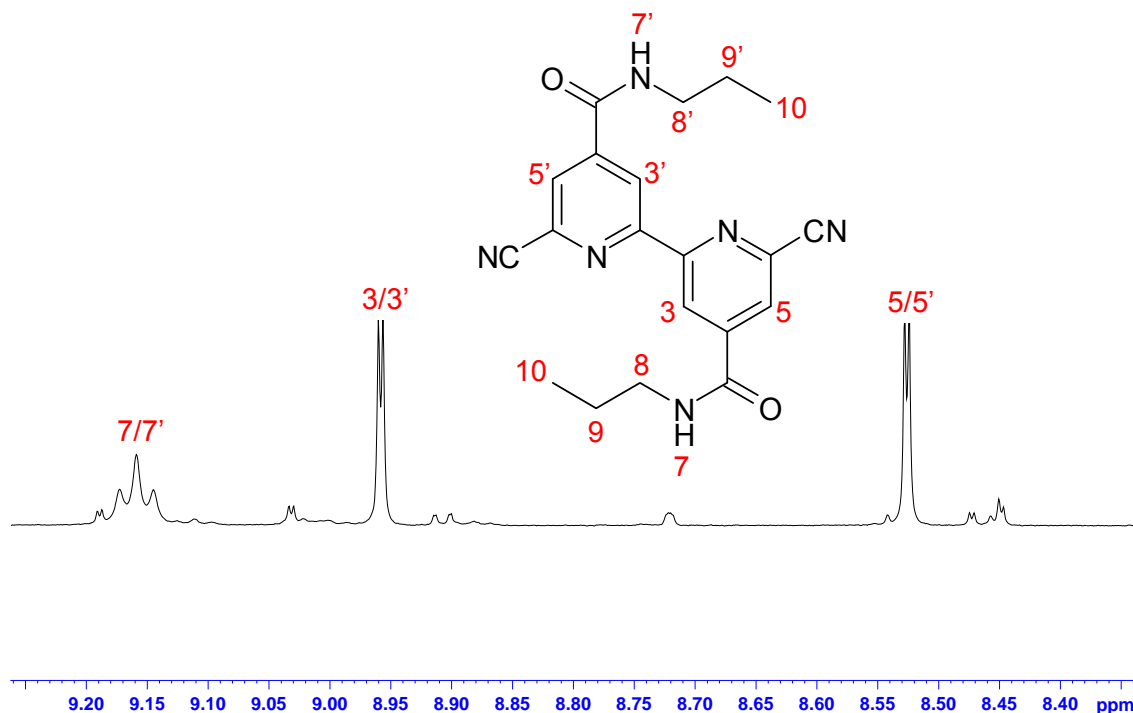


**Figure 3.13:** Aromatic region of the  $^1\text{H}$  NMR ( $d_6$ -DMSO) spectrum of **[6]**

The bis-thioamide **[7]** was produced as a yellow solid by purging hydrogen sulfide through a solution of **[6]** in ethanol in the presence of triethylamine. The appearance of two broad singlets (unresolved) corresponding to the thioamide at  $\delta$  10.34 and 10.09 in the  $^1\text{H}$  NMR spectrum (Figure 3.14) confirmed complete conversion of the nitrile derivative, as these peaks are indicative of thioamide formation.

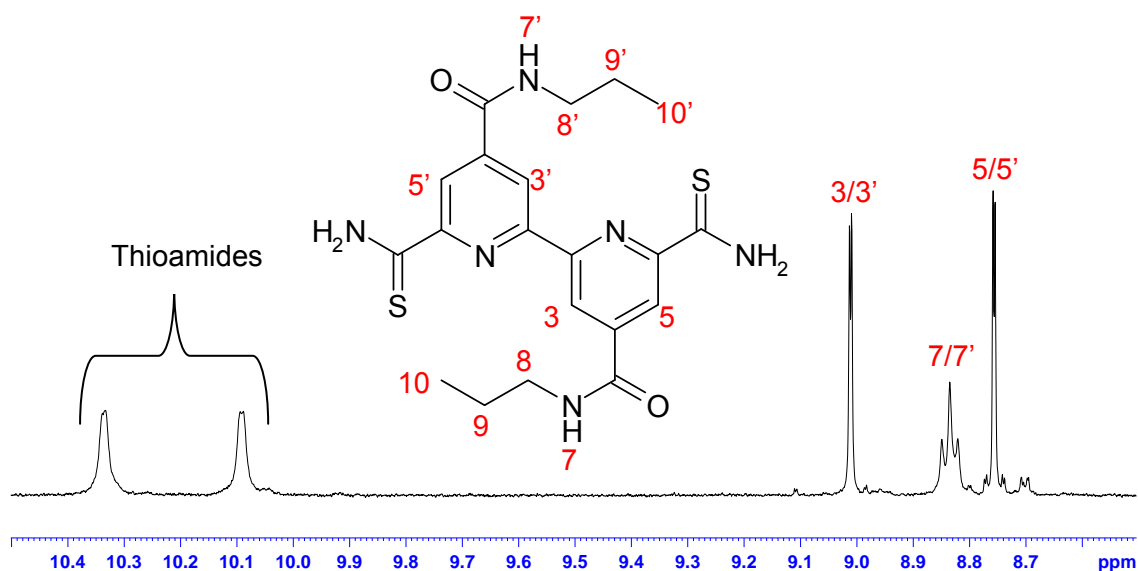


**Figure 3.14:** Aromatic region of the  $^1\text{H}$  NMR ( $d_6$ -DMSO) spectrum of product **[7]**

The spectrum also shows two doublet aromatic signals which represent the hydrogens labelled 3/3' and 5/5' on the bipyridine ring.

The resulting bis-thioamide derivative [7] was heated in ethanol in the presence of chloroacetone and tetra-n-butylammonium bromide at 90°C for a total of 4 hours. This resulted in a yellow precipitate and, when isolated by filtration, gave a yellow solid which in turn was allowed to stand in aqueous ammonia for 10 hours, before filtration gave the final desired ligand  $L^3$  as a yellow solid.

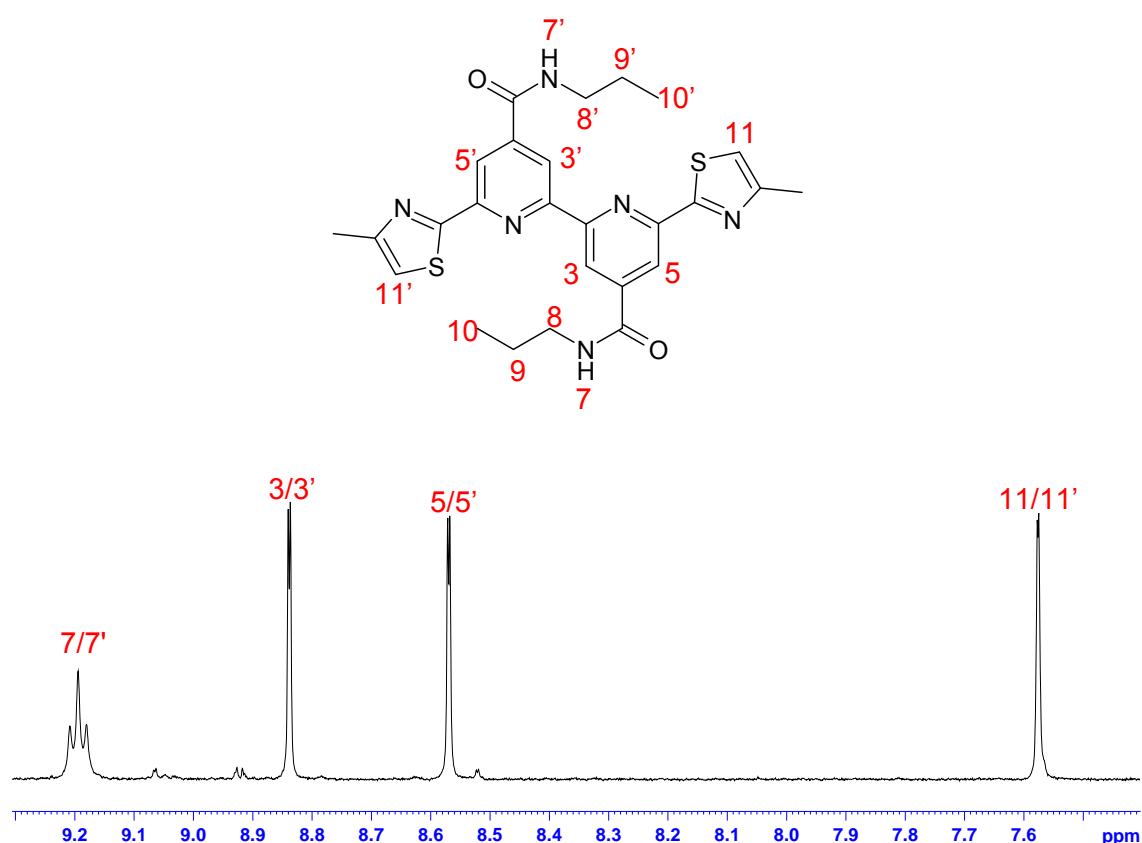


**Figure 3.15:** Aromatic region of the  $^1\text{H}$  NMR ( $d_6$ -DMSO) spectrum of  $L^3$

The  $^1\text{H}$  NMR spectrum reveals three doublet aromatic signals, two signals are from the bipyridine ring at  $\delta$  8.84 and 8.57 which represent the hydrogens labelled 3/3' and 5/5' shown in Figure 3.15. The other doublet aromatic signal relates to the thiazoyl ring at  $\delta$  7.58 which represents the single hydrogen in position 11/11'.

## 3.4.2 Coordination Chemistry - $L^3$

### 3.4.2.1 Reaction of $L^3$ with zinc (II)

The ligand  $L^3$  was not very soluble in common organic solvents. However, upon reaction with one equivalent of  $Zn(ClO_4)_2 \cdot 6H_2O$  in acetonitrile the ligand dissolved and produced a colourless solution. Slow diffusion of ethyl acetate into this resulting solution afforded colourless crystals. Single crystal x-ray analysis of the crystals shows the ligand  $L^3$  acting as a planar tetradentate donor, coordinating the zinc metal ion in the equatorial position, as shown in Figure 3.16.

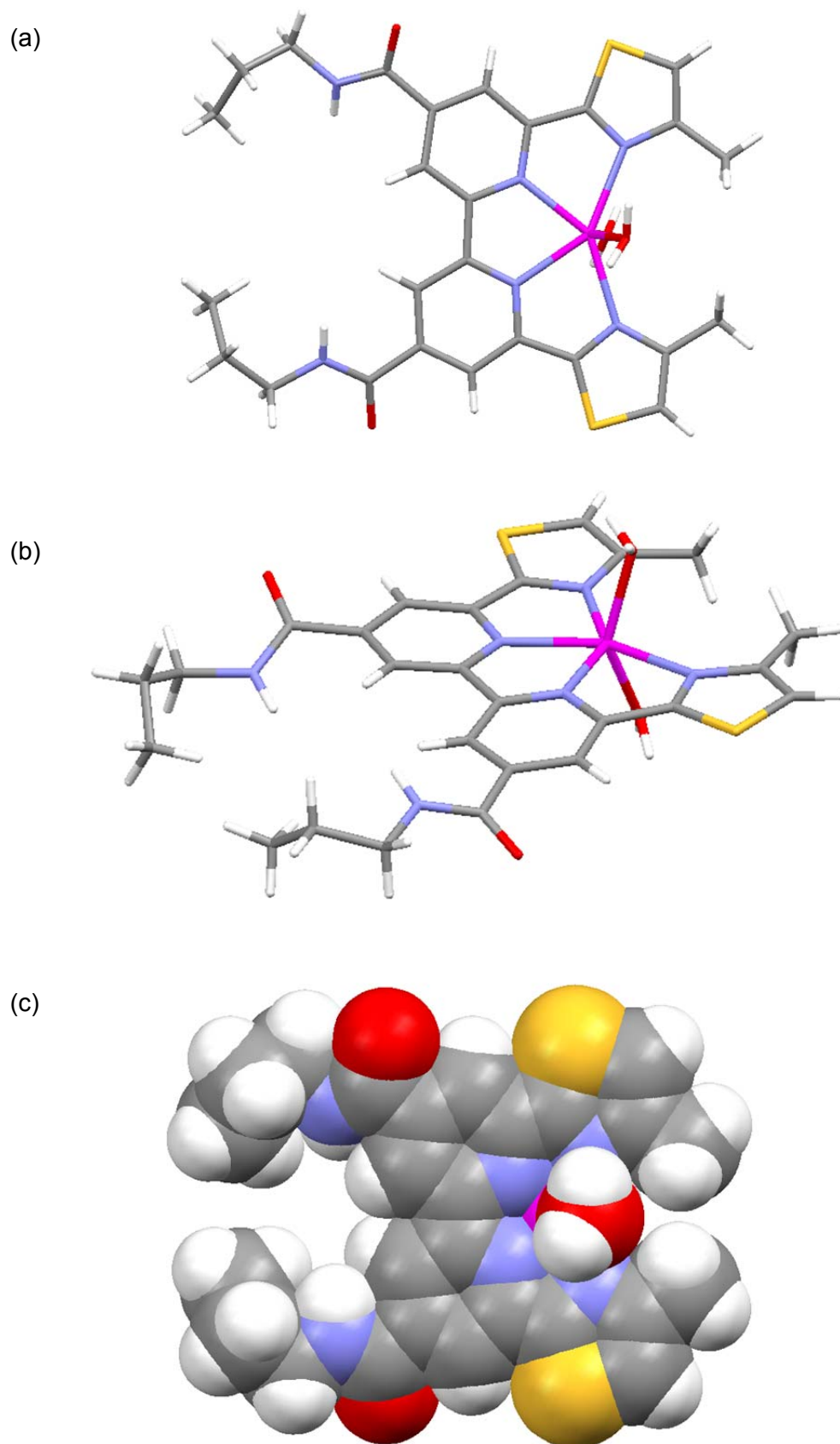


**Figure 3.16:** (a, b) Single crystal X-ray structure of  $[\text{Zn}(\text{L}^3)(\text{H}_2\text{O})_2](\text{ClO}_4)_2$ , anions omitted for clarity; (c) as a space-filling model

The cation adopts a distorted octahedral coordination geometry, with four nitrogen donor atoms from the ligand occupying four of the coordination sites (Zn-N distances 2.158(3) – 2.321(3) Å). Two water molecules are also coordinated to the zinc ion (Zn-O distances 2.006(3) - 2.039(2) Å), which results in a six-coordinate metal centre. Selected bond lengths and angles are shown in Tables 3.2 and 3.3.

Bond	Bond length (Å)
Zn(1)-O(3)	2.006(3)
Zn(1)-O(4)	2.039(2)
Zn(1)-N(1)	2.321(3)
Zn(1)-N(2)	2.173(3)
Zn(1)-N(3)	2.158(3)
Zn(1)-N(4)	2.305(3)

**Table 3.2:** Selected bond lengths (Å) for the complex cation  $[\text{Zn}(\text{L}^3)]^{2+}$

Bond	Bond angle (°)
O(3)-Zn(1)-O(4)	141.77(12)
O(3)-Zn(1)-N(1)	82.56(12)
O(3)-Zn(1)-N(2)	103.01(11)
O(3)-Zn(1)-N(3)	106.49(13)
O(3)-Zn(1)-N(4)	86.76(11)
O(4)-Zn(1)-N(1)	82.58(10)
O(4)-Zn(1)-N(2)	72.67(11)
O(4)-Zn(1)-N(3)	105.75(10)
O(4)-Zn(1)-N(4)	83.35(10)
N(2)-Zn(1)-N(1)	72.63(11)
N(2)-Zn(1)-N(4)	145.91(11)
N(3)-Zn(1)-N(1)	145.27(11)
N(3)-Zn(1)-N(4)	73.25(11)
N(4)-Zn(1)-N(1)	141.44(11)

**Table 3.3:** Selected bond angles (°) for the complex cation  $[\text{Zn}(\text{L}^3)]^{2+}$

The most interesting feature of the crystal structure is the binding of a perchlorate anion by the hydrogen bond donors of the ligand (Figure 3.17). In the solid state a disordered perchlorate is bound to both the amide hydrogen atom and the hydrogen atoms on the 3,3'-position of the bipyridine unit, although the shortest contact (2.421 Å) for the CH...anion interaction is substantially longer than the NH...anion interaction (2.026 Å).

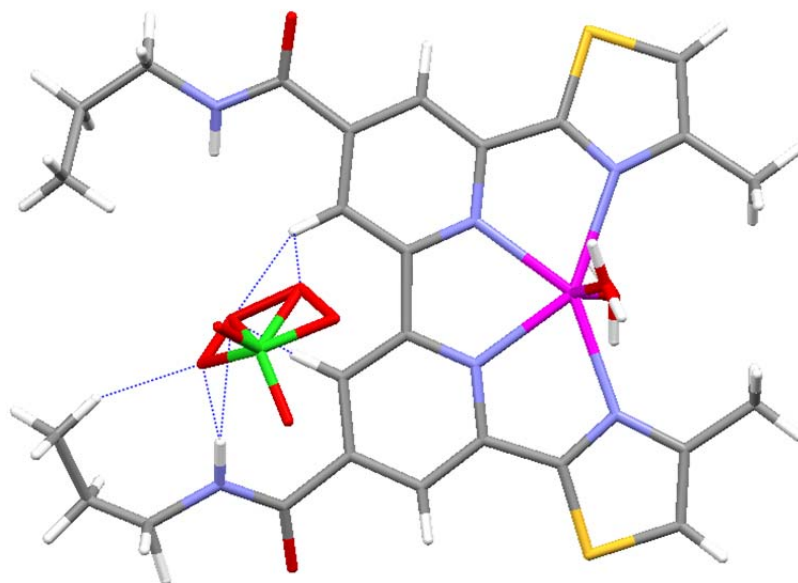


**Figure 3.17:** Single crystal X-ray structure of  $\{[\text{Zn}(\text{L}^3)(\text{H}_2\text{O})_2](\text{ClO}_4)\}^+$ ; the remaining anion is omitted for clarity

It is clear that the anion cavity formed by the complex is too large to interact with a single perchlorate anion and the oxygen atoms of the same perchlorate cannot “reach” both amides. However, the other amide interacts with the remaining perchlorate (Figure 3.18).

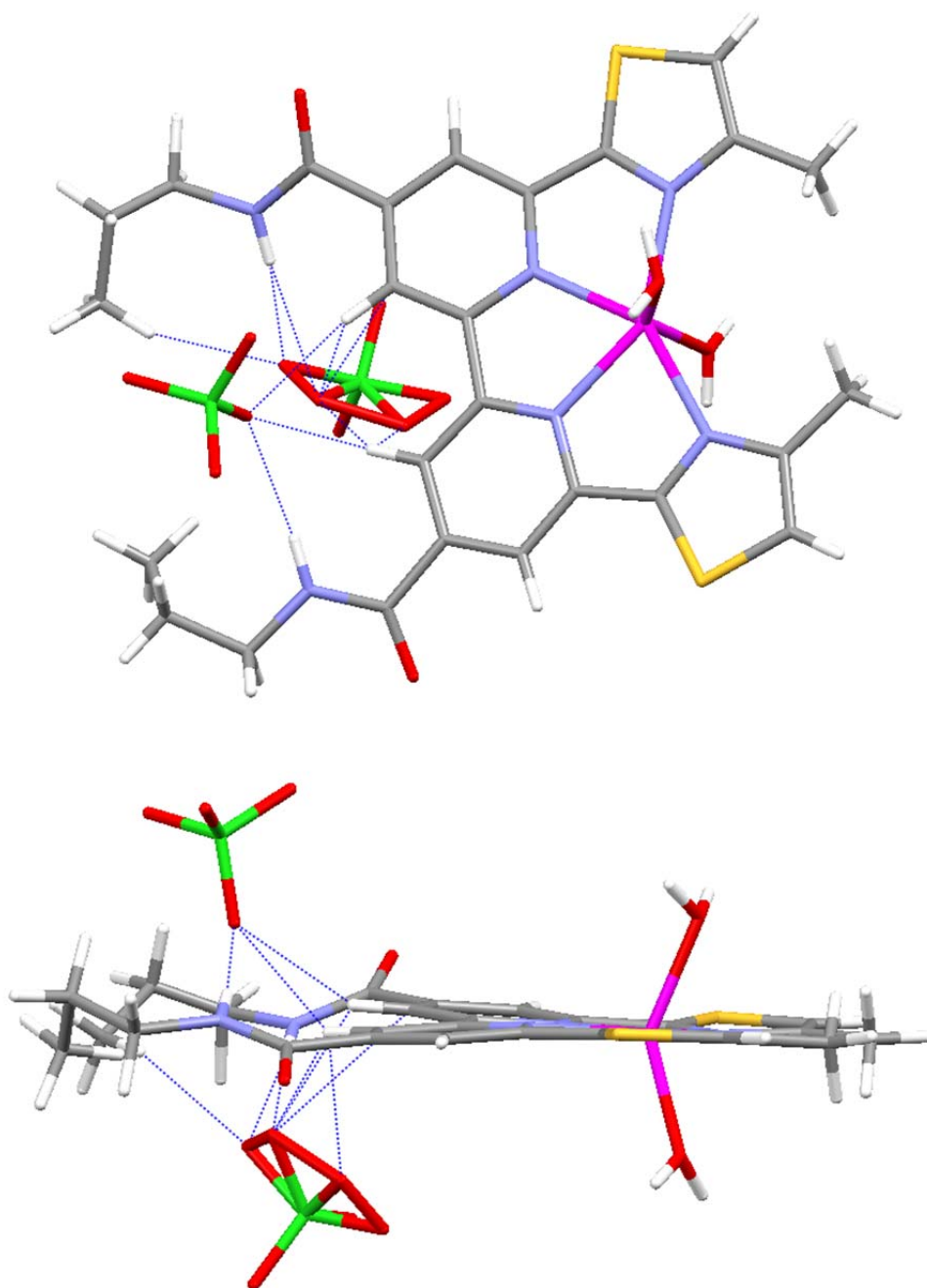


**Figure 3.18:** Two views of the single crystal X-ray structure of  $\{[\text{Zn}(\text{L}^3)(\text{H}_2\text{O})_2](\text{ClO}_4)_2\}$

ESI-MS analysis showed that a mononuclear species is also formed in solution; an ion was observed at  $m/z$  683 corresponding to  $\{[\text{Zn}(\text{L}^3)](\text{ClO}_4)\}^+$ .

#### 3.4.2.2 Reaction of $L^3$ with copper (I)

In a similar fashion to the previous ligand,  $L^3$  demonstrated poor solubility but upon reaction with  $Cu(MeCN)_4 \cdot PF_6$  in nitromethane the ligand dissolved and produced a dark red solution, typical of Cu(I) coordinated to a diimine.<sup>34</sup> Addition of  $Et_4NClO_4$  to this solution and slow diffusion of ethyl acetate into it gave large red crystals. Single crystal X-ray analysis of these shows the formation of a dinuclear species  $[Cu_2(L^3)_2](ClO_4)(PF_6)$  in the solid state. The ligand splits into two bidentate pyridyl-thiazole domains and each of the metal centres is coordinated by two of these domains, each from a different ligand (Figure 3.19).

The cation has assumed a distorted tetrahedral coordination geometry, with four nitrogen donor atoms from the ligands (Cu-N distances 2.007(3)–2.091(4) Å). Selected bond lengths and angles are shown in Tables 3.4 and 3.5.

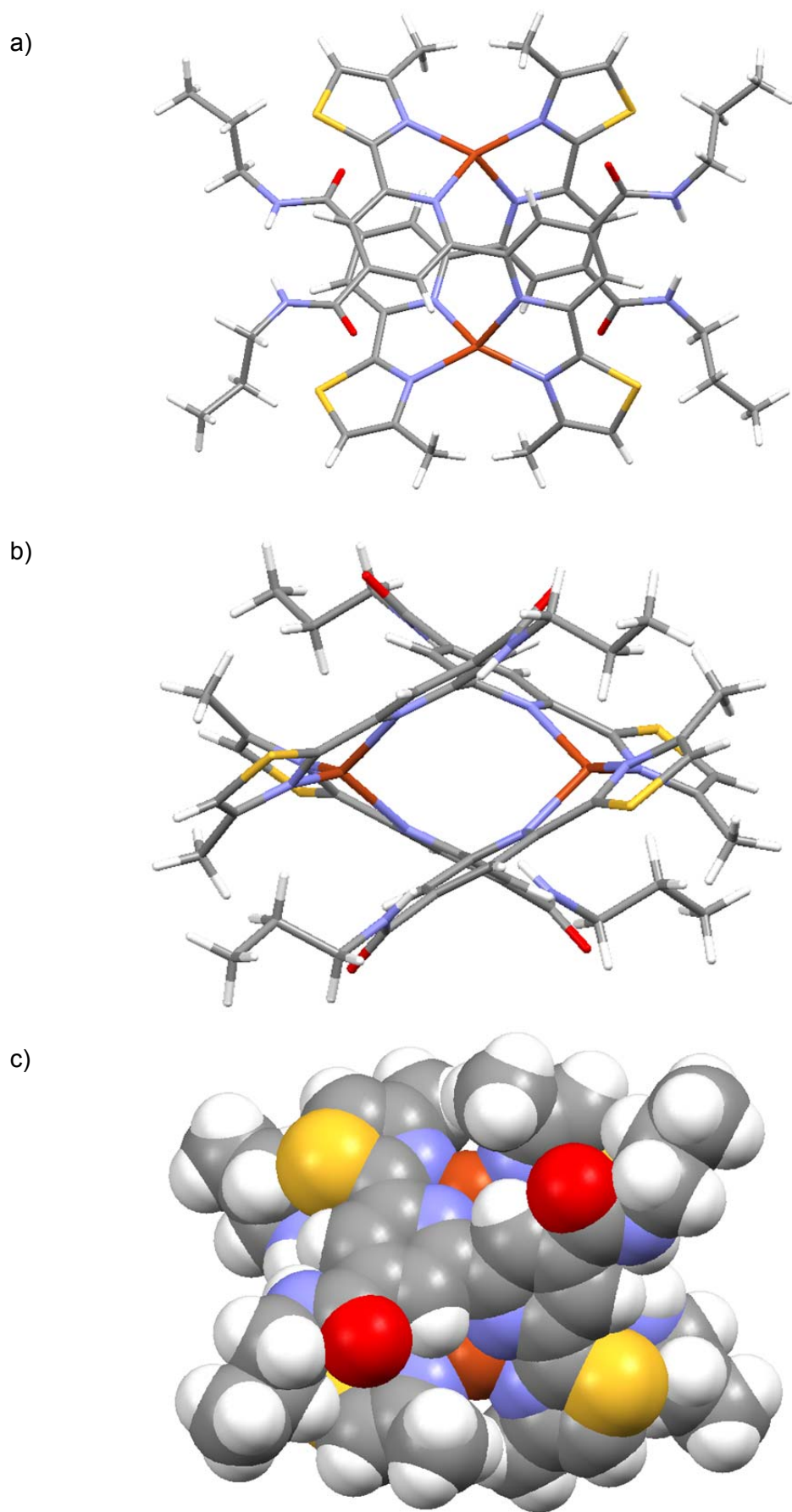


**Figure 3.19:** (a, b) Single crystal X-ray structure of  $[\text{Cu}_2(\text{L}^3)_2](\text{PF}_6)_2$ , anions omitted for clarity; (c) as a space-filling model

Bond	Bond length (Å)
Cu(I)-N(1)	2.091(4)
Cu(I)-N(2)	2.007(3)

**Table 3.4:** Selected bond lengths (Å) for the complex cation  $[\text{Cu}_2(\text{L}^3)_2]^{2+}$ ; other bond lengths are generated by symmetry

Bond	Bond angle (°)
N(1)-Cu(I)-N(1')	106.41(18)
N(2)-Cu(I)-N(1)	134.52(15)
N(2)-Cu(I)-N(1')	80.30(15)
N(2)-Cu(I)-N(2')	127.2(2)

**Table 3.5:** Selected bond angles (°) for the complex cation  $[\text{Cu}_2(\text{L}^3)_2]^{2+}$

Again the most interesting feature of this complex is the ability of the amides to bind anions. In the solid state perchlorate counter anions are bound *via* both the amide and the hydrogen atoms on the 5,5'-position of the bipyridine unit (Figure 3.20). However, in the Cu-containing example the shortest ligand-anion distance is the CH...anion interaction (2.345 Å) which is considerably shorter than the NH...anion interaction (2.897 Å).

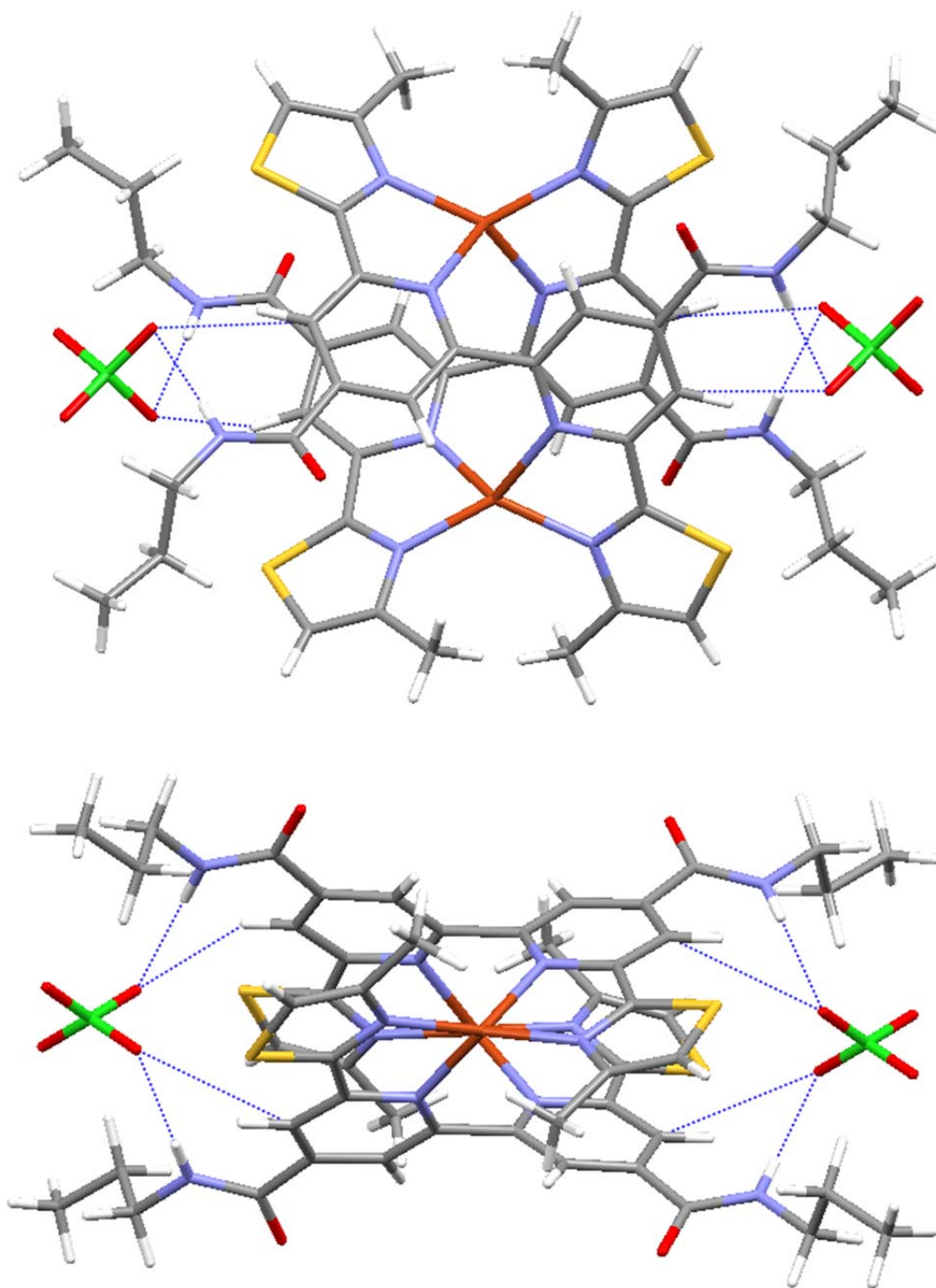


**Figure 3.20:** Selected views of the single crystal X-ray structure of  $\{[\text{Cu}_2(\text{L}^3)](\text{ClO}_4)\}^+$ ,  $\text{PF}_6^-$  omitted for clarity

Unlike the zinc complex ( $[\text{Zn}(\text{L}^3)(\text{H}_2\text{O})_2]^{2+}$ ) the perchlorate anions bridge the two amides from different ligand strands (Figure 3.21). Obviously the arrangement of the amides is closer in the double helicate complex (NHHN for  $[\text{Cu}_2(\text{L}^3)_2]^{2+} = 4.730 \text{ \AA}$ ;  $[\text{Zn}(\text{L}^3)(\text{H}_2\text{O})_2]^{2+} = 5.326 \text{ \AA}$ ) so that in the double helicate complex the arrangement of

the amide groups allows bonding of the two oxygen atoms of the *same* perchlorate anion.

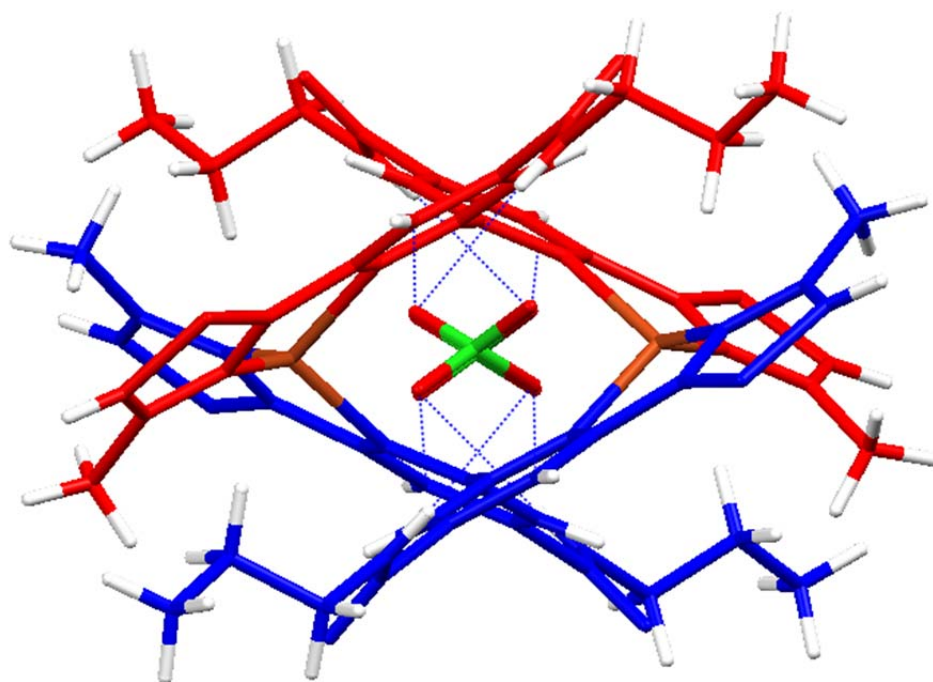


**Figure 3.21:** Selected view of the single crystal X-ray structure of  $\{[\text{Cu}_2(\text{L}^3)_2](\text{ClO}_4)\}^+$  showing the perchlorate bridging the two amides and binding two different ligand strands.  $\text{PF}_6^-$  counter ions are omitted for clarity

The double helicate is also formed in solution; ESI-MS analysis showed an ion at  $m/z$  1313 which corresponds to  $\{[\text{Cu}_2(\text{L}^3)_2](\text{PF}_6)\}^+$ .

This ability of the “ends” of the double helicate complex to bind two oxygen atoms of the perchlorate results in a 1-dimensional polymer in the solid state (Figure 3.22). Each of the perchlorate anions binds two complexes, such that all the oxygen atoms of the anion interact with amide or pyridyl hydrogen atoms (Figure 3.23).

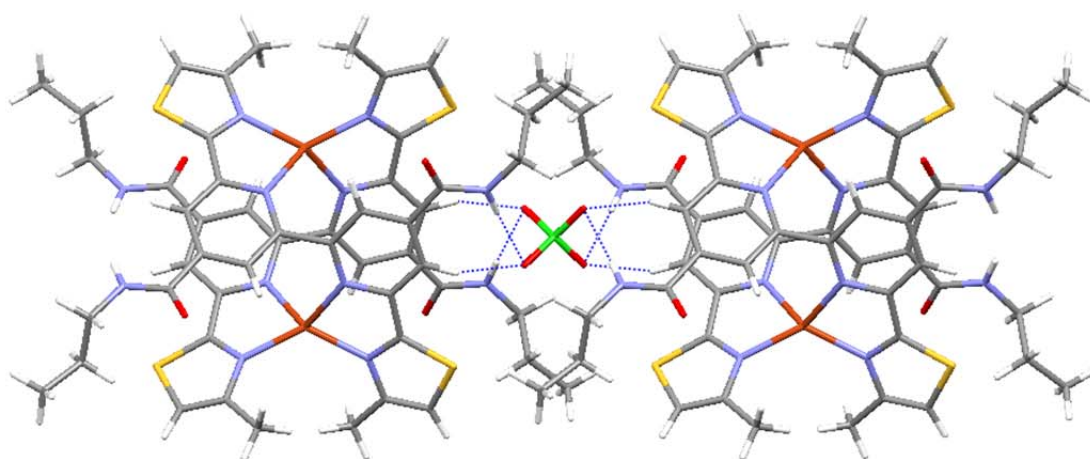


**Figure 3.22:** The 1-dimensional polymer structure of  $\{[\text{Cu}_{2n}(\text{L}^3)_{2n}](\text{ClO}_4)\}^{n+}$  formed in the solid state showing the perchlorate ion bridging two double helicate complexes

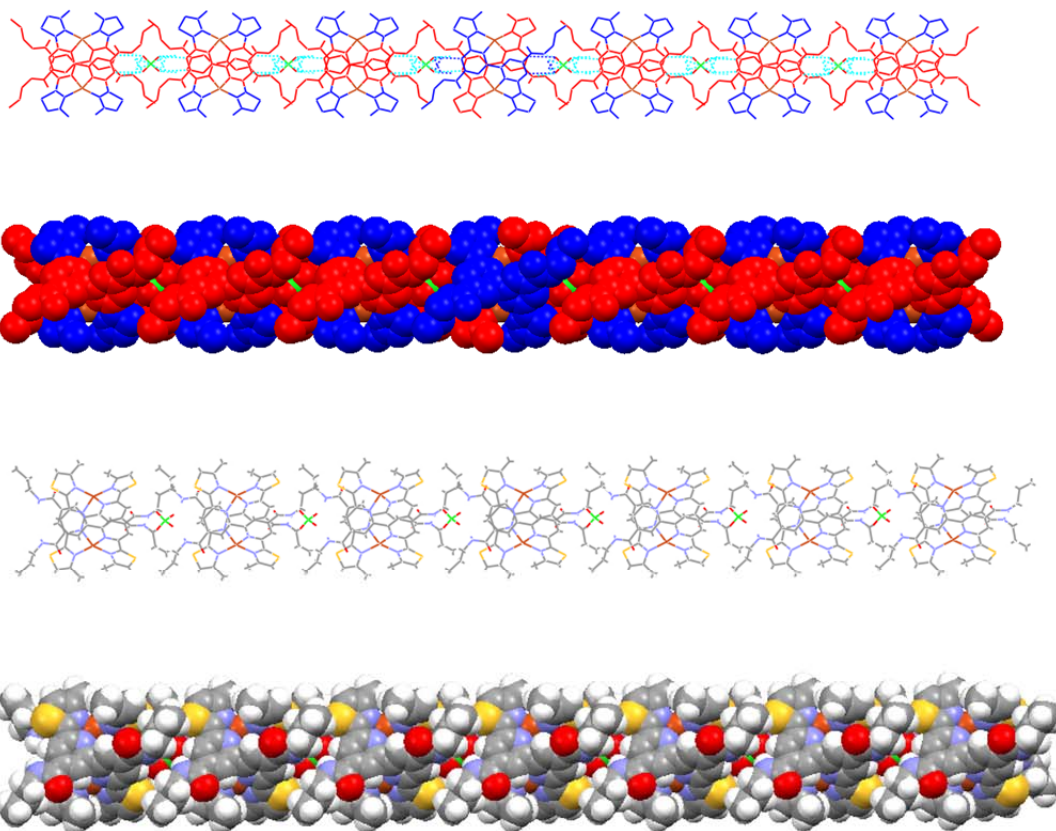


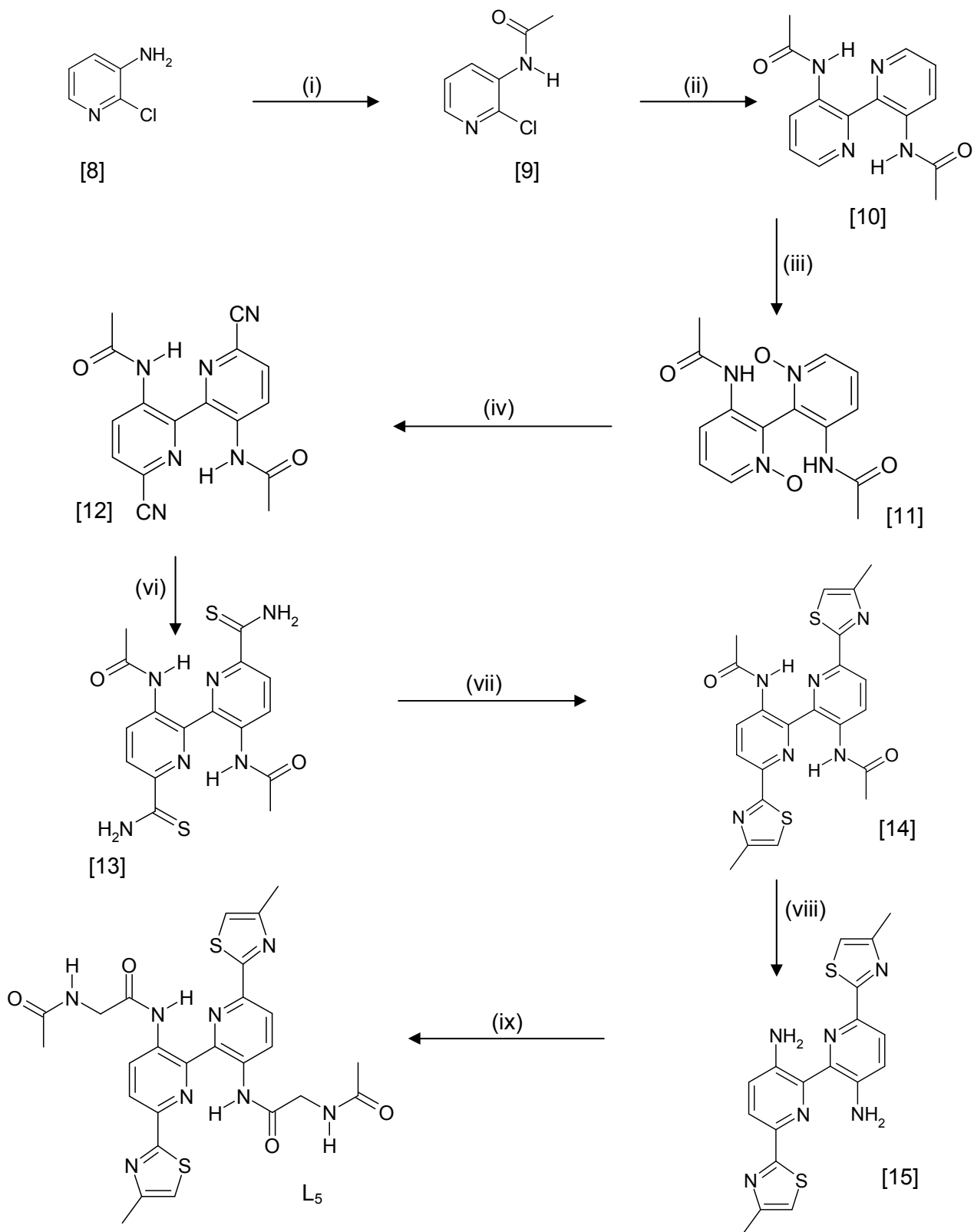
**Figure 3.23:** The 1-dimensional polymer structure of  $\{[\text{Cu}_{2n}(\text{L}^3)_{2n}](\text{ClO}_4)\}^{n+}$  formed in the solid state. Hexafluorophosphate anions (not shown) are present between the polymeric strands

Due to the difference in binding of the anion dependent upon the metal centre (e.g.  $[\text{Zn}(\text{L}^3)(\text{H}_2\text{O})_2]^{2+}$  vs.  $[\text{Cu}_2(\text{L}^3)_2]^{2+}$ ) it would be very interesting to study the relative

binding strengths of each of the amide pockets. However, studies were hampered by the relative solubilities of the complexes. The Cu(I) complex only formed in nitromethane (only colourless solutions were formed with Cu(I) and  $L^3$  in MeCN) whereas the Zn(II) complex did not dissolve in MeNO<sub>2</sub>. Addition of MeOH (e.g. 5% MeOH in MeNO<sub>2</sub>) did dissolve the zinc-containing complex but in this protic solution shifts in the <sup>1</sup>H NMR on addition of anions were very small.

### 3.4.3 Results and Discussion – $L^4$

The synthesis of the ligand  $L^4$  was performed using a five-step linear synthesis, once the starting materials had been produced (Scheme 2). Structural elucidation was performed at each step of the synthesis using <sup>1</sup>H NMR and mass spectrometry.



**Scheme 3.2.** Synthesis of L<sup>4</sup> from 3-amino-2-chloropyridine [8]. Reagents and conditions: (i) acetic anhydride, RT, 24 hrs (ii) Cu bronze, DMF, 80°C, 16 hrs (iii) DCM, mCPBA, RT, 8-10 days (iv) dimethylsulphate, 60°C, 24 hrs, (v) H<sub>2</sub>O, NaHCO<sub>3</sub>, sodium cyanide (vi) triethylamine, DMF, H<sub>2</sub>S (vii) DMF, chloroacetone, 80°C, 4 hrs (viii) conc. HCl, reflux, NH<sub>3</sub>, RT, 12 hrs (ix) N-acetylglycine, anhydrous pyridine, 0°C, oxalylchloride, RT, 72 hrs

The first step of the synthesis was performed using previous literature methods<sup>33</sup>, therefore **[9]** was reacted with Cu bronze in dimethylformamide at 80°C for 16 hours under an atmosphere of nitrogen. Filtration followed and the solid was washed with aqueous ammonia. Extraction using DCM produced a brown solid **[10]**.

Structural elucidation was performed using <sup>1</sup>H NMR. The structure of the ligand is symmetrical and therefore there are only 5 different hydrogen environments. The spectrum reveals three doublet of doublets aromatic signals at δ 9.12, 8.36 and 7.40 (Figure 3.24). These peaks represent the aromatic hydrogen environments labelled 4/4', 5/5' and 6/6' on the bipyridine ring.

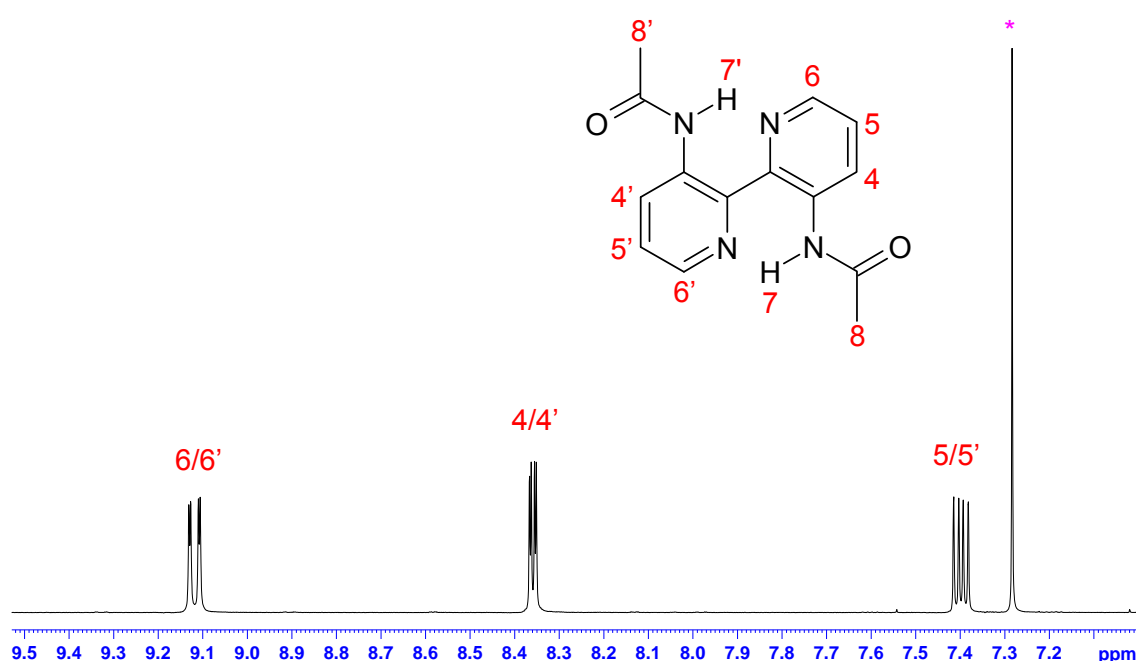


**Figure 3.24:** Aromatic region of the <sup>1</sup>H NMR (CDCl<sub>3</sub>) spectrum of **[10]** (\* corresponds to the solvent peak)

To achieve the bis-N-oxidation of **[10]**, the complex was allowed to stand in DCM with an excess of mCPBA for a period of 8-10 days, and the reaction was monitored by TLC. Once all the starting material had been consumed, the *bis-N,N*-dioxide product **[11]** was purified by column chromatography to give a white solid.

The <sup>1</sup>H NMR spectrum of **[11]** (Figure 3.25) again shows three signals in the aromatic region relating to the hydrogen atoms on the bipyridine ring. When comparing the NMR spectra for compounds **[10]** and **[11]** the aromatic signals show a considerable shift compared to those in Figure 3.24 due to the presence of the N-oxidised nitrogen atoms.

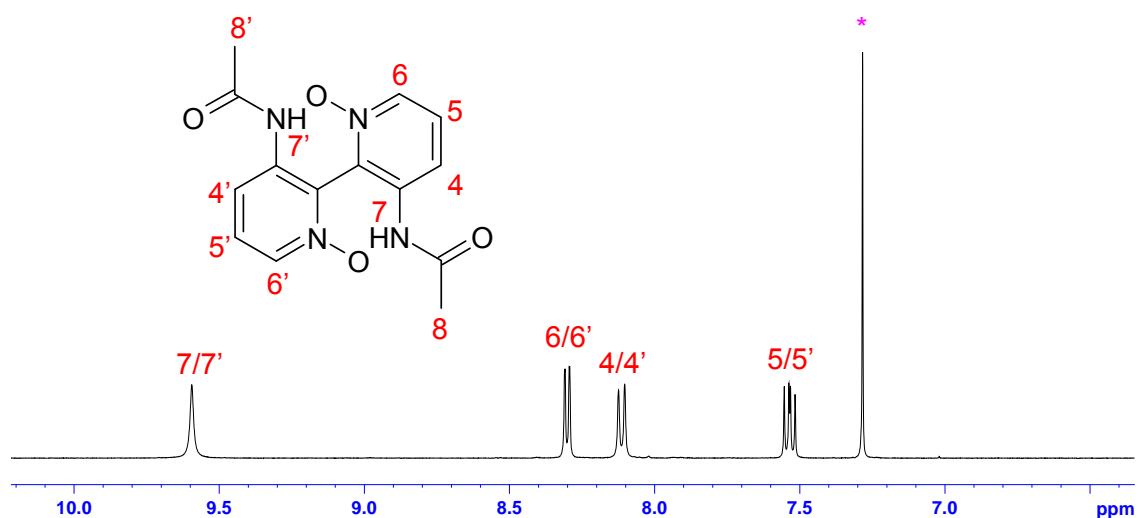


**Figure 3.25:** Aromatic region of  $^1\text{H}$  NMR ( $\text{CDCl}_3$ ) spectrum of **[11]** (\* corresponds to the solvent peak)

The *bis-N-N*-dioxide was reacted with dimethylsulphate at  $60^\circ\text{C}$  for 24 hours. This resulted in a yellow precipitate which when isolated by filtration gave a yellow solid. After suspending the yellow solid in an aqueous solution of sodium cyanide, a cream solid **[12]** precipitated out which was isolated by another filtration step.

The  $^1\text{H}$  NMR spectrum (Figure 3.26), shows two doublet aromatic signals which represent the single hydrogen atoms labelled 4/4' and 5/5' on the bipyridine ring.

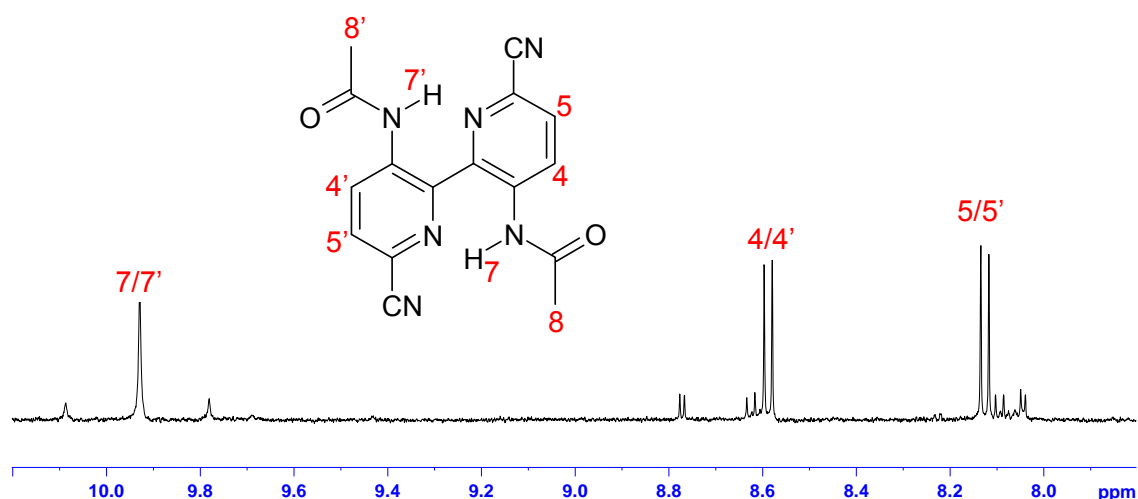


**Figure 3.26:** Aromatic region of  $^1\text{H}$  NMR ( $d_6$ -DMSO) spectrum of **[12]**

The thioamide **[13]** was produced as a yellow solid by purging hydrogen sulfide through a solution of **[12]** in dimethylformamide in the presence of triethylamine.

The appearance of two broad singlets corresponding to the thioamide at  $\delta$  10.17 and 9.76 in the  $^1\text{H}$  NMR spectrum confirmed complete conversion of the nitrile derivative (Figure 3.27).

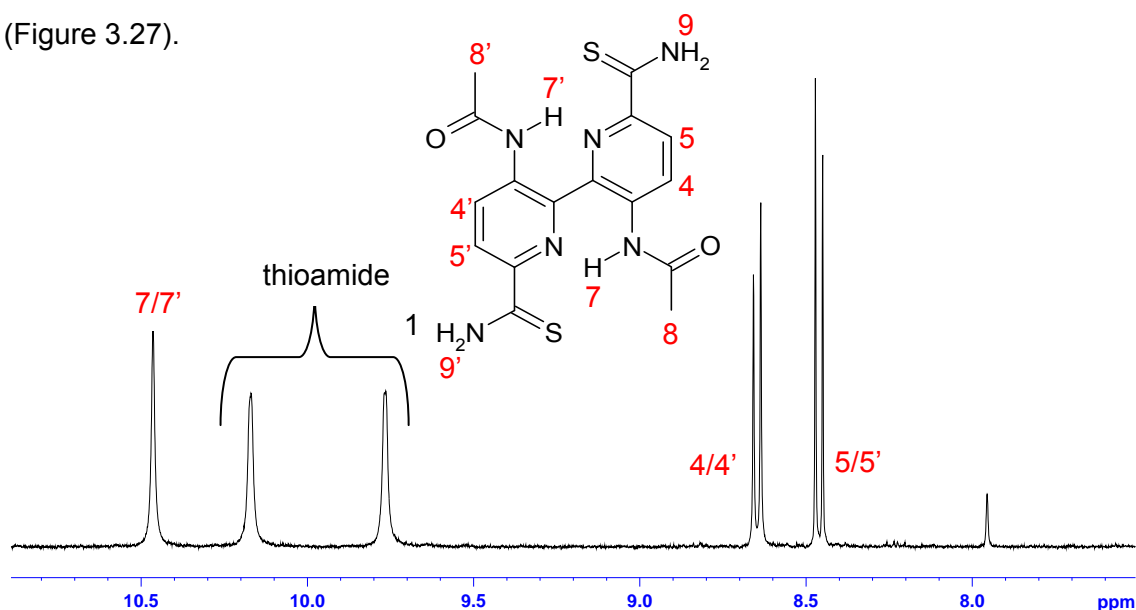


**Figure 3.27:** Aromatic region of  $^1\text{H}$  NMR ( $d_6$ -DMSO) spectrum of [13]

The resulting bis-thioamide derivative was reacted in dimethylformamide in the presence of chloroacetone at  $80^\circ\text{C}$  for a total of 4 hours. This resulted in a yellow precipitate which when isolated by filtration produced a yellow solid [14]. The  $^1\text{H}$  NMR spectrum reveals two doublet aromatic signals from the bipyridine ring at  $\delta$  8.75 and 8.18. The remaining singlet signal relates to the thiazoyl ring at  $\delta$  7.42 (Figure 3.28). The broad signal at 10.4 ppm is due to the amide proton; its relatively high chemical shift is due to hydrogen bonding to the pyridine nitrogen atom.

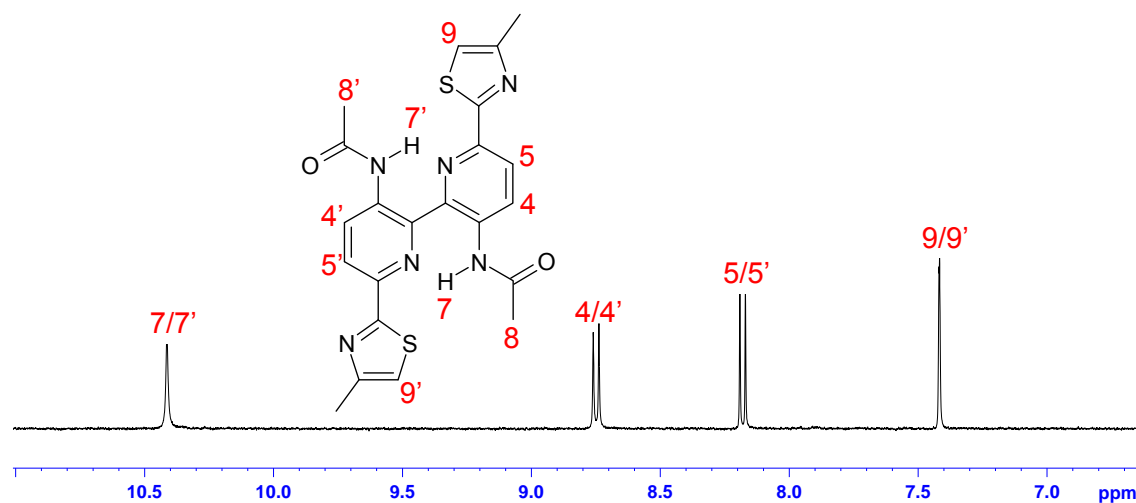


**Figure 3.28:** Aromatic region of  $^1\text{H}$  NMR ( $d_6$ -DMSO) spectrum of [14]

Compound **[14]** was reacted in conc. HCl at 80°C for a total of 3 hours. This resulted in an orange precipitate when suspended in H<sub>2</sub>O and this was isolated by filtration producing an orange hygroscopic solid which was suspended in aqueous ammonia for 12 hours during which time a bright yellow precipitate was produced, which was isolated by filtration to give **[15]** as a yellow solid.

<sup>1</sup>H NMR spectrum, shown in Figure 3.29., shows three different doublet aromatic signals, two of which represent the hydrogens labelled 4/4' and 5/5' on the bipyridine ring at  $\delta$  7.89 and 7.34. The remaining signal represents the single hydrogen atom (labelled 7/7') of the thiazoyl ring.

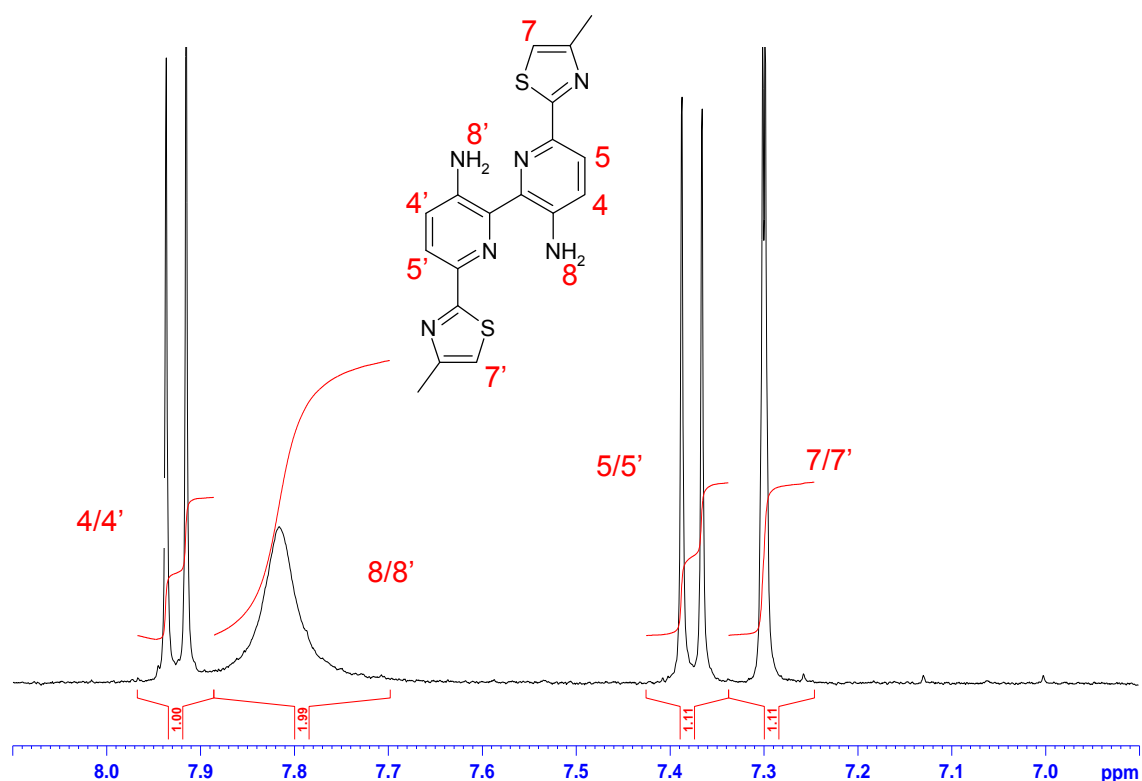


**Figure 3.29:** Aromatic region of <sup>1</sup>H NMR (d<sub>6</sub>-DMSO) spectrum of **[15]**

In the final step N-acetylglycine was reacted with oxalylchloride in anhydrous pyridine at 0°C. Compound **[15]** was added to the reaction and it was allowed to stir at room temperature for 72 hours, after which time a yellow precipitate had formed. When isolated by filtration, **L<sup>4</sup>** resulted as an orange solid.

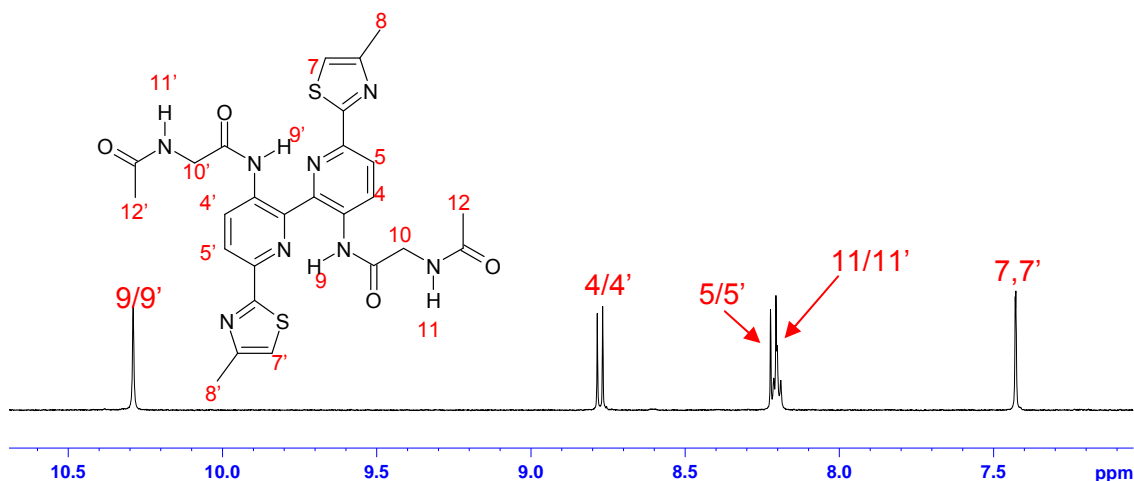


**Figure 3.30:** Aromatic region of  $^1\text{H}$  NMR ( $d_6$ -DMSO) spectrum of  $\text{L}^4$

The  $^1\text{H}$  NMR spectrum shown in Figure 3.30 shows three different doublet aromatic signals, two of which represent the hydrogens on the bipyridine ring at  $\delta$  8.78 and 8.21 (labelled 4/4' and 5/5'). The remaining aromatic signal corresponds to the thiazolyl proton (7,7') at  $\delta$  7.43. The signal at 10.3 ppm corresponds to the amide proton (its chemical shift is indicative of the formation of this group) and coincident with one of the bipyridine signals is the aliphatic amide proton (11), which is a triplet due to coupling to the adjacent  $-\text{CH}_2-$ .

### 3.4.4 Coordination Chemistry - $\text{L}^4$

#### 3.4.4.1 Reaction of $\text{L}^4$ with copper (I)

The ligand  $\text{L}^4$  was again not soluble in common organic solvents however upon reaction with one equivalent of  $\text{Cu}(\text{MeCN})_4\cdot\text{PF}_6$  in nitromethane a red solution was produced, indicative of complex formation. Reaction of this with  $\text{Et}_4\text{NNO}_3$  and slow diffusion of ether afforded red crystals.

Single crystal X-ray analysis of the red crystals showed the formation of a dinuclear species,  $[\text{Cu}_2(\text{L}^4)_2]^{2+}$ , in the solid state (Figure 3.31). The crystal structure shows how the ligand has partitioned into two bidentate pyridyl-thiazole nitrogen donor domains.

Each of the copper ions is coordinated by two of the bidentate domains, one from each ligand as shown in Figure 3.31. The cation has assumed a distorted tetrahedral coordination geometry, with four nitrogen donor atoms from the ligand (Cu-N distances 1.982 (8) – 2.101 (7) Å), shown in Table 3.6 as well as selected bond angles shown in Table 4.7. The crystal contains one hexafluorophosphate counter ion and a nitrate anion disordered over three positions.

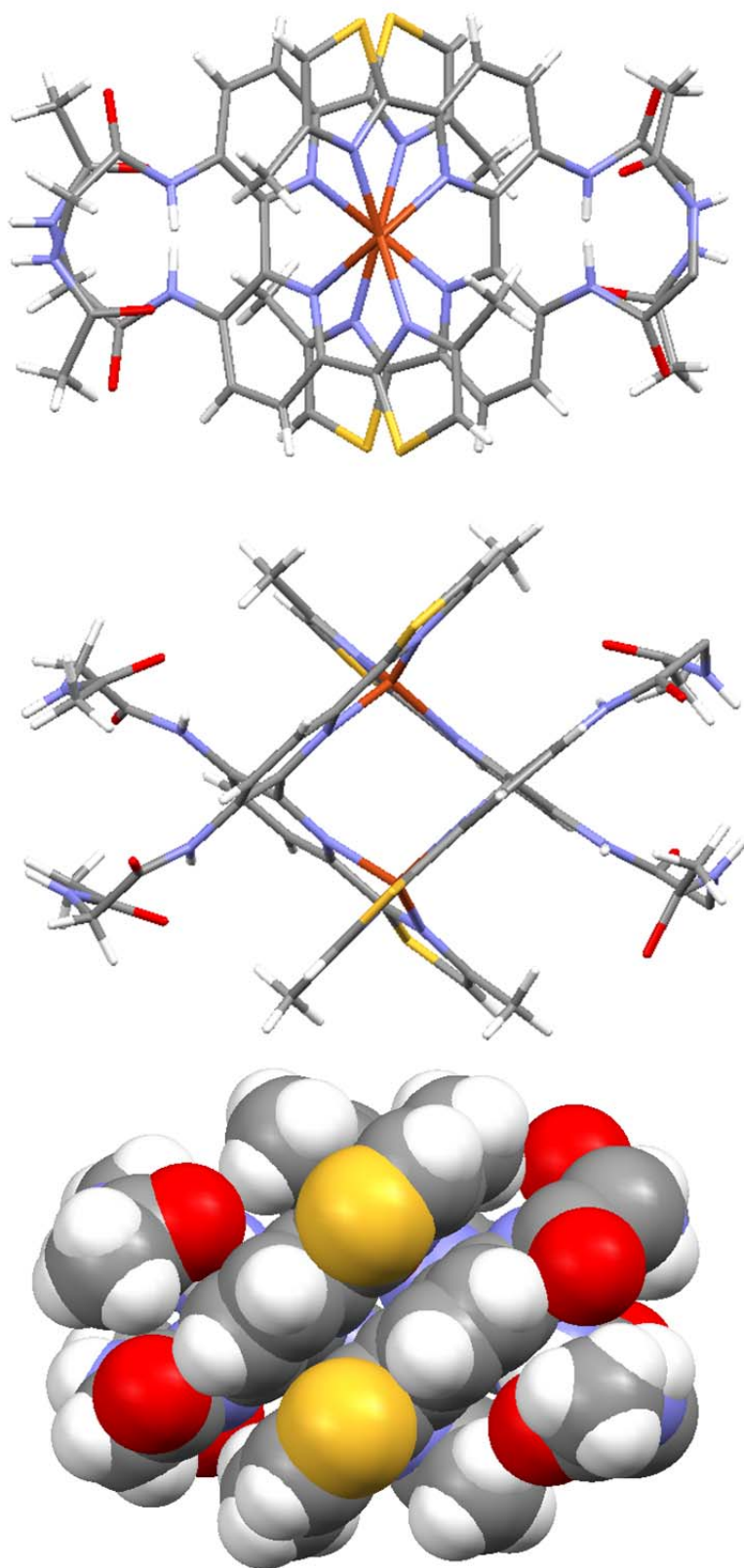


**Figure 3.31:** (a, b) Single crystal X-ray structure of [Cu<sub>2</sub>(L<sup>4</sup>)<sub>2</sub>]<sup>2+</sup>; (c) as a space-filling model

Bond	Bond length (Å)
Cu(I)-N(1)	1.982(8)
Cu(I)-N(2)	2.101(7)
Cu(I)-N(3)	2.079(7)
Cu(I)-N(4)	1.984(8)

**Table 3.6:** Selected bond lengths (Å) for the complex cation  $[(\text{Cu}_2(\text{L}^4)_2)]^{2+}$ ; other bond lengths are generated by symmetry

Bond	Bond angle (°)
N(1)-Cu(I)-N(2)	82.0(3)
N(1)-Cu(I)-N(3)	120.6(3)
N(1)-Cu(I)-N(4)	139.2(3)
N(3)-Cu(I)-N(2)	117.5(3)
N(4)-Cu(I)-N(2)	119.7(3)
N(4)-Cu(I)-N(3)	81.8(3)

**Table 3.7:** Selected bond angles (°) for the complex cation  $[(\text{Cu}_2(\text{L}^4)_2)]^{2+}$ ; other bond angles are generated by symmetry

Again the most interesting feature of the complex is its ability to interact with anions. On both sides of the double helicate the terminal, aliphatic amides from different ligands interact with hexafluorophosphate anions (Figures 3.32 and 3.33).

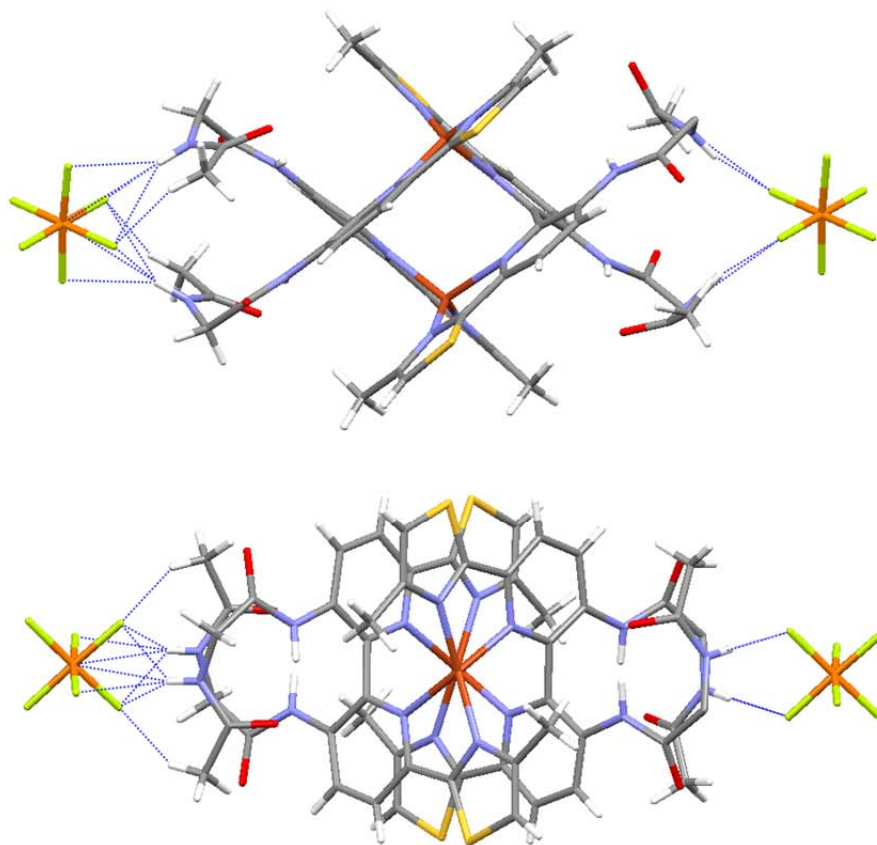


**Figure 3.32:** Single crystal X-ray structure of  $[Cu_2(L^4)_2]^{2+}$  showing the interaction of the cation with  $PF_6^-$

In an analogous fashion to  $\{[Cu_2(L^3)_2](ClO_4)_2\}$  this complex forms a 1-dimensional polymer in the solid state.

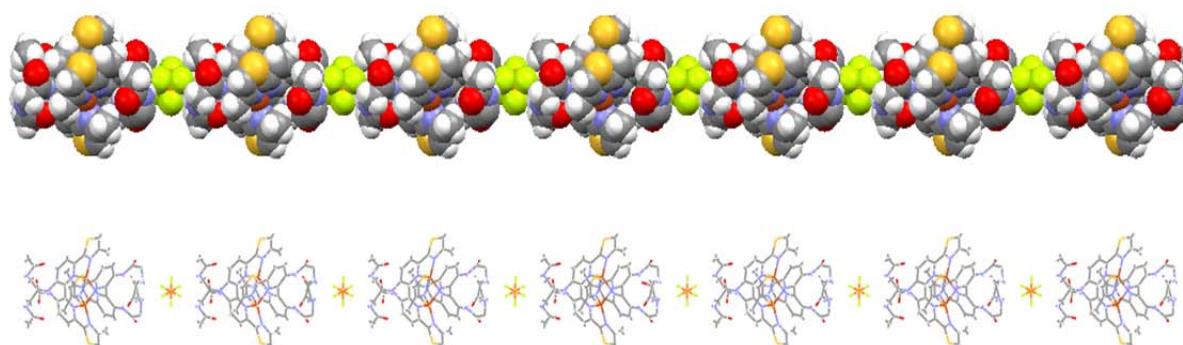


**Figure 3.33:** The 1-dimensional polymer structure of  $[Cu_{2n}(L^4)_{2n}(PF_6)_n]^{n+}$  formed in the solid state. Nitrate anions (not shown) are present between the polymeric strands

Interestingly the nitrate anion does not seem to interact with the amides on the complex. However, this could be a geometric constraint i.e. the two terminal amides might not interact as strongly with the *three* oxygen donors of the nitrate as opposed to the *six* fluorides of the phosphate. Also the aromatic amides do not appear to interact with any of the anionic species. It is probable that these are not of the correct geometry to interact with either the nitrate or hexafluorophosphate ions.

A double helicate species is also formed in solution; ESI-MS analysis gave an ion at  $m/z$  1429 which corresponds to  $\{[\text{Cu}_2(\text{L}^4)_2(\text{PF}_6)]^+\}$ .

It would be very interesting to compare the coordination chemistry of this ligand with different metal ions. For example, reaction with Zn(II) should produce the mononuclear structure and its ability to bind anions would make a good comparison with the double helicate structure. However, the final step in the synthesis of the ligand was at best unreliable and made production of usable and pure samples of the ligand  $\text{L}^4$  difficult, precluding further study.

### 3.5 Conclusion

Two novel pyridyl-thiazole ligands which are capable of binding both transition metal cations, *via* their N-donor units, and anions, *via* the amide-containing substituents, have been successfully prepared. Both  $\text{L}^3$  and  $\text{L}^4$  form complexes with Zn(II) and/or Cu(I) which can bind anions.  $\text{L}^3$  forms a mononuclear complex with Zn(II) which loosely binds two perchlorate anions *via* the amide groups on the two substituents. However, with Cu(I), both  $\text{L}^3$  and  $\text{L}^4$  form dinuclear double helicates which have a binding "pocket" at each end of the complex.  $[\text{Cu}_2(\text{L}^3)_2]^{2+}$  binds a perchlorate anion in each pocket *via* two of its oxygen atoms; the other two oxygen atoms interact with amide groups on adjacent molecules forming a one-dimensional polymer with bridging perchlorate anions. An analogous complex is formed by reaction of Cu(I) with  $\text{L}^4$ , this time forming a one-dimensional polymer with bridging hexafluorophosphate anions.

### 3.6 References

1. Steed, J. W., Turner, D. R., Wallace, K. J., (2007). *Core Concepts in Supramolecular Chemistry and Nanochemistry*. Chichester: John Wiley & Sons.
2. Beer, P. D., Gale, P. A., Smith, D. K., (1999). *Supramolecular Chemistry*. New York: Oxford University Press Inc.
3. Steed, J. W. & Atwood, J. L., (2000). *Supramolecular Chemistry*. Chichester: John Wiley & Sons.
4. Pedersen, C. J., The Discovery of Crown Ethers (Nobel Lecture), *Angew. Chem. Int. Ed. Engl.*, 1988, **27**, 1021-1027.
5. Cram, D. J., The Design of Molecular Hosts, Guests, and Their Complexes (Nobel Lectures), *Angew. Chem.*, 1988, **27**, 1009-1112.
6. Beer, P. D., Gale, P. A., Anion Recognition and Sensing: The State of the Art and Future Perspectives, *Angew. Chem. Int. Ed.*, 2001, **40**, 486-516.
7. Beer, P. D., Schmitt, P., Molecular Recognition of Anions by Synthetic Receptors, *Current Opinion in Chemical Biology*, 1997, **1**, 475-482.
8. Kavalieratos, K., de Gala, S. R., Austin, D. J., Crabtree, R. H., A Readily Available Non-preorganized Neutral Acyclic Halide Receptor with an Unusual Nonplanar Binding Conformation, *J. Am. Chem. Soc.*, 1997, **119**, 2325-2326.
9. Davis, A. P., Perry, J. J., Williams, R. P., Anion Recognition by Tripodal Receptors Derived from Cholic Acid, *J. Am. Chem. Soc.*, 1997, **119**, 1793-1794.
10. Rice, C. R., Metal Assembled Anion Receptors, *Coord. Chem. Rev.*, 2006, **250**, 3190-3199.
11. Beer, P. D., Transition-Metal Receptor Systems for the Selective Recognition and Sensing of Anionic Guest Species, *Acc. Chem. Res.*, 1998, **31**, 71-80.

12. Beer, P. D., Anion Selective Recognition and Optical/Electrochemical Sensing by Novel Transition-Metal Receptor Systems, *J. Chem. Soc. Chem. Commun.*, 1996, 689-696.
13. Beer, P. D., Dent, S. W., Wear, T. J., Spectral and Electrochemical Recognition of Halide Anions by Acyclic Mononuclear Ruthenium(II) Bipyridyl Receptor Molecules, *J. Chem. Dalton Trans.*, 1996, 2341-2346.
14. Wenzel, M., Hiscock, J. R., Gale, P. A., Anion Receptor Chemistry: highlights from 2010, *Chem. Soc. Rev.*, 2012, **41**, 480-520.
15. Brooks, S. J., Gale, P. A., Light, M. E., Anion-Binding Modes in a Macrocyclic Amidourea, *Chem. Commun.*, 2006, 4344-4346.
16. Gale, P. A., Camiolo, S., Tizzard, G. J., Chapman, C. P., Light, M. E., Coles, S. J., Hursthouse, M. B., 2-Aminopyrroles and 2,5-Diamidopyrroles as Simple Anion Binding Agents, *J. Org. Chem.*, 2001, **66**, 7849-7853.
17. Camiolo, S., Gale, P. A., Hursthouse, M. B., Light, M. E., Confirmation of a 'cleft-mode' of Binding in a 2,5-diamidopyrrole Anion Receptor in the Solid State, *Tetrahedron Letters.*, 2002, **43**, 6995-6996.
18. Beer, P. D., Drew, M. G. B., Graydon, A. R., Smith, D. K., Stokes, S. E., Quantitative and Structural Investigations of Hydrogen-Bonding Interactions in Anion Binding of Mono- and 1,1'-bis-substituted Aryl Cobaltocenium Receptors, *J. Chem. Soc. Dalton Trans.*, 1995, 403-408.
19. Beer, P. D., Hazlewood, C., Heseck, D., Hodacova, J., Stokes, S. E., Anion Recognition by Acyclic Redox-Responsive Amide-Linked Cobaltocenium Receptors, *J. Chem. Soc. Dalton Trans.*, 1993, 1327-1332.
20. Beer, P. G., Drew, M. G. B., Heseck, D., Nam, K. C., A New Carboxylate Anion Selective Cobaltocenium Calix[4]arene Receptor, *J. Chem. Soc. Chem. Commun.*, 1997, 107-108.

21. Beer, P. D., Graydon, A. R., Johnson, A. O. M., Smith, D. K., Neutral Ferrocenoyl Receptors for the Selective Recognition and Sensing of Anionic Guests, *Inorg. Chem.*, 1997, **36**, 2112-2118.
22. Pratt, M. D., Beer, P. D., Anion Recognition and Sensing by mono- and bis-urea Substituted Ferrocene Receptors, *Polyhedron.*, 2003, **22**, 649-653.
23. Gale, P. A., Chen, Z., Drew, M. G. B., Heath, J. A., Beer, P. D., Lower-rim Ferrocenyl Substituted Calixarenes: New Electrochemical Sensors for Anions, *Polyhedron.*, 1998, **17**, 405-412.
24. Constable, E. C., Expanded Ligands-An Assembly Principle for Supramolecular Chemistry, *Coord. Chem. Rev.*, 2008, **252**, 842-855.
25. Pitt, M. A., Johnson, D. W., Main Group Supramolecular Chemistry, *Chem. Soc. Rev.*, 2007, **36**, 1441-1453.
26. Harding, L. P., Jeffery, J. C., Riis-Johannessen, T., Rice, C. R., Zeng, Z., Anion Control of Ligand Self-Recognition in a Triple Helical Array, *J. Chem. Soc. Chem. Commun.*, 2004, 654-655.
27. Rice, C. R., Wörl, S., Jeffery, J. C., Paul, R. L., Ward, M. D., New Multidentate Ligands for Supramolecular Coordination Chemistry: Double and Triple Helical Complexes of Ligands Containing Pyridyl and Thiazoyl Donor Units, *J. Chem. Soc., Dalton Trans.*, 2001, 550-559.
28. Piguet, C., Bernardinelli, G., Hopfgartner, G., *Chem. Rev.*, 1997, **97**, 2005; Constable, E. C., *Polynuclear Transition Metal Helicates*, vol. 9, *Comprehensive Supramolecular Chemistry*, editor: Sauvage, J. P., Elsevier, Oxford, 1996, 213-252.
29. Lehn, J. M., Rigault, A., Siegel, J., Harrowfield, J., Chevrier, B., Moras, D., Spontaneous Assembly of Double-Stranded Helicates from Oligobipyridine Ligands and Copper(I) Cations: Structure of an Inorganic Double Helix, *Proc. Natl. Acad. Sci.*, 1987, **84**, 2565-2569.

30. Machado, V. G., Baxter, P. N., Lehn, J. M., Self-Assembly in Self-Organized Inorganic Systems: A View of Programmed Metallosupramolecular Architectures, *J. Braz. Chem. Soc.*, 2001, **12**, 431-462.
31. Uppadine, L. H., Drew, M. G. B., Beer, P. D., Anion Selectivity Properties of Ruthenium(II) Tris(5,5'-diamide-2,2'-bipyridine) Receptors Dictated by Solvent and Amide Substituent, *J. Chem. Soc. Chem. Commun.*, 2001, 291-292.
32. Garelli, N., Vierling, P., Synthesis of New Amphiphilic Perfluoroalkylated Bipyridines, *J. Org. Chem.*, 1992, **57**, 3046-3051.
33. Rice, C. R., Onions, S., Vidal, N., Wallis, J. D., Senna, M. C., Pilkington, M., Stoeckli-Evans, H., The Coordination Chemistry of 3,3'-Diamino-2,2'-bipyridine and Its Dication: Exploring the Role of the Amino Groups by X-ray Crystallography, *Eur. J. Inorg. Chem.*, 2002, 1985-1997.
34. Clayton, H. J., Harding, L. P., Irvine, J. P., Jeffery, J. C., Riis-Johannessen, T., Laws, A. P., Rice, C. R., Whitehead, M., Metal-Specific Allosteric Activation and Deactivation of a Diamine, *Chem. Commun.*, 2008, 108-110.

### 3.7 Appendix: Crystallographic Data Tables

Compound	$\{[\text{Zn}(\text{L}^3)(\text{H}_2\text{O})_2](\text{ClO}_4)_2\}$
Formula	$\text{C}_{26}\text{H}_{33}\text{Cl}_2\text{N}_6\text{O}_{12.5}\text{S}_2\text{Zn}$
M	829.97
System, space group	Triclinic, P-1
$a/\text{\AA}$	10.4026(7)
$b/\text{\AA}$	12.5464(8)
$c/\text{\AA}$	13.5468(9)
$\alpha/^\circ$	81.0770(10)
$\beta/^\circ$	82.2150(10)
$\gamma/^\circ$	87.926(2)
$V/\text{\AA}^3$	1730.4(2)
Z	2
$\rho_{\text{calc}}/\text{Mg m}^{-3}$	1.593
$F(000)$	854
Dimensions/mm	0.20 x 0.10 x 0.10
$\mu/\text{mm}^{-1}$	0.71073
T/K	150(2)
Reflections collected (range)	37356 ( $1.98 \leq \theta \leq 30.03^\circ$ )
$hkl$ range indices	$-14 \leq h \leq 14, -17 \leq k \leq 17, -19 \leq l \leq 14$
Unique reflections	10038
Total, independent $R_{\text{int}}$	0.0330
$R_w$	0.1646
R	0.0651
Reflections with $I > 2\sigma(I)$	7836
GOF	1.048
Refined parameters	503
Restraints	93
Largest peak and hole/ $\text{e}\text{\AA}^{-3}$	1.675, -1.493

Compound	<b>{[Cu<sub>2</sub>(L<sup>3</sup>)<sub>2</sub>](ClO<sub>4</sub>)(PF<sub>6</sub>)}</b>
Formula	C <sub>52</sub> H <sub>56</sub> ClCu <sub>2</sub> F <sub>6</sub> N <sub>12</sub> O <sub>8</sub> PS <sub>4</sub>
M	1412.83
System, space group	Tetragonal, P-4 <sub>2</sub> /c
a/Å	14.1507(7)
b/Å	14.1507(7)
c/Å	14.9643(7)
V/ Å <sup>3</sup>	2996.5(3)
Z	2
ρ <sub>calc</sub> /Mg m <sup>-3</sup>	1.566
F(000)	1448
Dimensions/mm	0.25 x 0.10 x 0.10
μ/mm <sup>-1</sup>	0.71073
T/K	150(2)
Reflections collected (range)	12040 (1.98 ≤ θ ≤ 26.02°)
hkl range indices	-8 ≤ h ≤ 17, -17 ≤ k ≤ 17, -17 ≤ l ≤ 18
Unique reflections	2972
Total, independent R <sub>int</sub>	0.0358
R <sub>w</sub>	0.1343
R	0.0483
Reflections with I > 2σ(I)	2456
GOF	1.047
Refined parameters	199
Restraints	0
Largest peak and hole/eÅ <sup>-3</sup>	0.882, -0.472

Compound	$\{[\text{Cu}_2(\text{L}^4)]_2(\text{PF}_6)_2(\text{NO}_3)\}$
Formula	$\text{C}_{52}\text{H}_{46.47}\text{Cu}_2\text{F}_6\text{N}_{18}\text{O}_{14.51}\text{PS}_4$
M	1556.03
System, space group	Monoclinic, $\text{P}2_1/\text{n}$
$a/\text{\AA}$	24.6698(13)
$b/\text{\AA}$	19.4476(10)
$c/\text{\AA}$	18.2642(9)
$\beta/^\circ$	122.9270(10)
$V/\text{\AA}^3$	7355.0(7)
Z	4
$\rho_{\text{calc}}/\text{Mg m}^{-3}$	1.405
$F(000)$	3166
Dimensions/mm	0.35 x 0.20 x 0.15
$\mu/\text{mm}^{-1}$	0.71073
T/K	150(2)
Reflections collected (range)	42976 ( $1.44 \leq \theta \leq 30.03^\circ$ )
$hkl$ range indices	$-17 \leq h \leq 34, -27 \leq k \leq 27, -25 \leq l \leq 15$
Unique reflections	10753
Total, independent $R_{\text{int}}$	0.0522
$R_w$	0.2362
R	0.0744
Reflections with $I > 2\sigma(I)$	6498
GOF	1.014
Refined parameters	571
Restraints	149
Largest peak and hole/ $\text{e}\text{\AA}^{-3}$	1.169, -0.578

## Chapter 4 Allosteric control of metal specificity in formation of coordination complexes

### 4.1 Introduction

The main focus of this chapter involves the synthesis of a ligand ( $L^5$ ) which is capable of coordinating transition metal cations and an investigation of the allosteric control of its coordination behaviour (Figure 4.1).

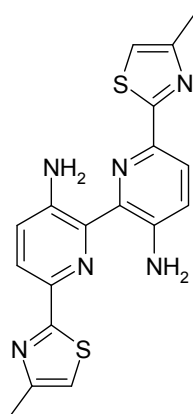


**Figure 4.1:** 3,3'-Diamino-6,6'-bis(4-methylthiazol-2-yl)-2,2'-bipyridine,  $L^5$

As explained earlier in the main introduction to this thesis, metallosupramolecular chemistry is a subdivision of supramolecular chemistry involving the spontaneous self-assembly of metal ions with ligands through coordinate bonds. Self-assembly and self-organization has become one of the major topics of supramolecular chemistry which has been demonstrated beautifully by Lehn *et al*, among others.<sup>1-3</sup>

Usually, N-donor heterocyclic ligands are reacted with metal ions which prefer either tetrahedral or octahedral coordination geometries. Metal ions have ideal coordination numbers and coordination geometries that can be matched with the intrinsic bonding properties of polydentate ligands to form supramolecular architectures. Lehn *et al*. demonstrated that a mixture of ligands, containing three bipyridine units linked by either ether or aliphatic units, will form only homonuclear, homoleptic trinuclear double and triple helicates, when reacted with the metal cations  $Ni^{2+}$  and  $Cu^+$  respectively, demonstrating *specific* recognition of the metals by the ligands.<sup>3</sup> (Figure 4.2)

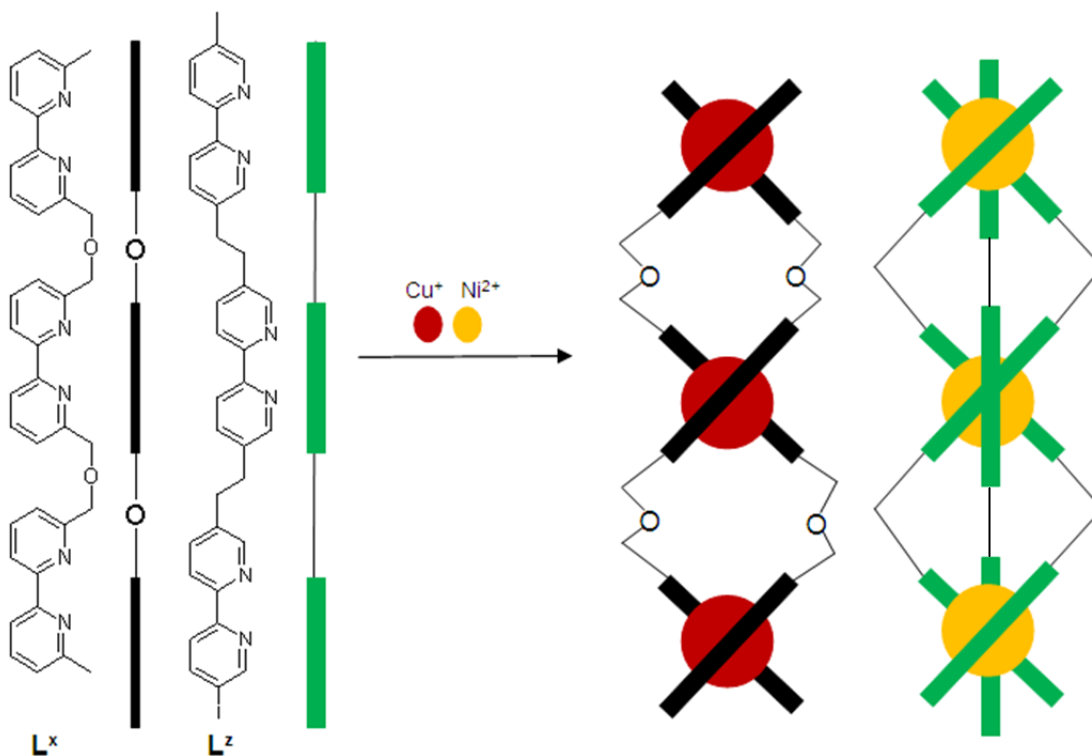


**Figure 4.2:** Schematic representation of the formation of homonuclear, homoleptic trinuclear double and triple helicates upon reaction of  $L^x$  and  $L^z$  with  $Ni^{2+}$  and  $Cu^+$  cations

Metal specificity can also be directed by introducing distinct binding domains within the ligand strand with each unit being specific to a particular metal geometry. Such ligands can be said to be *pre-programmed*, as the ligand system already contains the information needed to give selectivity for certain metals. This has already been prearranged during synthesis and consequently cannot be altered at a later stage.<sup>4</sup>

The brilliant research performed by Rebek<sup>5-8</sup> pioneered the field of artificial allosteric systems where there are numerous examples of catalysts and receptors.<sup>5-7,9</sup> Allosteric interactions involve a change in the behaviour of one part of a molecule, caused by a change to another part of the same molecule. However, the use of allosteric interactions which control reactivity has not received as much attention. Nonetheless, Rebek has demonstrated the use of metal ions to control the reactions in 3,3'-disubstituted-2,2'-bipyridines.<sup>8</sup> Rebek illustrated how the rate of an intramolecular condensation reaction of a 2,2'-bipyridine derivative with amide and ester moieties was increased by the coordination of metal cations at the diimine unit (Figure 4.3).

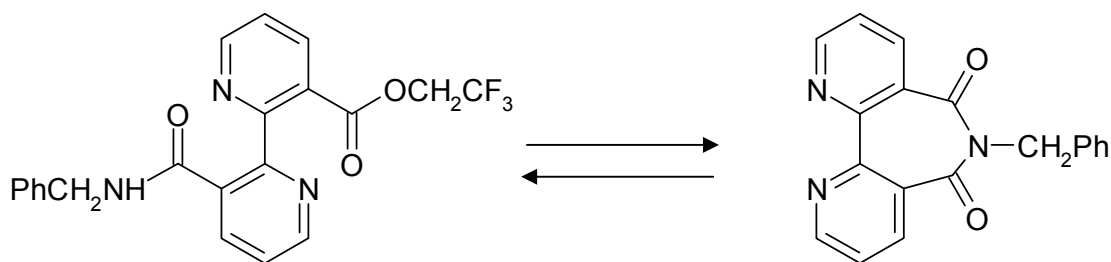


**Figure 4.3:** Scheme showing the intramolecular condensation reaction of a 2,2'-bipyridine derivative with amines

The half-life for the reaction was 60 minutes after complexation with  $\text{NiCl}_2$ , whereas without any metal ions, the reaction was significantly slower. Rebek proposed that, at least to some degree, the cyclisation reaction was accelerated by the coordination of the bipyridine unit to the  $\text{Ni(II)}$  centre, as this forces the two bipyridine rings to be approximately coplanar and therefore brings both the nucleophile and the electrophile units into close proximity. Other reported systems include the allosteric enhancement of both elimination and substitution reactions.<sup>8</sup> In these systems, the enhancement in the rate of reaction occurs upon coordination of a metal cation; it is not important which metal is used as long as the bipyridine unit is coordinated.

There are several reports of allosteric effects in coordination complexes; Rebek and coworkers have synthesised a range of ligands containing 2,2'-bipyridine substituted with a crown ether group at the 3,3'-positions (Figure 4.4).<sup>5,6,10</sup>

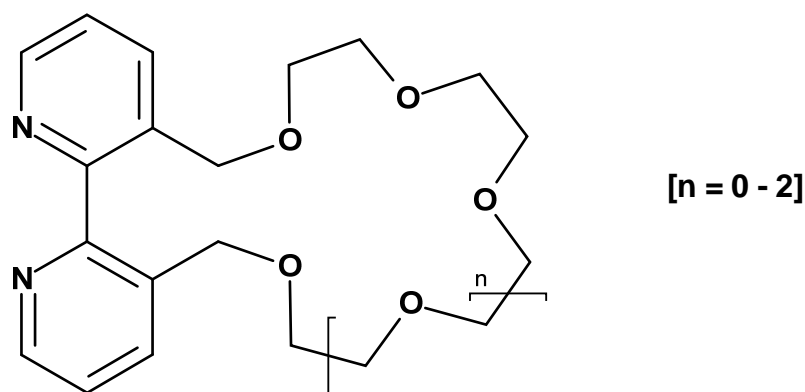


**Figure 4.4:** Ligands containing 2,2'-bipyridine appended with a crown ether used by Rebek<sup>10</sup>

The bipyridyl unit can coordinate transition metals and the crown ether moiety can bind alkali metal ions. These authors demonstrated that binding at one site altered the receptivity of the other, remote, site. They measured the selectivity of the ligand and its

[W(CO)<sub>4</sub>] complex for Li<sup>+</sup>, Na<sup>+</sup> and K<sup>+</sup> in ion transport experiments.<sup>6</sup> It was found that the free ligand preferentially bound potassium in its crown ether cavity, with both benzylic oxygen atoms also coordinating the metal ion. However, when the bipyridyl moiety was coordinated to a tungsten atom, the benzylic oxygens were forced into a conformation whereby only one of them could coordinate an alkali metal ion and so a preference for the smaller sodium ion was observed. Thus, the selectivity of the crown ether unit for metal ions was controlled allosterically by coordination of the bipyridyl unit.

Rice *et al.* have also demonstrated allosteric effects in coordination complexes containing crown ether and tetra-aza-crown units.<sup>11-16</sup> In the first case, a ligand was synthesised which contained a pyridyl-thiazolyl backbone and a crown ether group attached to the 3,3'-positions of the central bipyridyl core (Figure 4.5).

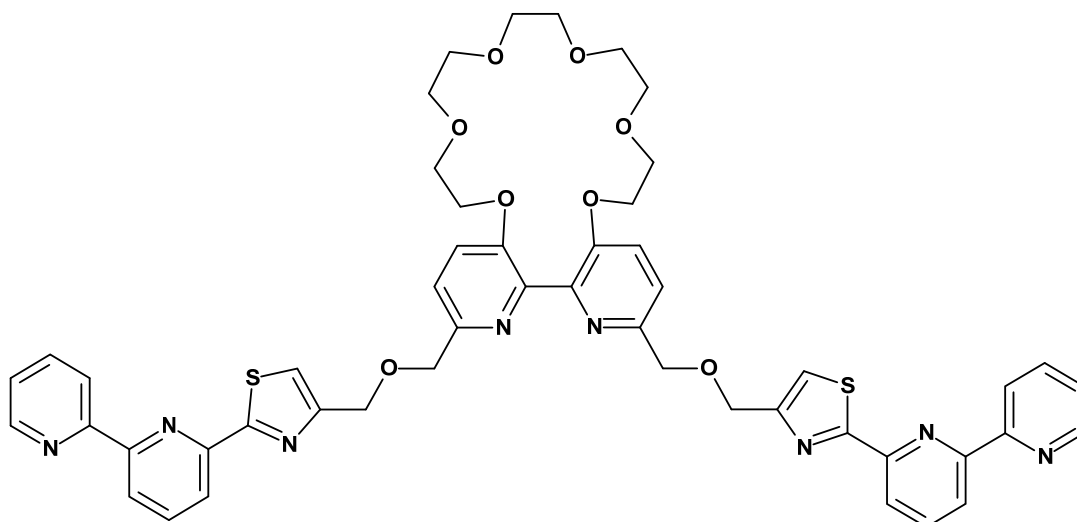


**Figure 4.5:** Crown ether-appended ligand used in studies of allosteric control of helicate formation<sup>11</sup>

This ligand contains two tridentate binding domains and a central bidentate binding domain separated by the ether spacer groups and thus forms a heterotrinnuclear double helicate with zinc and copper(I) ( $[Zn_2Cu(L)_2]^{5+}$ ). Binding of Ba<sup>2+</sup> ions to the crown ether moieties of the complex results in the central bipyridine no longer being able to coordinate the Cu(I) ion due to the decrease in the torsion angle of the bipy unit necessary for efficient coordination of the barium ions by the aryl oxygen atoms of the crown. A large number of species was observed in the <sup>1</sup>H NMR spectrum of the complex with added barium, indicating that the ligand had, effectively, been

allosterically *deprogrammed*, losing some of the pre-programmed information which caused it to form a double helicate complex.

A similar effect was observed using a ligand containing a bipyridyl unit and a tetra-aza-crown.<sup>12</sup> Both groups are capable of binding Cu(II) ions but it was discovered that the binding of copper by the aza-crown showed substantial negative cooperativity when the bipy unit was already coordinated. This was attributed to the fact that the tetra-aza-crown could coordinate copper through only three of its N-donors due to conformational restraints.

The ability of a ligand to change its preference for metal ions, *via* an allosteric interaction, has been reported.<sup>13</sup> In this example the ligand in Fig 4.6 contains both a potentially tetradentate N-donor domain and a crown ether unit on the back of the ligand strand. Reaction of this ligand with both Cu(I) and Zn(II) results in approximately equal amounts of both the mononuclear zinc-containing and dinuclear double helicate copper-containing species. In the mononuclear zinc(II) complex the four nitrogen atoms coordinate the metal centre in the four equatorial positions, whereas with Cu(I) the ligand splits about the inter-pyridine bond into two bidentate domains. Each of the two Cu(I) ions is coordinated by two of these domains from different ligands. A mixture of complexes occurs as the ligand can partition into either tetradentate or bis-bidentate binding domains. Upon addition of Sr(II) to this mixture of complexes a change is observed and by far the main species present is the zinc-containing complex. This change is attributed to an allosteric effect as the strontium ions coordinate the crown ether unit and upon doing so the ability of the ligand to twist about the inter-pyridine bond is diminished, thereby precluding helicate formation.

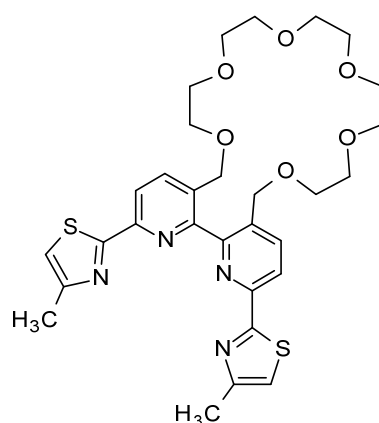


**Fig 4.6:** The potentially tetradentate crown ether-appended ligand used in studies of allosteric interactions<sup>13</sup>

This chapter focuses on developing the coordination chemistry of  $L^5$ , which has been previously studied by Rice *et al.*, and investigation of allosteric control of its coordination behaviour.<sup>17</sup> Previously, these authors showed that reaction of Cd(II) with a similar pyridyl-thiazole ligand which did not contain any amine functional groups on the 3,3'-position of the central bipyridine unit resulted in the formation of a mononuclear species.<sup>18</sup> This structure showed the ligand acting as a planar tetradentate donor which coordinated the Cd(II) ion in the equatorial positions. However, for  $L^5$  to be able to bind *one* metal *via* all four N-donors it would have to approach a planar geometry; this is unlikely due to unfavourable steric interactions between the two amine functional groups on the 3,3'-positions of the central bipyridine core. Therefore, when in the solid state,  $L^5$  prefers the formation of a dinuclear double helicate as this minimises unfavourable interactions between the two substituents. Indeed, single crystal X-ray diffraction studies showed that when the ligand was reacted with Cd(II) ions, the ligand partitioned in to two bis-bidentate pyridyl-thiazole binding domains. Figure 4.7 shows the dicadmium(II) double stranded helicate  $[Cd_2(L^5)_2]^{4+}$ . The coordination spheres of the metal ions are completed by an acetonitrile molecule and a perchlorate anion in each case, which in turn produces two identical distorted octahedral geometries.

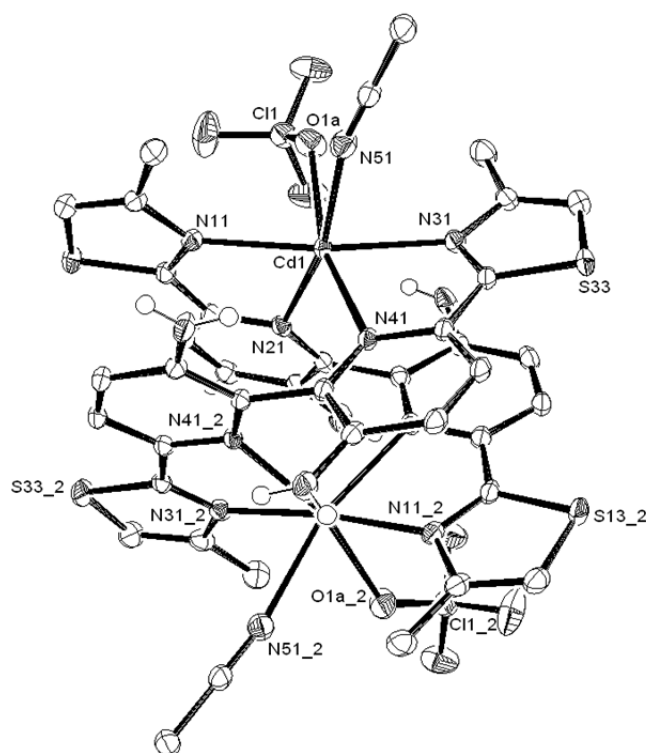


**Figure 4.7:** Solid-state structure of the  $[Cd_2(L^5)_2(MeCN)_2(ClO_4)_2]^{2+}$  complex cation (thermal ellipsoids are shown at a 50% probability level). All hydrogens (except amine) have been omitted for clarity. The “\_2” symbol in the atom labels indicates that these atoms are at equivalent positions (1 - x, y, - z)

$^1\text{H}$  NMR studies were performed<sup>17</sup> and the spectrum of crystals dissolved in  $\text{CD}_3\text{CN}$  showed that, in solution, the complex of  $\text{L}^5$  with cadmium exists as an equilibrium mixture of mononuclear species and dinuclear helicate  $2[\text{Cd}(\text{L}^5)(\text{CD}_3\text{CN})_2]^{2+} \leftrightarrow [\text{Cd}_2(\text{L}^5)_2(\text{CD}_3\text{CN})_4]^{4+}$ . As expected from the symmetry, the  $^1\text{H}$  NMR spectra of both the dinuclear and the mononuclear species clearly show three signals in the aromatic region (Figure 4.8a), with additional signals from the  $\text{NH}_2$  and  $\text{CH}_3$  moieties observed at lower shift (not shown). On average, signals which are assigned to the helicate will appear more upfield, as they are shielded by the aromatic rings on the neighbouring helical ligand strand.

Reaction of the mixture of the  $\text{Cd}(\text{II})$ -containing dinuclear double helicate and mononuclear complexes with acetone showed the solution change in colour from yellow to dark orange.  $^1\text{H}$  NMR studies were performed and the spectrum now shows only one set of signals present within the aromatic region (Figure 4.8b). The chemical shifts of these signals are further downfield for this new species than those which are expected for a dinuclear helicate species.

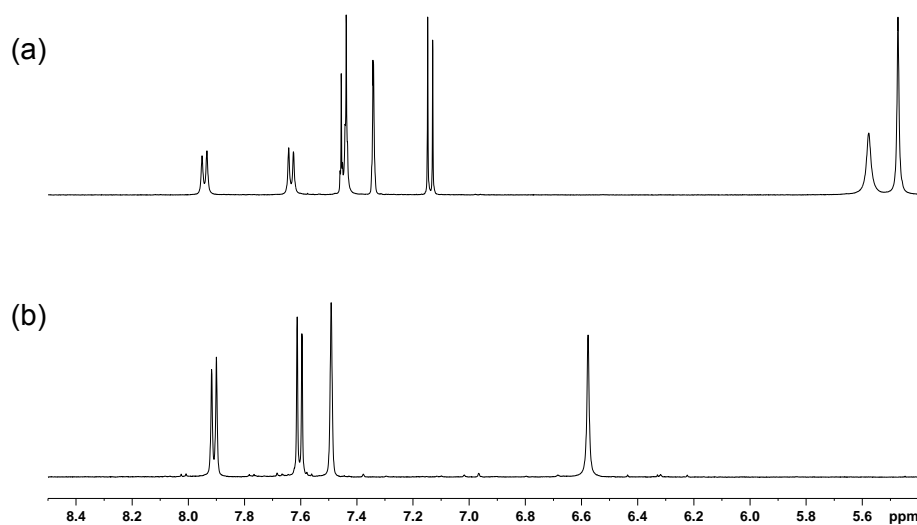


**Figure 4.8:** Selected regions of the  $^1\text{H}$  NMR spectra of  $\text{CD}_3\text{CN}$  solutions of (a)  $[\text{Cd}(\text{L}^5)]^{2+}$  and  $[\text{Cd}_2(\text{L}^5)_2]^{4+}$  and (b)  $[\text{Cd}(\text{L}^{5a})]^{2+}$ , where  $\text{L}^{5a}$  is the ligand after reaction with acetone

Single crystal X-ray diffraction confirmed formation of a mononuclear  $\text{Cd}(\text{II})$  complex (Figure 4.9).

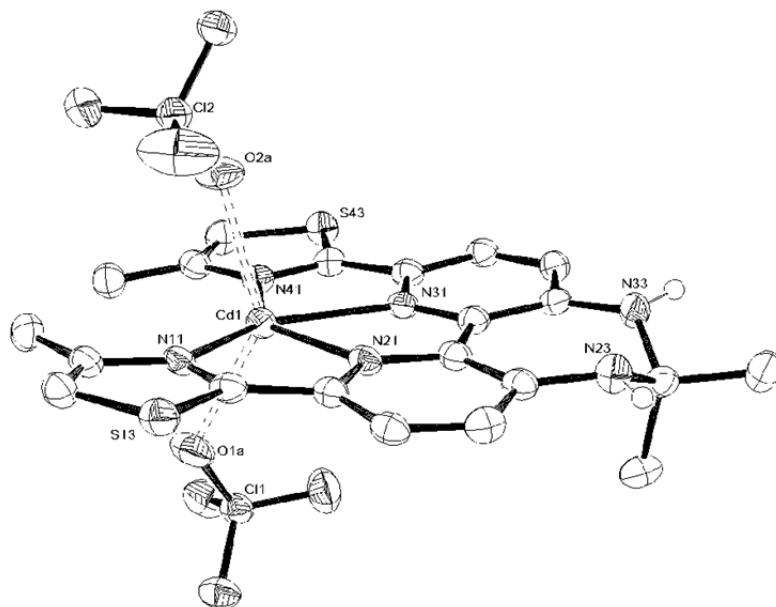


**Figure 4.9:** Solid-state structure of the  $[\text{Cd}(\text{L}^{5a})(\text{ClO}_4)_2]$  complex (thermal ellipsoids are shown at a 50% probability level)

Two monodentate perchlorate anions occupy the axial positions of the cadmium ion, with the ligand acting as a near planar ‘equatorial’ ligand. Even more interestingly, the amino groups of  $\text{L}^5$  have reacted with the acetone covalently bonding both to the 2-position on the propyl unit forming a 7-membered aminal ring.

When reacting  $\text{L}^5$  with  $[\text{Cu}(\text{MeCN})_4]\text{PF}_6$ , X-ray crystallography showed the formation of a copper-containing dinuclear double helicate (Figure 4.10). ESI-MS showed two ions present at  $m/z$  444 and 1033 which corresponded to  $\{[\text{Cu}_2(\text{L}^5)_2]\}^{2+}$  and  $\{[\text{Cu}_2(\text{L}^5)_2]\text{PF}_6\}^+$ , respectively.

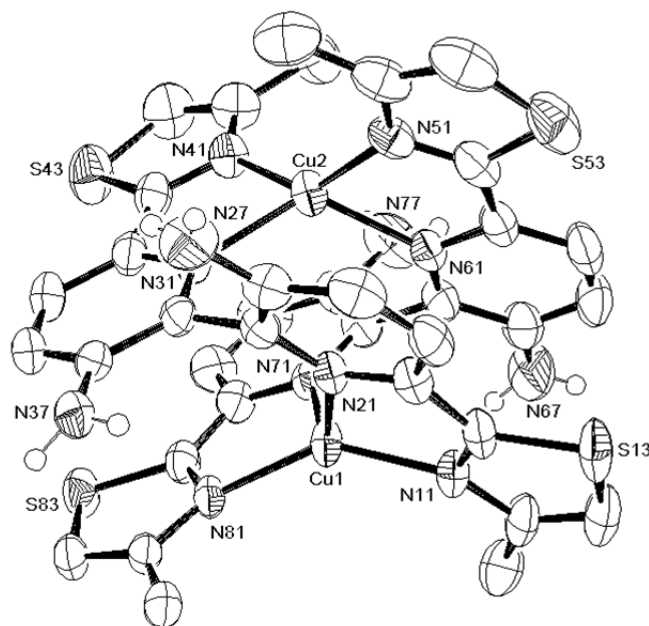


**Figure 4.10:** Solid state structure of the  $\{Cu_2(L^5)_2\}^{2+}$  complex cation (thermal ellipsoids are shown at a 50% probability level)

The ligand has partitioned into two bidentate binding domains in a similar manner to that of the Cd(II) helicate complex. The metal centre has adopted a 4-coordinate geometry with each Cu(I) centre coordinated by two pyridyl-thiazole units, one from each ligand.

The  $^1H$  NMR spectrum of the complex in  $CD_3CN$  solution clearly showed three signals in the aromatic region. The spectrum also shows one signal for both the amino and methyl groups which indicates that only one complex is formed in solution. The chemical shifts of these signals are consistent with formation of a dinuclear helicate when in solution. This agrees with the signals that are attributed to a helicate species in the  $[Cd_2(L^5)_2]^{4+}$  system.

## 4.2 Aims

The aim of this chapter was to form transition metal complexes of  $L^5$  and to examine whether the metal specificity of complexation can be controlled allosterically. This was to be achieved by means of constraining rotation about the interpyridine bond by reacting the diamino groups at the 3,3'-positions of the bipyridyl rings with cyclohexanone, forming a cyclic aminal product, as shown in the general reaction scheme shown in Fig. 4.11.

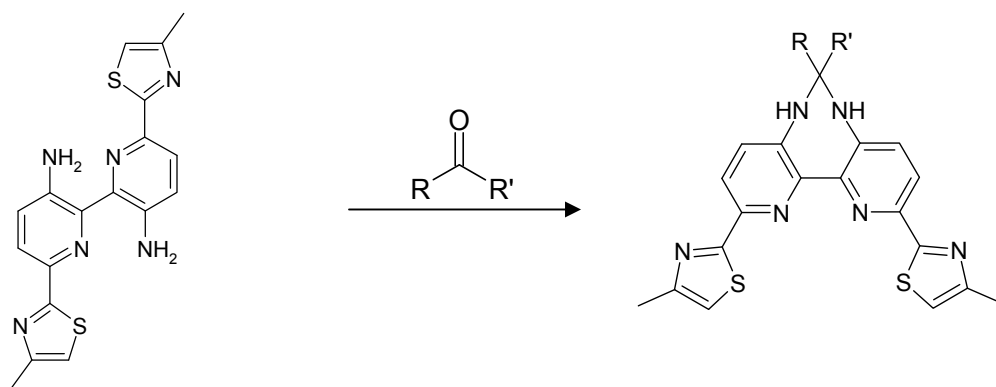
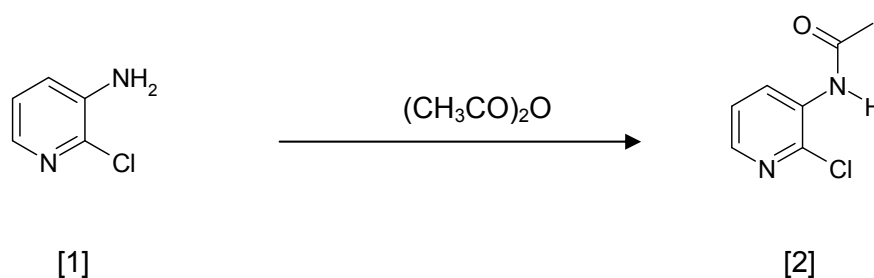


**Figure 4.11:** General reaction scheme of  $L^5$  with ketones

## 4.3 Experimental

### 4.3.1 Ligand synthesis (L<sup>5</sup>)

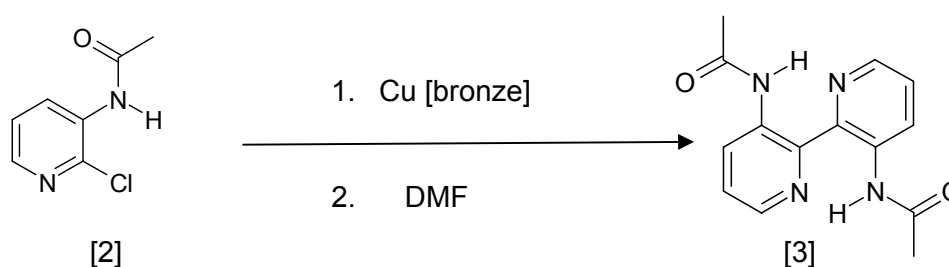
#### 4.3.1.1 Synthesis of 2-chloro-3-acetylamidopyridine, [2]



To a round bottom flask charged with 3-amino-2-chloropyridine **[1]** (1.40 g, 10.98 mmol) was added acetic anhydride (20 mL) and the reaction was allowed to stir for 24 hrs. Removal of the solvent by rotary evaporation gave the product as a clear oil, resulting in **[2]** as a beige crystalline solid upon cooling (1.80 g, 97%).

<sup>1</sup>H NMR (500 MHz, CDCl<sub>3</sub>) δ 9.10 (dd, 1H, *J* = 8.4, 1.57, py), 8.13 (dd, 1H, *J* = 4.5, 1.55), 7.30 (d, 1H, *J* = 8.4, 4.5 Hz, py), 7.1 (s, 1H, -CONH). High res. ESI-MS found *m/z* 171.0316 C<sub>7</sub>H<sub>8</sub>N<sub>2</sub>O<sub>1</sub>Cl<sub>1</sub> ([M+H]<sup>+</sup>) requires *m/z* 171.0320.

#### 4.3.1.2 Synthesis of 2,2'-bipyridine-3,3'-diacetylamide, [3]

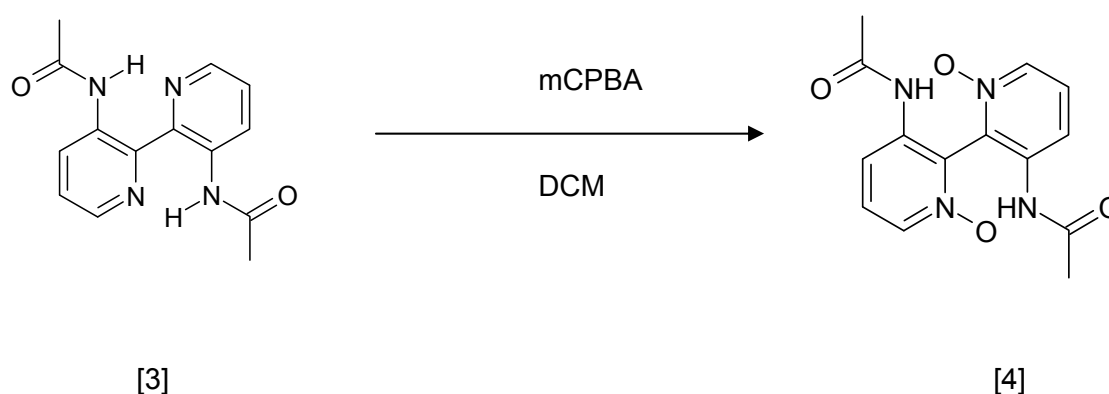


Under an atmosphere of nitrogen, a 250 mL two necked round bottom flask was charged with **[2]** (7 g, 0.04 mmol) and copper bronze (7 g, 0.12 mmol) and dimethylformamide (40 mL) was added. The reaction was stirred at 80 °C for 16 hrs then cooled to 0 °C and poured over ice (200 mL). The cold solution was filtered

through a sintered glass funnel charged with celite then washed with  $\text{NH}_3$  (aq.) (400 mL) giving a turquoise solid. The product was extracted into DCM (10 x 50 mL) and left to dry for 24 hrs which gave **[3]** as a brown solid (2.8 g, 25%).

$^1\text{H}$  NMR (500 MHz,  $\text{CDCl}_3$ )  $\delta$  13.17 (s, 2H, NH), 9.12 (dd, 2H, py,  $J = 8.54, 1.60$ ), 8.36 (dd, 2H, py,  $J = 4.58, 1.60$ ), 7.40 (dd, 2H, py,  $J = 8.20, 4.60$  Hz), 2.26 (s, 6H,  $\text{CH}_3$ ). High res. ESI-MS found  $m/z$  271.1193  $\text{C}_{14}\text{H}_{15}\text{N}_4\text{O}_2$  ( $[\text{M}+\text{H}]^+$ ) requires  $m/z$  271.1190.

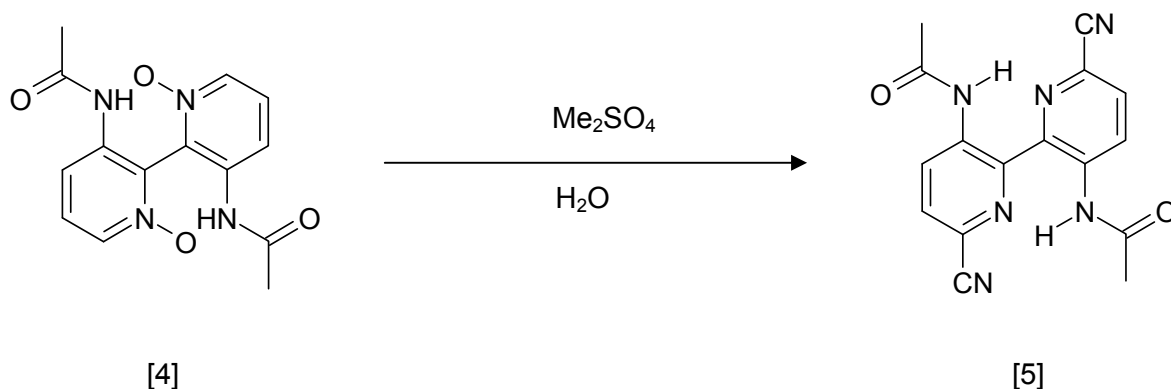
#### 4.3.1.3 Synthesis of 3,3'-diacetylamino-2,2'-bipyridine-*N,N*-dioxide, **[4]**



A solution of **[3]** (1 g, 3.7 mmol) in DCM (100 mL) was stirred at room temperature. To this was added mCPBA (77%, 2.74 g, 15.86 mmol) and the reaction was stirred at room temperature for 12 hrs. The reaction was followed by TLC and upon completion purification *via* column chromatography (10% MeOH in DCM,  $\text{Al}_2\text{O}_3$ ) gave **[4]** as a white solid (1.14 g, 100%).

$^1\text{H}$  NMR (500 MHz,  $\text{CDCl}_3$ )  $\delta$  9.41 (s, 2H, NH), 8.15 (d, 2H,  $J = 6.4$ , py), 7.66 (d, 2H,  $J = 8.4$ ), 7.46 (dd, 2H,  $J = 6.5, 8.4$ , py), 1.84 (s, 3H,  $-\text{CH}_3$ ). High res. ESI-MS found  $m/z$  303.1093  $\text{C}_{14}\text{H}_{15}\text{N}_4\text{O}_4$  ( $[\text{M}+\text{H}]^+$ ) requires  $m/z$  303.1088.

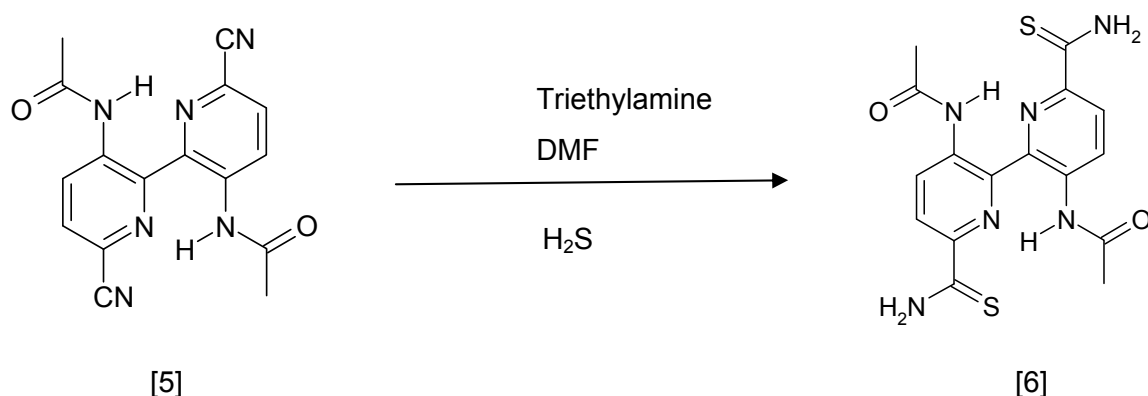
#### 4.3.1.4 Synthesis of 3,3'-diacetylamino-6,6'-dicyano-2,2'-bipyridine, [5]



A solution of **[4]** (1.04 g, 3.72 mmol), dimethyl sulphate (30 mL) and DCM (10 mL) was stirred at 60 °C for 24 hrs during which time a yellow solid slowly precipitated out. Ethanol (20 mL) was added to the reaction followed by filtration. The solid was suspended in a solution of NaCN (0.5 g, 10.2mmol) in H<sub>2</sub>O (100 mL), after which time a cream solid slowly precipitated out. Filtration followed by washing with H<sub>2</sub>O (4 x 20 mL) gave **[5]** as a cream solid (0.832 g, 70%).

<sup>1</sup>H NMR (500 MHz, DMSO-*d*<sub>6</sub>) δ 9.93 (s, 2H, NH), 8.57 (d, 2H, J = 8.6 Hz, py), 8.01 (brs, 2H, py), 1.98 (s, 6H, -CH<sub>3</sub>). High res. ESI-MS found *m/z* 343.0912 C<sub>16</sub>H<sub>12</sub>N<sub>6</sub>O<sub>2</sub>Na<sub>1</sub> ([M+Na]<sup>+</sup>) requires *m/z* 343.0914.

#### 4.3.1.5 Synthesis of 3,3'-diacetylamino-6,6'-dithioamide-2,2'-bipyridine, [6]

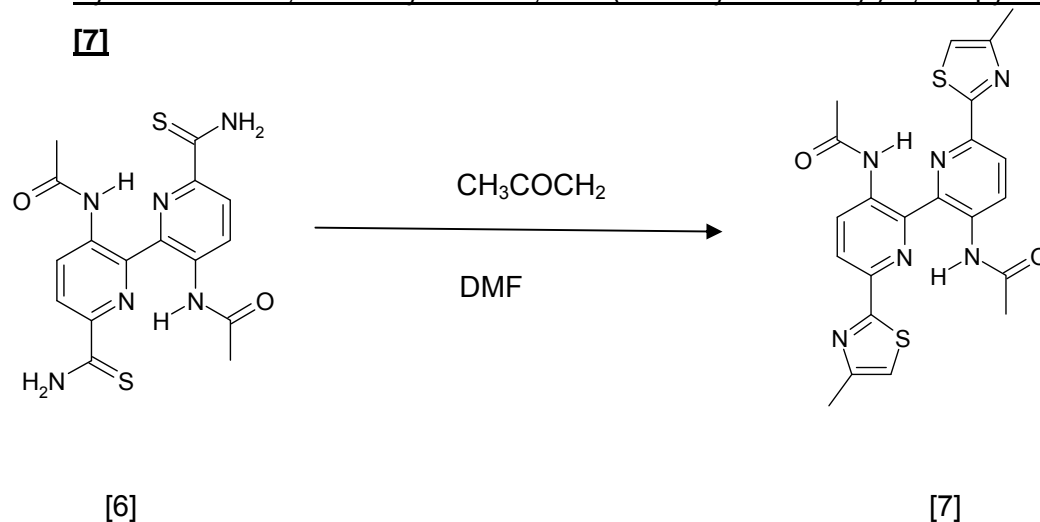


A solution of **[5]** (0.832 g, 2.60 mmol) and triethylamine (1 mL) in DMF (10 mL) was placed in a flask and H<sub>2</sub>S was slowly bubbled through the solution for 15 minutes,

during which time the solution turned yellow. The yellow solution was allowed to stand for 48 hrs during which time a yellow solid slowly precipitated out. Collection via filtration gave pure 2,2'-bipyridine bis-thioamide-3,3'-diacetylamide **[6]** as a yellow solid (0.56 g, 56%).

$^1\text{H}$  NMR (500 MHz, DMSO- $d_6$ )  $\delta$  10.48 (s, 2H, CONH), 10.15 (s, 2H, CSNH $_2$ ), 9.75 (s, 2H, CSNH $_2$ ), 8.65 (d, 2H, J = 8.7, py), 8.46 (d, 2H, J = 8.7 Hz, py), 2.03 (s, 6H, -COCH $_3$ ). High res. ESI-MS found  $m/z$  389.0846 C $_{16}$ H $_{17}$ N $_6$ O $_2$ S $_2$  ([M+H] $^+$ ) requires  $m/z$  389.0849.

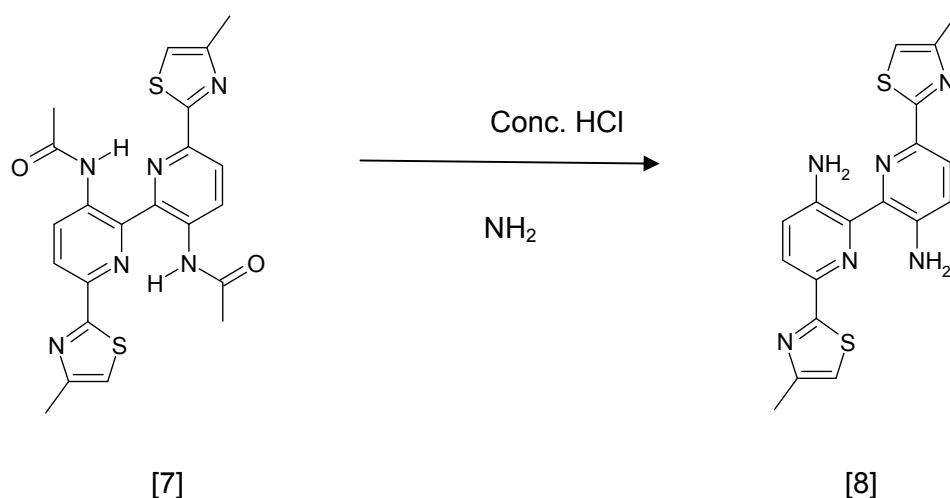
#### 4.3.1.6 Synthesis of 3,3'-diacetylamino-6,6'-bis(4-methylthiazol-2-yl)-2,2'-bipyridine,



To a round bottom flask charged with **[6]** (0.56 g, 1.44 mmol) was added DMF (20 mL) and chloroacetone (0.2 mL) and the reaction was heated at 80 °C with stirring for 4 hrs. A yellow solid slowly precipitated out and the precipitate was filtered and washed with EtOH (4 x 20 mL) and Et $_2$ O (4 x 20 mL) which gave **[7]** as a yellow solid (0.32 g, 47%).

$^1\text{H}$  NMR (500 MHz, DMSO- $d_6$ )  $\delta$  10.44 (s, 2H, NH), 8.76 (d, 2H, J = 8.7, py), 8.18 (d, 2H, J = 8.7 Hz, py), 7.41 (s, 2H, tz), 2.47 (s, 3H, tz-CH $_3$ ), 2.08 (s, 3H, -COCH $_3$ ). High res. ESI-MS found  $m/z$  465.1171 C $_{22}$ H $_{21}$ N $_6$ O $_2$ S $_2$  ([M+H] $^+$ ) requires  $m/z$  465.1162.

#### 4.3.1.7 Synthesis of 3,3'-diamino-6,6'-bis(4-methylthiazol-2-yl)-2,2'-bipyridine, [8]

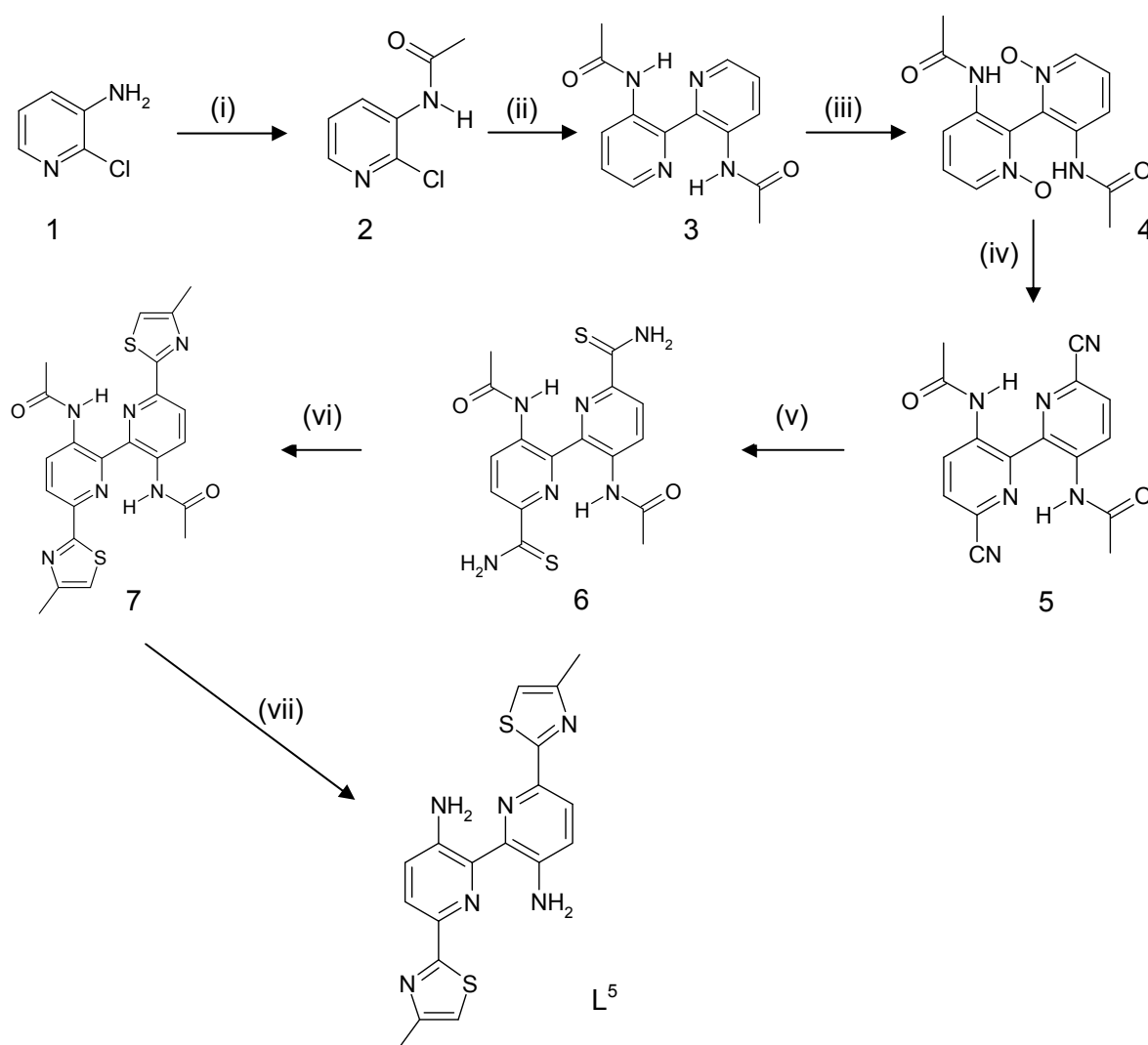


The yellow solid **[7]** (0.596 g, 1.28 mmol) was suspended in HCl (conc., 50 mL) and refluxed for 3 hrs. The solution was then suspended in H<sub>2</sub>O (100 mL) followed by filtration, resulting in an orange solid. The solid was suspended in NH<sub>3</sub> (aq.) (40 mL) for 12 hrs after which time the colour changed from orange to yellow. The solution was allowed to stir at room temperature for 1 hr. Filtration followed by washing with H<sub>2</sub>O (4 x 20 mL), EtOH (4 x 20 mL) and Et<sub>2</sub>O (4 x 20 mL) gave **[8]** as a yellow solid (0.362 g, 74%).

<sup>1</sup>H NMR (500 MHz, DMSO-*d*<sub>6</sub>) δ 7.90 (d, 2H, J = 8.55, py), 7.77 (brs, 4H, -NH<sub>2</sub>), 7.35 (d, 2H, J = 8.55 Hz, py), 7.26 (s, 2H, tz), 2.43 (s, 6H, tz-CH<sub>3</sub>). High res. ESI-MS found *m/z* 381.0962 C<sub>18</sub>H<sub>17</sub>N<sub>6</sub>S<sub>2</sub> ([M+H]<sup>+</sup>) requires *m/z* 381.0951.

## 4.4 Results and Discussion

The synthesis of  $L^5$ , including all reagents and conditions, was carried out in exactly the same manner as used in the synthesis of  $L^4$  shown in the previous chapter. The synthesis of  $L^5$  was performed using a six-step linear synthesis (Scheme 4.1); the ligand was produced by omitting the final step in the synthesis of  $L^4$ . Structural elucidation was performed using  $^1H$  NMR and mass spectrometry at each step of the synthesis and compared with spectra of  $L^4$ .



**Scheme 4.1:** Synthesis of  $L^5$  from 3-amino-2-chloropyridine [**1**]. Reagents and conditions: (i) acetic anhydride, RT, 24 hrs (ii) Cu bronze, DMF, 80°C, 16 hrs (iii) DCM, mCPBA, RT, 12 hrs (iv) dimethylsulphate, DCM, 60°C, 24 hrs, ethanol,  $H_2O$ , sodium cyanide (v) triethylamine, DMF,  $H_2S$  (vi) DMF, chloroacetone, 80°C, 4 hrs (vii) conc. HCl, reflux,  $NH_3$ , RT, 12 hrs

#### 4.4.1 Coordination Chemistry of $L^5$

##### 4.4.1.1 Reaction of $L^5$ with silver(I)

The ligand  $L^5$  was not very soluble in common organic solvents. However, upon reaction with one equivalent of  $Ag(CF_3SO_3)$  in acetonitrile the ligand dissolved and produced a yellow solution. The slow diffusion of ethyl acetate into this resulting solution afforded yellow crystals. Single crystal X-ray analysis of these crystals showed the formation of a dinuclear double helicate species  $[Ag_2(L^5)_2]^{2+}$  in the solid state (Figure 4.12).

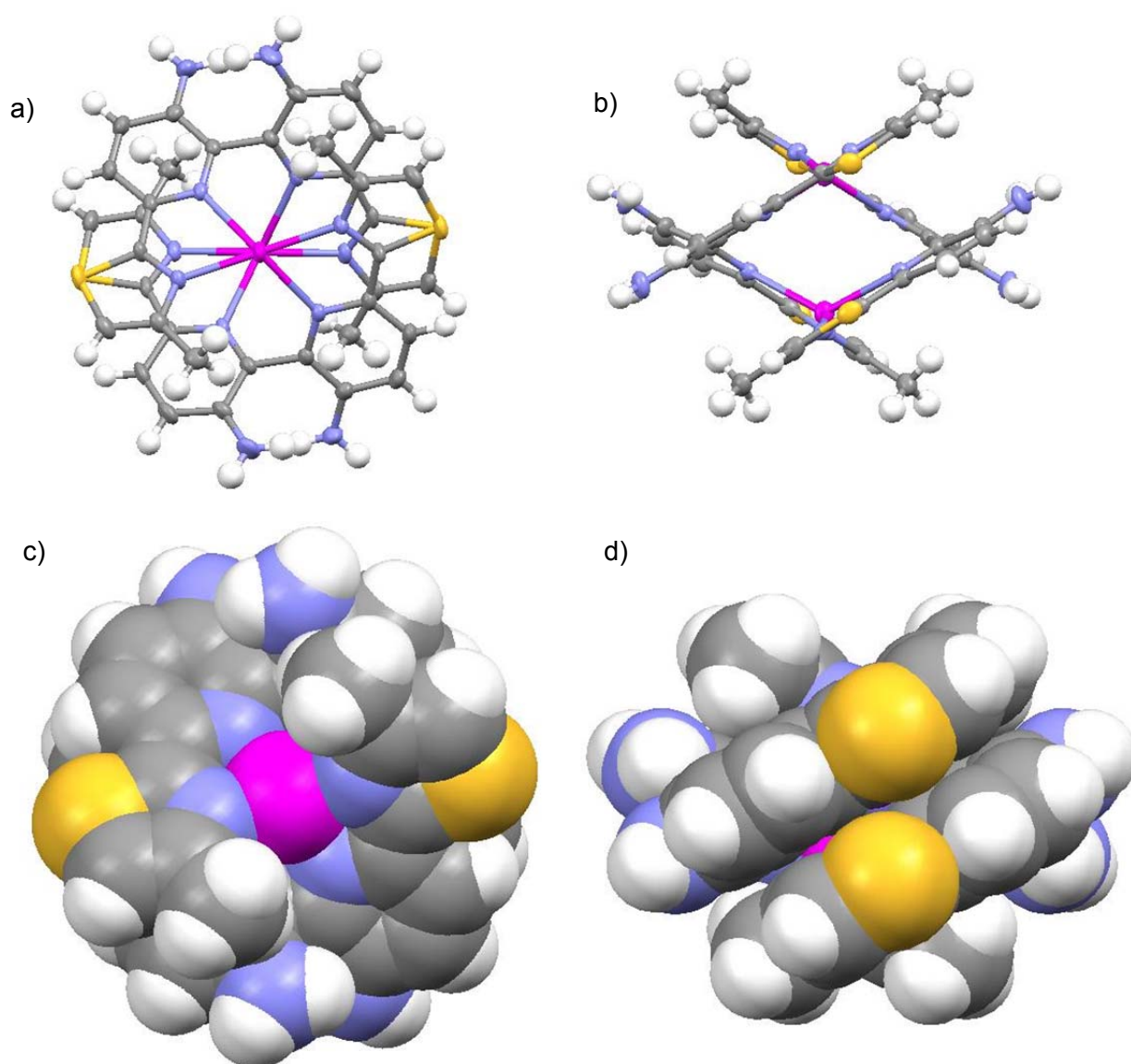


**Figure 4.12:** (a, b) Single crystal X-ray structure of  $[Ag_2(L^5)_2]^{2+}$ ; (c, d) as the space-filling model

The crystal structure of the complex shows how the ligand has partitioned into two bidentate binding domains. The metal centre has adopted a 4-coordinate tetrahedral geometry with each Ag(I) centre coordinated by two pyridyl-thiazole units, one from each ligand strand. Selected bond lengths and angles are shown in Tables 4.1 and 4.2.

Bond	Bond length (Å)
Ag(1)-N(3)	2.3726(19)
Ag(1)-N(6)	2.2604(19)
Ag(2)-N(1)	2.2161(19)
Ag(2)-N(2)	2.3918(18)

**Table 4.1:** Selected bond lengths (Å) for the complex cation  $[\text{Ag}_2(\text{L}^5)_2]^{2+}$ ; other bond lengths are generated by symmetry

Bond	Bond angle (°)
N(3)-Ag(1)-N(3)	131.07(9)
N(6)-Ag(1)-N(3)	74.05(7)
N(6)-Ag(1)-N(3)	118.89(7)
N(6)-Ag(1)-N(6)	150.87(10)
N(1)-Ag(2)-N(1)	155.54(11)
N(1)-Ag(2)-N(2)	73.86(7)
N(1)-Ag(2)-N(2)	117.80(7)
N(2)-Ag(2)-N(2)	127.18(9)

**Table 4.2:** Selected bond angles (°) for the complex cation  $[\text{Ag}_2(\text{L}^5)_2]^{2+}$ ; other bond angles are generated by symmetry

As we have previously shown  $^1\text{H}$  NMR analysis can determine if there are mononuclear and/or dinuclear double helicate complexes present, as the double helicate signals tend to be at lower chemical shift. The  $^1\text{H}$  NMR spectrum of the

crystals dissolved in acetonitrile (Figure 4.13) reveals that, in solution, reaction of  $L^5$  with silver has formed a double helical complex as expected. As stated earlier, signals ascribed to the helicate species appear, on average, more upfield due to shielding by aromatic rings that are on the adjacent ligand strand. These signals are consistent with dinuclear double helicate formation when in solution, with additional signals relating to the  $NH_2$  and  $CH_3$  functional groups.

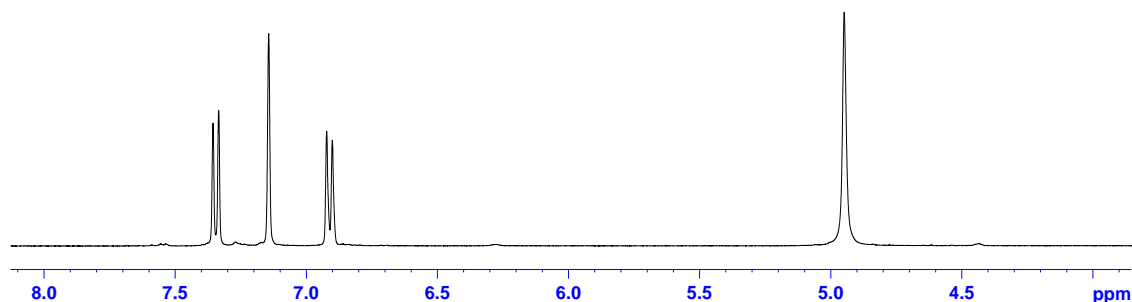


**Figure 4.13:** Aromatic region of the  $^1H$  NMR ( $CD_3CN$ ) spectrum of  $[Ag_2(L^5)_2]^{2+}$

ESI-MS showed two ions present at  $m/z$  488 and 1125 which corresponded to  $\{[Ag_2(L^5)_2]\}^{2+}$  and  $\{[Ag_2(L^5)_2](CF_3SO_3)\}^+$  respectively, which is also consistent with the NMR data produced.

#### 4.4.1.2 Reaction of $L^5$ with silver(I) and cyclohexanone

The  $[Ag_2(L^5)_2]^{2+}$  complex was reacted with cyclohexanone and a catalytic amount of camphorsulfonic acid, forming a cyclic aminal product with the bipy-diamine moiety of the ligand. Yellow crystals were obtained by slow diffusion of ethyl acetate into a yellow solution of the product; single crystal X-ray analysis of these showed the formation of a mononuclear species  $[Ag(L^{5a})]^+$  in the solid state as shown in Figure 4.14 (where  $L^{5a}$  is the modified ligand).

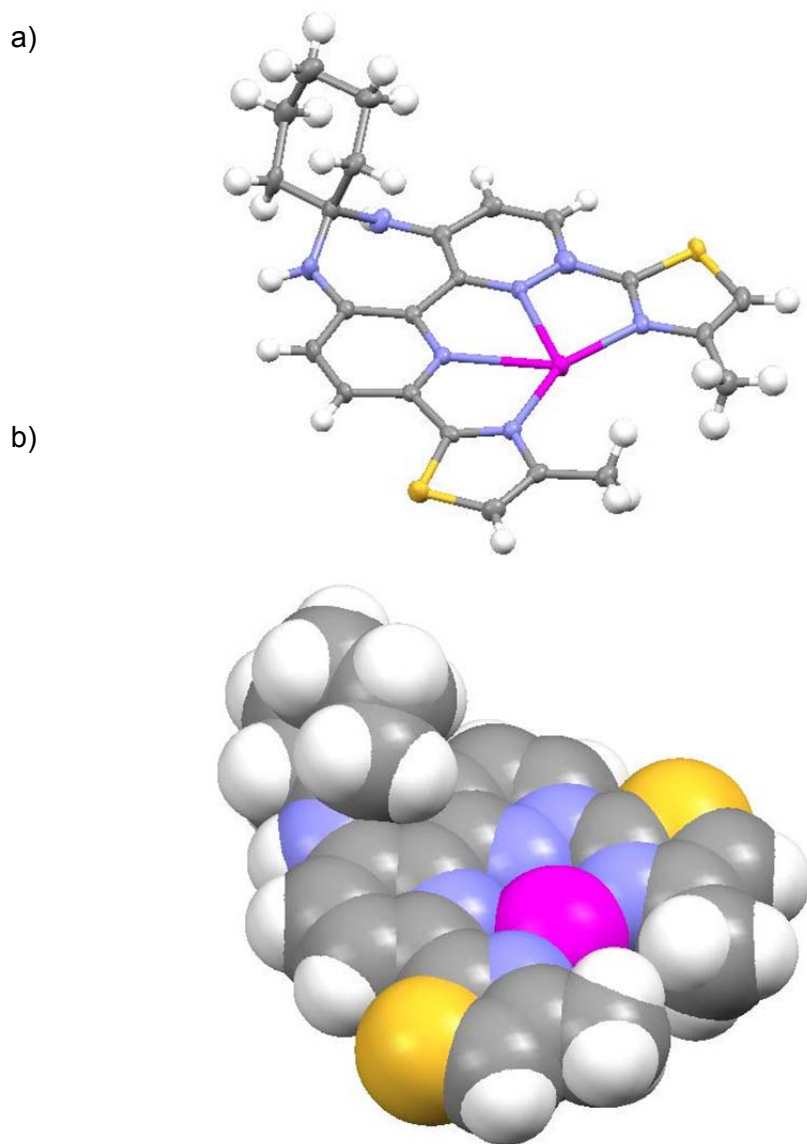


**Figure 4.14:** a) Single crystal X-ray structure of  $[\text{Ag}(\text{L}^{5a})]^+$ ; b) as the space filling model

The crystal structure of  $[\text{AgL}^{5a}]^+$  shows that the silver ion has now adopted an unusual 4-coordinate distorted square planar geometry. Due to reaction with cyclohexanone, the amine functional groups have been constrained, preventing rotation about the inter-pyridine bond and thus prohibiting formation of the double helicate. Selected bond lengths and angles are shown in Tables 4.3 and 4.4.

Bond	Bond length (Å)
Ag(1)-N(1)	2.2125(19)
Ag(1)-N(2)	2.5262(17)
Ag(1)-N(3)	2.5148(19)
Ag(1)-N(4)	2.2184(18)

**Table 4.3:** Selected bond lengths (Å) of the complex cation  $[\text{Ag}(\text{L}^{5a})]^+$

Bond	Bond angle (°)
N(1)-Ag(1)-N(2)	71.33(6)
N(1)-Ag(1)-N(3)	132.65(6)
N(1)-Ag(1)-N(4)	156.17(7)
N(3)-Ag(1)-N(2)	61.33(6)
N(4)-Ag(1)-N(2)	132.07(7)
N(4)-Ag(1)-N(3)	70.96(6)

**Table 4.4:** Selected bond angles (°) of the complex cation  $[\text{Ag}(\text{L}^{5a})]^+$

The  $^1\text{H}$  NMR spectrum for the reaction of  $\text{L}^5$  with silver and cyclohexanone (shown in Figure 4.15) is somewhat surprising, with the main signals observed very similar to the uncyclised starting material (*i.e.*  $[\text{Ag}_2(\text{L}^5)_2]^{2+}$ ). One possible explanation is that the cyclised species is not very soluble and has precipitated out of solution (there was some solid material present in the NMR tube). Indeed broad signals at slightly higher chemical shift could be due to the presence of the poorly soluble cyclised complex. We can assume the main signals that are observed are due to the residual amounts of  $[\text{Ag}_2(\text{L}^5)_2]^{2+}$  which has not as yet reacted upon the addition of cyclohexanone.

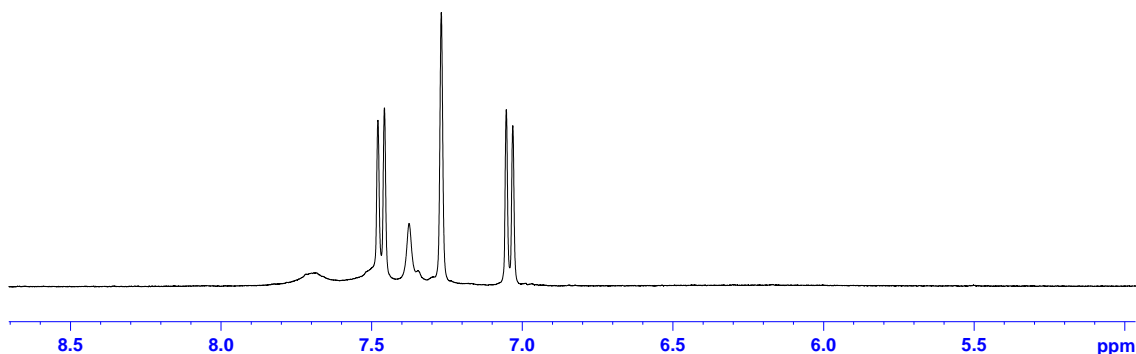


**Figure 4.15:** Aromatic region of the  $^1\text{H}$  NMR ( $\text{CD}_3\text{CN}$ ) spectrum of  $[\text{Ag}(\text{L}^{5a})]^+$

However, the crystal data is supported by ESI-MS analysis shows the presence of an ion at  $m/z$  569 which corresponds to  $[\text{Ag}(\text{L}^{5a})]^+$ .

#### 4.4.1.3 Reaction of $\text{L}^5$ with mercury(II)

Upon reaction of  $\text{L}^5$  with one equivalent of  $\text{Hg}(\text{ClO}_4)_2 \cdot 3\text{H}_2\text{O}$  in acetonitrile, the ligand dissolved and a yellow solution was formed from which a solid material was produced upon slow diffusion of ethyl acetate. The  $^1\text{H}$  NMR spectrum of this material dissolved in acetonitrile, shown in Figure 4.16, shows only one species is present in solution and, due to the relative chemical shift of the aromatic groups, that in solution a double helicate species has been formed.

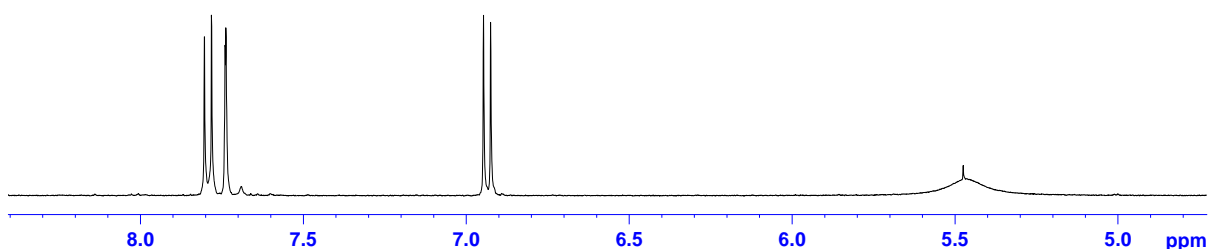


**Figure 4.16:** Aromatic region of the  $^1\text{H}$  NMR ( $\text{CD}_3\text{CN}$ ) spectrum of  $[\text{Hg}_2(\text{L}^5)_2]^{4+}$

The spectrum also contains one signal for both the  $\text{NH}_2$  and  $\text{CH}_3$  groups (not shown). Further confirmation of the formation of a dinuclear double helicate was given from the use of ESI-MS, where studies showed an ion present at  $m/z$  1461 corresponding to  $\{[\text{Hg}_2(\text{L}^5)_2](\text{ClO}_4)_3\}^+$ .

#### 4.4.1.4 Reaction of $L^5$ with mercury(II) and cyclohexanone

The ligand  $L^5$  was reacted with one equivalent of  $Hg(ClO_4)_2 \cdot 3H_2O$  in acetonitrile with the addition of cyclohexanone and a catalytic amount of camphorsulfonic acid. Yellow crystals were obtained by slow diffusion of ethyl acetate into a yellow solution of the product; single crystal X-ray analysis of these showed the formation of a mononuclear complex  $[Hg(L^{5a})]^{2+}$  in the solid state as shown in Figure 4.17.

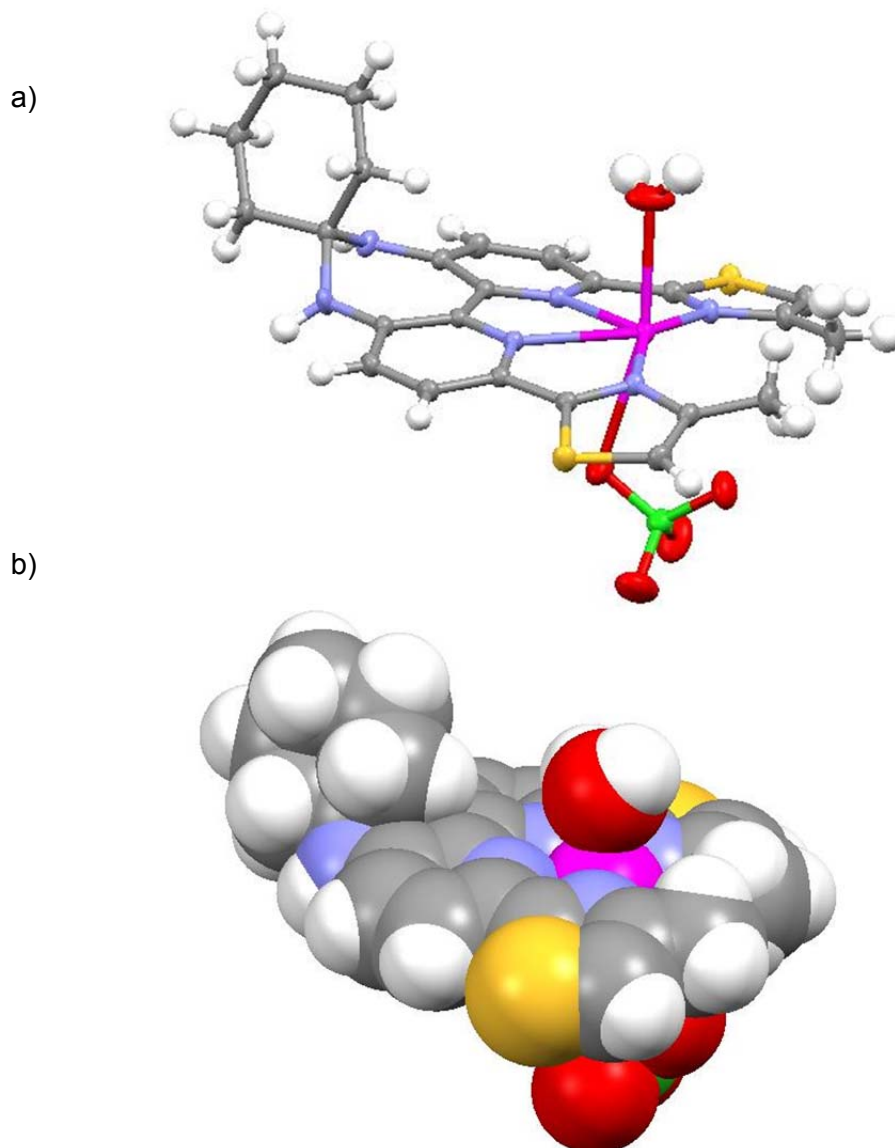


**Figure 4.17:** a) Single crystal X-ray structure of  $[Hg(L^{5a})]^{2+}$ ; b) as the space filling model

The crystal structure of  $[Hg(L^{5a})]^{2+}$  shows the mercury centre has now adopted a distorted octahedral geometry coordinated by four nitrogen atoms from the ligand in the equatorial positions and two oxygen donors in the axial positions, one from a water

molecule and the other from a perchlorate anion. Selected bond lengths and angles are shown in Tables 4.7 and 4.8.

Bond	Bond lengths (Å)
Hg(1)-N(1)	2.4281(15)
Hg(1)-N(2)	2.4626(15)
Hg(1)-N(5)	2.1990(15)
Hg(1)-N(6)	2.1878(15)
Hg(1)-O(1)	2.7349(17)
Hg(1)-O(1')	2.4988(18)

**Table 4.7:** Selected bond lengths (Å) of the complex cation  $[\text{Hg}(\text{L}^{5a})]^{2+}$

Bond	Bond angle (°)
N(1)-Hg(1)-N(2)	63.57(5)
N(5)-Hg(1)-N(1)	72.52(5)
N(5)-Hg(1)-N(2)	135.60(5)
N(6)-Hg(1)-N(1)	134.97(5)
N(6)-Hg(1)-N(2)	71.80(5)
N(6)-Hg(1)-N(5)	149.78(6)
N(1)-Hg(1)-O(1)	73.34(5)
N(1)-Hg(1)-O(1')	92.76(7)
N(2)-Hg(1)-O(1)	79.73(5)
N(2)-Hg(1)-O(1')	88.41(6)
N(5)-Hg(1)-O(1)	81.99(6)
N(5)-Hg(1)-O(1')	100.24(6)
N(6)-Hg(1)-O(1)	93.76(6)
N(6)-Hg(1)-O(1')	91.67(7)
O(1')-Hg(1)-O(1)	164.69(7)

**Table 4.8:** Selected bond angles (°) of the complex cation  $[\text{Hg}(\text{L}^{5a})]^{2+}$

The  $^1\text{H}$  NMR spectrum shows three signals present in the aromatic region, indicating that there is only one species present (Figure 4.18) which, based on the chemical shifts, is a mononuclear complex.

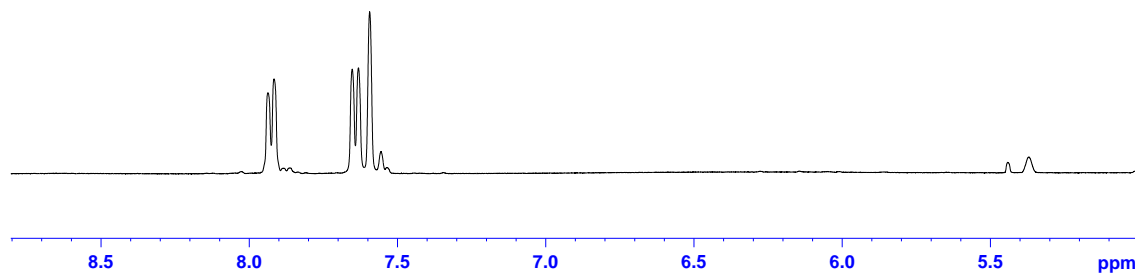


**Figure 4.18:** Aromatic region of the  $^1\text{H}$  NMR ( $\text{CD}_3\text{CN}$ ) spectrum of  $[\text{Hg}(\text{L}^{5a})]^{2+}$

ESI-MS studies showed only formation of the mononuclear species; two ions were present in the mass spectrum at  $m/z$  761 and 893 corresponding to  $\{[\text{Hg}(\text{L}^{5a})]\cdot\text{ClO}_4\}^+$  and  $\{[\text{Hg}(\text{L}^{5a})]\cdot\text{CSA}\}^+$  (where CSA = camphorsulfonic acid).

#### 4.4.1.5 Reaction of $\text{L}^5$ with zinc(II)

The reaction of  $\text{L}^5$  with  $\text{Zn}(\text{CF}_3\text{SO}_3)_2$  in acetonitrile, followed by slow diffusion of ethyl acetate produced yellow crystals, single crystal X-ray diffraction studies of which showed the formation of a dinuclear double helicate species  $[\text{Zn}_2(\text{L}^5)_2]^{4+}$  in the solid state (Figure 4.19).

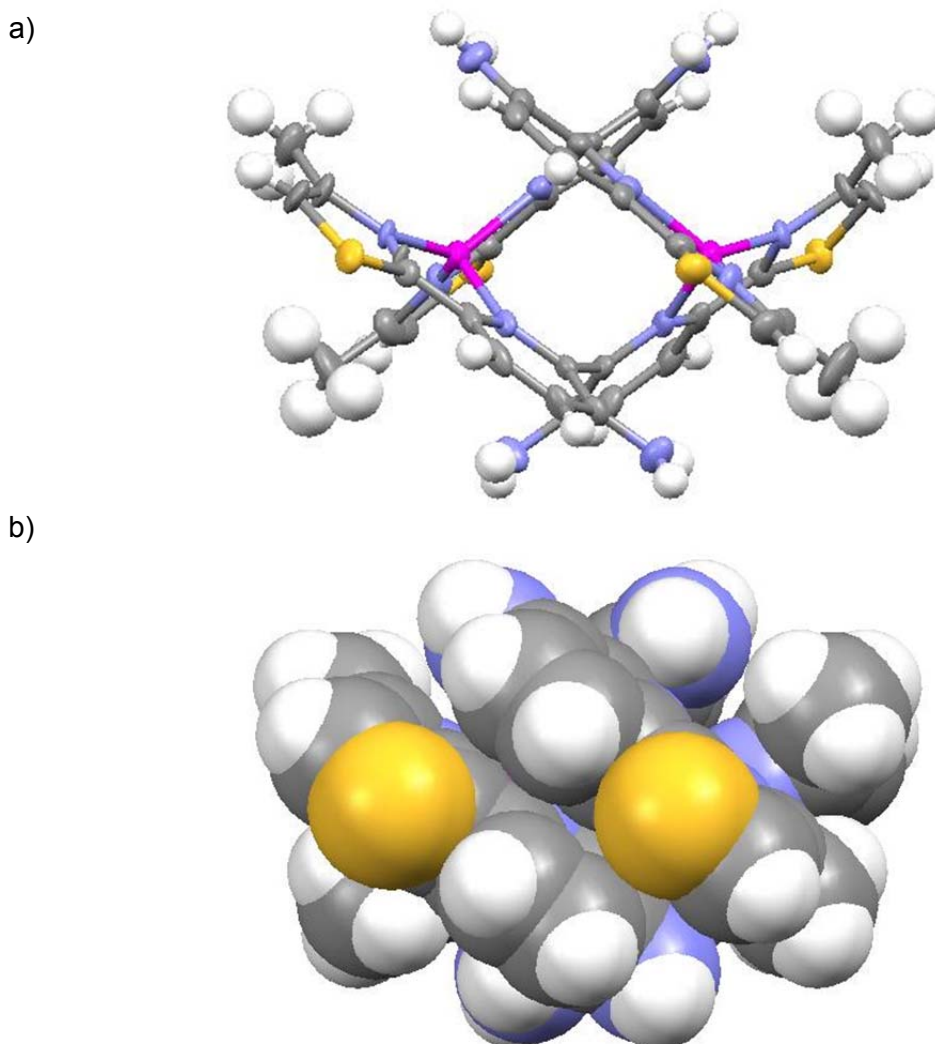


**Figure 4.19:** a) Single crystal X-ray structure of  $[\text{Zn}_2(\text{L}^5)_2]^{4+}$ , b) as the space-filling model

The ligand has again partitioned into two bidentate binding domains. Each Zn(II) centre is coordinated by two pyridyl-thiazole units, one from each ligand, with the metal adopting a 4-coordinate tetrahedral geometry.

Bond	Bond lengths (Å)
Zn(1)-N(1)	1.979(4)
Zn(1)-N(2)	2.041(3)
Zn(1)-N(3)	2.033(3)
Zn(1)-N(4)	2.071(9)
Zn(1)-N(4')	1.806(17)

**Table 4.9:** Selected bond lengths (Å) for the complex cation  $[\text{Zn}_2(\text{L}^5)_2]^{4+}$ ; other bond lengths are generated by symmetry

Bond	Bond angles (°)
N(1)-Zn(1)-N(2)	82.63(14)
N(1)-Zn(1)-N(3)	126.89(13)
N(1)-Zn(1)-N(4)	132.7(3)
N(2)-Zn(1)-N(4)	129.4(3)
N(3)-Zn(1)-N(2)	109.00(12)
N(3)-Zn(1)-N(4)	79.8(3)
N(4')-Zn(1)-N(1)	123.8(7)
N(4')-Zn(1)-N(2)	126.5(9)
N(4')-Zn(1)-N(3)	91.2(6)
N(4')-Zn(1)-N(4)	11.5(7)

**Table 4.10:** Selected bond angles (°) for the complex cation  $[\text{Zn}_2(\text{L}^5)_2]^{4+}$ ; other bond angles are generated by symmetry

NMR analysis of the crystals dissolved in  $\text{CD}_3\text{CN}$  shows three signals present in the aromatic region of the spectrum, along with a signal in both the  $\text{NH}_2$  and  $\text{CH}_3$  regions and comparison with those observed for  $[\text{Ag}_2(\text{L}^5)_2]^{2+}$  and  $[\text{Hg}_2(\text{L}^5)_2]^{4+}$  indicates that only a mononuclear species is present (Figure 4.20), contradicting the solid state result. Thus the data suggest that *in solution* the Zn(II) complex is the mononuclear species  $[\text{Zn}(\text{L}^5)]^{2+}$ . Although such phase dependant behaviour (*i.e.* the formation of a mononuclear species in MeCN solution and a dinuclear double helicate in the solid state) is unusual it is not unknown and such behaviour has been observed in other metallocupramolecular systems.<sup>19</sup>

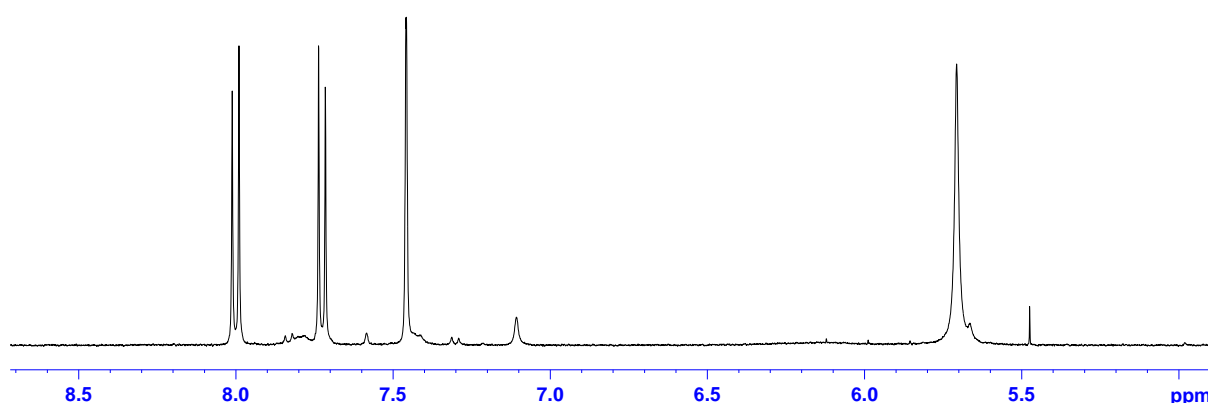


**Figure 4.20:** Aromatic region of the  $^1\text{H}$  NMR ( $\text{CD}_3\text{CN}$ ) spectrum of  $[\text{Zn}_2(\text{L}^5)_2]^{4+}$

The formation of a dinuclear double helicate was also observed in the ESI-mass spectrum, which showed an ion present at  $m/z$  973 corresponding to  $\{[\text{Zn}_2(\text{L}^5)_2](\text{CF}_3\text{SO}_3)_3\}^+$ .

#### 4.4.1.6 Reaction of $\text{L}^5$ with zinc(II) and cyclohexanone

The  $[\text{Zn}_2(\text{L}^5)_2]^{4+}$  (or  $[\text{Zn}(\text{L}^5)]^{2+}$ ) complex was reacted with cyclohexanone in the presence of a catalytic amount of camphorsulfonic acid and a yellow material was obtained by slow diffusion of ethyl acetate into a yellow solution of the product. The  $^1\text{H}$  NMR spectrum of the reaction indicated formation of a mononuclear species since the chemical shifts of the signals are relatively high (Figure 4.21).

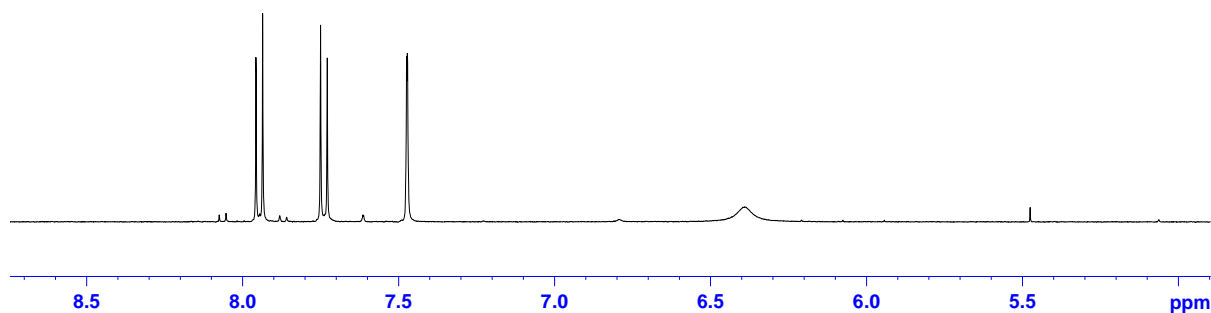


**Figure 4.21:** Aromatic region of the  $^1\text{H}$  NMR ( $\text{CD}_3\text{CN}$ ) spectrum of  $(\text{Zn}(\text{L}^{5a}))^{2+}$

ESI-MS analysis showed ions present at  $m/z$  673 and 755 which corresponded to  $\{[\text{ZnL}^{5a}](\text{CF}_3\text{SO}_3)\}^+$  and  $\{[\text{ZnL}^{5a}]\text{CSA}\}^+$ , which is also consistent with the NMR data.

#### 4.4.2 Metal specificity of $\text{L}^5$

As the ligand's ability to coordinate metal ions can be changed by reaction of the amino groups with a suitable ketone, competitive experiments were performed using  $\text{L}^5$  with various octahedral and tetrahedral metals to investigate the selectivity of the ligand  $\text{L}^5$  and to see if this could be controlled allosterically by reaction of cyclohexanone with the diamino groups of the bipyridine ligand. A series of experiments was performed using  $^1\text{H}$  NMR analysis to examine the solution behaviour of these systems.

##### 4.4.2.1 Reaction of $\text{L}^5$ with cadmium(II) and mercury(II)

A solution was prepared which contained one equivalent of  $\text{L}^5$  and one equivalent both of  $\text{Cd}^{2+}$  and  $\text{Hg}^{2+}$  and its  $^1\text{H}$  NMR spectrum was recorded (Fig. 4.22b). The  $^1\text{H}$  NMR spectra for  $\text{L}^5+\text{Cd}(\text{II})$  and  $\text{L}^5+\text{Hg}(\text{II})$  are shown for comparison in Figs 4.22a and 4.22c respectively. As discussed previously, the spectrum of the cadmium complex (Fig. 4.22a) shows a total of six signals in the aromatic region which indicates that a mixture of mononuclear and dinuclear species is present in solution. However, the spectrum of the mercury complex (Fig. 4.22c) shows a more simplified spectrum with three signals present in the aromatic region, showing that only the double helicate species is present in solution.

When analysing the spectrum of the mixed species (Fig. 4.22b), the spectrum clearly shows only three signals in the aromatic region, which correspond to the dinuclear mercury complex  $[\text{Hg}_2(\text{L}^5)_2]^{4+}$ .

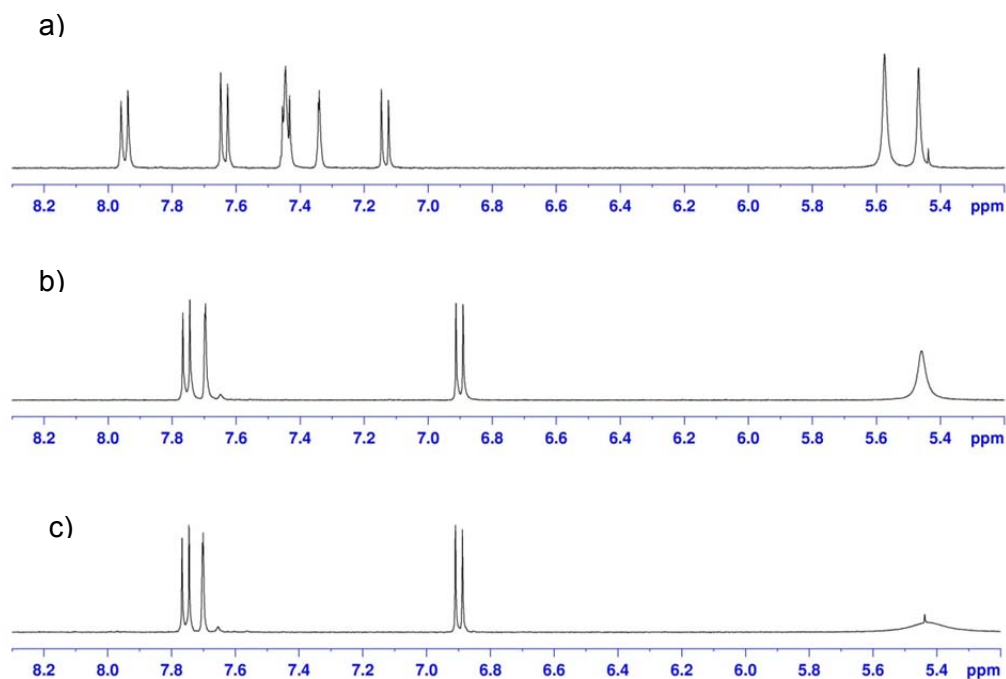


**Figure 4.22:** Selected regions of the  $^1\text{H}$  NMR spectra (CD<sub>3</sub>CN) of a)  $\text{L}^5+\text{Cd}(\text{II})$ , b)  $\text{L}^5+\text{Cd}(\text{II})+\text{Hg}(\text{II})$  and c)  $\text{L}^5+\text{Hg}(\text{II})$

Cyclohexanone and a catalytic amount of camphorsulfonic acid were added to all three solutions and the  $^1\text{H}$  NMR spectra were re-run; their spectra are shown in Fig. 4.23. The spectra of the cadmium-containing species (Fig. 4.23a) and mercury-containing species (Fig. 4.23c) showed three signals in the aromatic region whose chemical shift strongly indicated that only the mononuclear species is present in solution ( $[\text{CdL}^{5a}]^{2+}$ ) and ( $[\text{HgL}^{5a}]^{2+}$ ).

The spectrum of the mixed species  $\text{L}^5+\text{Cd}(\text{II})+\text{Hg}(\text{II})+$  cyclohexanone (Fig. 4.23b) shows the presence of two species. The major product is the cyclised mercury-containing complex  $[\text{HgL}^{5a}]^{2+}$  (here the thiazole singlet at 7.6 ppm is useful for comparison) and the minor product corresponds to the unreacted mercury complex  $[\text{Hg}_2(\text{L}^5)_2]^{4+}$  (Figure 4.23 (c)). The spectrum shows no signals corresponding to any cadmium-containing complexes.

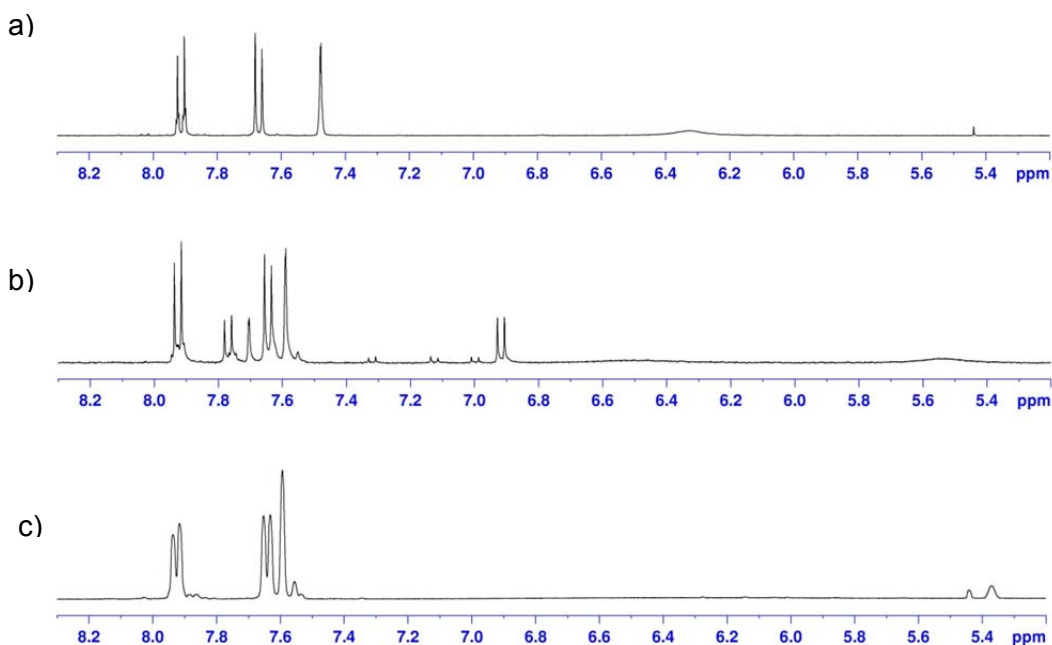


**Figure 4.23:** Selected regions of the  $^1\text{H}$  NMR spectra ( $\text{CD}_3\text{CN}$ ) of a)  $[\text{Cd}(\text{L}^{5a})_2]^{2+}$ , b)  $\text{L}^5+\text{Cd}(\text{II})+\text{Hg}(\text{II})+\text{cyclohexanone}$  and c)  $[\text{Hg}(\text{L}^{5a})_2]^{2+}$

#### 4.4.2.2 Reaction of $\text{L}^5$ with cadmium(II) and zinc(II)

A solution containing  $\text{L}^5+\text{Cd}(\text{II})+\text{Zn}(\text{II})$  was prepared and its  $^1\text{H}$  NMR spectrum was recorded (Fig. 4.24b). The spectra for  $\text{L}^5+\text{Cd}$  and  $\text{L}^5+\text{Zn}$  are shown for comparison in Figs 4.24a and c respectively. As discussed above, the  $\text{L}^5+\text{Cd}$  solution contains both mono- and dinuclear species (Fig. 4.24a), while the  $\text{L}^5+\text{Zn}$  solution contains the mononuclear complex (Fig. 4.24c).

When analysing the spectrum of the mixed reaction  $\text{L}^5+\text{Cd}(\text{II})+\text{Zn}(\text{II})$  a major component from the cadmium-containing species  $[\text{Cd}(\text{L}^5)]^{2+}$  and  $[\text{Cd}_2(\text{L}^5)_2]^{4+}$  is observed, and also a minor component corresponding to  $[\text{Zn}_2(\text{L}^5)_2]^{4+}$  (Fig. 4.24b).

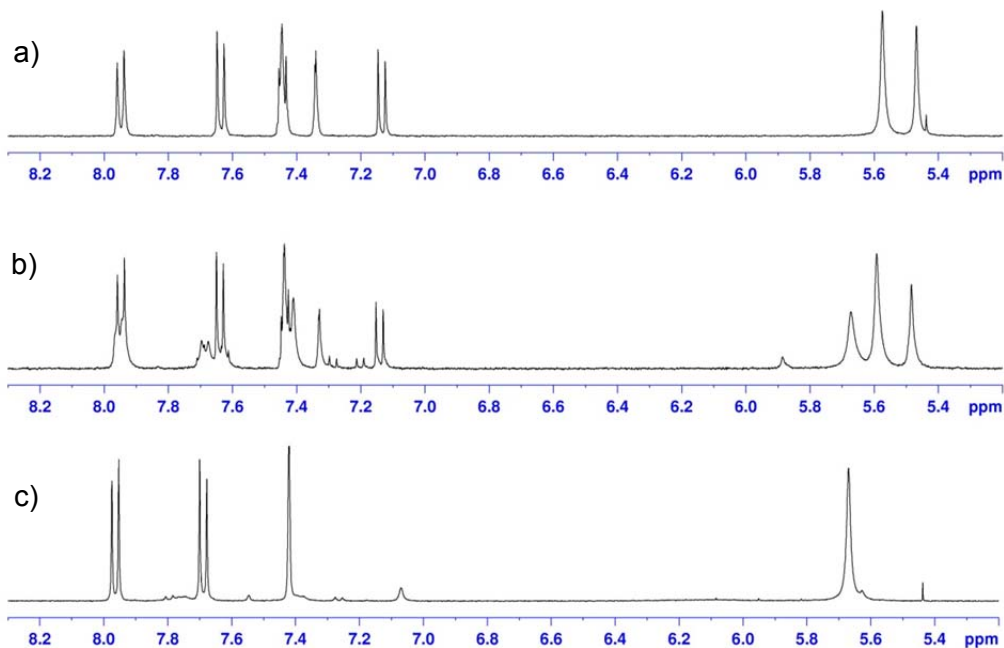


**Figure 4.24:** Selected regions of the <sup>1</sup>H NMR spectra (CD<sub>3</sub>CN) of a)  $L^5+Cd(II)$ , b)  $L^5+Cd(II)+Zn(II)$  and c)  $L^5+Zn(II)$

The <sup>1</sup>H NMR spectra of the three solutions were re-run after reaction with cyclohexanone (Figure 4.25). In the individual systems mononuclear species are formed both with cadmium(II) ( $[Cd(L^{5a})]^{2+}$ , Fig. 4.25a) and with Zn(II) ( $[Zn(L^{5a})]^{2+}$ , Fig. 4.25c). The <sup>1</sup>H NMR spectrum for the solution containing  $L^5+Cd(II)+Zn(II)+cyclohexanone$  in acetonitrile shows species relating to both  $[Cd(L^{5a})]^{2+}$  and  $[Zn(L^{5a})]^{2+}$  (Fig. 4.25b).

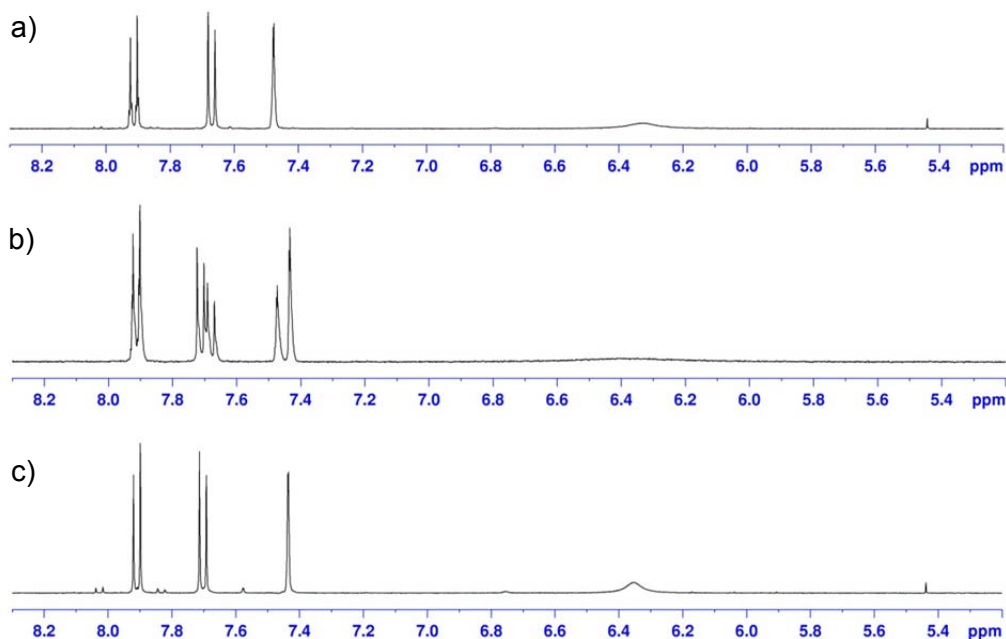


**Figure 4.25:** Selected regions of the  $^1\text{H}$  NMR spectra ( $\text{CD}_3\text{CN}$ ) of a)  $[\text{Cd}(\text{L}^{5\text{a}})]^{2+}$ , b)  $\text{L}^5+\text{Cd}(\text{II})+\text{Zn}(\text{II})+\text{cyclohexanone}$  and c)  $[\text{Zn}(\text{L}^{5\text{a}})]^{2+}$

#### 4.4.2.3 Reaction of $\text{L}^5$ with cadmium(II) and silver(I)

The  $^1\text{H}$  NMR spectrum of a solution containing  $\text{L}^5+\text{Cd}(\text{II})+\text{Ag}(\text{I})$  was recorded and is shown in Figure 4.26b, along with the spectra of  $[\text{CdL}^5]^{2+}/[\text{Cd}_2\text{L}^5_2]^{4+}$  (Fig. 4.26a) and  $[\text{Ag}_2\text{L}^5_2]^{2+}$  (Fig. 4.26c). As before,  $\text{L}^5+\text{Cd}(\text{II})$  shows both mono- and dinuclear species present in solution whereas the spectrum of the silver system shows only signals attributable to the dinuclear double helicate  $[\text{Ag}_2\text{L}^5_2]^{2+}$ .

The spectrum of  $\text{L}^5+\text{Cd}(\text{II})+\text{Ag}(\text{I})$  (Fig. 4.26b) shows that it consists predominantly of cadmium-containing species (both the mono- and dinuclear species) and does not contain the silver complex  $[\text{Ag}_2\text{L}^5_2]^{2+}$ . There are several small signals which do not correspond to either of the homometallic species and therefore may be due to the presence of a small amount of the mixed species,  $[\text{AgCdL}^5_2]^{3+}$ .

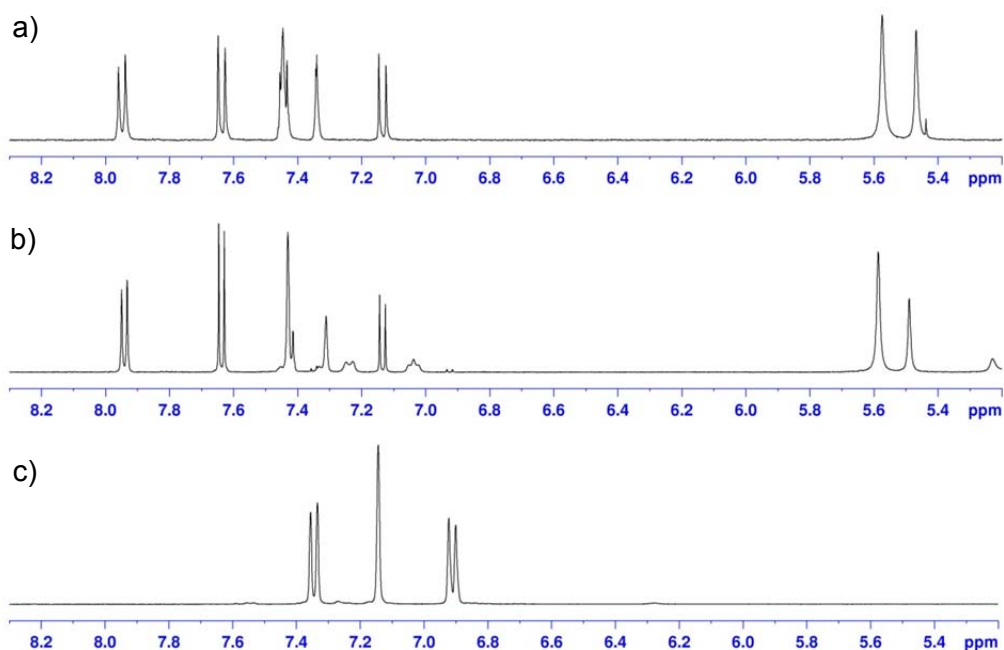


**Figure 4.26:** Selected regions of the <sup>1</sup>H NMR spectra (CD<sub>3</sub>CN) of a) L<sup>5</sup>+Cd(II), b) L<sup>5</sup>+Cd(II)+Ag(I) and c) L<sup>5</sup>+Ag(I)

The <sup>1</sup>H NMR spectra of the three solutions were re-run after reaction with cyclohexanone (Figure 4.27). In the individual systems, a mononuclear species was formed with cadmium(II) ([Cd(L<sup>5a</sup>)]<sup>2+</sup>, Fig. 4.27a), and as explained earlier, only the double helical species was observed with silver(I), (Fig. 4.27c). In the solution containing L<sup>5a</sup>+Cd(II)+Ag(I), Figure 4.27b, only species relating to the cadmium complex are observed. It is possible that some of the silver-containing species was formed but due to its low solubility is not observed in solution (as discussed earlier). However, there was no precipitate present in the NMR tube indicating that all the materials were in solution and only the Cd(II) complex was formed.

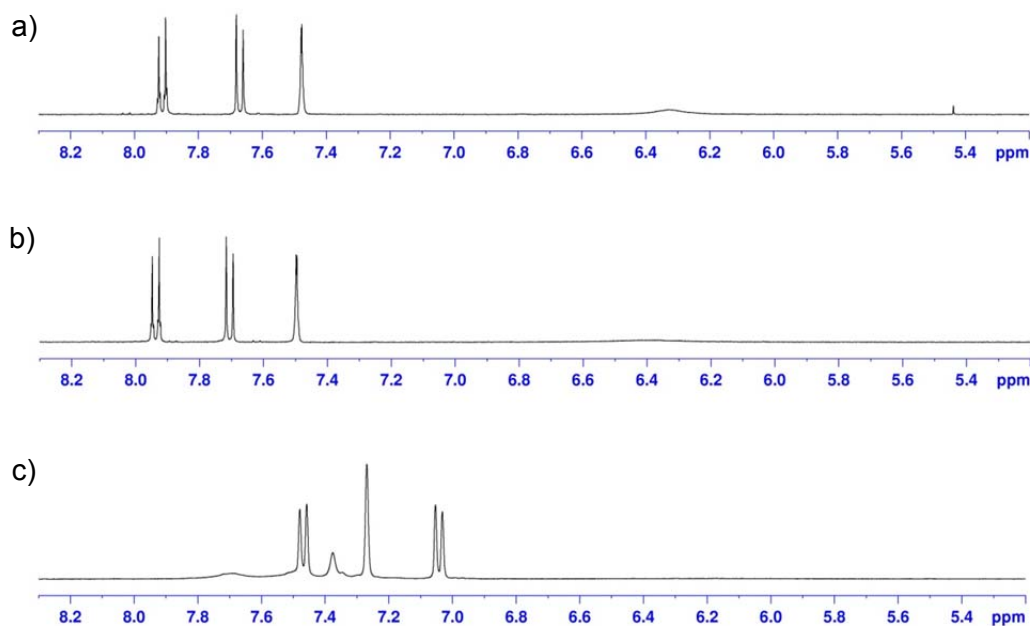


**Figure 4.27:** Selected regions of the <sup>1</sup>H NMR spectra (CD<sub>3</sub>CN) of a) [Cd(L<sup>5a</sup>)]<sup>2+</sup>, b) L<sup>5</sup>+Cd(II)+Ag(I)+cyclohexanone and c) [Ag<sub>2</sub>(L<sup>5a</sup>)<sub>2</sub>]<sup>2+</sup>

#### 4.4.2.4 Reaction of L<sup>5</sup> with cadmium(II) and copper(I)

The <sup>1</sup>H NMR spectrum of a solution containing L<sup>5</sup>+Cd(II)+Cu(I) was recorded and is shown in Figure 4.28b, along with the spectra of [Cd(L<sup>5</sup>)]<sup>2+</sup>/[Cd<sub>2</sub>(L<sup>5</sup>)<sub>2</sub>]<sup>4+</sup> (Fig. 4.28a) and [Cu<sub>2</sub>(L<sup>5</sup>)<sub>2</sub>]<sup>2+</sup> (Fig. 4.28c). Once again, the spectrum of the cadmium system shows the presence of two species in solution, whereas the spectrum of L<sup>5</sup>+Cu(I) shows the presence of one species formed in solution; from the chemical shifts, this species is the dinuclear double helicate [Cu<sub>2</sub>(L<sup>5</sup>)<sub>2</sub>]<sup>2+</sup>.

In an analogous fashion to the reaction of L<sup>5</sup> with Cd(II) and Ag(I), the spectrum of L<sup>5</sup>+Cd(II)+Cu(I) (Fig. 4.28b) shows that the predominant species in solution are related to cadmium ([Cd(L<sup>5</sup>)]<sup>2+</sup>/[Cd<sub>2</sub>(L<sup>5</sup>)<sub>2</sub>]<sup>4+</sup>) and that no [Cu<sub>2</sub>(L<sup>5</sup>)<sub>2</sub>]<sup>2+</sup> is present. However, a small amount of a new species is observed which, similar to the Cd/Ag system, is probably the heterometallic helicate [CuCd(L<sup>5</sup>)<sub>2</sub>]<sup>3+</sup>.

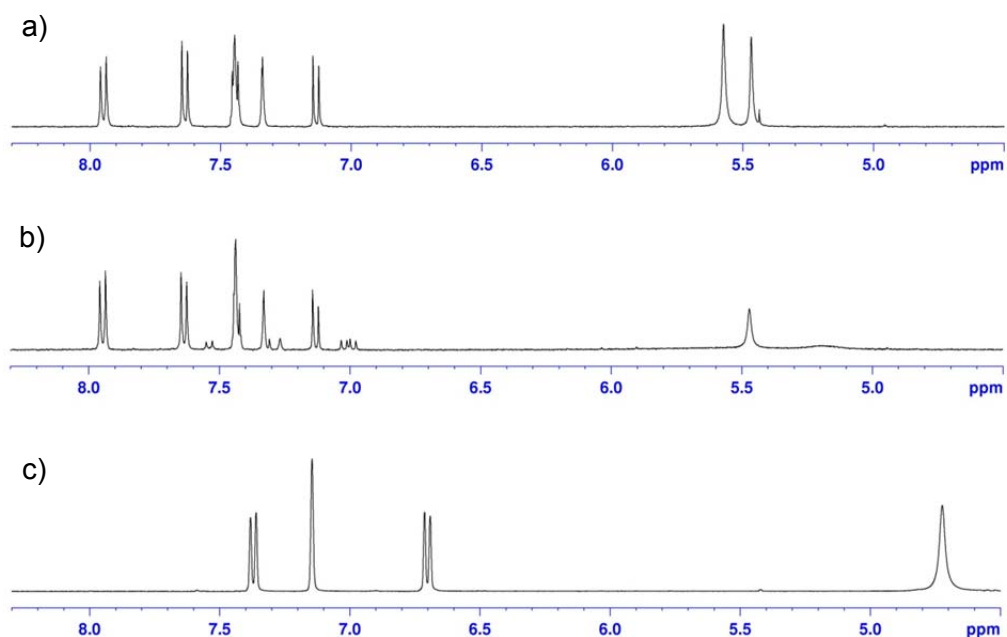


**Figure 4.28:** Selected regions of the <sup>1</sup>H NMR spectra (CD<sub>3</sub>CN) of a)  $L^5+Cd(II)$ , b)  $L^5+Cd(II)+Cu(I)$  and c)  $L^5+Cu(I)$

The <sup>1</sup>H NMR spectra of the three solutions were re-run after reaction with cyclohexanone (Fig. 4.29). In the individual systems a mononuclear species was formed with cadmium(II) ( $[CdL^{5a}]^{2+}$ , Fig. 4.29a). Figure 4.29c shows three signals present in the aromatic region of the copper(I)/ $L^5$  system indicating again that only one species is present. The chemical shifts of these signals however, indicate the species formed with copper(I) is a dinuclear double helical species; it is likely therefore that the ligand has not reacted with cyclohexanone. The <sup>1</sup>H NMR spectra for the solution containing  $L^5+Cd(II)+Cu(I)+cyclohexanone$  in acetonitrile (Fig. 4.29b) shows three signals present relating to only the cadmium complex.

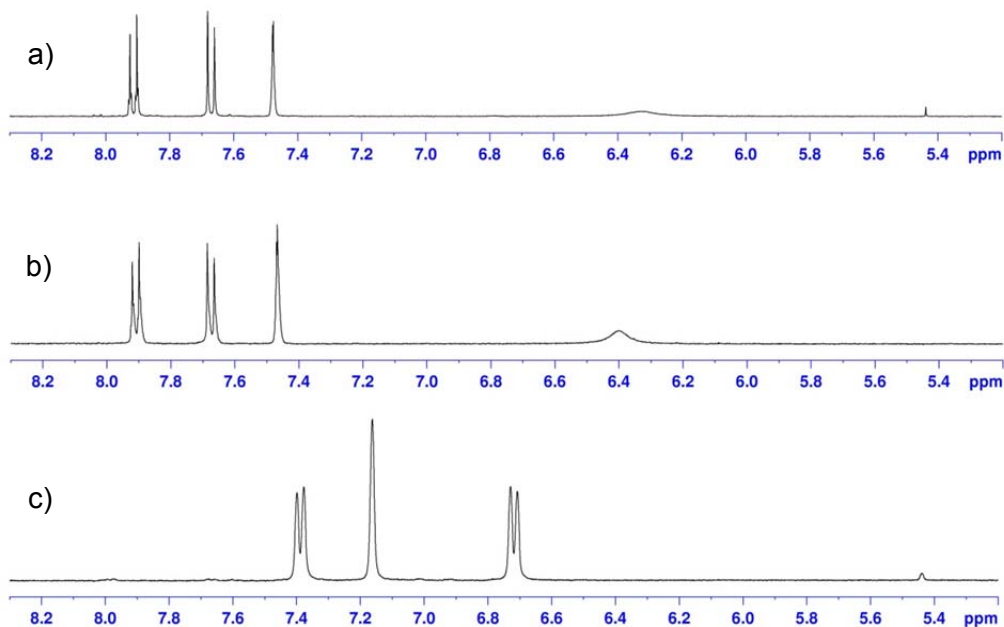


**Figure 4.29:** Selected regions of the <sup>1</sup>H NMR spectra (CD<sub>3</sub>CN) of a) [CdL<sup>5a</sup>]<sup>2+</sup>, b) L<sup>5</sup>+Cd(II)+Cu(I)+cyclohexanone and c) [Cu<sub>2</sub>(L<sup>5a</sup>)<sub>2</sub>]<sup>2+</sup>

#### 4.4.2.5 Reaction of L<sup>5</sup> with mercury(II) and zinc(II)

Figure 4.30 shows the <sup>1</sup>H NMR spectra for the solutions containing L<sup>5</sup>+Hg(II) (Fig. 4.30a), L<sup>5</sup>+Hg(II)+Zn(II) (Fig. 4.30b) and L<sup>5</sup>+Zn(II) (Fig. 4.30c).

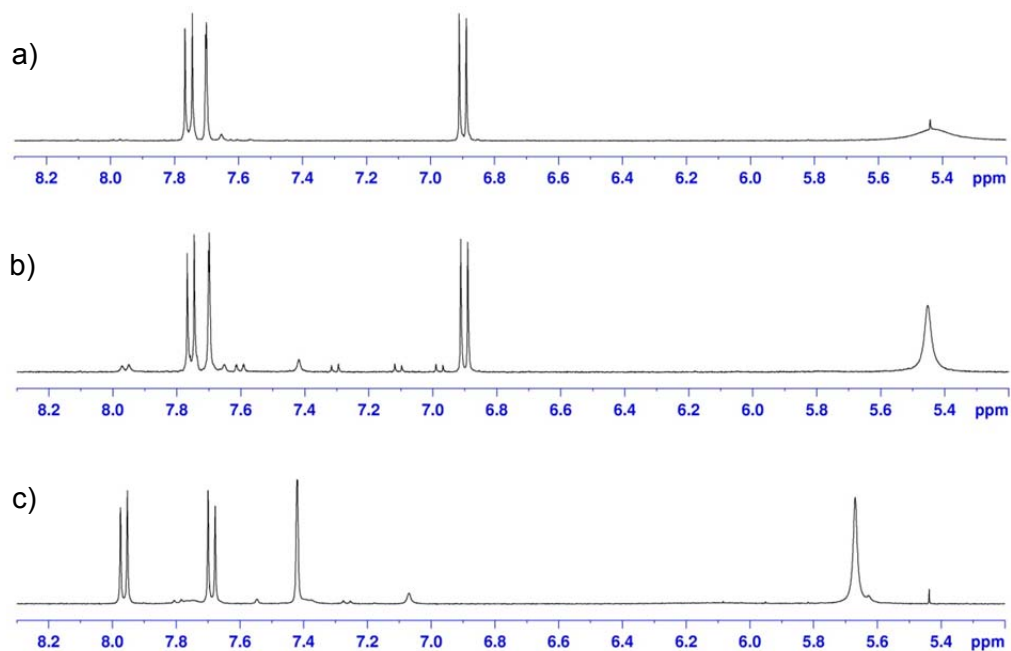


**Figure 4.30:** Selected regions of the <sup>1</sup>H NMR spectra (CD<sub>3</sub>CN) of a) L<sup>5</sup>+Hg(II), b) L<sup>5</sup>+Hg(II)+Zn(II) and c) L<sup>5</sup>+Zn(II)

The spectrum of  $L^5+Hg(II)$  showed three signals in the aromatic region (Fig. 4.30a), which indicates the presence of only one species; the chemical shifts of these peaks indicate that this is the dinuclear double helicate  $[Hg_2(L^5)_2]^{4+}$ . The spectrum of  $L^5+Zn(II)$  also contains three signals (Fig. 4.30c) but in this case the chemical shifts indicate a mononuclear species is formed ( $[Zn(L^5)]^{2+}$ ). When analysing the spectrum for the mixed species in solution (Fig. 4.30b), the dinuclear species  $[Hg_2(L^5)_2]^{4+}$  is clearly present, and only a very small amount of  $[Zn(L^5)]^{2+}$  is observed. There are, however, some small signals that represent the mixed species  $[HgZn(L^5)_2]^{4+}$ .

The  $^1H$  NMR spectra of the three solutions were re-run after reaction with cyclohexanone (Fig. 4.31); the spectra of  $[Hg(L^{5a})]^{2+}$  (Fig. 4.31a) and  $[Zn(L^{5a})]^{2+}$  (Fig. 4.31c) are shown for comparison. As discussed previously, the spectrum of the mercury system contains three signals in the aromatic region indicating that the mononuclear species is present in solution. The spectrum of the zinc species shows that a mononuclear complex  $[Zn(L^{5a})]^{2+}$  is also formed in solution. The spectrum of the  $L^5+Hg(II)+Zn(II)+cyclohexanone$  system (Fig. 4.31b) shows that there is a mixture of species and from comparison of the chemical shifts it is clear that the mixed solution mainly comprises the cyclised Hg(II) species  $[Hg(L^{5a})]^{2+}$ , some unreacted mercury-containing complex  $[Hg_2(L^5)_2]^{4+}$  and a very small amount of cyclised zinc complex  $[Zn(L^{5a})]^{2+}$ . Again, a set of weak signals is present corresponding to the heteronuclear helicate.

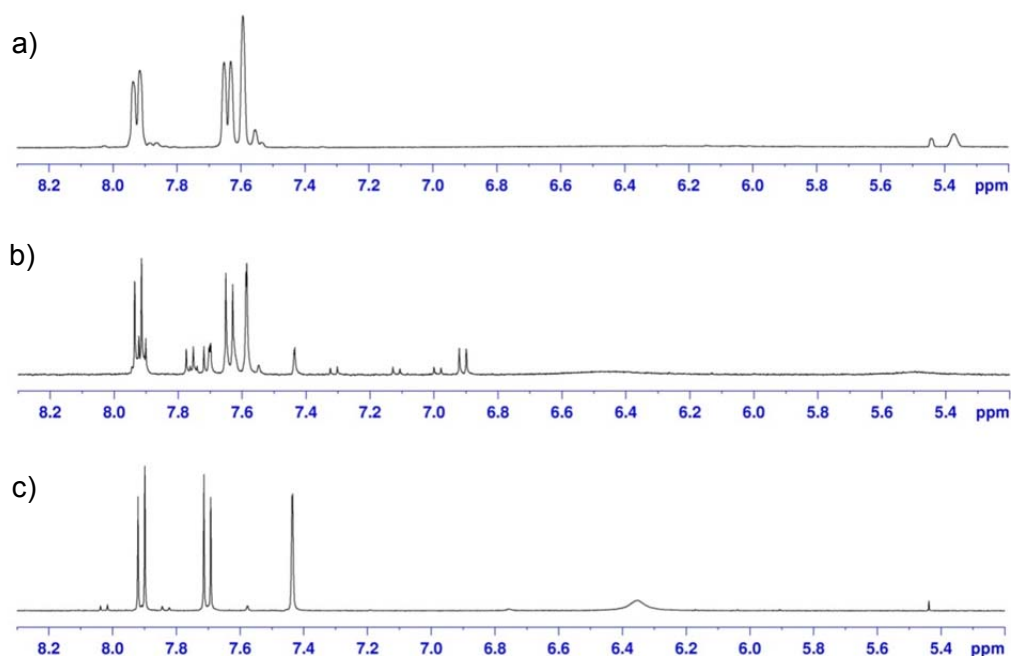


**Figure 4.31:** Selected regions of the  $^1H$  NMR spectra ( $CD_3CN$ ) of a)  $[Hg(L^{5a})]^{2+}$ , b)  $L^5+Hg(II)+Zn(II)+cyclohexanone$  and c)  $[Zn(L^{5a})]^{2+}$

#### 4.4.2.6 Reaction of $L^5$ with mercury(II) and silver(I)

The  $^1H$  NMR spectra for the solutions containing  $L^5+Hg(II)$  (Fig. 4.32a),  $L^5+Hg(II)+Ag(I)$  (Fig. 4.32b) and  $L^5+Ag(I)$  (Fig 4.32c) were recorded. The spectrum of the mixed system,  $L^5+Hg(II)+Ag(I)$ , shows that the mercury-containing dinuclear double helicate is the most abundant species, with a number of small signals which do not correspond to either the  $Hg(II)$  or  $Ag(I)$  species formed in the individual experiments, and are therefore likely to be due to a mixed species (perhaps  $[HgAg(L^5)_2]^{3+}$ ).

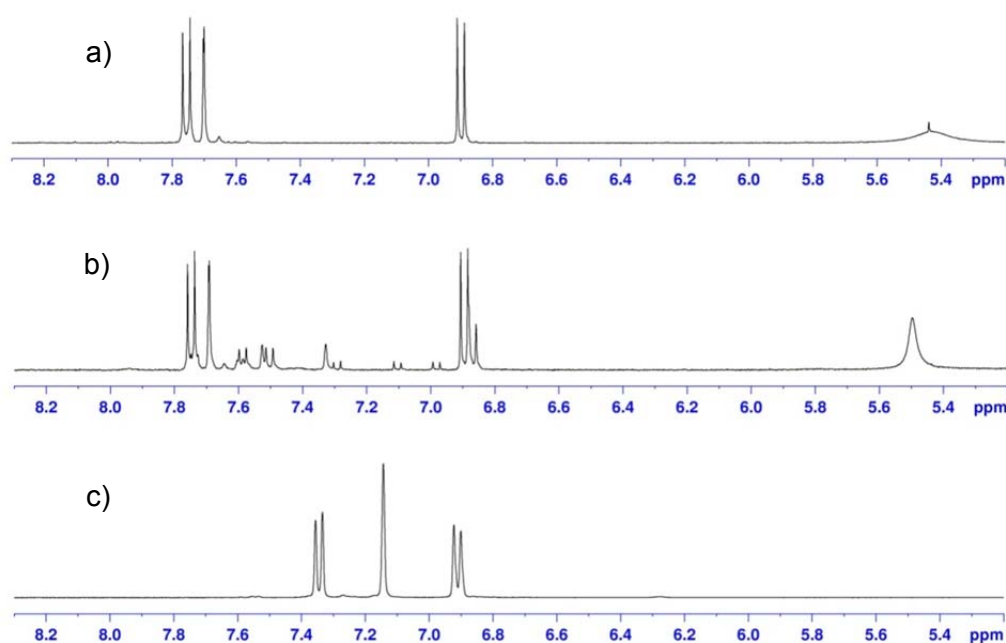


**Figure 4.32:** Selected regions of the  $^1H$  NMR spectra ( $CD_3CN$ ) of a)  $[Hg_2(L^5)_2]^{4+}$ , b)  $L^5+Hg(II)+Ag(I)$  and c)  $[Ag_2(L^5)_2]^{2+}$

The  $^1H$  NMR spectra for the three solutions were re-run after reaction with cyclohexanone; these are shown in Figure 4.33 along with the spectra of  $[HgL^{5a}]^{2+}$  and “ $[Ag(L^{5a})]^{+}$ ” for comparison. The spectrum of the  $L^5+Hg(II)+Ag(I)+cyclohexanone$  system (Figure 4.33b) shows that in solution the mononuclear mercury species is the only complex present in solution. Again no precipitate was observed.

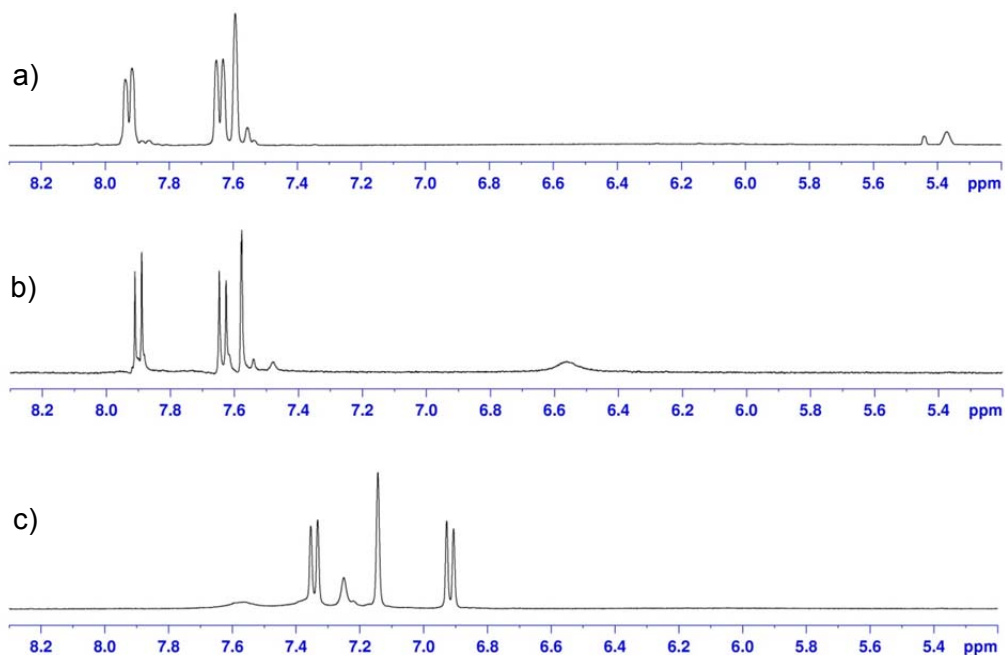


**Figure 4.33:** Selected regions of the <sup>1</sup>H NMR spectra (CD<sub>3</sub>CN) of a) L<sup>5a</sup>+Hg(II), b) L<sup>5a</sup>+Hg(II)+Ag(I) and c) L<sup>5a</sup>+Ag(I)

#### 4.4.2.7 Reaction of L<sup>5</sup> with mercury(II) and copper(I)

The <sup>1</sup>H NMR spectra for solutions containing L<sup>5</sup>+Hg(II) (Fig. 4.34a), L<sup>5</sup>+Hg(II)+Cu(I) (Fig. 4.34b) and L<sup>5</sup>+Cu(I) (Fig. 4.34c) were recorded. The spectra of both of the homometallic solutions indicated formation of the dinuclear double helicates [Hg<sub>2</sub>(L<sup>5</sup>)<sub>2</sub>]<sup>4+</sup> and [Cu<sub>2</sub>(L<sup>5</sup>)<sub>2</sub>]<sup>2+</sup>. In the mixed experiment (Fig. 4.34b), the predominant species was again the mercury-containing helicate, with a small number of signals corresponding, presumably, to the mixed species [HgAg(L<sup>5</sup>)<sub>2</sub>]<sup>3+</sup>; no signals arising from the silver complex were observed.

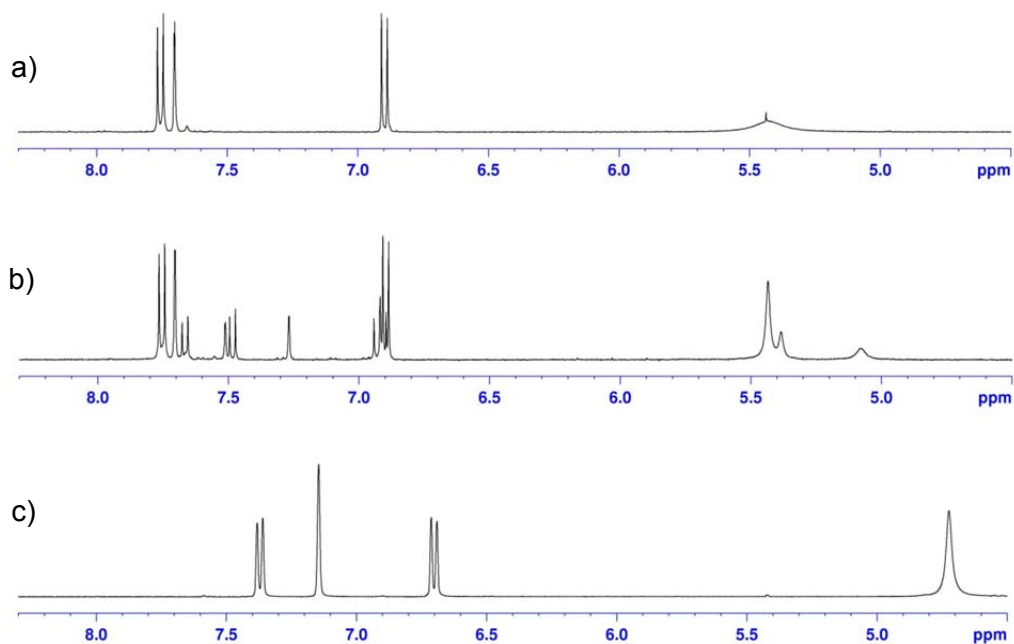


**Figure 4.34:** Selected regions of the  $^1\text{H}$  NMR spectra (CD<sub>3</sub>CN) of a)  $\text{L}^5+\text{Hg}(\text{II})$ , b)  $\text{L}^5+\text{Hg}(\text{II})+\text{Cu}(\text{I})$  and c)  $\text{L}^5+\text{Cu}(\text{I})$

The  $^1\text{H}$  NMR spectra for the three solutions were re-run after the addition of cyclohexanone; these are shown in Figure 4.35 along with the spectra of  $[\text{HgL}^{5a}]^{2+}$  and  $[\text{Cu}_2(\text{L}^5)_2]^{2+}$  for comparison. The spectrum of the  $\text{L}^5+\text{Hg}(\text{II})+\text{Cu}(\text{I})+\text{cyclohexanone}$  system (Fig. 4.35b) shows that in solution a mixture of both mononuclear mercury(II) species as well as the copper(I) dinuclear species can be seen; the latter presumably has not reacted with cyclohexanone. However, the predominant species is the mononuclear mercury complex  $[\text{Hg}(\text{L}^{5a})]^{2+}$ .

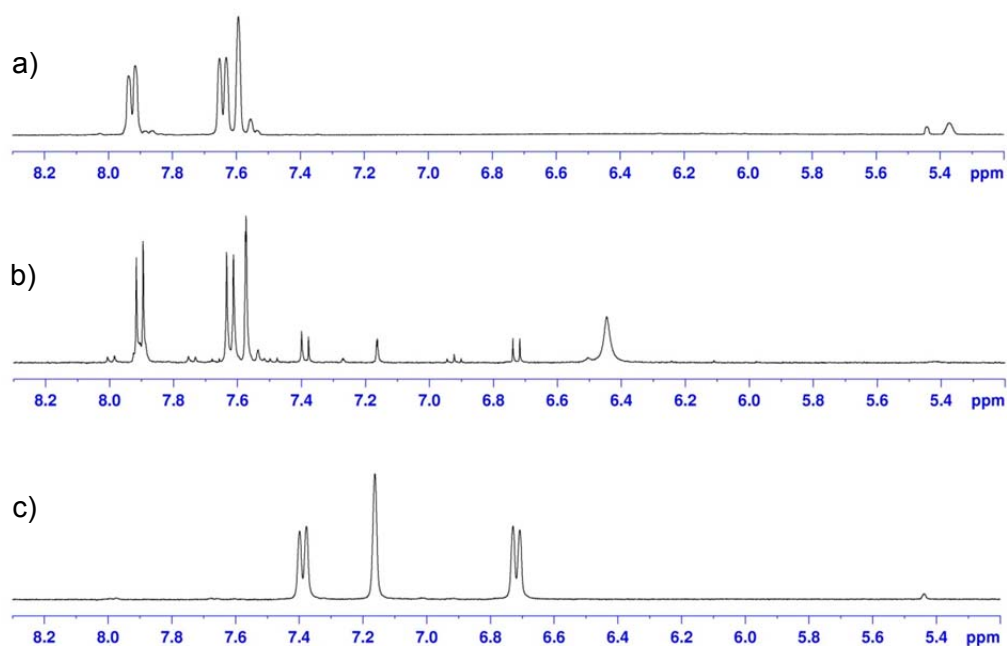


**Figure 4.35:** Selected regions of the  $^1\text{H}$  NMR spectra ( $\text{CD}_3\text{CN}$ ) of a)  $[\text{HgL}^{5a}]^{2+}$ , b)  $\text{L}^5 + \text{Hg}(\text{II}) + \text{Cu}(\text{I}) + \text{cyclohexanone}$  and c)  $[\text{Cu}_2\text{L}^{5a}]^{2+}$

#### 4.4.2.8 Reaction of $\text{L}^5$ with zinc(II) and silver(I)

The  $^1\text{H}$  NMR spectra for solutions containing  $\text{L}^5 + \text{Zn}(\text{II})$  (Fig. 4.36a),  $\text{L}^5 + \text{Zn}(\text{II}) + \text{Ag}(\text{I})$  (Fig. 4.36b) and  $\text{L}^5 + \text{Ag}(\text{I})$  (Fig. 4.36c) were recorded. When analysing the spectrum of the mixed reaction (Fig. 4.36b), multiple signals can be seen in the aromatic region. The spectra clearly show the presence of the mononuclear zinc complex and a (very) small amount of the dinuclear silver helicate is also seen. A number of other, small, peaks are present in the spectrum which may correlate to the mixed species  $[\text{ZnAg}(\text{L}^5)_2]^{3+}$ .

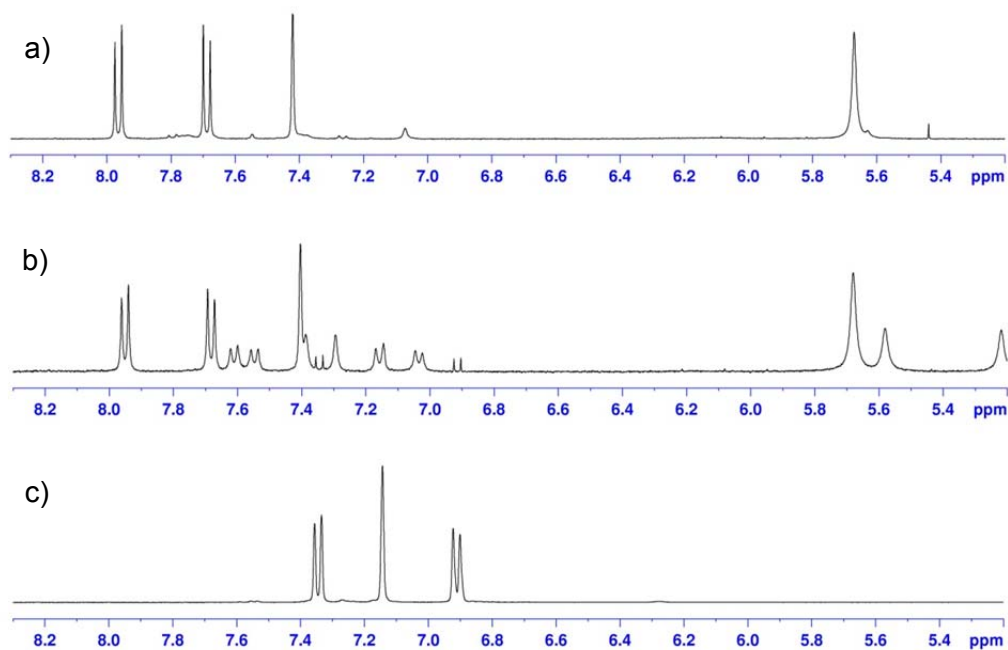


**Figure 4.36:** Selected regions of the <sup>1</sup>H NMR spectra (CD<sub>3</sub>CN) of a)  $L^5+Zn(II)$ , b)  $L^5+Zn(II)+Ag(I)$  and c)  $L^5+Ag(I)$

The <sup>1</sup>H NMR spectra of the three solutions were re-run after reaction with cyclohexanone (Fig. 4.37). The spectrum of the  $L^5+Zn(II)+Ag(I)+cyclohexanone$  system (Fig. 4.37b) shows that, in solution, the cyclised mononuclear zinc species is the only complex present in solution. As with the other systems all the materials were soluble confirming the sole formation of the Zn(II)-containing complex.

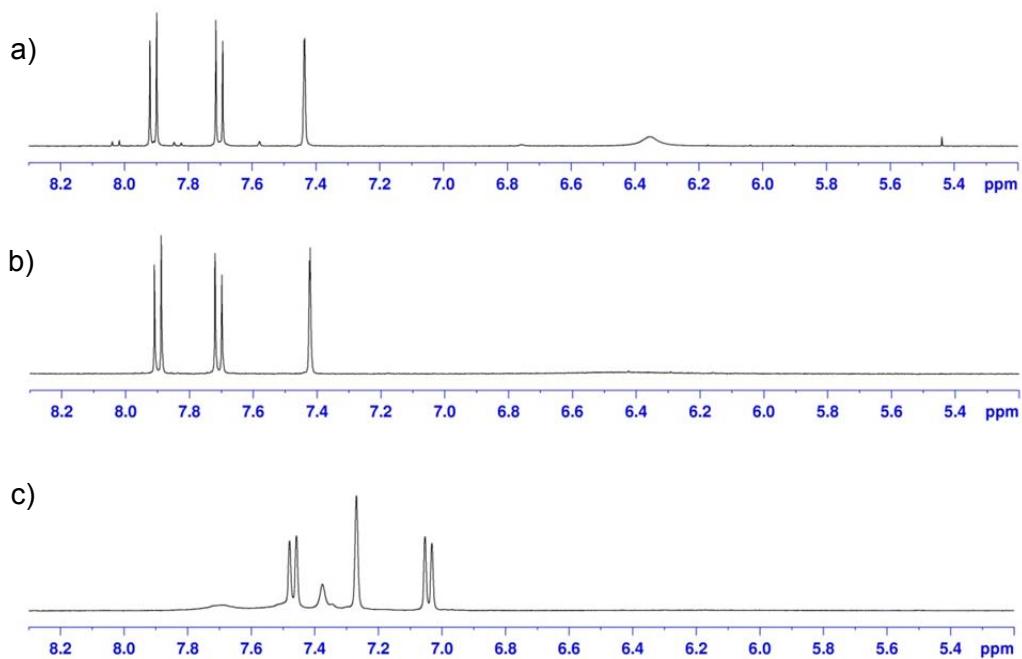


**Figure 4.37:** Selected regions of the <sup>1</sup>H NMR spectra (CD<sub>3</sub>CN) of a) L<sup>5a</sup>+Zn, b) L<sup>5a</sup>+Zn(II)+Ag(I) and c) L<sup>5a</sup>+Ag(I)

#### 4.4.2.9 Reaction of L<sup>5</sup> with zinc(II) and copper(I)

Figure 4.38 shows the <sup>1</sup>H NMR spectra for solutions containing; a) L<sup>5</sup>+Zn(II), b) L<sup>5</sup>+Zn(II)+Cu(I) and c) L<sup>5</sup>+Cu(I).

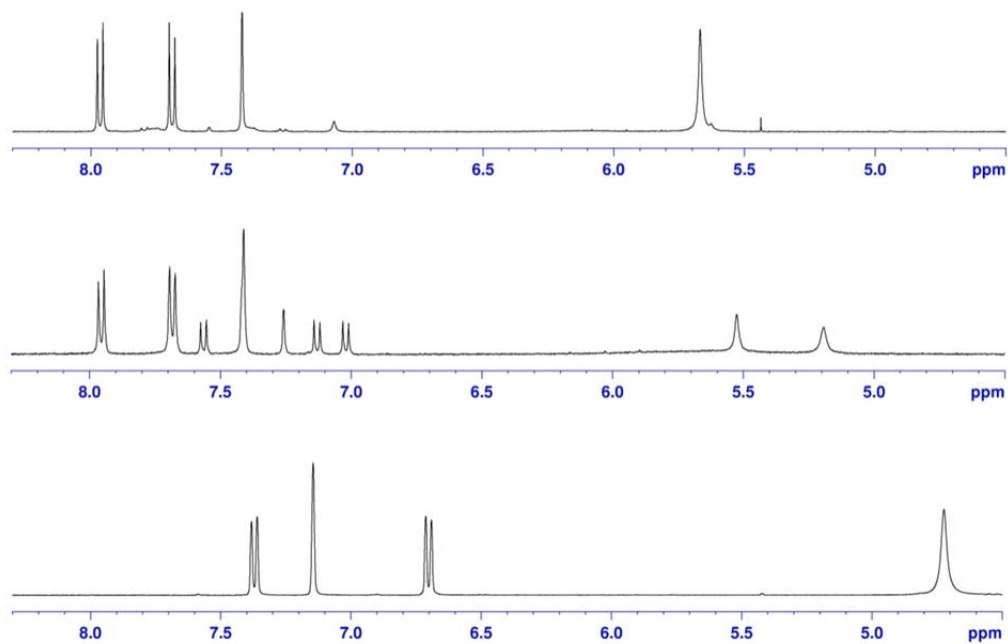


**Figure 4.38:** Selected regions of the <sup>1</sup>H NMR spectra (CD<sub>3</sub>CN) of a) L<sup>5</sup>+Zn(II), b) L<sup>5</sup>+Zn(II)+Cu(I) and c) L<sup>5</sup>+Cu(I)

The spectrum of  $L^5$  with both zinc(II) and copper(I) ions shows multiple signals in the aromatic region (Fig. 4.38b). Three of those signals correspond to the  $[Zn(L^5)]^{2+}$  complex seen in spectrum 4.38a but no peaks are seen which correspond to the copper helicate. Again, a number of new signals are present which are likely due to formation of a small amount of the heterometallic helicate,  $[ZnCu(L^5)_2]^{3+}$ .

The  $^1H$  NMR spectra of the solutions were re-run after reaction with cyclohexanone; these are shown in Figure 4.39 along with the spectra of  $[Zn(L^{5a})]^{2+}$  and  $[Cu_2(L^5)_2]^+$  for comparison. The spectrum of the  $L^5+Zn(II)+Cu(I)+cyclohexanone$  system (Fig. 4.39b) shows that the mononuclear zinc species is the only complex present in solution.

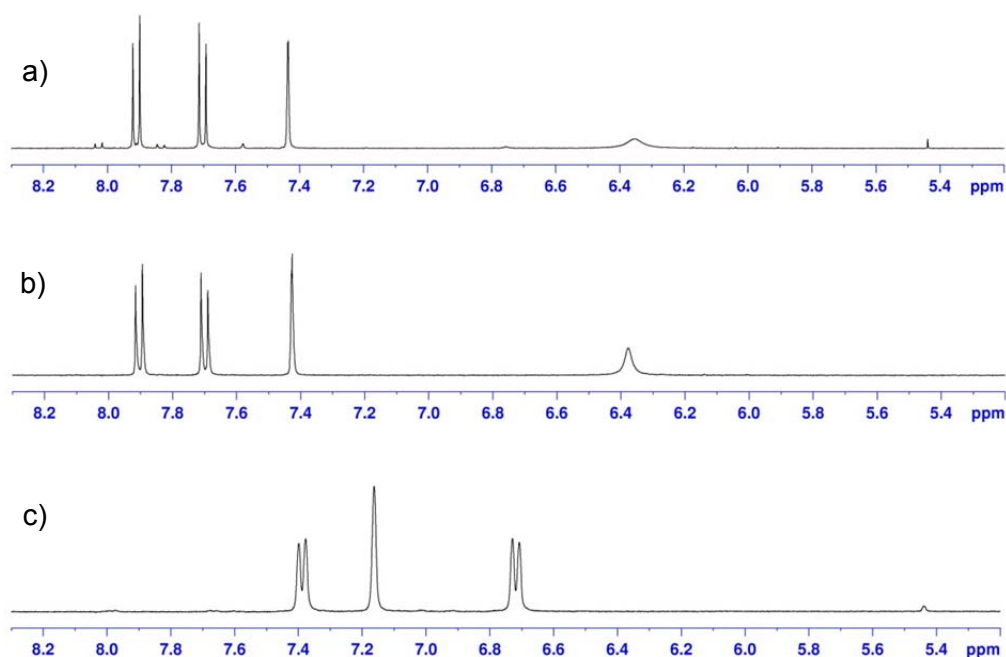


**Figure 4.39:** Selected regions of the  $^1H$  NMR spectra ( $CD_3CN$ ) of a)  $[Zn(L^{5a})]^{2+}$ , b)  $L^5+Zn(II)+Cu(I)+cyclohexanone$  and c)  $L^5+Cu(I)+cyclohexanone$

Table 4.11 shows the overview of all the metal specificity results for the reactions with the ligand  $L^5$ .

COMPLEX	NMR	MS	X-Ray
$L^5+Hg^{2+}$	Dinuclear double helicate	Dinuclear double helicate & mononuclear	Dinuclear double helicate
$L^5+Hg^{2+}+cyclohexanone$	Mononuclear	Mononuclear	Mononuclear
$L^5+Ag^+$	Dinuclear double helicate	Dinuclear double helicate & small amount of mononuclear	Dinuclear double helicate
$L^5+Ag^++cyclohexanone$	Mononuclear	Mononuclear	Mononuclear
$L^5+Zn^{2+}$	Mononuclear	Dinuclear double helicate & mononuclear	Dinuclear double helicate
$L^5+Zn^{2+}+cyclohexanone$	Mononuclear	Mononuclear	Mononuclear
$L^5+Cd^{2+}$	Dinuclear double helicate & mononuclear (~50:50)	Dinuclear double helicate & mononuclear (~50:50)	Dinuclear double helicate
$L^5+Cd^{2+}+cyclohexanone$	Mononuclear	Mononuclear	Mononuclear

**Table 4.11:** Results for the complex formation of  $L^5$  with various metal ions

Reaction of  $L^5$  with various metals affords differing distributions of mononuclear and dinuclear double helicate complexes, depending on their preferred coordination geometries. With mercury, which can adopt octahedral or tetrahedral coordination modes, the ligand forms a dinuclear double helicate in which it can be assumed that the Hg(II) centres are 4-coordinate. With silver, which prefers tetrahedral coordination, a dinuclear double helicate is formed as expected. In the case of zinc, there is a discrepancy between the solution and solid state results. A mononuclear complex is formed in solution but the solid state structure showed a dinuclear double helicate. However, the solid state structure results from crystallisation of the least soluble product, and is not necessarily representative of the bulk solution. Finally, with

cadmium an approximately equal mixture of mono- and dinuclear species was observed, since Cd(II) can adopt either tetrahedral or octahedral geometries.

On reaction of all four complexes with cyclohexanone, mononuclear species were observed in all cases. These results show clearly that reaction of the complexes with cyclohexanone controls the coordination geometry of the metal ions Hg(II), Ag(I), Zn(II) and Cd(II). Constraint of the pyridyl rings by formation of the cyclic aminal derivatives promotes formation of planar, mononuclear species, even with silver which normally prefers tetrahedral coordination geometry, rather than a square planar geometry.

Table 4.12 shows the overview of all mixed metal results for the reactions with the ligand  $L^5$ . The reaction of  $L^5$  with various mixed metals affords differing distributions of mononuclear and dinuclear double helicate complexes, again, depending on their preferred coordination geometries.

REACTION	NMR
$L^5 + Cd + Hg$	$[Hg_2(L^5)_2]^{4+}$
$L^5 + Cd + Hg + \text{cyclohexanone}$	$[Hg(L^{5a})]^{2+}$ Small $[CdHg(L^5)_2]^{4+}$
$L^5 + Cd + Zn$	$[Cd(L^5)]^{2+} / [Cd_2(L^5)_2]^{4+}$ Small $[Zn(L^5)]^{2+}$ , small $[CdZn(L^5)_2]^{4+}$
$L^5 + Cd + Zn + \text{cyclohexanone}$	$[Zn(L^{5a})]^{2+} / [Cd(L^{5a})]^{2+}$ (~60:40)
$L^5 + Cd + Ag$	$[Cd(L^5)]^{2+} / [Cd_2(L^5)_2]^{4+}$ Small $[AgCd(L^5)_2]^{3+}$
$L^5 + Cd + Ag + \text{cyclohexanone}$	$[Cd(L^{5a})]^{2+}$
$L^5 + Cd + Cu(I)$	$[Cd(L^5)]^{2+} / [Cd_2(L^5)_2]^{4+}$ Small $[CdCu(L^5)_2]^{3+}$
$L^5 + Cd + Cu(I) + \text{cyclohexanone}$	$[Cd(L^{5a})]^{2+}$
$L^5 + Hg + Zn$	$[Hg_2(L^5)_2]^{4+}$ Small $[Zn(L^5)]^{2+}$ , small $[HgZn(L^5)_2]^{3+}$
$L^5 + Hg + Zn + \text{cyclohexanone}$	$[Hg(L^{5a})]^{2+}$ Small $[Zn(L^{5a})]^{2+}$ , small $[HgZn(L^5)_2]^{4+}$
$L^5 + Hg + Ag$	$[Hg_2(L^5)_2]^{4+}$ Small mixed helicate $[HgAg(L^5)_2]^{3+}$
$L^5 + Hg + Ag + \text{cyclohexanone}$	$[Hg(L^{5a})]^{2+}$
$L^5 + Hg + Cu^+$	$[Hg_2(L^5)_2]^{4+}$ Small mixed helicate $[HgCu(L^5)_2]^{3+}$
$L^5 + Hg + Cu^+ + \text{cyclohexanone}$	$[Hg(L^{5a})]^{2+}$ Small $[Cu_2(L^5)_2]^{2+}$ , small $[HgCu(L^5)_2]^{3+}$
$L^5 + Zn + Ag$	$[Zn(L^5)]^{2+}$ Small $[Ag_2(L^5)_2]^{2+}$ , small $[ZnAg(L^5)_2]^{3+}$
$L^5 + Zn + Ag + \text{cyclohexanone}$	$[Zn(L^{5a})]^{2+}$
$L^5 + Zn + Cu^+$	$[Zn(L^5)]^{2+}$ Small mixed helicate $[ZnCu(L^5)_2]^{3+}$
$L^5 + Zn + Cu^+ + \text{cyclohexanone}$	$[Zn(L^{5a})]^{2+}$

**Table 4.12:** Results for the complex formation of  $L^5$  with various mixed metals

The reactions of the mixed metal systems have shown two clear trends: firstly, when  $L^5$  is mixed with an octahedral metal and a tetrahedral metal, species containing the octahedral metal are favoured (Table 4.13). Secondly, where two octahedral metals are present, species containing the metal with the larger ionic radius are formed preferentially. The possible reason for this is the divergent nature of the thiazole ring. Due to this 5-membered ring the binding pocket is larger than other tetradentate aromatic donors (e.g. quaterpyridine) and this may favour the larger metal ions (e.g. the affinity increases down the group 12 metal ions).

	Hg	Zn	Ag	Cu(I)
Cd	$[\text{Hg}_2(\text{L}^5)_2]^{4+}$	$[\text{Cd}(\text{L}^5)]^{2+}/[\text{Cd}_2(\text{L}^5)_2]^{4+}$	$[\text{Cd}(\text{L}^5)]^{2+}/[\text{Cd}_2(\text{L}^5)_2]^{4+}$	$[\text{Cd}(\text{L}^5)]^{2+}/[\text{Cd}_2(\text{L}^5)_2]^{4+}$
Hg		$[\text{Hg}_2(\text{L}^5)_2]^{4+}$	$[\text{Hg}_2(\text{L}^5)_2]^{4+}$	$[\text{Hg}_2(\text{L}^5)_2]^{4+}$
Zn			$[\text{Zn}(\text{L}^5)]^{2+}$	$[\text{Zn}(\text{L}^5)]^{2+}$

**Table 4.13:** Showing the predominant species formed on reaction of  $L^5$  with mixed metals

Upon reaction with cyclohexanone, only the mononuclear species of the octahedral metals are formed in all cases (Table 3.14).

	Hg	Zn	Ag	Cu(I)
Cd	$[\text{Hg}(\text{L}^{5a})]^{2+}$	$[\text{Cd}(\text{L}^{5a})]^{2+}/[\text{Zn}(\text{L}^{5a})]^{2+}$	$[\text{Cd}(\text{L}^{5a})]^{2+}$	$[\text{Cd}(\text{L}^{5a})]^{2+}$
Hg		$[\text{Hg}(\text{L}^{5a})]^{2+}$	$[\text{Hg}(\text{L}^{5a})]^{2+}$	$[\text{Hg}(\text{L}^{5a})]^{2+}$
Zn			$[\text{Zn}(\text{L}^{5a})]^{2+}$	$[\text{Zn}(\text{L}^{5a})]^{2+}$

**Table 4.14:** Showing the predominant species formed on reaction of  $L^5$  with mixed metals after addition of cyclohexanone

This is because the ligand becomes planar after reaction with cyclohexanone; the two amino-groups in the 3,3'-positions are constrained by formation of the 7-membered aminal ring and hence rotation about the inter-pyridine bond is prevented. The planar ligand cannot coordinate all four positions of a tetrahedral metal with formation of the double helicate prevented due to the lack of rotation between the central pyridyl

groups and so no species containing Ag(I) or Cu(I) are seen in their respective experiments. However,  $L^{5a}$  can coordinate the equatorial coordination sites of octahedral metals, giving rise to mononuclear species; indeed, these are observed in every case.

#### 4.5 Conclusion

For the most part in these experiments there is little, if any change in the affinity of the ligand upon reaction of the amine units to form the aminal. This is because the ligand  $L^5$  prefers to coordinate in the equatorial region of octahedral metal ions. Reaction with cyclohexanone does not change this behaviour (as upon cyclization it acts as a planar tetradentate chelate) and as a result no allosteric change is observed.

The only exception is the experiment with zinc and cadmium, where reaction of these metal ions with  $L^5$  gives the cadmium-containing species but upon reaction with cyclohexanone (giving  $L^{5a}$ ) a 3:2 mixture of  $[Zn(L^{5a})]^{2+}$  and  $[Cd(L^{5a})]^{2+}$  is formed. The reason that this change occurs is not clear. Both metal ions can adopt octahedral coordination geometry but due to the divergent nature of the thiazole units  $L^5$  may be more selective to the larger metal ion. Formation of the aminal will lock the ligand into a planar tetradentate unit and it would appear that in doing so the ligand has effectively no preference for the two different metal ions.

## 4.6 References

1. Smith, V. C. M., Lehn, J. M., Helicate Self-Assembly from Heteroleptic Ligand Strands of Specific Binding Site Sequence, *J. Chem. Soc. Chem. Commun.*, 1996, 2733-2734.
2. Lehn, J. M., Towards Self-Organization and Complex Matter, *Science*, 2002, **295**, 2400-2403.
3. Krämer, R., Lehn, J. M., Marquis-Rigault, A., Self-Recognition in Helicate Self-Assembly: Spontaneous Formation of Helical Metal Complexes from Mixtures of Ligands and Metal Ions, *Proc. Natl. Acad. Sci.*, 1993, **90**, 5394-5398.
4. Steed, J. W. & Atwood, J. L., (2000). *Supramolecular Chemistry*. Chichester: John Wiley & Sons.
5. Rebek, Jr. J., Trend, J. E., Wattley, R. V., Chakravorti, S., Allosteric Effects in Organic Chemistry. Site-Specific Binding, *J. Am. Chem. Soc.*, 1979, **101**, 4333-4337.
6. Rebek, Jr. J., Wattley, R. V., Allosteric Effects. Remote Control of Ion Transport Selectivity, *J. Am. Chem. Soc.*, 1980, **102**, 4853-4854.
7. Rebek, Jr. J., Binding Forces, Equilibria, and Rates: New Models for Enzyme Catalysis, *Acc. Chem. Res.*, 1984, **17**, 258-264.
8. Rebek, Jr. J., Costello, T., Wattley., Binding Forces and Catalysis. The Use of Bipyridyl-Metal Chelation to Enhance Reaction Rates, *J. Am. Chem. Soc.*, 1985, **107**, 7487-7493.
9. Kovbasyuk, L., Krämer, R., Allosteric Supramolecular Receptors and Catalysis, *Chem. Rev.*, 2004, **104**, 3161-3187.
10. Rebek, Jr. J., Marshall, L., Allosteric Effects: An On-Off Switch, *J. Am. Chem. Soc.*, 1983, **105**, 6668-6670.

11. Riis-Johannessen, T., Harding, L. P., Jeffery, J. C., Moon, R., Rice, C. R., Allosteric Deprogramming of a Trinuclear Heterometallic Helicate, *Dalton Trans.*, 2007, 1577-1587.
12. Sutton, C. E., Harding, L. P., Hardie, M., Riis-Johannessen, T., Rice, C. R., Allosteric Effects in a Ditopic Ligand Containing Bipyridine and Tetra-aza-crown Donor Units, *Chem. Eur. J.*, 2012, **18**, 3464-3467.
13. Baylies, C. J., Riis-Johannessen, T., Harding, L. P., Jeffery, J. C., Moon, R., Rice, C. R., Whitehead, M., Allosteric-Controlled Metal Specificity of a Ditopic Ligand, *Angew. Chem.*, 2005, **117**, 7069-7072.
14. Bokolinis, G., Riis-Johannessen, T., Harding, L. P., Jeffery, J. C., McLay, N., Rice, C. R., Facile Interconversion of Dinuclear Double Helicates and Side-by-Side Species: A Reprogrammable Ligand with Potential Sensor Applications, *Chem. Commun.*, 2006, 1980-1982.
15. Baylies, C. J., Harding, L. P., Jeffery, J. C., Riis-Johannessen, T., Rice, C. R., Allosteric and Electrostatic Reprogramming of a Ditopic Ligand, *Angew. Chem. Int. Ed.*, 2004, **43**, 4515-4518.
16. Baylies, C. J., Harding, L. P., Jeffery, J. C., Moon, R., Rice, C. R., Riis-Johannessen, T., Electrostatic Control of the Formation of Heteroleptic Transition metal Helicates, *New. J. Chem.*, 2007, **31**, 1525-1529.
17. Clayton, H. J., Harding, L. P., Irvine, J. P., Jeffery, J. C., Riis-Johannessen, T., Laws, A. P., Rice, C. R., Whitehead, M., Metal-Specific Allosteric Activation and Deactivation of a Diamine, *Chem. Commun.*, 2008, 108-110.
18. Riis-Johannessen, T., Jeffery, J. C., Robson, A. P. H., Rice, C. R., Harding, L. P., Solution and Solid-state Complexes of the Potentially Tetradentate Pyridyl-thiazole Ligand 6,6'-bis(4-methylthiazol-2-yl)-2,2'-bipyridine with  $\text{Co}^{\text{II}}$ ,  $\text{Ni}^{\text{II}}$ ,  $\text{Cu}^{\text{II}}$ ,  $\text{Hg}^{\text{II}}$ ,  $\text{Cu}^{\text{I}}$  and  $\text{Ag}^{\text{I}}$ , *Inorganica Chimica Acta*, 2005, **358**, 2781-2798.

19. Hannon, M. J., Painting, C. L., Plummer, E. A., Childs, L. J., Alcock, N. W., Competing Supramolecular Interactions Give a New Twist to Terpyridyl Chemistry: Anion- and Solvent- Induced Formation of Spiral Arrays in Silver(I) Complexes of a Simple Terpyridine, *Chem., Eur. J.*, 2002, **8**, 2225-2238.

## 4.7 Appendix: Crystallographic Data Tables

<b>Compound</b>	<b>{[Ag<sub>2</sub>(L<sup>5</sup>)<sub>2</sub>](ClO<sub>4</sub>)<sub>2</sub>}</b>
Formula	C <sub>40</sub> H <sub>38</sub> Ag <sub>2</sub> Cl <sub>2</sub> N <sub>14</sub> O <sub>8</sub> S <sub>4</sub>
M	1257.72
System, space group	Monoclinic, C2/c
a/Å	30.8604(7)
b/Å	8.0709(2)
c/Å	24.3888(6)
β/°	124.40
V/ Å <sup>3</sup>	5012.2(2)
Z	4
ρ <sub>calc</sub> /Mg m <sup>-3</sup>	1.667
F(000)	2528
Dimensions/mm	0.33x0.26x0.2
μ/mm <sup>-1</sup>	0.71073
T/K	150(2)
Reflections collected (range)	34259 (2.65 ≤ θ ≤ 32.03°)
hkl range indices	-46 ≤ h ≤ 46, -12 ≤ k ≤ 11, -36 ≤ l ≤ 36
Unique reflections	8651
Total, independent R <sub>int</sub>	0.0217
R <sub>w</sub>	0.1191
R	0.0396
Reflections with I > 2σ(I)	7410
GOF	1.085
Refined parameters	320
Restraints	0
Largest peak and hole/eÅ <sup>-3</sup>	1.836, -0.866

<b>Compound</b>	<b>{[Ag(L<sup>5a</sup>)](CF<sub>3</sub>SO<sub>3</sub>)}</b>
Formula	C <sub>27</sub> H <sub>27</sub> AgF <sub>3</sub> N <sub>7</sub> O <sub>3</sub> S <sub>3</sub>
M	758.61
System, space group	Triclinic, P-1
a/Å	7.5013(3)
b/Å	12.3497(6)
c/Å	17.8272(8)
β/°	96.4250(10)
V/ Å <sup>3</sup>	1493.03(12)
Z	2
ρ <sub>calc</sub> /Mg m <sup>-3</sup>	1.687
F(000)	768
Dimensions/mm	0.40x0.20x0.05
μ/mm <sup>-1</sup>	0.71073
T/K	151(2)
Reflections collected (range)	26907 (1.81 ≤ θ ≤ 27.88°)
hkl range indices	-9≤h≤9, -15≤k≤16, -23≤l≤23
Unique reflections	7112
Total, independent R <sub>int</sub>	0.0385
R <sub>w</sub>	0.0634
R	0.0303
Reflections with I > 2σ(I)	5765
GOF	1.015
Refined parameters	400
Restraints	0
Largest peak and hole/eÅ <sup>-3</sup>	0.643, -0.519

<b>Compound</b>	<b>{[Hg(L<sup>5a</sup>)](ClO<sub>4</sub>)<sub>2</sub>}</b>
Formula	C <sub>24</sub> H <sub>26</sub> Cl <sub>2</sub> HgN <sub>6</sub> O <sub>9</sub> S <sub>2</sub>
M	878.12
System, space group	Triclinic, P-1
a/Å	8.3955(3)
b/Å	13.1833(4)
c/Å	14.9044(7)
β/°	96.5860(10)
V/ Å <sup>3</sup>	1462.38(10)
Z	2
ρ <sub>calc</sub> /Mg m <sup>-3</sup>	1.994
F(000)	860
Dimensions/mm	0.20x0.20x0.10
μ/mm <sup>-1</sup>	0.71073
T/K	150(2)
Reflections collected (range)	31204 (1.73 ≤ θ ≤ 29.57)
hkl range indices	-11 ≤ h ≤ 11, -18 ≤ k ≤ 18, -20 ≤ l ≤ 20
Unique reflections	8196
Total, independent R <sub>int</sub>	0.0158
R <sub>w</sub>	0.0401
R	0.0159
Reflections with I > 2σ(I)	7894
GOF	1.003
Refined parameters	399
Restraints	0
Largest peak and hole/eÅ <sup>-3</sup>	0.835, -0.877

<b>Compound</b>	<b>{[Zn<sub>2</sub>(L<sup>5</sup>)<sub>2</sub>](CF<sub>3</sub>SO<sub>3</sub>)<sub>4</sub>}</b>
Formula	C <sub>40</sub> H <sub>32</sub> F <sub>12</sub> N <sub>12</sub> O <sub>12</sub> S <sub>8</sub> Zn <sub>2</sub>
M	1488.00
System, space group	Monoclinic, C2/2
a/Å	26.510(5)
b/Å	10.536(2)
c/Å	20.807(4)
β/°	109.76(3)
V/ Å <sup>3</sup>	5469.4(19)
Z	4
ρ <sub>calc</sub> /Mg m <sup>-3</sup>	1.807
F(000)	2992
Dimensions/mm	0.20x0.20x0.15
μ/mm <sup>-1</sup>	0.71073
T/K	100(2)
Reflections collected (range)	25017 (2.08 ≤ θ ≤ 25.00)
hkl range indices	-31 ≤ h ≤ 31, -12 ≤ k ≤ 12, -24 ≤ l ≤ 24
Unique reflections	4823
Total, independent R <sub>int</sub>	0.0514
R <sub>w</sub>	0.1388
R	0.0419
Reflections with I > 2σ(I)	3700
GOF	0.709
Refined parameters	578
Restraints	495
Largest peak and hole/eÅ <sup>-3</sup>	0.446, -0.599

## Appendix: Publication